STUDIES ON A CLASS OF NON-AUTONOMOUS EVOLUTIONARY EQUATIONS: INTEGRABILITY, EXACT SOLUTIONS, QUALITATIVE ANALYSIS, AND APPLICATIONS IN PLASMA DYNAMICS

Thesis

submitted for the Degree of

Doctor of Philosophy

in Science

by

Tanay Sarkar
(Index No. 62/19/Maths./26)

to

Department of Mathematics
Jadavpur University
Kolkata - 700032, India

January, 2025

This thesis is dedicated to my parents

Sri Abhiram Sarkar & Smt. Lakshi Sarkar

CERTIFICATE FROM THE SUPERVISOR(S)

This is to certify that the thesis entitled "**Studies on a Class of Non-autonomous Evolutionary Equations: Integrability, Exact Solutions, Qualitative Analysis, and Applications in Plasma Dynamics**" submitted by Sri Tanay Sarkar who got his name registered on 02.09.2019 (Index No. 62/19/Maths./26) for the award of Ph.D. (Science) Degree of Jadavpur University, is absolutely based upon his own work under the supervision of Professor (Dr.) Prakash Chandra Mali and Dr. Santanu Raut and that neither this thesis nor any part of it has been submitted for either any degree / diploma or any other academic award anywhere before.

24.01.2025

Prof. (Dr.) Prakash Chandra Mali
(Supervisor)

Professor (RETD.)
DEPARTMENT OF MATHEMATICS
Jadavpur University
Kolkata - 700 032, West Bengal

Santanu Raut 24/01/25

Dr. Santanu Raut
(Supervisor)

Assistant Professor
Mathabhanga College
Mathabhanga, Cooch Behar
West Bengal, Pin - 736146

ACKNOWLEDGEMENT

First and foremost, I would like to extend my sincere gratitude to my respected supervisors, Dr. Prakash Chandra Mali, Professor, Department of Mathematics, Jadavpur University, and Dr. Santanu Raut, Assistant Professor, Mathabhanga College. Their unwavering support, thoughtful guidance, and constructive feedback have been instrumental in shaping the course of my research. I am deeply appreciative of their encouragement and the confidence they placed in me during times of doubt, as well as their invaluable direction in helping me navigate challenges and avoid errors.

I also extend my sincere thanks to the other members of my research advisory committee, Prof. Abhijit Lahiri and Prof. Sagnik Sinha (Head of the Department), for their constant support, critical insights, and stimulating discussions. Their thoughtful feedback and dedicated time have been pivotal in refining and shaping the direction of my research, for which I am truly grateful.

I wish to convey my deepest respect and heartfelt gratitude to Professor Sujit Kumar Sardar, from the Department of Mathematics, Jadavpur University. I am profoundly thankful for his invaluable guidance and unwavering encouragement throughout the course of my research.

I would like to extend my sincere appreciation to the faculty members, fellow research scholars, and non-teaching staff of the Department of Mathematics, Jadavpur University. Their invaluable support and cooperation have been instrumental in shaping my efforts and bringing this work to fruition.

I am deeply grateful to the University Grants Commission, Government of India, for providing financial support through the Junior Research Fellowship (JRF) and Senior Research Fellowship (SRF), which enabled me to carry out this research work in its entirety.

I am also deeply thankful to my dear friends and fellow researchers, Dr. Sampad Das and Dr. Biswaranjan Khanra, for their unwavering support and unconditional assistance throughout my research journey.

I would also like to extend my gratitude to all my co-authors of various articles, with special thanks to Subrata Roy for his invaluable contributions and support.

Finally, I would like to express my heartfelt gratitude to my parents, Sri Abhiram Sarkar and Smt. Lakshi Sarkar, who have been the guiding light in my life. They have always taught me the values of patience, kindness, and perseverance through every stage of life. Words may fall short to convey my appreciation, but I extend my deepest thanks to them for their unwavering love, sacrifices, understanding, encouragement, support, and prayers. Their blessings and motivation have been the foundation of all that I have achieved.

To everyone who contributed in any way to this journey, I am forever grateful

Kolkata **Tanay Sarkar**

ABSTRACT

In chapter (1), the goals and importance of the current study are discussed. Definitions, a few essential properties, and the basic equations required for the research project are also provided.

Chapter (2) illustrates the infinite conservation law, quasi-periodic wave, breather, lump, and characteristic of integrability of the non-autonomous Kadomtsev-Petviashvili (NKP) equation through bilinear Bäcklund and lax pair. We derive the quasi-periodic solution and examine the periodic wave's asymptotic behaviour. Furthermore, lump, breather, and different complex structures solution for the NKP equation are investigated.

Chapter (3) uses Painlevé analysis, bilinear Bäcklund, and lax pairs to illustrate the integrability of the nonautonomous KP-modified KP equation. Several sorts of solutions including multi-solitons, smooth positons, and breathers are investigated through Hirota's bilinear technique. Using bifurcation theory, a qualitative study of the nonautonomous KP-modified KP equation is performed.

The Kadomtsev-Petviashvili-modified Kadomtsev-Petviashvili (KP-mKP) equation is shown to have some forms of efficient solutions in Chapter (4). The introduction of Liu's method for the full polynomial discrimination system addresses periodic wave profiles as well as shock waves and solitary waves.

The damped Gardner-Burgers (dGB) equation is discussed in Chapter (5), where several solutions are investigated using the (G'/G)-expansion approach and the approach of Undetermined Coefficient. These solutions produce various wave shapes and contain discrete sets of arbitrary functions, such as exponential and hyperbolic functions.

In Chapter (6), the propagating properties of dust acoustic waves (DAWs) in collisionless, unmagnetized, viscous dusty plasma are analysed through the KP equation and the Kadomtsev-Petviashvili Burgers (KPb) equation. Using various techniques, shock, solitary, and periodic solutions are obtained from the appropriate frameworks. Lastly, numerical examples are provided to show how the physical characteristics affect the wave propagation in the current system.

Chapter (7) examines the properties of ion-acoustic waves propagating through a relativistic electron-positron-ion (EPI) plasma when a relativistic positron beam is present. The Korteweg-de Vries (KdV) equation and modified Korteweg-de Vries (mKdV) equation are derived using the fundamental set of fluid equations. Different sorts of solutions, including periodic and breather ones, are derived in both models. The wave propagation model incorporates numerical information of several physical parameters in the physical environment.

A summary of our complete investigation, along with a discussion of possible avenues for future research, is provided in Chapter (8).

List of Acronyms

BT : Bäcklund transformation

CDSPM : complete discrimination system for polynomial method

dGB : damped Gardner-Burgers

DAW : dust acoustic wave

DIAW : dust ion acoustic wave

IST : inverse scattering transform

IAW : ion-acoustic wave

KP : Kadomstev-Petviashvili

KPb : Kadomtsev-Petviashvili Burgers

KP-mKP : Kadomtsev-Petviashvili-modified Kadomtsev-Petviashvili

KdV : Korteweg-de Vries

mKP: modified Kadomtsev-Petviashvili

mKdV : modified Korteweg-de Vries

NKP : non-autonomous Kadomtsev-Petviashvili

NLEE : nonlinear evolution equation

NSE : nonlinear Schrödinger equation

ODE : ordinary differential equation

PDE : partial differential equation

RPM : Reductive Perturbation Method

RPT : Reductive Perturbation Technique

SHBM : simplified Hirota bilinear method

WTC : Weiss, Tabor, and Carnevale

ZK : Zakharov-Kuznestev

List of Figures

Contents

Chapter 1

Introduction

Nonlinear evolution equations (NLEEs) are pivotal in modeling a diverse array of physical phenomena across multiple disciplines, including fluid dynamics, plasma dynamics, biological systems, chemistry, Astronomy, water-wave phenomena, ocean engineering, etc [1, 2, 3, 4, 5, 6, 7, 8]. These equations capture the complexity and richness of nonlinear interactions, where traditional linear models often fall short. The study of NLEEs has gained significant attention due to their intricate structures and the mathematical challenges they present. The general representation of a NLEE can be written as

$$\frac{\partial u}{\partial t} = N(u, u_x, u_{xx}, , , ,).$$

Here, $u = u(x, t)$ is a state variable that depends on both space x and time t, and N is a nonlinear operator function that often includes spatial derivatives and other nonlinear terms. Non-autonomous NLEEs are a class of partial differential equations (PDEs) that serve to characterize systems exhibiting temporal changes that are not governed by a linear or predictable framework. Such behavior is often a result of the effects of time-dependent variables or external conditions. Unlike autonomous systems, which are time-invariant, non-autonomous systems are influenced by external factors that vary over time, making the system's behavior depend explicitly on time. These equations capture processes where the system's rules change continuously or at intervals, driven by external or internal changes to the environment. The general form of a non-autonomous NLEE can be described as,

$$\frac{\partial u}{\partial t} = N(t, u, u_x, u_{xx}, , , ,).$$

In non-autonomous equations, N also explicitly depends on t, making the system's evolution directly tied to external temporal factors. These equations arise in diverse fields such as engineering, physics, biology and economics, where systems evolve over time under the influence of external or internal non-stationary forces [9, 10, 11, 12, 13, 14, 15, 16, 17, 18].

Integrability is a mathematical property that enhances the ability to predict and gain qualitative insights into a system's dynamics, both locally and globally [19]. The concept of integrability for nonlinear PDEs is not precisely defined, and no single, universally accepted definition exists [20]. However, several working definitions are commonly used to investigate whether a nonlinear PDE is integrable. Few of them are Inverse Scattering Transform (IST) Method [20, 21, 22], Lax pair [23, 24, 25], Existence of N-Soliton Solutions [4, 26, 27], Painlevé Analysis or Singularity Structure Analysis [28, 29], Bäcklund Transformations (BT) [30, 31], Infinitely Many Conservation Laws [2, 20, 31, 32, 33], Infinitely Many Generalized Symmetries [34, 24] etc. Numerous integrable NLEEs, particularly those that support soliton solutions, have been identified and extensively studied. These integrable NLEEs reveal a rich mathematical structure and play a critical role in advancing science and technology. Therefore, the search for new integrable NLEEs remains a valuable pursuit. An exact solution of a NLEE is an explicit, closed-form expression that satisfies the equation without approximation. Exact solutions provide a complete and explicit understanding of a system's behavior, offering a crucial tool in both theoretical and applied contexts. Finding exact solutions to NLEEs can be challenging due to the inherent nonlinearity. However, several powerful techniques are commonly used to obtain exact solutions such as inverse scattering transformations [20], Hirota direct method [27, 35], Bäcklund transformations [36], Tanh method [37], G'/G-expansion method [38], etc. Exact solutions of NLEEs come in various forms, some of the common types are solitons [4, 27], positons [39, 40], breathers [41, 42, 43], lumps [44, 45], shock or kink, periodic, quasi-periodic [46, 47] etc. These exact solutions provide diverse insights into nonlinear evolution equations, from stable particle-like behavior (solitons) to complex oscillatory structures (breathers), shock waves, etc. These solutions are vital for understanding phenomena in fluid dynamics, optics, quantum mechanics, and beyond.

Again, Qualitative analysis of NLEEs focuses on understanding the general behavior, stability, and patterns of solutions without necessarily solving the equations exactly [48, 49]. When NLEEs are often difficult (or impossible) to solve explicitly, qualitative analysis is essential for gaining insights into their behavior. Various approaches in dynamical system provide the mathematical framework and tools essential for conducting qualitative analysis [50, 51]. A dynamical system is a mathematical framework used to describe how a point in a certain space changes over time according to a set of rules or equations. This concept is widely used in fields like biology, physics, economics, engineering and many other disciplines to model the evolution of systems over time [52]. Dynamical systems can help in understanding complex phenomena by examining the relationships and interactions between variables over time. Nonlinear systems are capable of displaying chaotic behavior [52, 53], in which minor variations in initial conditions result in vastly different outcomes, making the system highly sensitive and unpredictable. Qualitative analysis helps understand how changes in system parameters affect the behavior of solutions [51, 54].

Plasma is an extremely hot state of matter in which atoms are so energized that their electrons break free, creating an ionized gas. In the night sky, we see plasma glowing as stars, nebulae, and auroras shimmering near the poles [55]. Lightning flashes in the sky are plasma, as are the neon signs that light up our city streets. The Sun, too, is a massive ball of plasma, the source of energy that sustains life on Earth. With so much of the universe in a plasma state, scientists across many fields are deeply interested in its behavior and properties [56, 57]. In particular, at the extreme temperatures required for practical fusion energy, matter becomes plasma. Beyond fusion, plasmas are harnessed in many fields, from manufacturing computer chips and powering rocket engines to environmental cleanup, destroying biological hazards, wound healing, and many other innovative applications [58, 59, 60, 61]. Due to imbalances in the distribution or movement of charged particles, such as ions and electrons, within a plasma, many plasma waves are formed. IAWs is one such plasma waves form when there is a difference in pressure (temperature) between ions and electrons. These are low-frequency waves caused by the oscillations of ions in a plasma. Since ions have significantly greater mass compared to electrons, they oscillate more slowly. They can occur in magnetized or unmagnetized plasmas, and are parallel to the magnetic field in magnetized plasmas. Charged dust particles within plasmas not only modify the electron-ion composition and affect conventional wave modes, like IAWs, but also give rise to novel low-frequency wave modes known as DAWs [62, 63]. DAWs can be thought of as a dust-dominated analog to IAWs, where the massive dust grains replace ions as the dominant inertial component. In the limiting case where dust density is low, DAWs reduce in behavior closer to IAWs. DAWs are a distinctive mode of propagation in a three-component dusty plasma system consisting of electrons, ions, and micrometer-sized charged dust particles with significant mass [64]. These waves exhibit a phase velocity significantly lower than the thermal velocities of electrons and ions. In DAWs, the restoring force is generated by the pressure of the electrons and ions, while the dust grains provide the necessary inertia.

1.1 Historical background

The modern study of integrable equations began with the landmark work of Martin Kruskal and his collaborators on the Cauchy problem for the KdV equation, using what would later be known as the IST method [65, 26]. A significant advancement came with Peter Lax, who showed that the essential feature of an integrable equation is its expression as the compatibility condition of two linear eigenvalue equations, later termed a "Lax pair" [66]. The presence of a Lax pair remains a fundamental criterion for integrability [67]. One of the most common characteristic for a nonlinear equation to be integrable, it often admits multi-soliton solutions [2]. The Hirota method systematically constructs these solutions by rewriting the equation in bilinear form and using perturbative expansions [4]. A remarkable characteristic of nonlinear equations in this category is

their possession of an infinite number of conservation laws [32]. In 1983, Weiss, Tabor, and Carnevale (WTC) introduced the Painlevé integrability analysis method [68], originally developed by Paul Painlevé to assess the integrability of nonlinear PDEs.

The study of exact solutions for NLEEs has a rich historical background that spans several decades, highlighting significant mathematical and physical developments. The roots of nonlinear equations can be traced back to 19th-century mathematical physics, particularly in the context of fluid dynamics and wave motion. Early researchers like Bernoulli and Navier-Stokes began formulating nonlinear equations to describe various physical phenomena. The KdV equation, introduced by Korteweg and de Vries, emerged in 1895 to describe shallow water waves [69]. Its soliton solutions were discovered much later, in the 1960s, through the work of Zabusky and Kruskal [65]. They used numerical simulations to reveal soliton behavior, which sparked interest in finding exact solutions and many new methods are discovered. The inverse scattering transform, developed by Gardner, Greene, Kruskal, and Miura, provided a powerful technique to find exact solutions of certain nonlinear equations, including the KdV equation [26]. The Hirota direct method, developed by Ryogo Hirota in the early 1970s, is particularly effective in finding multi-soliton solutions of integrable equations [27]. Techniques such as Bäcklund transformations and Darboux transformations [70, 71, 72] emerged, enabling the construction of new exact solutions from known ones.

Dynamical systems were initially applied to astronomical studies in the early seventeenth century by Johannes Kepler and Galileo Galilei, who conducted qualitative analysis of planetary motion. Later, Isaac Newton formalized these studies mathematically through ordinary differential equations. Since then, mathematical analysis has become integral to studying various natural and physical systems. Towards the late nineteenth century, Henri Poincaré pioneered the topological study of dynamical systems [49], using it to explore the three-body problem in celestial mechanics [73, 74]. In the early twentieth century, George Birkhoff extended this work by applying the qualitative theory of dynamical systems to problems in ergodic theory [75]. These foundational studies inspired further research, leading to widespread use of dynamical systems theory in approximating natural and physical phenomena across multiple scientific and engineering fields. In recent times, the theory of dynamical systems has been used extensively to predict the long term behaviour of various physical and natural systems occurring around us [76, 52].

The study of plasma waves, particularly IAWs and DAWs, has a fascinating history rooted in the exploration of both theoretical and experimental plasma physics[77, 78, 79, 80]. The history of IAWs dates back to the early development of plasma physics in the 20th century. Langmuir and Tonks developed the concept of plasma oscillations, which set the stage for understanding plasma waves [81]. After the Second World War, interest in plasmas grew, especially due to research in nuclear fusion and astrophysical plasmas [82, 83]. Scientists studied the collective behavior of charged particles in plasma and began understanding the significance of wave-like disturbances.

Researchers like David Bohm and Igor Tamm (among others) formulated the concepts of plasma oscillations and waves in plasmas. They described how low-frequency oscillations could occur due to the interaction between ions and electrons.

DAWs emerged as a significant area of study more recently, with developments primarily in the late 20th century. They involve plasmas that contain charged dust particles in addition to ions and electrons. Plasma physicists began focusing on the behavior of dusty plasmas, particularly as researchers observed that the presence of charged dust particles could significantly alter plasma dynamics. The concept of the DAW was first introduced by physicist P. K. Shukla at the First Capri Workshop on Dusty Plasmas in 1989. The following year, Rao, Shukla, and Yu conducted a theoretical investigation of dust acoustic waves in 1990 [84]. The existence of DAWs was later confirmed through experiments by Barkan, Merlino, and D'Angelo in 1995 [85].

1.2 Literature review

The KP equation, a two-dimensional nonlinear dispersive long-wave model, characterizes weakly transverse water waves in the long-wavelength limit with minimal surface tension effects [86]. It was later developed by Ablowitz and Segur [87] as a model for surface and internal water waves and applied to nonlinear optics by Pelinovsky, Stepanyants, and Kivshar [88]. Additionally, this equation has found relevance in various physical contexts, such as reduced models in Bose-Einstein condensation, string theory, and ferromagnetics. Over the years there are many authors who studied the integrability and exact solutions of KP equation. The linear scattering problem, or Lax form, linked to the KP equation was formulated by Dryuma in 1974, providing a strong indication that the equation is integrable. The following year, Chen solved the KP equation using the Bäcklund transformation method [89]. Satsuma was the first to find the bilinear form and obtain an exact N-soliton solution for the KP equation applying Hirota's method [90]. Subsequently, the inverse scattering approach was applied to the KP equation by Manakov [91], Fokas and Ablowitz [92], and Ablowitz, Bar Yaacov, and Fokas [93]. Recently, many authors studied integrability and exact solutions of extended KP equation. Li et al [94] and Wazwaz [95] investigated the characteristic integrability of extended KP equation via Painlevé test and derived N-soliton, breathers, lump solutions. Konopelchenko study the completely integrability of the KP-mKP equation [96]. The integrability characteristics of the KP-mKP or Gardner-KP equations have been investigated through infinite conservation laws by Naz et al [97], and Lax pairs by Wazwaz [98].

Some researchers have studied the integrability and exact solutions of the non-autonomous KP equation and its extended forms, particularly the KP equation with time-dependent coefficients. Clarkson [99] studied the integrability of variable coefficient KP equation via painlevé analysis. Tian and Zhang [100] investigated the integrability of the generalized variable coefficient KP equation us-

ing the Bell polynomial approach, and derived the soliton solutions and periodic wave solutions expressed through Riemann theta functions. Yan et al. [101] studied the characteristic of integrability of (2+1)-dimensional variable coefficient KP equation via Painlevé analysis and derived N-soliton solution. Many authors have studied exact solutions of the KP equation in the form of lump, shocks, periodic, N-soliton, positon and other types of solutions [44, 102, 103, 104, 105, 106, 107].

The KP-mKP equation has applications in modeling real physical systems, including fluid dynamics, plasma waves, and nonlinear optics. Exact solutions can predict how wave patterns will behave under constant environmental conditions, which is important for designing wave-based applications in fields such as communication, energy transfer, and fluid flow management. Since the KP-mKP equation is highly nonlinear and multidimensional, so finding exact solution is not so easy. Konopelchenko find the exact solutions including rational solutions, lump solutions of the KP-mKP equation [108].

Wazwaz exploited Hirota bilinear method to derive multiple singular and multi-solitary solutions for the KP-mKP equation, showcasing the diversity of solutions through numerical analysis [109]. Liu et al. [110] explored the phase portrait of the KP-mKP model using bifurcation theory of dynamical systems, deriving exact traveling wave solutions such as solitary, periodic, kink (anti-kink), and breaking wave solutions. Jawad et al. [111] applied the improved (G'/G) expansion method to obtain various solutions for the KP-mKP equation, including soliton and hyperbolic solutions. Boateng et al. [112] employed the Modified Extended Direct Algebraic Method to derive trigonometric and hyperbolic solutions for the $(2+1)$-dimensional KP-mKP equation.

The Gardner-Burgers equation combines features of the Burgers and Gardner equations. It models a range of physical phenomena, including turbulence, shock waves, and dissipative systems in fluid dynamics. Wang studied the exact solution of Gardner-Burgers equation employing homogeneous balance method [113]. Zhang et al find the kink type solitary solution for Gardner-Burgers equation using proper transformation [114]. Li et al derived the hyperbolic and trigonometric function solutions for Gardner-Burgers equation using proper transformation [115]. Kaya obtained the exact solution of Gardner-Burgers equation by using Adomian's decomposition method [116]. The addition of damping terms can represent friction or energy loss, which are often present in real-world applications.

Recently, there is a considerable interest in studying two-dimensional nonlinear DAWs due to their significance in understanding the complex dynamics of dusty plasma. Duan studied the DAWs for (2+1) dimensional KP equation [117]. Lin and Duan studied KP equation in a two-ion-temperature cold dusty plasma [118]. Dorranian and Sabetkar [119] analytically investigated nonlinear dust acoustic solitary waves in a dusty plasma containing two nonthermal ion species at different temperatures. Saini et al. [120] investigated nonlinear dust acoustic solitary waves in a dusty plasma with superthermal charged particles (electrons and ions) using the KP equation.

There are also several literature in which dust acoustic waves has been studied in the framework of KP equation [121, 122, 123]. Xue studied the dust acoustic shock waves in dusty plasma in the framework of KP Burgers equation [124].

In recent years, significant attention has been focused on the nonlinear wave propagation in plasmas composed of electron, ion, and positron beams. The nonlinear structure of a plasma can undergo significant alterations in the presence of positron beams. The effects of an positron beam on nonlinear energy transport in positron beam-plasma system has been studied by Shah and Mahmood [125]. Shan et al.[126] demonstrated that the increased velocity of the positron beam, along with the presence of super-thermal electrons, can influence the existence domain, amplitude, and width of solitons. Shah et al. [127] examined ion-acoustic shock waves in a superthermal electron-ion plasma influenced by the presence of a positron beam. The effect of the cold positron beam on growth and damping of the waves in a plasma system investigated by Shan et al.[128]. Sarma et al. studied the propagation properties of ion-acoustic solitary waves in an unmagnetized thermal electron-ion plasma influenced by a relativistic positron beam flow [129].

1.3 Motivation

The study of nonautonomous NLEEs focuses on determining whether these time-dependent versions retain the integrability of their autonomous counterparts, which is critical for understanding long-term system behavior. Nonautonomous terms, influenced by external forces, or spatial variations, can complicate dynamics and potentially lead to chaos or irregularity. Investigating their integrability provides insights into transitions between predictable (integrable) and complex (non-integrable) behaviors, making their study an important and challenging aspect of nonlinear partial differential equations. Exact solutions are crucial for exploring phenomena like time-dependent solitons, breathers, and localized structures. They also help assess whether nonautonomous deformations preserve integrable features such as Lax pairs or Bäcklund transformations, providing deeper insights into the structure and behavior of these systems.

Nonetheless, many evolution equations lack explicit solutions, rendering them either inaccessible or impractical. The presence of time-dependence introduces additional complexities, demanding a thorough approach to evaluate time-dependent stability, which is shaped by changing external factors. Furthermore, understanding the implications of periodic and aperiodic forcing is crucial, as these can give rise to phenomena including resonance, quasi-periodicity, or chaos. In such scenarios, qualitative analysis assumes a significant role by exploring essential questions, including the potential for the system to stabilize over time, the resilience of solutions against perturbations or changes in parameters, and the presence of periodic or chaotic behavior within the system. A thorough understanding of these phenomena is critical for advancing theoretical knowledge and for

effectively controlling such behaviors in real-world contexts. This insight empowers researchers to anticipate system dynamics, ensure stability, and implement interventions or optimizations as required. The interest in studying the qualitative analysis of evolution equations is motivated by a combination of theoretical exploration, the imperative to understand nonlinear and time-dependent dynamics, and the goal of addressing practical challenges in a diverse array of fields.

These equations provide a more accurate representation of real-world systems, including fluid dynamics with seasonal changes, plasma waves influenced by time-varying fields, and optical systems with variable refractive indices. We employed these models to investigate the propagation characteristics of plasma waves in various plasma environments. IAWs and DAWs play a vital role in plasma physics as they are key to understanding the behavior and dynamics of plasmas in both natural and laboratory settings. These fundamental plasma waves are often modeled by nonlinear evolution equations such as the KdV and KP equations, which describe the intricate nonlinear interactions within plasmas. These equations elucidate the complex nonlinear interactions occurring within plasmas. Analyzing precise solutions to these equations, such as solitons and shocks, yields vital understanding of how plasma characteristics, including density and temperature, affect wave dynamics and nonlinear phenomena. Furthermore, these exact solutions enable researchers to identify transitions, bifurcations, and dynamic behaviors that are crucial for the progression of both theoretical models and experimental endeavors in the field of plasma science.

This thesis is devoted to the investigation of a particular category of NLEEs, emphasizing the concept of integrability. By conducting an in-depth analysis, this work aims to enhance the comprehension of NLEEs, illuminating their integrability, the diversity of their exact solutions, and the qualitative characteristics that influence their dynamics. Ultimately, the established frameworks are employed to analyze the propagation behavior of IAWs and DAWs across different plasma environments.

1.4 Nonlinear Partial Differential Equations

Nonlinear PDEs are a rich area of study, with ongoing research focused on integrability, finding solutions, analyzing stability, and applying them to real-world problems. In this section we discussed the NLEEs which are used in this thesis.

1.4.1 KdV equation

The KdV equation explains the behavior of water waves traveling through long, narrow, and shallow channels. Originally proposed in 1895 by Dutch mathematicians Diederik Johannes Korteweg and Gustav de Vries [69], the equation is typically written in its standard form after

suitable scaling adjustments as the following

$$u_t - 6uu_x + u_{xxx} = 0, \tag{1.1}$$

and in general can be written as

$$u_t + Auu_x + Bu_{xxx} = 0, \tag{1.2}$$

In the equation, $u(x,t)$ represents the vertical displacement of the water from its equilibrium position at a given location x and time t. The KdV equation is classified as a nonlinear PDE because of the uu_x term, where subscripts indicate partial derivatives. The presence of the u_{xxx} term introduces dispersive effects.

The significance of the KdV equation became evident in 1965 when Zabusky and Kruskal [65] provided an explanation for the Fermi-Pasta-Ulam puzzle using solitary-wave solutions of the KdV equation. Through their numerical analysis, they identified solitary-wave pulses, which they termed solitons due to their particle-like properties. These solitons exhibited nonlinear interactions, yet remarkably, their size and shape remained virtually unchanged after such interactions. This intriguing behavior of soliton solutions to the KdV equation generated considerable interest, though, at the time, the only method for solving this nonlinear PDE was numerical.

1.4.2 mKdV equation

The mKdV equation is a nonlinear PDE often encountered in the study of wave dynamics, such as in plasma physics, shallow water waves, and nonlinear optics [130]. It is a variant of the KdV equation that includes a cubic nonlinearity instead of a quadratic one. The standard form of the mKdV equation is given by [131]

$$u_t + 6u^2u_x + u_{xxx} = 0, \tag{1.3}$$

and in general can be written as

$$u_t + A_1u^2u_x + Bu_{xxx} = 0, \tag{1.4}$$

The mKdV equation indeed holds a pivotal place in the history of Soliton Theory and nonlinear dynamics. It was instrumental in deriving infinitely many conservation laws for the KdV equation [132], which ultimately led to the discovery of the KdV equation's Lax pair and the development of the IST.

1.4.3 KP equation

In mathematical physics, the KP equation, attributed to Boris B. Kadomtsev and Vladimir I. Petviashvili, is a PDE used to model the behavior of nonlinear wave motion [86]. The KP equation

is commonly expressed as

$$(u_t + 6uu_x + u_{xxx})_x - \sigma u_{yy} = 0, \qquad \sigma = \pm 1 \tag{1.5}$$

and in general can be written as

$$(u_t + Auu_x + Bu_{xxx})_x + Du_{yy} = 0, \tag{1.6}$$

In this context, $u = u(x, y, t)$ represents a scalar function, where x and y denote the longitudinal and transverse spatial coordinates, respectively. Partial derivatives are indicated by subscripts x, y and t.

The KP equation serves as a universal integrable system in two spatial dimensions, analogous to the role of the KdV equation in one spatial dimension, as many other integrable systems can be derived as its reductions. Over the past five decades, it has been a significant focus of study within the mathematical community. It naturally appears as a distinguished limit in asymptotic analyses, retaining only the leading-order terms while assuming a balance between weak dispersion, quadratic nonlinearity, and diffraction. The asymmetry between the two spatial variables is reflected in their distinct roles within the equation.

1.4.4 KPb equation

The KPb equation is a modified version of the KP equation that includes dissipative effects. It is used to model the dynamics of certain types of waves in dissipative media, where energy is lost due to viscosity or other dissipative mechanisms. The KPb equation is particularly relevant in the study of wave phenomena in fluid dynamics and related fields. The KP-Burger equation is given by

$$(u_t + Auu_x + Bu_{xxx} + Cu_{xx})_x + Du_{yy} = 0 \tag{1.7}$$

The presence of the dissipative term Cu_{xx} introduces a damping effect, causing the wave amplitude to decrease over time. This term models the physical processes responsible for energy dissipation in the medium, such as viscosity in fluid flow. The KPb equation retains many of the mathematical properties of the KP equation, including soliton solutions and other nonlinear wave behaviors. However, the presence of dissipation alters the dynamics of the system, leading to different types of wave propagation and interaction phenomena. Research on the KPb equation and its solutions contributes to the understanding of wave dynamics in dissipative media and has applications in various fields, including fluid mechanics, nonlinear optics, and plasma physics.

1.4.5 Damped forced KP equation

The damped forced KP equation is a modification of the classical KP equation that incorporates external forcing and damping effects. The general form of the damped, forced KP equation

is

$$(u_t + Puu_x + Qu_{xxx} + Du)_x + \alpha u_{yy} = f(x,t), \tag{1.8}$$

The damped, forced KP equations are used to model a variety of physical systems, including shallow water waves in the presence of external forces and dissipation, Plasma physics, nonlinear optics with external driving forces.

1.4.6 KP-mKP equation

The KP-mKP equation is a generalization of the KP equation that includes additional higher order nonlinear terms to account for more complex behavior. It is particularly used when dealing with situations where both quadratic and cubic nonlinearities are important. The KP-mKP equation can be written as

$$(u_t + Puu_x + Qu^2u_x + Ru_{xxx})_x + Tu_{yy} = 0 \tag{1.9}$$

Due to its ability to describe the interplay between nonlinearity, dispersion, and multi-dimensional effects, the KP-mKP equation is widely utilized across several branches of physics such as plasma physics, fluid dynamics, quantum field theory etc.

1.4.7 Damped forced KP-mKP equation

The damped forced KP-mKP equation is a nonlinear PDE that extends the standard KP equation by incorporating higher-order (modified) nonlinearities, damping, and external forcing. This equation appears in contexts such as shallow water waves, plasma physics, and other nonlinear wave phenomena where transverse effects, nonlinearity, and dispersion interact in complex ways. The damped forced KP-mKP equation can be written as

$$(u_t + Puu_x + Qu^2u_x + Ru_{xxx} + Su)_x + Tu_{yy} = f(x,t), \tag{1.10}$$

where P, Q are the coefficients of nonlinear terms, R is the coefficient for third-order dispersion, T is the coefficient for transverse dispersion, S is damping coefficient, and $f(x,t)$ is the forcing term.

1.4.8 Damped Gardner-Burgers equation

The dGB equation is a modified nonlinear PDE that combines features of the Gardner equation, Burgers equation, and damping effects. It is used to model various physical phenomena where nonlinear, dispersive, and dissipative effects interact, along with an external damping

mechanism. The general form of the dGB equation can be written as

$$u_t + Auu_x + Bu^2u_x + Cu_{xxx} + Duxx + Eu = 0. \tag{1.11}$$

1.5 Integrability of nonlinear partial differential equations

The integrability of nonlinear PDEs has become a prominent area of research in recent years. An integrable system is often perceived as one that is theoretically solvable. Numerous strategies have been utilized to establish the concept of integrability in this area. As of now, there is no universally accepted definition in mathematics that delineates what constitutes an integrable or exactly solvable system. The exploration of what defines an integrable system is closely linked to its classification. Integrability is defined in a number of ways, including the presence of Lax representation, Painlevé property, conservation laws, Bäcklund transformations, etc.

1.5.1 Description of the Painlevé test

Painlevé and Gambier at the beginning of this century initiated the Painlevé analysis for the classification of nonlinear ordinary differential equations (ODEs) (without movable critical points) in an algebraic manner. The Painlevé analysis for nonlinear PDEs is introduced by WTC in 1983 [68] as an extension of the method initiated by Painlevé and Gambier. The Painlevé test serves as a useful tool for providing necessary conditions to identify whether PDEs exhibit complete integrability. A PDE is said to exhibit the Painlevé property if its solutions remain single-valued around movable singularity manifolds. We consider a general nonlinear PDE with the unknown $\phi = \phi(x, y, z, \tau)$ as,

$$\phi_\tau = \mathcal{N}(\phi, \phi_x, \phi_y, \phi_z, \phi_{x,x}, \phi_{\tau x}, \phi_{xxx}, \phi_{yy}...). \tag{1.12}$$

Through a generalized Laurent expansion, we offer the solution to Eq.(1.12) as

$$\nu = \phi^{-\gamma}(x, y, z, \tau) \sum_{j=0}^{\infty} \nu_j(x, y, z, \tau)\phi^j(x, y, z, \tau) \tag{1.13}$$

in which $\phi(x, y, z, \tau) = 0$ reduces a singular manifold. The positive integer γ needs to be evaluated, and $\phi(x, y, z, \tau)$ and $\nu_j(x, y, z, \tau)$ are both taken to be analytic functions. In order to assess the higher order of the Eq.(1.13), we first set

$$\nu(x, y, z, \tau) = \nu_0(x, y, z, \tau)\phi^{-\gamma}(x, y, z, \tau) \tag{1.14}$$

where $\psi_0(x, y, z, \tau)$ is analytic.

Step 1. In order to obtain $\gamma = k$, substitute Eq.(1.14) into Eq.(1.12) and balance the highest

order derivative with the nonlinear terms.

Step 2. For the recursion formula, we set

$$\nu(x, y, z, t) \approx \nu_0(x, y, z, \tau)\phi^{-k} + \nu_j(x, y, z, \tau)\phi^{j-k}(x, y, z, \tau). \tag{1.15}$$

We acquire the recursion formula by substituting Eq.(1.15) into Eq.(1.12) and collect the terms affecting ν_j. Resonances are now characterized as the values of j where the recursion formula fails to be defined, resulting in ν_j becoming arbitrary.

Step 3. The reduced expansion is now expressed as follows for the compatibility condition:

$$\nu = \nu_0\phi^{-k} + \sum_{j=1}^{k_h} \nu_j\phi^{j-k}. \tag{1.16}$$

Our consideration is limited to the highest resonance ($j = k_h$). For simplicity, we employ the Kruskal anasatz [133] of the singular manifold [68] in this scenario. Thus, we view as

$$\phi(x, y, z, \tau) = x + y + z - \chi(\tau) \tag{1.17}$$

where the analytic function $\chi(\tau)$ is selected at random. (1.16) and (1.17) are substituted into Eq.(1.12), with the collecting power of ϕ being equal to zero. Thus, one can determine whether or not all positive resonances satisfy the compatibility criterion.

1.5.2 Bilinearization using Bell polynomials

It is widely recognized that the initial phase in assessing the integrability of a NLEE involves the exploration of a bilinear representation of that equation. The Hirota bilinear method and the Bell-polynomial framework are intricately connected. To begin with, one may apply the necessary adjustments to the Bell polynomials. In the early 1930s, Bell introduced three distinct varieties of exponential polynomials [134, 135, 136, 137].

Definition 1 Let r be defined as a constant positive integer, and let n represent any arbitrary non-negative integer. The polynomial in relation to the independent variables ξ and τ is subsequently expressed as follows:

$$\zeta_n(\xi, \tau) \equiv exp(-\tau\xi^r)\partial_\xi^n exp(\tau\xi^r). \tag{1.18}$$

This is known as the classical Bell polynomials, or specifically the Hermite-Bell polynomials when $r = 2$, as introduced by Bell. The Bell polynomials of the initial lower orders are as follows,

$\zeta_0(\xi, \tau) = 1$, $\zeta_1(\xi, \tau) = r\tau\xi^{r-1}$, $\zeta_2(\xi, \tau) = r^2\tau^2\xi^{2r-2} + r(r-1)\tau\xi^{r-2}$,

and in general

$\zeta_n(\xi,\tau) = n!\sum_{j=a}^{n}\frac{\tau^j\xi^{rj-n}}{j!}\sum_{l=0}^{b}(-1)^l\binom{j}{l}\binom{r(j-l)}{n}$,
where $a = n-[n(r-1)/r]$ and $b = [(rh-n)/r]$ in which square brackets denote the integer part.

Definition 2 Let $u = u(\xi_1,..,\xi_l))$ be an arbitrary non-negative integer, represented by n_k for $k = 1,2,\ldots,l$. We will consider C^∞ as a multivariable function that follows this criterion:

$$Y_{n_1\xi_1,\ldots,n_l\xi_l}(u) \equiv \exp(-u)\partial_{\xi_1}^{n_1}\ldots\partial_{\xi_l}^{n_l}\exp(u), \tag{1.19}$$

Multi-dimensional Bell polynomials, often referred to as generalized Bell polynomials or Y-polynomials, are defined as polynomials involving the partial derivatives of u with respect to the variables $\xi_1,\cdots,\xi_l$. In the expression $Y_{n_1\xi_1,\cdots,n_l\xi_l}(u)$, the subscripts indicate the highest order of derivatives of u concerning x_k, where k ranges from 1 to l. Specifically, with $u = u(\xi,\tau)$, the associated two-dimensional Bell polynomials derived from equation (1.19) are presented as follows:

$Y_\xi(u) = u_\xi$, $Y_{2\xi}(u) = u_{2\xi}+u_\xi^2$, $Y_{3\xi}(u) = u_{3\xi}+3u_\xi u_{2\xi}+u_\xi^3$, $Y_{\xi,\tau}(u) = u_{\xi,\tau}+u_\xi u_\tau$,...

Specifically, when $n_1 = n$, $n_2 = 0$, and $u = u(\xi,\tau) = \tau\xi^r$, multi-dimensional Bell polynomials (1.19) serve as a precise reduction of the classical Bell polynomials (1.18).

$$Y_{n\xi}(u) = \exp(-\tau\xi^r)\partial_\xi^n\exp(\tau\xi^r) = \zeta_n(\xi,\tau).$$

This suggests that the multi-dimensional Bell polynomials presented in equation (1.19) represent an extended form of the conventional Bell polynomials depicted in equation (1.18).

Definition 3 The multi-dimensional binary Bell polynomials, referred to as $\mathcal{Y}$-polynomials, can be formulated using the aforementioned Bell polynomials (1.19) in the manner described below.

$$\mathcal{Y}_{n_1\xi_1,\ldots,n_l\xi_l}(v,w) = Y_{n_1\xi_1,\ldots,n_l\xi_l}(u)\Big|_{u_{r_1\xi_1,\ldots,r_l\xi_l}=\begin{cases}v_{r_1\xi_1,\ldots,r_l\xi_l}, r_1+..+r_l \text{ is odd},\\ w_{r_1\xi_1,\ldots,r_l\xi_l}, r_1+..+r_l \text{ is even},\end{cases}} \tag{1.20}$$

The multivariable polynomials are with respect to all partial derivatives $v_{r_1\xi_1,\ldots,r_l\xi_l}$ and $w_{r_1\xi_1,\ldots,r_l\xi_l}$. The initial binary Bell Polynomials are listed.

$\mathcal{Y}_\xi(v) = v_\xi$, $\mathcal{Y}_{2\xi}(v,w) = w_{2\xi}+v_\xi^2$, $\mathcal{Y}_{\xi,\tau}(v,w) = w_{\xi,\tau}+v_\xi v_\tau$, $\mathcal{Y}_{3\xi}(v,w) = v_{3\xi}+3v_\xi w_{2\xi}+v_\xi^3$,...

Proposition 1: The correlation between the Bell polynomials $\mathcal{Y}_{n_1\xi_1,\ldots,n_l\xi_l}(v,w)$ and standard Hirota bilinear equation $D_{\xi_1}^{n_1}\cdots D_{\xi_l}^{n_l}F\cdot G$ can be obtained using the following identity.

$$\mathcal{Y}_{n_1\xi_1,\ldots,n_l\xi_l}(v=\ln F/G, w=\ln FG) = (FG)^{-1}D_{\xi_1}^{n_1}\cdots D_{\xi_l}^{n_l}F\cdot G, \tag{1.21}$$

where $n_1+\cdots+n_l \geqslant 1$ and the Hirota bilinear operators $D_{\xi_l},\ldots,D_{\xi_l}$ are characterized by

$$D_{\xi_1}^{n_1}\cdots D_{\xi_l}^{n_l}F\cdot G = (\partial\xi_1-\partial\xi_1')^{n_1}\cdots(\partial\xi_1-\partial\xi_l')^{n_l}F(\xi_1,\ldots,\xi_l)G(\xi_1',\ldots,\xi_l')\Big|_{\xi_i'=\xi_i}.$$

When F and G are equal, (1.21) becomes

$$G^{-2}D_{\xi_1}^{n_1}\cdots D_{\xi_l}^{n_l}G\cdot G = \mathcal{Y}_{n_1\xi_1,\ldots,n_l\xi_l}(v=0,w=2\ln G=q) = \begin{cases} 0, \text{ when } n_1+\cdots+n_l \text{is odd}, \\ P_{n_1\xi_1,\ldots,n_l\xi_l}(q), \text{ when } n_1+\cdots+n_l \text{is even}. \end{cases} \tag{1.22}$$

The first handful can be clearly described as

$$P_{2\xi}(q) = q_{2\xi},\ P_{\xi,\tau} = q_{\xi\tau},\ P_{4\xi}(q) = q_{4\xi}+3q_{2\xi}^2 \tag{1.23}$$

In particular, the use of equations (1.22) and (1.23) will be beneficial in connecting nonlinear equations to their corresponding bilinear equations. This means that a nonlinear equation can be transformed into a linear equation if it can be expressed as a linear collection of P-polynomials.

Proposition 2: The binary Bell polynomials $\mathcal{Y}_{n_1\xi_1,\ldots,n_l\xi_l}(v,w)$ can be classified into two distinct types: P-polynomials and Y-polynomials.

$$\begin{aligned} (FG)^{-1}D_{\xi_1}^{n_1}\cdots D_{\xi_l}^{n_l}F\cdot G &= \mathcal{Y}_{n_1\xi_1,\ldots,n_l\xi_l}(v,w)|_{v=\ln F/G,w=\ln FG} \\ &= \mathcal{Y}_{n_1\xi_1,\ldots,n_l\xi_l}(v,v+q)|_{v=\ln F/G,q=2\ln G} \\ &= \sum_{r_1=0}^{n_1}\cdots\sum_{r_l=0}^{n_l}\binom{n_1}{r_1}\cdots\binom{n_l}{r_l}P_{r_1\xi_1,\ldots,r_l\xi_l}(q)Y_{(n_1-r_1)\xi_1,\ldots,(n_l-r_l)\xi_l}(v). \end{aligned} \tag{1.24}$$

The primary characteristic of the Bell polynomials

$$Y_{n_1\xi_1,\ldots,n_l\xi_l}(v)|_{v=\ln\phi} = \frac{\phi_{n_1\xi_1,\ldots,n_l\xi_l}}{\phi}, \tag{1.25}$$

The binary Bell polynomials $\mathcal{Y}_{n_1\xi_1,\ldots,n_l\xi_l}(v,w)$ can be expressed in a linear form through the application of the Hopf-Cole transformation, where $v=\ln\phi$ and $\phi = F/G$. By employing the equations (1.24) and (1.25), one can efficiently derive the corresponding Lax system associated with particular nonlinear equations.

1.5.3 Bilinear Bäcklund Transformation

Bilinear BT serve as a powerful technique for addressing nonlinear equations, especially when these equations can be represented in a bilinear format through the Hirota bilinear approach. The Bell-polynomial scheme, previously mentioned, is also relevant for managing BT in the context of NLEEs. Numerous examples found in the literature illustrate the utilization of this scheme for equations such as the Burgers-Hopf hierarchy, potential KdV, modified KdV, potential Sawada-Kotera, sine-Gordon, Boussinesq equations, and the Ablowitz-Kaup-Newell-Segur system [135, 138, 139, 140]. The implementation of the Bell-polynomial scheme consists of several essential steps.

(A) Employ the scale transformations to derive the Bell-polynomial representation of the original NLEE, ensuring that its invariance is duly considered.
(B) Additionally, devise an appropriate decomposition of the homogeneous constraint, or two-field condition, that exists between the primary field and a replica field. This will facilitate the development of a Bell-polynomial-type BT, which generally consists of a linear combination of Bell-polynomials along with their derivatives.
(C) Finally, implement the Hopf-Cole transformation to achieve a linearized form of the Bell-polynomial-type BT, leading to the corresponding Lax pair.
We shall now explore the process of constructing a BT through the application of binary Bell polynomials. To illustrate this, we will examine a nonlinear partial differential equation.

$$u_\tau = \mathcal{N}(u,\, u_\xi,\, u_{2\xi},\, u_{\tau\xi},\, u_{3\xi}, ...). \tag{1.26}$$

The study involves two independent variables, identified as ξ and τ. By utilizing a field transformation represented by $u = f(q)$, we seek to establish a link between equation (1.26) and a collection of P-polynomials.

$$H(q) = \sum_i c_i P_{k_i\xi, s_i\tau}(q) = 0. \tag{1.27}$$

The expression in question signifies a finite summation, where the variables k_i and s_i are integers, and c_i can be either constants or functions of ξ and τ. By implementing the transformation $q = 2\ln G$ on equation (1.27), we derive the following bilinear form (1.26).

$$\sum_i c_i D_\xi^{k_i} D_\tau^{s_i} G \cdot G = 0, \tag{1.28}$$

Let us consider that q and $\bar{q}$ represent two distinct solutions of the potential equation (1.28). To analyze these solutions independently, we will decouple the two-field condition,

$$E(v, w) = H(\bar{q} = w + v) - H(q = w - v). \tag{1.29}$$

The expression can be represented as a combination of binary Bell Y-polynomials along with their corresponding derivatives.

$$\sum_j c_{1j} Y_{n_j\xi, m_j\tau}(v, w) = 0, \quad \sum_k c_{2k} Y_{\bar{n}_k\xi, \bar{m}_k\tau}(v, w) = 0 \tag{1.30}$$

subject to suitable supplementary limitations. The application of the transformation $v = \ln G/F$, $w = \ln FG$ results in equation (1.30) producing the BT for equation (1.26).

$$\sum_j c_{1j} D_\xi^{n_j} D_\tau^{m_j} F \cdot G = 0, \quad \sum_k c_{2k} D_\xi^{\bar{n}_k} D_\tau^{\bar{m}_k} F \cdot G = 0. \tag{1.31}$$

1.5.4 Lax Pairs

In the field of integrable systems concerning nonlinear PDEs, numerous methodologies have been proposed. Among these methodologies, the Lax pair is particularly noteworthy. This pair comprises time-dependent matrices or operators that adhere to the Lax equation. The concept was introduced by Peter Lax, drawing inspiration from the inverse scattering method formulated by Gardner, Greene, Kruskal, and Miura in 1967. Through the application of the Lax equation, one can derive soliton equations from the Lax pair [141]. Lax examined two operators, denoted as L and M, where L is linked to the spectral problem, while M is responsible for the temporal evolution of the eigen functions.

$$L\nu = \lambda\nu, \quad \nu_t = M\nu. \tag{1.32}$$

The evaluation of the partial derivative of (1.32) in relation to time leads to,

$$L_t\nu + LM\nu = \lambda_t\nu + ML\nu. \tag{1.33}$$

Upon additional simplification, it can be inferred that,

$$(L_t + LM - ML)\nu = \lambda_t\nu. \tag{1.34}$$

For the purpose of deriving nontrivial eigenfunctions $\nu(x,t)$, we investigate the Lax Equation,

$$L_t + [L, M] = 0, \tag{1.35}$$

The expression $[L, M] := LM - ML$ holds true if and only if $\lambda_t = 0$. Lax's equation represents a nonlinear evolution equation, where L and M are defined appropriately. Lax pair can be identified through the use of binary Bell-polynomials. We will initiate our analysis by considering the nonlinear partial differential equation (1.26). Subsequently, by substituting $\nu = \ln\,\phi$ and $w = q + \ln\,\phi$ into equations (1.24) and (1.25), we will derive a connection between binary Bell-polynomials and ϕ.

$$\mathcal{Y}_{n\xi_1,m\xi_l}(\nu,w)|_{\nu=\ln\,\phi, w=q+\ln\,\phi} = \sum_{r=0}^{n}\sum_{s=0}^{m}\binom{n}{r}\binom{m}{s}P_{r\xi,s\tau}(q)Y_{(n-r)\xi,(m-s)\tau}(\nu = \ln\,\phi) \tag{1.36}$$

A select few among them are

$\mathcal{Y}_\tau(\nu) = \phi_\tau/\phi$, $\mathcal{Y}_\xi(\nu) = \phi_\xi/\phi$, $\mathcal{Y}_{2\xi}(\nu,w) = q_{2\xi} + \phi_{2\xi}/\phi$, $\mathcal{Y}_{3\xi}(\nu,w) = 3q_{2\xi}\phi_\xi/\phi + \phi_{3\xi}/\phi, \ldots$

The relationships previously mentioned facilitate the transformation of equations (1.30) into Lax pairs,

$$L_1(q)\phi = \sum_j c_{1j}L_{n_j,m_j}(q)\phi = 0, \quad L_2(q)\phi = \sum_j c_{2k}L_{\bar{n}_k,\bar{m}_k}(q)\phi = 0, \tag{1.37}$$

where

$L_{n_j,m_j}(q) = \sum_{r_{1j}=0}^{n_j}\sum_{r_{2j}=0}^{m_j}\binom{n_j}{r_{1j}}\binom{m_j}{r_{2j}}P_{r_{1j}\xi,r_{2j}\tau}(q)\partial_\xi^{n_j-r_{1j}}\partial_\tau^{m_j-r_{2j}}$

$L_{\bar{n}_k,\bar{m}_k}(q) = \sum_{\bar{r}_{1k}=0}^{\bar{n}_k}\sum_{\bar{r}_{2k}=0}^{\bar{m}_k}\binom{\bar{n}_k}{\bar{r}_{1k}}\binom{\bar{m}_k}{\bar{r}_{2k}}P_{\bar{r}_{1k}\xi,\bar{r}_{2k}\tau}(q)\partial_\xi^{\bar{n}_k-\bar{r}_{1k}}\partial_\tau^{\bar{m}_k-\bar{r}_{2k}}$

1.5.5 Infinite number of conservation laws

An integral aspect of integrability lies in the existence of an infinite number of conservation laws. Additionally, the presence of an infinite number of conservation laws (in involution, in the context of a Hamiltonian system) serves as another criterion for determining integrability. In the case of a scalar partial differential equation with two independent variables, namely x and t, and a single dependent variable u, a conservation law (which is local in nature) can be expressed in the following manner.

$$\partial_t G + \partial_x F = 0, \tag{1.38}$$

As a consequence of the equation, F, G, known as "the components of the conservation law", are functions of x, t, u and a finite number of partial derivatives of u. G is identified as the conserved density and F as the conserved flow. It is assumed that the function $u(x,t)$ and its derivatives with respect to x diminish rapidly as $|x| \to \infty$,

$$I[u(x,t)] = \int_{-\infty}^{\infty} G(x,t)dx \tag{1.39}$$

The constant of motion is obtained as a consequence. For instance, if u meets the requirements of the KdV equation.

$$u_t = \frac{1}{4}\, u_{xxx} + 3uu_x \tag{1.40}$$

Subsequently, we come across the initial three conservation laws,

$$\partial_t(u) + \partial_x(-\frac{1}{4}\, u_{xx} - \frac{3}{2}u^2) = 0 \tag{1.41}$$

$$\partial_t(u^2) + \partial_x(-\frac{1}{2}\, uu_{xx} + \frac{1}{4}\, u_x^2 - 2u^3) = 0 \tag{1.42}$$

$$\partial_t(4u^3 - u_x^2) + \partial_x(-9u^4 + \frac{1}{2}\, u_x u_{xxx} - \frac{1}{4}\, u_{xx}^2 - 3u^2 u_{xx} + 6uu_x^2) = 0 \tag{1.43}$$

Now we discuss how to find infinite conservation laws with the help of binary Bell-polynomials. Let us consider the nonlinear partial differential equation (1.26). To find infinite conservation laws first thing we have to do is to find binary Bäcklund transformation which already discussed in the above section. By introducing appropriate transformation, rewrite the $\mathcal{Y}$-polynomials Bäcklund transformation (1.30) as a Riccati-type equation and a divergence-type equation. In terms of the series expansion method, obtain the infinite conservation laws.

1.6 Analytical methods for solving nonlinear PDEs

The comprehension of physical phenomena linked to nonlinear evolution equations is fundamentally dependent on the discovery of solutions. This endeavor, however, is complex and necessitates the use of suitable techniques. In our research, we have utilized a variety of methods, including

the Discrimination method, the (G'/G)-expansion method, the F-function method, the simplified Hirota bilinear method (SHBM), the Hirota bilinear method, among others, to derive various types of solutions for distinct nonlinear evolution equations. For instance, the Discrimination method is employed to ascertain all potential single traveling wave solutions, such as soliton, shock, and elliptic function solutions, for the KP-mKP equation. The F-function method is applied to obtain elliptic function solutions for the KPb equation, while the Hirota bilinear method is used to discover multi-soliton solutions for the NKP equation. In the following subsections, we will present a brief overview of these methods, which have been thoroughly examined in the existing literature.

1.6.1 Description of the (G'/G)-expansion method

Wang et al. [38] proposed a direct methodology for identifying traveling wave solutions of nonlinear evolution equations. This technique allows for the derivation of solitary waves, shock waves, and various other related solutions by appropriately choosing parameter values. The core principle of this approach is that the traveling wave solutions can be expressed as a polynomial in the ratio (G'/G). In this study, we investigate a general nonlinear PDE characterized by the unknown variable $\phi = \phi(\xi, \eta, \tau)$.

$$\phi_\tau = \mathcal{N}(\phi, \phi_\xi, \phi_{\xi\xi}, \phi_{\tau\xi}, \phi_{\xi\xi\xi}, \phi_{\eta\eta} \ldots). \tag{1.44}$$

θ is introduced as a blend of ξ, η, and τ.

$$\phi(\xi, \eta, \tau) = U(\theta), \quad \theta = l\xi + m\eta - V\tau, \tag{1.45}$$

The wave's velocity is represented by V, and in this context, equation (1.44) is converted into an ODE as,

$$\mathcal{Q}(U, -VU', U', l^2U'', l^3U''', \cdots) = 0, \tag{1.46}$$

The fundamental procedures of the approach are concisely outlined below as:

Step 1. The application of the wave transformation equation (1.45) to the variables ξ, η, and τ in equation (1.44) leads us to the discovery of the ordinary differential equation (1.46).
Step 2. The solution $U(\theta)$ of Eq. (1.46) is expressed as

$$U(\theta) = \sum_{j=0}^{N} P_i \left(\frac{G'(\theta)}{G(\theta)} \right)^j. \tag{1.47}$$

Now, it is necessary to determine the values of the constants $P_j, (j = 0 \cdots N)$, where $P_N \neq 0$, and find the positive integer N. Furthermore, the function $G(\theta)$ is governed by the auxiliary linear ODE,

$$G''(\theta) + \lambda G'(\theta) + \mu G(\theta) = 0. \tag{1.48}$$

The real constants λ and μ are assigned specific numerical values, and their interpretations will be explained subsequently.

Step 3. To compute N, one must balance the derivative of the highest order with the highest order nonlinear terms in Equation (1.46).

Step 4. Upon substituting Equation (1.47) into Equation (1.46) and utilizing the relation in Equation (1.48), one can derive a polynomial of (G'/G). By collecting all the coefficients of the same power terms in that polynomial and setting them to zero, a set of algebraic equations for P_j, λ, μ, V, and l can be obtained. These equations can then be solved using computational aids such as Maple, Matlab, etc., thereby determining the unknown constants. Subsequently, by substituting the values of these constants into Equation (1.47), the solutions of Equation (1.46) can be derived.

1.6.2 Description of the F-function method

Yomba [142] introduced an innovative technique referred to as the indirect F-function method, aimed at identifying Jacobi elliptic function solutions for specific NLEEs. By employing this F-function method, one can effectively obtained a wide array of wave solutions in a thorough manner. This research centers on a general nonlinear PDE with the unknown variable represented as $\phi = \phi(\xi, \eta, \tau)$.

$$\phi_\tau = \mathcal{N}(\phi, \phi_\xi, \phi_\tau, \phi_{\xi\xi}, \phi_{\tau\xi}, \phi_{\xi\xi\xi}, \phi_{\eta\eta}...). \tag{1.49}$$

We introduce ζ combining ξ, η and τ such that

$$\phi(\xi, \eta, \tau) = U(\zeta), \quad \zeta = l\xi + m\eta - V\tau, \tag{1.50}$$

Here, the variable V indicates the velocity of the wave, while equation (1.49) is adapted into an ODE as shown below,

$$Q(U, lU', -VU', l^2U'', -VlU', \cdots) = 0, \tag{1.51}$$

The essential phases of the process are briefly summarized as follows:

Step 1. The derivation of the ODE indicated by (1.51) is achieved through the application of the wave transformation equation (1.50) to the variables ξ, η, and τ present in equation (1.49).

Step 2. The formulation of the solution $U(\zeta)$ for Eq. (1.51) is represented as,

$$U(\zeta) = \lambda(\tau)F^s(\zeta), \tag{1.52}$$

In this scenario, λ is designated as a parameter, and the positive integer s is to be established. Ultimately, the function $F(\zeta)$ is governed by the ODE,

$$F'^2(\zeta) = PF^4(\zeta) + QF^2(\zeta) + R, \tag{1.53}$$

P, Q, and R are real constants that play an important role.

Step 3. Identify the value of s by balancing the highest order derivative against the highest order nonlinear terms found in Equation (1.51).

Step 4. By substituting Equation (1.52) into Equation (1.51) and utilizing the relationship established in Equation (1.53), one can formulate a polynomial in terms of F. By aggregating the coefficients associated with like power terms and equating them to zero, a system of algebraic equations involving λ, V, and l is generated. These equations can be solved using computational tools such as Maple or Matlab, resulting in expressions for λ and V in terms of P, Q, and R. Subsequently, the constants can be reinserted into Equation (1.52) to derive the solutions for Equation (1.51).

1.6.3 Description of Discrimination method

Liu [143] proposed a methodology for identifying all possible exact travelling wave solutions for a NLEE. The fundamental principle of this approach involves expressing the NLEE in an integral format, which is then solved to derive the exact travelling wave solutions [144, 145]. In this context, we are investigating a general nonlinear PDE in which the variable $\nu = \nu(x, y, \tau)$ remains unknown.

$$\mathcal{N}(\nu, \nu_\tau, \nu_x, \nu_{xx}, \nu_{\tau x}, \nu_{xxx}, \nu_{yy} \ldots) = 0. \tag{1.54}$$

The new variable ζ is introduced through the combination of the original variables x, y, and τ,

$$\nu(x, y, \tau) = \phi(\zeta), \quad \zeta = k_1 x + k_2 y - c\tau, \tag{1.55}$$

Let k_1 and k_2 represent constants, with c indicating the speed of the traveling wave. Consequently, the equation (1.54) is restructured into an ODE.

$$\mathcal{M}(\phi, -c\phi', k_1\phi', k_1^2\phi'', -ck_1\phi'', \cdots) = 0, \tag{1.56}$$

Here, $\mathcal{M}$ represents a polynomial in ϕ along with its derivatives, while the symbol (') indicates differentiation with respect to ζ. By integrating equation (1.56), one can derive an expression,

$$(\phi')^2 = G(\phi), \tag{1.57}$$

where $G(\phi)$ might be any kind of function, rational or irrational, including polynomials. The form in which the integral of (1.57) can be represented is

$$\pm(\zeta - \zeta_0) = \int \frac{d\phi}{\sqrt{G(\phi)}}. \tag{1.58}$$

The above described technique yields several significant results, one of which is the identification of ζ_0 as an integral constant.

1.6.4 Basic idea of method of undetermined coefficients

The undetermined coefficients method presents an uncomplicated means of finding the solution of ODE when specific criteria are fulfilled. The following discussion focuses on a general nonlinear PDE, where the unknown function is expressed as $\phi = \phi(\xi, \eta, \tau)$ where,

$$\phi_\tau = \mathcal{N}(\phi, \phi_\xi, \phi_{\xi\xi}, \phi_{\tau\xi}, \phi_{\xi\xi\xi}, \phi_{\eta\eta}...). \tag{1.59}$$

By combining ξ, η, and τ, we define θ as,

$$\phi(\xi, \tau) = U(\theta), \quad \theta = l\xi - V\tau. \tag{1.60}$$

The wave's velocity is denoted by V, and the equation (1.59) is reformulated into an ODE,

$$Q(U, -VU', U', l^2U'', l^3U''', \cdots) = 0. \tag{1.61}$$

The key procedures of the technique are outlined concisely in the following section.

Step 1. The ODE presented in (1.61) can be derived by utilizing the wave transformation outlined in (1.60), incorporating the variables ξ, η, and τ as defined in equation (1.59).
Step 2. The solution $U(\theta)$ of Eq. (1.61) some time indicates the expression for the bright soliton as,

$$U(\theta) = \lambda\ \mathrm{sech}^m(\theta). \tag{1.62}$$

In addition, pertaining to the dark soliton, it is significant to mention that

$$U(\theta) = \lambda\ \tanh^m(\theta). \tag{1.63}$$

It is necessary to ascertain the values of the constants λ (with the condition that $\lambda \neq 0$) and m (where m belongs to the set of positive integers, denoted as $\mathcal{J}^+$).
Step 3. By setting the highest order derivatives equal to the nonlinear terms in Eq.(1.61), it is possible to determine the value of m.
Step 4. By substituting Eq.(1.62), which may relate to the dark soliton described in Eq.(1.63), into Eq.(1.61), one can gather all terms that share the same power of $\mathrm{sech}(\theta)$, $\tanh(\theta)$, and $\mathrm{sech}(\theta)\sinh(\theta)$. This process enables us to set each coefficient to zero, leading to the formulation of a system of algebraic equations.
Step 5. A precise solution for equation (1.59) can be attained by inserting the values of λ and V into equation (1.62), which is determined through the resolution of this system of equations.

1.6.5 Basic description of simplified Hirota bilinear method

Awawdeh et al. [146] introduced a streamlined version of the Hirota bilinear method by integrating Hirota's direct approach with the simplified technique developed by Hereman et al. [147]. This integration demonstrated that soliton solutions can be represented as polynomials of exponential functions. The SHBM can be effectively employed to derive solutions for evolution equations, as it does not necessitate the bilinear form of the equation. We examine a general nonlinear PDE with the unknown function $\phi = \phi(\xi, \eta, \tau)$.

$$\phi_\tau = \mathcal{N}(\phi, \phi_\xi, \phi_{\xi\xi}, \phi_{\tau\xi}, \phi_{\xi\xi\xi}, \phi_{\eta\eta}...). \tag{1.64}$$

We define θ by integrating ξ, η, and τ in a way that

$$\phi(\xi, \eta, \tau) = e^\theta, \quad \theta = l\xi + m\eta - V\tau, \tag{1.65}$$

Step 1. By utilizing the wave transformation equation (1.65) with the variables ξ, η, and τ in the linear terms of equation (1.64), we derive the dispersion relation that yields the value of V.
Step 2. The solution $\phi(\xi, \eta, \tau)$ of Eq. (1.64) is expressed as

$$\phi(\xi, \eta, \tau) = R\ (\ln\ f)_\xi, \tag{1.66}$$

It is necessary to ascertain the constant R. In the end, the function $f(\xi, \eta, \tau)$ is defined accordingly,

$$f(\xi, \eta, \tau) = 1 + e^\theta, \tag{1.67}$$

Step 3. By incorporating equations (1.66) and (1.67) into equation (1.64), it is possible to derive a polynomial involving e^θ. Moreover, by organizing all coefficients of similar power terms from this polynomial and equating them to zero, a collection of algebraic equations can be formulated.
Step 4. The process of solving the algebraic equations with the assistance of computational tools, including Maple and Matlab, allows for the determination of the unknown constant R. Once R is established, it is inserted into Equation (1.66) to extract the solutions for Equation (1.64).

1.6.6 Basic description of Hirota Bilinear method

The bilinear method, which was developed by Hirota several decades ago, has been instrumental in the exploration of integrable nonlinear systems [27]. This formalism is exceptionally effective for deriving not only multi-soliton solutions but also various types of special solutions for numerous NLEEs. Additionally, it has been employed to examine the algebraic structure of integrable

evolution equations and to derive extensions of these systems. The essence of the bilinear method is centered on identifying an appropriate transformation of the dependent variable. By utilizing this transformation along with the Hirota D-operator, one can derive bilinear representations of the nonlinear equation [148, 149]. Following the establishment of these bilinear forms, the subsequent task is to determine the solution. Let us consider the bilinear form as

$$F_1(D)f \cdot f = 0, \tag{1.68}$$

or

$$F_2(D)f \cdot g = 0, \tag{1.69}$$

In certain instances, the equation may encompass two distinct types, and this is entirely contingent upon the transformation of the dependent variable. At this point, we will apply the standard perturbation method, expanding f into a formal power series with respect to a small parameter, which yields the following expression.

$$f = 1 + \epsilon f_1 + \epsilon^2 f_2 + \epsilon^3 f_3 + \cdots, \tag{1.70}$$

By substituting these expressions into (1.68) and organizing the terms according to each order of the exponent of the expansion parameter ϵ, one may derive a system of equations.

$$\epsilon^0 : F_1(D)(1 \cdot 1) = 0, \tag{1.71}$$

$$\epsilon^1 : F_1(D)(1 \cdot f_1 + f_1 \cdot 1) = 0, \tag{1.72}$$

$$\epsilon^2 : F_1(D)(1 \cdot f_2 + f_1 \cdot f_1 + f_2 \cdot 1) = 0, \tag{1.73}$$

For deriving single-soliton solution one may consider $f = 1 + \epsilon f_1 = 1 + exp(\theta)$, where $\theta = px + qy + w\tau + .. + \theta^0$ and the perturbation coefficient ϵ absorbed into the constant θ^0 in the exponent. On the other hand for exploring two-soliton solution we take $f = 1 + f_1 + f_2 = 1 + exp(\theta_1) + exp(\theta_2) + A_{12} exp(\theta_1) \cdot exp(\theta_2)$. Finally different types of solitons can be acquired from these expression.

1.7 Dynamical System

Dynamics is primarily the study of the time-evolutionary process and the corresponding system of equations is referred to as a dynamical system [150]. In general, within an n-dimensional space $\mathbb{R}^n$, the nature of this evolutionary process is described by a collection of n first-order differential equations, referred to as an n-dimensional dynamical system. These evolutionary processes may exhibit various properties, including determinacy or non-determinacy, finite or infinite dimensionality, and differentiability. A process is classified as deterministic if its entire future and past can

be uniquely determined by its current state; otherwise, it is termed non-deterministic. Evolutionary processes can be categorized into continuous and discrete-time processes. Continuous-time processes are represented through differential equations, while maps are utilized for discrete-time processes. Let the dynamics of a continuous-time framework be represented by the vector $x = x(t)$ The system can be mathematically formulated as

$$\frac{dx}{dt} = \dot{x} = f(x, t) \tag{1.74}$$

In this context, $f(x, t)$ is a sufficiently smooth function which is nonlinear in general and time is represented by the variable parameter t. The interval of time may be finite, semi-finite, or infinite.

In contrast, the discrete framework is associated with a discrete mapping defined solely at equidistant points of time such that starting from x_0, one can derive x_1, which subsequently maps to x_2 and so forth. This can be expressed as

$$x_{n+1} = f(x_n) = f(f(x_{n-1})) = ...$$

It can also be represented as

$$x_{n+1} = f(x_n) = f^2(x_{n-1}) = ...$$

The sequence of iterations can be constructed as

$$x_0, f(x_0), f(f(x_0)), f(f(f(x_0)))...$$

This sequence may be either finite or infinite, and it will be intriguing to observe the behaviour of this sequence after multiple iterations.

A system is classified as autonomous if the right-hand side of (1.74) is independent of time explicitly. Consequently, the trajectories of such system remain unaffected by time. In contrast, a system is identified as nonautonomous if the right-hand side of (1.74) exhibits a clear dependence on time. An n-dimensional nonautonomous system can be transformed into an autonomous one by introducing an additional dependent variable, denoted as x_{n+1}, where $x_{n+1} = t$. In general, finding a solution to the system (1.74) becomes challenging or sometimes unfeasible when $f(x, t)$ is nonlinear, except in a few simplified instances.

The second-order differential equation $\ddot{x} + a_1\dot{x} + a_2x = 0$, with $a_1, a_2 > 0$, is an example of an autonomous system. This equation characterizes a damped linear harmonic oscillator, with the parameters a_1 and a_2 representing the strength of the damping and the linear restoring forces, respectively.

1.7.1 Flows

Flows in $\mathbb{R}$: Consider a one-dimensional autonomous model represented by the equation $\dot{x} = f(x)$, $x \in \mathbb{R}$. One can visualize a fluid, referred to as phase fluid is moving along the real line,

known as the phase line. In this context, $f(x)$ represents the fluid's velocity. The direction of flow is determined by the sign of $f(x)$; specifically, the flow is directed to the right if $f(x) > 0$ and to the left if $f(x) < 0$.

To derive the solution for $\dot{x} = f(x)$, a fictional particle, termed a phase point, is positioned at an arbitrary initial location x_0 and then observe the particle's movement with the flow along the phase line.

As time t progresses, the phase point advances along the phase line according to a specific function $\psi(t, x_0)$.

This function is called the trajectory associated with the initial position x_0, and the collection $\psi(t, x_0) : t \in \mathbb{R}$ is referred to as the orbit of $x_0 \in \mathbb{R}$. The phase portrait consists of all qualitative trajectories of the system.

Flows in $\mathbb{R}^2$: Consider a two-dimensional autonomous system described by the equations $\dot{x} = f_1(x, y)$, $\dot{y} = f_2(x, y)$, $(x, y) \in \mathbb{R}^2$. This system can be visualized as a fluid flowing within the xy-plane, which is referred to as the phase plane. The states are expressed parametrically as $x = x(t), y = y(t)$.

A curve that traces the evolution of states through an initial point $A(x(t_0), y(t_0))$ is known as a phase path. The orbit corresponding to $x_0 \in \mathbb{R}2$is represented by the collection $\psi(t, x_0) : t \in \mathbb{R}$.

Although there are infinitely many trajectories, depicting a few of them under different initial circumstances can elucidate the qualitative behaviour of the system. The phase portrait illustrates how the qualitative behaviour of the system changes as x and y change over time.

An orbit is classified as periodic if, for all t and for some $\mu > 0$, the condition $x(t+\mu) = x(t)$ holds.

The prime period of an orbit is defined as the smallest positive integer μ that satisfies the condition $x(t + \mu) = x(t)$.

Flows in $\mathbb{R}^n$: Consider an autonomous system in n-dimension, described by

$$\dot{x_1} = f_1(x_1, x_2, ..., x_n)$$

$$\dot{x_2} = f_2(x_1, x_2, ..., x_n)$$

$$...$$

$$\dot{x_n} = f_n(x_1, x_2, ..., x_n)$$

This can be formulated as $\dot{x} = f(x)$ where $x = (x_1, x_2, \ldots, x_n)$ and $f = (f_1, f_2, \ldots, f_n)$. The solution corresponding to the initial condition $x(t_0) = x_0$ can be considered as a continuous curve, referred to as the phase curve within the space $\mathbb{R}^n$. This space is identified as the phase space. Solutions arising from various initial circumstances illustrate a collection of phase curves in the space $\mathbb{R}^n$, which is termed the phase portrait of the system. The vector field $f(x)$ is tangent everywhere to these curves and their orientation is governed by the direction of the tangent vector of $f(x)$.

1.7.2 Fixed Points and their Stability

The concept of a fixed point is crucial for understanding the behaviour of a dynamical system. A fixed point refers to a constant or unchanging solution of the system, often described as an equilibrium solution of the system. In the context of a continuous system, fixed points can be obtained by setting $\dot{x} = 0 \implies f(x) = 0$ a time-dependent framework, fixed points can be defined for a specific time interval. Fixed points may also be referred to as critical points or equilibrium points. The number of fixed points in a flow along a phase line can be either finite or infinite, and it is possible for a flow to have no fixed points at all. For instance, the equations $\dot{x} = 3, \dot{x} = x - 1$, and $\dot{x} = \cos x$ illustrate flows with no fixed points, one fixed point, and infinitely many fixed points, respectively.

To illustrate it further, let us consider following examples:

(a) $\dot{x} = x^3 + x^2 - 6x$

The fixed points of this system are $-3, 0$ and 2. It is observed that

$$\dot{x} < 0 \quad \text{if } x < -3,$$

$$\dot{x} > 0 \quad \text{if } -3 < x < 0,$$

$$\dot{x} < 0 \quad \text{if } 0 < x < 2,$$

$$\dot{x} > 0 \quad \text{if } x > 2.$$

Figure 1.1(a) illustrates the flow of the system graphically. The direction of flow is to the right when $\dot{x} > 0$, and to the left when $\dot{x} < 0$. It is noticed that the fixed points $x = -3$ and $x = 2$ function as sources, while the fixed point $x = 0$ acts as a sink. Consequently, the fixed points -3 and 2 are classified as unstable, while the fixed point 0 is deemed stable.

(b) $\dot{x} = x^2 - 5x + 4$

The fixed points for this system are 1 and 4. It is observed that

$$\dot{x} > 0 \quad \text{if } x < 1,$$

$$\dot{x} < 0 \quad \text{if } 1 < x < 4,$$

$$\dot{x} > 0 \quad \text{if } x > 4.$$

Figure 1.1(b) illustrates the flow of the system graphically. The flow is directed to the right when $\dot{x} > 0$, which occurs when $x^2 - 5x + 4 > 0$, and to the left when $\dot{x} < 0$, which is true when

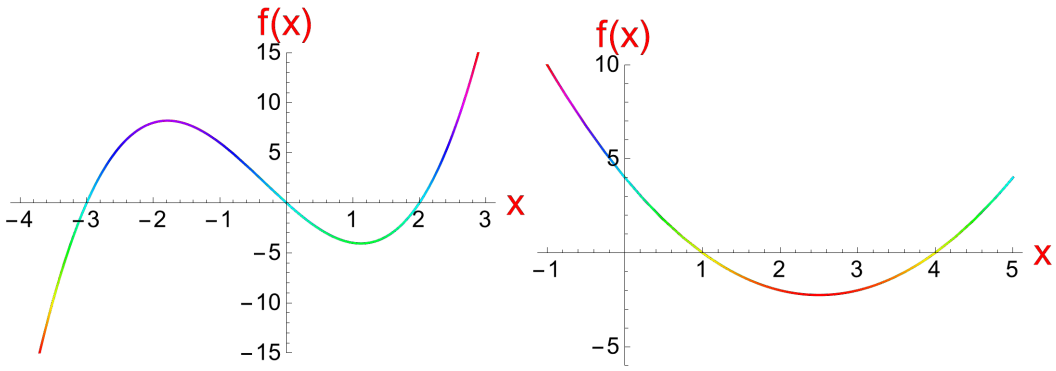

(a) (b)

Figure 1.1: (a) Graphical display of $f(x) = x^3 + x^2 - 6x$. (b) Graphical display of $f(x) = x^2 - 5x + 4$.

$x^2 - 5x + 4 < 0$. It is noticed that fixed point $x = 1$ acts as a sink, while fixed point $x = 4$ functions as a source. Consequently, 1 is classified as a stable fixed point, while 4 is identified as an unstable fixed point.

1.7.3 Birfurcations

A structural alteration in the orbit of a system is referred to as bifurcation [150, 151]. The first observation of this phenomenon was made by Henri Poincaré, a renowned French mathematician. The study of bifurcation focuses on how the orbit's structure is affected by changes in parameters. The location at which bifurcation occurs is referred to as the bifurcation point. At this point, there may be substantial changes in the characteristics of equilibrium points and the trajectories. Typically, the nature of sources and sinks is altered during bifurcation. The bifurcation diagram, which graphically represents various parameter values in relation to equilibrium points, is an essential tool for understanding the dynamics of a system. The dynamics of a continuous system represented by the equation $\dot{x} = f(x, \lambda)$are governed by the parameter $\lambda \in \mathbb{R}$. It is frequently observed that when λ surpasses a critical value, various characteristics of the system, such as stability, equilibrium points, and periodicity, may change. Furthermore, this can lead to the formation of a totally new orbit. Overall, bifurcation signifies a system with an unstable configuration. Codimension-1 bifurcations involve a single parameter, whereas codimension-2 bifurcations are associated with two parameters. These bifurcations provide insights into many significant dynamics within the framework. The implications of bifurcation are significant in both physical and biological sciences. Bifurcations and their related theories are vital for the analysis of nonlinear dynamical systems.

1.7.4 Limit Cycles

A limit cycle refers to an isolated closed trajectory, indicating that the trajectories in its vicinity are open. These nearby trajectories move either towards or away from the closed trajectory spirally. Limit cycles represent a nonlinear phenomenon. They cannot occur within a linear system. Limit cycles can be observed in various physical systems, including satellite orbits, predator-prey dynamics, cardiac rhythms, and self-excited vibrations in bridges. Limit cycles can be classified into three types: stable, unstable, and half-stable. A limit cycle is classified as stable if all adjacent trajectories converge towards the closed path. A limit cycle is classified as unstable when all trajectories in its vicinity move away from the closed path. In the case of a half-stable limit cycle, trajectories move towards the closed path from one side and away from the other side. Among these three classifications of limit cycles, the stable limit cycle holds considerable scientific importance. In this circumstance, systems oscillate without the influence of any external periodic forces. Numerous examples exist, including the beating of the heart and the daily fluctuations in human body temperature.

1.7.5 Poincaré Map

Achieving an analytical solution for nonlinear continuous systems is often challenging, and at times, it may be deemed impossible. Furthermore, the analysis of the complex dynamical behaviour of such systems is extremely difficult. Therefore, rather than focusing on continuous frameworks, we can shift our attention to their discrete counterparts, where the flow paths are depicted by a series of points in phase space. This method, developed by Henri Poincaré, serves as a connection between continuous systems and their discrete equivalents. At times, chaotic motion can be more readily analysed using the discrete approach. This process is known as the Poincaré map.

1.8 Study of plasma

Plasma can be characterized as a quasineutral assemblage of charged and neutral particles that demonstrates collective behavior. The word "plasma" has its roots in the Greek language, initially coined by American physicists Langmuir and Tonks in 1929. Often regarded as the fourth state of matter, plasma is considered part of the continuum that includes solid, liquid, gas, and plasma. In reality, when specific conditions are met, a collection of charged and neutral particles exhibits characteristics typical of plasma. Plasma is viewed as the most fundamental state of matter. Over 99% of the matter in the universe is estimated to exist in the plasma state, while we reside in the 1% of the universe that typically does not feature plasma. Stellar interiors, gaseous nebulae,

and a significant portion of interstellar space are all filled with plasma. In our sun, plasma is evident through solar flares and sunspots. Closer to Earth, plasmas can be observed in the form of the solar wind and the Van Allen radiation belts. Natural occurrences of plasma include phenomena such as lightning bolts and the Aurora Borealis, while artificially generated plasma can be found in fluorescent tubes and various industrial applications.

1.8.1 Conditions for an ionized gas to be a plasma

An ionized gas needs to meet following conditions to become a plasma.

1. The linear dimension L must be much larger than the Debye length λ_d. In other words, $L >> \lambda_d$. Charge neutrality at macroscopic level is confirmed by this condition.

2. The particle number n_d in Debye Sphere must be much larger than the unity. i.e., $n_d >> 1$. Here $n_d = \frac{4}{3}\pi\lambda_d^3 n$, n is the plasma density. Now $n_d >> 1 \Rightarrow \lambda_d^3 n >> 1$. If this condition is not met, the conception of Debye shielding will not be valid statistically. Again $\lambda_d^3 n >> 1 \Rightarrow n^{-\frac{1}{3}} << \lambda_d$. This indicates that the interparticle distance must be significantly smaller than λ_d.

3. Third requirement is related to the collision. Plasma particles and neutral atoms collide often in a weakly ionized gas. If τ represents the average time between the collisions and ω_p represents the plasma frequency, then $\omega_p\tau > 1$ is necessary for an ionized gas to transition to plasma.

1.8.2 Plasma Oscillation

A key feature of plasma is its tendency to uphold electrical charge neutrality on a macroscopic level under equilibrium conditions. Consequently, if electrons are displaced from a homogeneous ion background within the plasma, an electric field will arise, attempting to return the displaced electrons to their original positions. However, due to their inertia, the electrons will exceed their initial positions, creating a restoring electric field that acts in the opposite direction. This results in the oscillation of electrons about their equilibrium position. The frequency of this oscillation is referred to as the plasma frequency. Such oscillation typically occurs at a very high frequency, while ions, having greater mass, are unable to keep pace with this high-frequency motion and can be regarded as stationary.

1.8.3 Fluid equations for a simple plasma system

A plasma is typically composed of a large number of particles. It is practically impossible to follow the complex trajectories of each of these particles and predict the behaviour of the plasma. Thankfully, the majority of plasma phenomena observed in real experiments can be elucidate by a basic model known as the fluid model. Here, only the motion of the fluid particles, similar to fluid mechanics is taken into account, disregarding the identity of any individual particle. In this

conjecture, it is assumed that each species of plasma may preserve a local equilibrium. Thereafter, each species can be conceptualized as a fluid characterized by local density, temperature, and macroscopic velocity. To understand how these quantities evolve over time, fluid equations, which resemble hydrodynamic equations but are generally more intricate, are utilized.
Let us consider a simple plasma having only ions and electrons. The fluid equations of plasma are the following:
Continuity equation

$$\frac{\partial n_j}{\partial t} + \nabla \cdot (n_j \mathbf{u_j}) = 0 \tag{1.75}$$

Momentum equation:

$$m_j n_j \left[\frac{\partial \mathbf{u_j}}{\partial t} + (\mathbf{u_j} \cdot \nabla)\,\mathbf{u_j}\right] = q_j n_j \left(\mathbf{E} + \mathbf{u_j} \times \mathbf{B}\right) - \nabla p_j \tag{1.76}$$

Energy equation:

$$p_j = C_j n_j^{\gamma_j} \tag{1.77}$$

where, $m_j, \mathbf{u_j}, n_j, q_j$ and p_j correspond to the mass, velocity, number density, charge, and pressure of the $j-$th species, with $j = i$ indicating ions and $j = e$ indicating electrons. The constant C_j is included, and γ_j signifies the ratio of specific heat at constant pressure to that at constant volume. The magnetic and electric fields are represented by $\mathbf{B}$ and $\mathbf{E}$, respectively. The motion of charged plasma particles leads to the generation of current density ($\mathbf{J}$) and charge density (ρ). These are described by the following Maxwell's equations:

$$\varepsilon_0 \nabla \cdot \mathbf{E} = \rho \tag{1.78}$$

$$\nabla \times \mathbf{E} = -\frac{\partial \mathbf{B}}{\partial t} \tag{1.79}$$

$$\nabla \cdot \mathbf{B} = 0 \tag{1.80}$$

$$\nabla \times \mathbf{B} = \mu_0 \left(\mathbf{J} + \varepsilon_0 \frac{\partial \mathbf{E}}{\partial t}\right) \tag{1.81}$$

Here $\rho = n_i q_i + n_e q_e$, $\mathbf{J} = n_i q_i \mathbf{u_i} + n_e q_e \mathbf{u_e}$ and ε_0, μ_0 are constant.

1.8.4 Kinetic Approach

A collection of numerous interacting charged particles is referred to as plasma. The fluid hypothesis provides a simple elucidation of plasma behaviour. Although it sufficiently describes a majority of plasma phenomena, there are occasions when it proves inadequate. A statistical kinetic approach can provide a more accurate representation of plasma. This approach requires the introduction of a distribution function. The macroscopic plasma variables necessary for a thorough

description of plasma behaviour can be systematically derived from the understanding of the distribution function. The distribution function holds all the physically significant information regarding plasma. The PDE that governs this function is referred to as the Boltzmann equation, which plays a vital role in the kinetic theory of plasma.

The distribution function $f(\mathbf{r}, \mathbf{v}, t)$ is formulated in such a way that the number of particles within the volume element $d^3r d^3v$, centered at the coordinates $(\mathbf{r}, \mathbf{v})$ at time t, is expressed as follows:

$$dn(\mathbf{r}, \mathbf{v}, t) = f(\mathbf{r}, \mathbf{v}, t)\, d^3r d^3v \tag{1.82}$$

where $d^3r d^3v = dx dy dz dv_x dv_y dv_z$.

This distribution function provides a thorough elucidation of the system from a statistical perspective. To analyse the system from a statistical perspective, it is necessary to have knowledge of the distribution function associated with the system under consideration. The Boltzmann equation describes the relationship of the distribution function $f(\mathbf{r}, \mathbf{v}, t)$ with the variables $\mathbf{r}, \mathbf{v}$ and t. In the absence of collisions within the system, the Boltzmann equation is expressed as

$$\frac{\partial f}{\partial t} + \mathbf{v} \cdot \nabla f + \mathbf{a} \cdot \nabla_v f = 0 \tag{1.83}$$

where $\mathbf{a} = \frac{\mathbf{F}}{m}$, with $\mathbf{F}$ denoting the force and m representing the mass of the particle. When collisions are present within the system, the Boltzmann equation is modified to

$$\frac{\partial f}{\partial t} + \mathbf{v} \cdot \nabla f + \mathbf{a} \cdot \nabla_v f = \left(\frac{\partial f}{\partial t}\right)_c \tag{1.84}$$

where $\left(\frac{\partial f}{\partial t}\right)_c$ signifies the collision term. In the case of collisions involving neutral particles, the collision term can be estimated as $\left(\frac{\partial f}{\partial t}\right)_c = \frac{f_n - f}{T_c}$ where f_n and T_c correspond to the distribution function of neutral particles and the constant collision time, respectively. Ignoring the collision term and considering the force $\mathbf{F}$ to be solely electromagnetic, equation (2) can be expressed as

$$\frac{\partial f}{\partial t} + \mathbf{v} \cdot \nabla f + \frac{q}{m}(\mathbf{E} + \mathbf{v} \times \mathbf{B}) \cdot \nabla_v f = 0 \tag{1.85}$$

This equation is referred to as the Vlasov equation. The Vlasov equation describes the evolution of the distribution function over time in phase space. From the distribution function $f(\mathbf{r}, \mathbf{v}, t)$, one can derive macroscopic variables such as number density $n(\mathbf{r}, t)$ and average velocity $\mathbf{u}(\mathbf{r}, t)$, by taking the appropriate velocity moments of $f(\mathbf{r}, \mathbf{v}, t)$. The number density $n(\mathbf{r}, t)$ is determined by integrating $f(\mathbf{r}, \mathbf{v}, t)$ over the velocity space. Thus

$$n(\mathbf{r}, t) = \int_v f d^3v. \tag{1.86}$$

The average velocity $\mathbf{u}(\mathbf{r}, t)$ is determined by taking first velocity moment of distribution function. Thus

$$\mathbf{u}(\mathbf{r}, t) = \frac{1}{n} \int_v \mathbf{v} f d^3v. \tag{1.87}$$

The continuity equation is established by taking the zeroth velocity moment of the Boltzmann equation, which involves integrating the Boltzmann equation over the velocity space. The continuity equation is represented as

$$\frac{\partial n}{\partial t} + \nabla \cdot (n\mathbf{u}) = 0 \tag{1.88}$$

The equation of motion is formulated by taking the first velocity moment of the Boltzmann equation. This involves multiplying the Boltzmann equation by $m\mathbf{v}$ and integrating it over the velocity space. The equation of motion is expressed as

$$mn\left(\frac{\partial}{\partial t} + \mathbf{u} \cdot \nabla\right)\mathbf{u} = qn\left(\mathbf{E} + \mathbf{u} \times \mathbf{B}\right) - \nabla \cdot \mathbf{P} + \mathbf{P_c} \tag{1.89}$$

In this equation, $\mathbf{P}$ indicates the pressure tensor, while $\mathbf{P_c}$ signifies the change in momentum due to collision.

In instances where effect of viscosity is negligible, one can omit all terms of the pressure tensor except for the diagonal ones. Furthermore, when the velocity distribution remains unchanged regarding direction, the pressure tensor $\mathbf{P}$ will have identical diagonal elements, which can be represented as a scalar pressure (p). Consequently, ∇p can substitute $\nabla \cdot \mathbf{P}$. If we also ignore collisions, the equation (3) simplifies to

$$mn\left(\frac{\partial}{\partial t} + \mathbf{u} \cdot \nabla\right)\mathbf{u} = qn\left(\mathbf{E} + \mathbf{u} \times \mathbf{B}\right) - \nabla p \tag{1.90}$$

The energy equation is derived by examining the second velocity moment of the Boltzmann equation. This involves multiplying the Boltzmann equation by $\frac{1}{2}mv^2$ and integrating it over the velocity space. If we ignore the influences of thermal conductivity, viscosity, and collisions, the energy equation simplifies to the adiabatic equation of state, expressed as

$$p = C\rho_m^{\gamma}$$

where C is a constant, ρ_m represents mass density, and γ is defined as $\frac{C_p}{C_v}$ (with C_p being the specific heat at constant pressure and C_v the specific heat at constant volume).

1.8.5 Dusty Plasma

Dust particles coexist with plasma frequently. These particles are positively or negatively charged, depending on the plasma environments; they are not neutral. The combination of ions, electrons, neutrals, and charged dust particles produces a “dusty plasma”. A dusty plasma is an electron-ion plasma that also includes charged particles that are micron or submicron in size. The complexity of the system increases even further with the addition of these particles. For this reason, ”complex plasma” is another term for dusty plasma. Dust grains vary in size from nanometers to

millimeters and are $10^6 - 10^8$ times heavier than protons. Dust grains will differ in size and shape unless they are artificial. The term "dust in a plasma" or "a dusty plasma" can be used to describe plasma that contains dust grains or particles, depending on how the average inter-grain distance (a), plasma Debye radius (λ_d), and dust grain radius (r_d) are arranged. The plasma is referred to as "dust in a plasma" if $r_d << \lambda_d < a$. On the other hand, if $r_d << a < \lambda_d$, the plasma is referred to as "a dusty plasma." It is important to consider the local plasma inhomogeneities when considering a plasma with isolated dust grains ($a >> \lambda_d$). On the other hand, under the opposite condition ($a << \lambda_d$), dust particles should be viewed as massive charged particles similar to multiple charged positive or negative ions. The presence of charged dust grains not only modifies already-existing low-frequency waves (like IAWs), but also causes the emergence of new low-frequency dust-related waves (like DAWs, and dust ion acoustic waves (DIAWs)).

It is important to note that nonlinear evolution model can be derived from the basic governing equation of plasma environment using different types of parametric stretching. Finally, solving these evolution equations, one can find the dynamical characteristic of IAW. For instance, some evolution equations deriving from governing principle are presented below.

1.8.6 The KdV equation

In order to observe the dynamics of IAWs, we consider KdV equation. Here we consider an unmagnetized collision-free two-component plasma consisting of electrons and ions, where ions are mobile and electron obey Maxwell distribution. Let the ion is moving in the background of Maxwell distributed electron. The governing equations which include the equation of continuity, equation of momentum balance and Poisson equation are stated as follows,

$$\frac{\partial n_i}{\partial t} + \frac{\partial}{\partial x}(n_i u_i) = 0 \tag{1.91}$$

$$\frac{\partial u_i}{\partial t} + u_i \frac{\partial u_i}{\partial x} = -\frac{e}{m_i}\frac{\partial \Psi}{\partial x} \tag{1.92}$$

$$\varepsilon_0 \frac{\partial^2 \Psi}{\partial x^2} = e(n_e - n_i) \tag{1.93}$$

where $n_e = N_{e0}\exp\left(\frac{e\Psi}{K_B T_e}\right)$. Here n_j is the density of the j-th species ($j = e,\ i$ stands for electron and ion respectively), u_i is the velocity of ion, m_i is mass of ion, e is the magnitude of electron charge, ε_0 is the dielectric constant and K_B is the Boltzmann constant. Ψ represents the electrostatic wave potential.

1.8.6.1 Normalization

To write equations (1.91)-(1.93) in dimensionless from we introduce the following normalization;

$$\frac{e\Psi}{K_B T_e} \to \psi,\ \frac{u_i}{c_{si}} \to U_i,\ \frac{n_i}{N_{i0}} \to N_i,\ \frac{n_e}{N_{e0}} \to N_e,\ \frac{x}{\lambda_{di}} \to X,\ \omega_{pi} t \to T \tag{1.94}$$

where $c_{si} = \sqrt{\frac{K_B T_e}{m_i}}$ is the ion acoustic speed, $\lambda_{di} = \sqrt{\frac{\varepsilon_0 K_B T_e}{N_{i0} e^2}}$ is the ion Debye length, $\omega_{pi}^{-1} = \sqrt{\frac{\varepsilon_0 m_i}{N_{i0} e^2}}$ is the ion plasma period. N_{i0} and N_{e0} represent respectively the unperturbed ion and electron number density.

Using (1.94) we get the dimensionless from of equation of continuity, equation of momentum balance and Poisson equation are as follows,

$$\frac{\partial N_i}{\partial T} + \frac{\partial}{\partial X}(N_i U_i) = 0 \tag{1.95}$$

$$\frac{\partial U_i}{\partial t} + U_i \frac{\partial U_i}{\partial X} = -\frac{\partial \psi}{\partial X} \tag{1.96}$$

$$\frac{\partial^2 \psi}{\partial X^2} = \exp(\psi) - N_i \tag{1.97}$$

1.8.6.2 Linearization

To linearized equations (1.95) -(1.97), let us consider the dependent variables as sum of equilibrium and perturbed parts, so that we write

$$N_i = 1 + \overline{N_i},\ U_i = \overline{U_i},\ \psi = \overline{\psi} \tag{1.98}$$

Using (1.98) into the equations (1.95)−(1.97) and neglecting the nonlinear term $\frac{\partial(\overline{N_i U_i})}{\partial x}$. we get the linearized form of as follows.

$$\frac{\partial \overline{N_i}}{\partial T} + \frac{\partial \overline{U_i}}{\partial X} = 0 \tag{1.99}$$

$$\frac{\partial \overline{U_i}}{\partial T} + \frac{\partial \overline{\psi}}{\partial X} = 0 \tag{1.100}$$

$$\frac{\partial^2 \overline{\psi}}{\partial X^2} = \overline{\psi} - \overline{N_i} \tag{1.101}$$

1.8.6.3 Dispersion relation

To obtain dispersion relation for low frequency wave, the perturbation is assumed proportional to $\exp i(lX - \omega T)$ and of the form

$$\overline{N_i} = N_0 e^{i(lX-\omega T)},\ \ \overline{U_i} = U_0 e^{i(lX-\omega T)},\ \ \overline{\phi} = \phi_0 e^{i(lX-\omega T)} \tag{1.102}$$

where l is the wave number and ω is the wave frequency for ion acoustic wave.
Substituting (1.102) in equations (1.99)-(1.101), we get

$$\omega N_0 - l U_0 = 0 \tag{1.103}$$
$$\omega U_0 - l \psi_0 = 0 \tag{1.104}$$
$$N_0 - \left(1 + l^2\right) \psi_0 = 0 \tag{1.105}$$

The system of equations (1.103)−(1.105) is a system of linear homogeneous equations in three variables N_0, U_0 and ψ_0. So for nontrivial solutions we must have

$$\begin{vmatrix} \omega & -l & 0 \\ 0 & \omega & -l \\ 1 & 0 & -\left(1 + l^2\right) \end{vmatrix} = 0$$

$$\text{or } \omega^2 = \frac{l^2}{1 + l^2}$$

which is the required dispersion relation.
For weak dispersion i.e., for small values of l, we have

$$\begin{aligned} \omega &= l\left(1 + l^2\right)^{-\frac{1}{2}} \\ &= l\left(1 - \frac{1}{2}l^2 + \cdots\right) \\ &= l - \frac{1}{2}l^3, \text{ neglecting } l^5 \text{ and higher order of } l. \end{aligned}$$

The phase velocity v_p is given by

$$\begin{aligned} v_p &= \frac{\omega}{l} \\ &= \frac{1}{\sqrt{1 + l^2}} \end{aligned}$$

Here $v_p \to 1$ as $l \to 0$ and $v_p \to 0$ as $k \to \infty$.

1.8.6.4 Derivation of KdV equation

To deduce KdV equation, the standard independent variables are stretched and written as:

$$\begin{aligned} \xi &= \epsilon^{\frac{1}{2}} (X - \lambda_0 T) \\ \tau &= \epsilon^{\frac{3}{2}} T \end{aligned} \tag{1.106}$$

where ϵ measures the strength of nonlinearity and λ_0 is the phase velocity of waves.
So

$$\frac{\partial}{\partial X} = \epsilon^{\frac{1}{2}} \frac{\partial}{\partial \xi}, \quad \frac{\partial}{\partial T} = \epsilon^{\frac{3}{2}} \frac{\partial}{\partial \tau} - \lambda_0 \epsilon^{\frac{1}{2}} \frac{\partial}{\partial \xi}, \quad \frac{\partial^2}{\partial X^2} = \epsilon \frac{\partial^2}{\partial \xi^2} \tag{1.107}$$

The dependent variables are expanded as follows:

$$\begin{aligned} N_i &= 1 + \epsilon N_i^{(1)} + \epsilon^2 N_i^{(2)} + \cdots \\ U_i &= \epsilon U_i^{(1)} + \epsilon^2 U_i^{(2)} + \cdots \\ \psi &= \epsilon \psi^{(1)} + \epsilon^2 \psi^{(2)} + \cdots \end{aligned} \tag{1.108}$$

Substituting (1.107) and (1.108) in equations (1.95)-(1.97) and collecting the coefficients of lower power of ϵ we get

$$-\lambda_0 \frac{\partial N_i^{(1)}}{\partial \xi} + \frac{\partial U_i^{(1)}}{\partial \xi} = 0, \quad -\lambda_0 \frac{\partial U_i^{(1)}}{\partial \xi} = -\frac{\partial \psi^{(1)}}{\partial \xi}, \quad \psi^{(1)} - N_i^{(1)} = 0 \tag{1.109}$$

and collecting the coefficients of next higher order of ϵ we get

$$\frac{\partial N_i^{(1)}}{\partial \tau} - \lambda_0 \frac{\partial N_i^{(2)}}{\partial \xi} + \frac{\partial U_i^{(2)}}{\partial \xi} + \frac{\partial}{\partial \xi}\left(N_i^{(1)} U_i^{(1)}\right) = 0 \tag{1.110}$$

$$\frac{\partial U_i^{(1)}}{\partial \tau} - \lambda_0 \frac{\partial U_i^{(2)}}{\partial \xi} + U_i^{(1)} \frac{\partial U_i^{(1)}}{\partial \xi} = -\frac{\partial \psi^{(2)}}{\partial \xi} \tag{1.111}$$

$$\frac{\partial^2 \psi^{(1)}}{\partial \xi^2} = \psi^{(2)} + \frac{1}{2}\left(\psi^{(1)}\right)^2 - N_i^{(2)} \tag{1.112}$$

Integrating first two of (1.109), and assuming all the variable vanish as $\xi \to \pm\infty$, we get from (1.109)

$$N_i^{(1)} = \frac{U_i^{(1)}}{\lambda_0}, \quad U_i^{(1)} = \frac{\psi^{(1)}}{\lambda_0}, \quad N_i^{(1)} = \psi^{(1)} \tag{1.113}$$

From (1.113), we get

$$\lambda_0^2 = 1$$

Differentiating (1.112) with respect to ξ, we get

$$\frac{\partial^3 \psi^{(1)}}{\partial \xi^3} = \frac{\partial \psi^{(2)}}{\partial \xi} + \psi^{(1)} \frac{\partial \psi^{(1)}}{\partial \xi} - \frac{\partial N_i^{(2)}}{\partial \xi} \tag{1.114}$$

From (1.110) and (1.111), we get

$$\frac{\partial \psi^{(2)}}{\partial \xi} - \frac{\partial N_i^{(2)}}{\partial \xi} = -\frac{\partial U_i^{(1)}}{\partial \tau} - U_i^{(1)} \frac{\partial U_i^{(1)}}{\partial \xi} - \lambda_0 \frac{\partial N_i^{(1)}}{\partial \tau} - \lambda_0 \frac{\partial}{\partial \xi}\left(N_i^{(1)} U_i^{(1)}\right) \tag{1.115}$$

From (1.114) and (1.115), we get

$$\frac{\partial^3 \psi^{(1)}}{\partial \xi^3} = -\frac{\partial U_i^{(1)}}{\partial \tau} - U_i^{(1)} \frac{\partial U_i^{(1)}}{\partial \xi} - \lambda_0 \frac{\partial N_i^{(1)}}{\partial \tau} - \lambda_0 \frac{\partial}{\partial \xi}\left(N_i^{(1)} U_i^{(1)}\right) + \psi^{(1)} \frac{\partial \psi^{(1)}}{\partial \xi}$$

$$
\begin{aligned}
\text{or } \frac{\partial^3\psi^{(1)}}{\partial\xi^3} &= -\frac{1}{\lambda_0}\frac{\partial\psi^{(1)}}{\partial\tau} - \psi^{(1)}\frac{\partial\psi^{(1)}}{\partial\xi} - \lambda_0\frac{\partial\psi^{(1)}}{\partial\tau} - \frac{\partial}{\partial\xi}\left(\psi^{(1)}\right)^2 + \psi^{(1)}\frac{\partial\psi^{(1)}}{\partial\xi} \\
\text{or } \frac{\partial^3\psi^{(1)}}{\partial\xi^3} &= -\frac{2}{\lambda_0}\frac{\partial\psi^{(1)}}{\partial\tau} - 2\psi^{(1)}\frac{\partial\psi^{(1)}}{\partial\xi} \\
\text{or } \frac{\partial\psi^{(1)}}{\partial\tau} &+ \lambda_0\psi^{(1)}\frac{\partial\psi^{(1)}}{\partial\xi} + \frac{\lambda_0}{2}\frac{\partial^3\psi^{(1)}}{\partial\xi^3} = 0 \\
\text{or } \frac{\partial\psi^{(1)}}{\partial\tau} &+ \mathcal{A}\psi^{(1)}\frac{\partial\psi^{(1)}}{\partial\xi} + \mathcal{B}\frac{\partial^3\psi^{(1)}}{\partial\xi^3} = 0
\end{aligned} \tag{1.116}
$$

where

$$
\mathcal{A} = \lambda_0,\ \mathcal{B} = \frac{\lambda_0}{2}
$$

The above equation (1.116) is known as Korteweg–de Vries (KdV) equation.

1.8.7 The KP equation

In order to study the propagation of ion-acoustic waves we consider the KP equation. Here we consider a two-dimensional unmagnetized collision-free three-component plasma consists of electrons, positrons and ions where ions are mobile and electrons and positrons obey the Maxwell distribution. The governing equations which include the equation of continuity, equation of momentum balance and Poisson equation are stated as follows,

$$
\frac{\partial n_i}{\partial t} + \nabla\cdot(n_i\mathbf{u}_i) = 0 \tag{1.117}
$$

$$
\frac{\partial \mathbf{u}_i}{\partial t} + (\mathbf{u}_i\cdot\nabla)\,\mathbf{u}_i = -\frac{e}{m_i}\nabla\Psi \tag{1.118}
$$

$$
\nabla^2\Psi = 4\pi e\,(n_e - n_i - n_p) \tag{1.119}
$$

where $n_e = N_{e0}\exp\left(\frac{e\Psi}{K_B T_e}\right)$ and $n_p = N_{p0}\exp\left(-\frac{e\Psi}{K_B T_p}\right)$.
Here n_j is the density of the j-th species ($j = e, p$, i stands for electron, positron and ion respectively), u_i is the velocity of ion, m_i is the mass of ion, e is the magnitude of electron charge and c is the velocity of light. Φ represents the electrostatic wave potential. T_e and T_p represent the temperature of the electron and positron respectively.

1.8.7.1 Normalization

To write equations (1.117)-(1.119) in dimensionless form, the normalization are as follows:

$$
\frac{e\Psi}{K_B T_e} \to \psi,\ \frac{u_i}{c_{si}} \to U_i,\ \frac{n_i}{N_{i0}} \to N_i,\ \frac{n_e}{N_{e0}} \to N_e,\ \frac{n_p}{N_{p0}} \to N_p,\ \frac{\nabla}{\lambda_{di}} \to \nabla,\ \omega_{pi}t \to T \tag{1.120}
$$

where $c_{si} = \sqrt{\frac{K_B T_e}{m_i}}$ is the ion acoustic speed, $\lambda_{di} = \sqrt{\frac{K_B T_e}{4\pi N_{i0} e^2}}$ is the ion Debye length, $\omega_{pi} = \sqrt{\frac{4\pi N_{i0} e^2}{m_i}}$ is the ion plasma frequency and $\mathcal{K}_B$ is the Boltzmann constant. N_{i0}, N_{e0} and N_{p0}

represent respectively the unperturbed ion, electron and positron number density. At equilibrium, the charge neutrality condition requires that $N_{e0} = N_{i0} + N_{p0}$.
Using (1.120) in equations (1.117)-(1.119), we get the normalized equations as

$$\frac{\partial N_i}{\partial T} + \nabla\cdot(N_i \mathbf{U}_i) = 0 \tag{1.121}$$

$$\frac{\partial \mathbf{U}_i}{\partial T} + (\mathbf{U}_i \cdot \nabla)\,\mathbf{U}_i = -\nabla\psi \tag{1.122}$$

$$\nabla^2\psi = (1+\rho)\exp(\psi) - N_i - \rho\exp(-\sigma\psi) \tag{1.123}$$

where $\sigma = \frac{T_e}{T_p}$ and $\rho = \frac{N_{po}}{N_{io}}$.
The normalized equations in the component form can be written as

$$\frac{\partial N_i}{\partial T} + \frac{\partial}{\partial x}(N_i U_{ix}) + \frac{\partial}{\partial y}(N_i U_{iy}) = 0 \tag{1.124}$$

$$\frac{\partial U_{ix}}{\partial T} + \left(U_{ix}\frac{\partial}{\partial x} + U_{iy}\frac{\partial}{\partial y}\right)U_{ix} = -\frac{\partial\psi}{\partial x} \tag{1.125}$$

$$\frac{\partial U_{iy}}{\partial T} + \left(U_{ix}\frac{\partial}{\partial x} + U_{iy}\frac{\partial}{\partial y}\right)U_{iy} = -\frac{\partial\psi}{\partial y} \tag{1.126}$$

$$\left(\frac{\partial^2}{\partial x^2} + \frac{\partial^2}{\partial y^2}\right)\psi = (1+\rho)\exp(\psi) - N_i - \rho\exp(-\sigma\psi) \tag{1.127}$$

1.8.7.2 Linearization

To linearized equations (1.124) -(1.127), let us consider the dependent variables as sum of equilibrium and perturbed parts, so that we write

$$N_i = 1 + \overline{N_i},\ U_{ix} = \overline{U_{ix}},\ U_{iy} = \overline{U_{iy}},\ \psi = \overline{\psi} \tag{1.128}$$

Using (1.128) into the equations (1.124)−(1.127) and neglecting the nonlinear terms $\frac{\partial(\overline{n_i}\ \overline{U_{ix}})}{\partial x}$, $\frac{\partial(\overline{N_i}\ \overline{U_{iy}})}{\partial y}$, $\overline{U_{ix}}\frac{\partial \overline{U_{iy}}}{\partial x}$, and $\overline{U_{iy}}\frac{\partial \overline{U_{iy}}}{\partial y}$. we get the linearized form of as follows.

$$\frac{\partial \overline{N_i}}{\partial T} + \frac{\partial \overline{U_{ix}}}{\partial x} + \frac{\partial \overline{U_{iy}}}{\partial y} = 0 \tag{1.129}$$

$$\frac{\partial \overline{U_{ix}}}{\partial T} = -\frac{\partial \overline{\psi}}{\partial x} \tag{1.130}$$

$$\frac{\partial \overline{U_{iy}}}{\partial T} = -\frac{\partial \overline{\psi}}{\partial y} \tag{1.131}$$

$$\left(\frac{\partial^2}{\partial x^2} + \frac{\partial^2}{\partial y^2}\right)\overline{\psi} = (1+\rho(1+\sigma))\,\overline{\psi} - \overline{N_i} \tag{1.132}$$

1.8.7.3 Dispersion relation

To obtain dispersion relation for low frequency wave, the perturbation is assumed proportional to $\exp i\left(l_x x + l_y y - \omega T\right)$ and of the form

$$\begin{aligned}
\overline{N_i} &= N_0 e^{i(l_x x + l_y y - \omega T)} \\
\overline{U_{ix}} &= U_{0x} e^{i(l_x x + l_y y - \omega T)} \\
\overline{v_{iy}} &= U_{0y} e^{i(l_x x + l_y y - \omega T)} \\
\overline{\psi} &= \psi_0 e^{i(l_x x + l_y y - \omega T)}
\end{aligned} \tag{1.133}$$

where l_x and l_y are the wave numbers in x and y directions respectively and ω is the wave frequency for ion acoustic wave.
Using (1.133) in equation (1.129), we get

$$\text{or } N_0 = \frac{l_x}{\omega} U_{0x} + \frac{l_y}{\omega} U_{0y} \tag{1.134}$$

Using (1.133) in equation (1.130), we get

$$U_{0x} = \frac{l_x}{\omega} \psi_0 \tag{1.135}$$

Using (1.133) in equation (1.131), we get

$$U_{0y} = \frac{l_y}{\omega^2} \psi_0 \tag{1.136}$$

Using (1.133) in equation (1.132), we get

$$-\left(l_x^2 + l_y^2\right)\psi_0 = \left(1 + \rho\left(1 + \sigma\right)\right)\psi_0 - \left(\frac{l_x}{\omega} U_{0x} + \frac{l_y}{\omega} U_{0y}\right)$$

$$\text{or } -\left(l_x^2 + l_y^2\right)\psi_0 = \left(1 + \rho\left(1 + \sigma\right)\right)\psi_0 - \frac{l_x^2}{\omega^2}\psi_0 - \frac{l_y^2}{\omega^2}\psi_0$$

$$\text{or } \frac{l_x^2 + l_y^2}{\omega^2} = 1 + \rho\left(1 + \sigma\right) + \left(l_x^2 + l_y^2\right)$$

$$\text{or } \frac{1}{\omega^2} = \frac{1 + \rho\left(1 + \sigma\right)}{l_x^2 + l_y^2} + 1$$

$$\text{or } \omega = \left[\frac{1 + \rho\left(1 + \sigma\right)}{l_x^2 + l_y^2} + 1\right]^{-\frac{1}{2}} \tag{1.137}$$

which is the required dispersion relation.

1.8.7.4 Derivation of KP equation

To deduce KP equation, the standard independent variables are stretched and written as:

$$\xi = \epsilon\,(x - \lambda_0 T)\,,\ \eta = \epsilon^2 y,\quad \tau = \epsilon^3 T \tag{1.138}$$

where ϵ measures the strength of nonlinearity and λ_0 is the phase velocity of waves.
So

$$\frac{\partial}{\partial x} = \epsilon\frac{\partial}{\partial \xi}, \frac{\partial}{\partial y} = \epsilon^2\frac{\partial}{\partial \eta}, \frac{\partial}{\partial T} = \epsilon^3\frac{\partial}{\partial \tau} - \lambda_0\epsilon\frac{\partial}{\partial \xi}, \frac{\partial^2}{\partial x^2} = \epsilon^2\frac{\partial^2}{\partial \xi^2}, \frac{\partial^2}{\partial y^2} = \epsilon^4\frac{\partial^2}{\partial \eta^2} \tag{1.139}$$

The dependent variables are expanded as follows:

$$\begin{aligned} N_i &= 1 + \epsilon^2 N_i^{(1)} + \epsilon^4 N_i^{(2)} + \cdots \\ u_{ix} &= \epsilon^2 u_{ix}^{(1)} + \epsilon^4 u_{ix}^{(2)} + \cdots \\ u_{iy} &= \epsilon^3 u_{iy}^{(1)} + \epsilon^5 u_{iy}^{(2)} + \cdots \\ \psi &= \epsilon^2 \psi^{(1)} + \epsilon^4 \psi^{(2)} + \cdots \end{aligned} \tag{1.140}$$

Substituting (1.139) and (1.140) in equation (1.124) and collecting the coefficients of ϵ^3 and ϵ^5,we get

$$-\lambda_0\frac{\partial N_i^{(1)}}{\partial \xi} + \frac{\partial u_{ix}^{(1)}}{\partial \xi} = 0 \tag{1.141}$$

$$\frac{\partial N_i^{(1)}}{\partial \tau} - \lambda_0\frac{\partial N_i^{(2)}}{\partial \xi} + \frac{\partial u_{ix}^{(2)}}{\partial \xi} + \frac{\partial}{\partial \xi}\left(N_i^{(1)} u_{ix}^{(1)}\right) + \frac{\partial u_{iy}^{(1)}}{\partial \eta} = 0 \tag{1.142}$$

Substituting (1.139) and (1.140) in equation (1.125) and collecting the coefficients of ϵ^3 and ϵ^5,we get

$$-\lambda_0\frac{\partial u_{ix}^{(1)}}{\partial \xi} = -\frac{\partial \psi^{(1)}}{\partial \xi} \tag{1.143}$$

$$\frac{\partial u_{ix}^{(1)}}{\partial \tau} - \lambda_0\frac{\partial u_{ix}^{(2)}}{\partial \xi} + u_{ix}^{(1)}\frac{\partial u_{ix}^{(1)}}{\partial \xi} = -\frac{\partial \psi^{(2)}}{\partial \xi} \tag{1.144}$$

Substituting (1.139) and (1.140) in equation (1.126) and collecting the coefficients of ϵ^4 and ϵ^6,we get

$$-\lambda_0\frac{\partial u_{iy}^{(1)}}{\partial \xi} = -\frac{\partial \psi^{(1)}}{\partial \eta} \tag{1.145}$$

$$\frac{\partial u_{iy}^{(1)}}{\partial \tau} - \lambda_0\frac{\partial u_{iy}^{(2)}}{\partial \xi} + u_{ix}^{(1)}\frac{\partial u_{iy}^{(1)}}{\partial \xi} = \frac{\partial \psi^{(2)}}{\partial \eta} \tag{1.146}$$

Substituting (1.139) and (1.140) in equation (1.127) and collecting the coefficients of ϵ^2 and ϵ^4,we

get

$$(1+\rho)\,\psi^{(1)} - N_i^{(1)} + \rho\sigma\psi^{(1)} = 0 \tag{1.147}$$

$$\frac{\partial^2\psi^{(1)}}{\partial\xi^2} = (1+\rho)\left(\psi^{(2)} + \frac{1}{2}\left(\psi^{(1)}\right)^2\right) - N_i^{(2)} + \rho\sigma\psi^{(2)} - \frac{1}{2}\rho\sigma^2\left(\psi^{(1)}\right)^2 \tag{1.148}$$

Integrating (1.141) and (1.143) and assuming all the variable vanish as $\xi \to \pm\infty$, we get

$$N_i^{(1)} = \frac{U_{ix}^{(1)}}{\lambda_0} \tag{1.149}$$

$$U_{ix}^{(1)} = \frac{\psi^{(1)}}{\lambda_0} \tag{1.150}$$

From (1.147) ,we get

$$N_i^{(1)} = (1+\rho\,(1+\sigma))\,\psi^{(1)} \tag{1.151}$$

From (1.149), (1.150) and (1.151), we get

$$\lambda_0^2 = \frac{1}{1+\rho\,(1+\sigma)}$$

Differentiating (1.148) with respect to ξ, we get

$$\frac{\partial^3\psi^{(1)}}{\partial\xi^3} = (1+\rho)\left(\frac{\partial\psi^{(2)}}{\partial\xi} + \psi^{(1)}\frac{\partial\psi^{(1)}}{\partial\xi}\right) - \frac{\partial N_i^{(2)}}{\partial\xi} + \rho\sigma\frac{\partial\psi^{(2)}}{\partial\xi} - \rho\sigma^2\psi^{(1)}\frac{\partial\psi^{(1)}}{\partial\xi}$$

$$\text{or } \frac{\partial^4\psi^{(1)}}{\partial\xi^4} = (1+\rho)\left(\frac{\partial^2\psi^{(2)}}{\partial\xi^2} + \frac{\partial}{\partial\xi}\left(\psi^{(1)}\frac{\partial\psi^{(1)}}{\partial\xi}\right)\right) - \frac{\partial^2 N_i^{(2)}}{\partial\xi^2} + \rho\sigma\frac{\partial^2\psi^{(2)}}{\partial\xi^2} - \rho\sigma^2\frac{\partial}{\partial\xi}\left(\psi^{(1)}\frac{\partial\psi^{(1)}}{\partial\xi}\right)$$

$$\text{or } \frac{\partial^4\psi^{(1)}}{\partial\xi^4} = (1+\rho\,(1+\sigma))\,\frac{\partial^2\psi^{(2)}}{\partial\xi^2} + \left(1+\rho\left(1-\sigma^2\right)\right)\frac{\partial}{\partial\xi}\left(\psi^{(1)}\frac{\partial\psi^{(1)}}{\partial\xi}\right) - \frac{\partial^2 N_i^{(2)}}{\partial\xi^2} \tag{1.152}$$

Differentiating (1.142) with respect to ξ, we get

$$\frac{\partial^2 N_i^{(1)}}{\partial\xi\partial\tau} - \lambda_0\frac{\partial^2 N_i^{(2)}}{\partial\xi^2} + \frac{\partial^2 U_{ix}^{(2)}}{\partial\xi^2} + \frac{\partial^2}{\partial\xi^2}\left(N_i^{(1)}U_{ix}^{(1)}\right) + \frac{\partial^2 U_{iy}^{(1)}}{\partial\xi\partial\eta} = 0$$

$$\text{or } \lambda_0\frac{\partial^2 N_i^{(1)}}{\partial\xi\partial\tau} - \lambda_0^2\frac{\partial^2 N_i^{(2)}}{\partial\xi^2} + \lambda_0\frac{\partial^2 U_{ix}^{(2)}}{\partial\xi^2} + \lambda_0\frac{\partial^2}{\partial\xi^2}\left(N_i^{(1)}U_{ix}^{(1)}\right) + \lambda_0\frac{\partial^2 U_{iy}^{(1)}}{\partial\xi\partial\eta} = 0 \tag{1.153}$$

Differentiating (1.144) with respect to ξ, we get

$$\frac{\partial^2 U_{ix}^{(1)}}{\partial\xi\partial\tau} - \lambda_0\frac{\partial^2 U_{ix}^{(2)}}{\partial\xi^2} + \frac{\partial}{\partial\xi}\left(U_{ix}^{(1)}\frac{\partial U_{ix}^{(1)}}{\partial\xi}\right) = -\frac{\partial^2\psi^{(2)}}{\partial\xi^2} \tag{1.154}$$

From (1.153) and (1.154), we get

$$\frac{\partial^2\psi^{(2)}}{\partial\xi^2}-\lambda_0^2\frac{\partial^2 N_i^{(2)}}{\partial\xi^2} = -\lambda_0\frac{\partial^2 N_i^{(1)}}{\partial\xi\partial\tau}-\lambda_0\frac{\partial^2}{\partial\xi^2}\left(N_i^{(1)}U_{ix}^{(1)}\right)-\lambda_0\frac{\partial^2 U_{iy}^{(1)}}{\partial\xi\partial\eta}-\frac{\partial^2 U_{ix}^{(1)}}{\partial\xi\partial\tau} -\frac{\partial}{\partial\xi}\left(U_{ix}^{(1)}\frac{\partial U_{ix}^{(1)}}{\partial\xi}\right)$$

From (1.152), we get,

$$\lambda_0^2\frac{\partial^4\psi^{(1)}}{\partial\xi^4}=\frac{\partial^2\psi^{(2)}}{\partial\xi^2}+\lambda_0^2\left(1+\rho\left(1-\sigma^2\right)\right)\frac{\partial}{\partial\xi}\left(\psi^{(1)}\frac{\partial\psi^{(1)}}{\partial\xi}\right)-\lambda_0^2\frac{\partial^2 N_i^{(2)}}{\partial\xi^2}$$

$$\text{or } \lambda_0^2\frac{\partial^4\psi^{(1)}}{\partial\xi^4} = -\lambda_0\frac{\partial^2 N_i^{(1)}}{\partial\xi\partial\tau}-\lambda_0\frac{\partial^2}{\partial\xi^2}\left(N_i^{(1)}U_{ix}^{(1)}\right)-\lambda_0\frac{\partial^2 U_{iy}^{(1)}}{\partial\xi\partial\eta}-\frac{\partial^2 U_{ix}^{(1)}}{\partial\xi\partial\tau} -\frac{\partial}{\partial\xi}\left(U_{ix}^{(1)}\frac{\partial U_{ix}^{(1)}}{\partial\xi}\right)+\lambda_0^2\left(1+\rho\left(1-\sigma^2\right)\right)\frac{\partial}{\partial\xi}\left(\psi^{(1)}\frac{\partial\psi^{(1)}}{\partial\xi}\right)$$

$$\text{or } \lambda_0^2\frac{\partial^4\psi^{(1)}}{\partial\xi^4} = -\frac{1}{\lambda_0}\frac{\partial^2\psi^{(1)}}{\partial\xi\partial\tau}-\frac{1}{\lambda_0^2}\frac{\partial^2}{\partial\xi^2}\left(\psi^{(1)}\right)^2-\frac{\partial^2\psi^{(1)}}{\partial\eta^2}-\frac{1}{\lambda_0}\frac{\partial^2\psi^{(1)}}{\partial\xi\partial\tau} -\frac{1}{\lambda_0^2}\frac{\partial}{\partial\xi}\left(\psi^{(1)}\frac{\partial\psi^{(1)}}{\partial\xi}\right)+\lambda_0^2\left(1+\rho\left(1-\sigma^2\right)\right)\frac{\partial}{\partial\xi}\left(\psi^{(1)}\frac{\partial\psi^{(1)}}{\partial\xi}\right)$$

$$\text{or } \lambda_0^3\frac{\partial^4\psi^{(1)}}{\partial\xi^4} = -2\frac{\partial^2\psi^{(1)}}{\partial\xi\partial\tau}-\frac{2}{\lambda_0}\frac{\partial}{\partial\xi}\left(\psi^{(1)}\frac{\partial\psi^{(1)}}{\partial\xi}\right)-\lambda_0\frac{\partial^2\psi^{(1)}}{\partial\eta^2} -\frac{1}{\lambda_0}\frac{\partial}{\partial\xi}\left(\psi^{(1)}\frac{\partial\psi^{(1)}}{\partial\xi}\right)+\lambda_0^3\left(1+\rho\left(1-\sigma^2\right)\right)\frac{\partial}{\partial\xi}\left(\psi^{(1)}\frac{\partial\psi^{(1)}}{\partial\xi}\right)$$

$$\text{or } \frac{\partial^2\psi^{(1)}}{\partial\xi\partial\tau}+\frac{1}{\lambda_0}\frac{\partial}{\partial\xi}\left(\psi^{(1)}\frac{\partial\psi^{(1)}}{\partial\xi}\right)+\frac{\lambda_0}{2}\frac{\partial^2\psi^{(1)}}{\partial\eta^2}+\frac{1}{2\lambda_0}\frac{\partial}{\partial\xi}\left(\psi^{(1)}\frac{\partial\psi^{(1)}}{\partial\xi}\right) -\frac{\lambda_0^3}{2}\left(1+\rho\left(1-\sigma^2\right)\right)\frac{\partial}{\partial\xi}\left(\psi^{(1)}\frac{\partial\psi^{(1)}}{\partial\xi}\right)+\frac{\lambda_0^3}{2}\frac{\partial^4\psi^{(1)}}{\partial\xi^4}=0$$

$$\text{or } \frac{\partial^2\psi^{(1)}}{\partial\xi\partial\tau}+\left(\frac{3}{2\lambda_0}-\frac{\lambda_0^3}{2}\left(1+\rho\left(1-\sigma^2\right)\right)\right)\frac{\partial}{\partial\xi}\left(\psi^{(1)}\frac{\partial\psi^{(1)}}{\partial\xi}\right)+\frac{\lambda_0^3}{2}\frac{\partial^4\psi^{(1)}}{\partial\xi^4} +\frac{\lambda_0}{2}\frac{\partial^2\psi^{(1)}}{\partial\eta^2}=0$$

$$\text{or } \frac{\partial}{\partial\xi}\left[\frac{\partial\psi^{(1)}}{\partial\tau}+\left(\frac{3}{2\lambda_0}-\frac{\lambda_0^3}{2}\left(1+\rho\left(1-\sigma^2\right)\right)\right)\psi^{(1)}\frac{\partial\psi^{(1)}}{\partial\xi}+\frac{\lambda_0^3}{2}\frac{\partial^3\psi^{(1)}}{\partial\xi 3}\right] +\frac{\lambda_0}{2}\frac{\partial^2\psi^{(1)}}{\partial\eta^2}=0$$

$$\text{or } \frac{\partial}{\partial\xi}\left[\frac{\partial\psi^{(1)}}{\partial\tau}+\mathcal{A}\psi^{(1)}\frac{\partial\psi^{(1)}}{\partial\xi}+\mathcal{B}\frac{\partial^3\psi^{(1)}}{\partial\xi^3}\right]+\mathcal{C}\frac{\partial^2\psi^{(1)}}{\partial\eta^2}=0 \tag{1.155}$$

where

$$\mathcal{A}=\frac{3}{2\lambda_0}-\frac{\lambda_0^3}{2}\left(1+\rho\left(1-\sigma^2\right)\right),\ \mathcal{B}=\frac{\lambda_0^3}{2},\ \mathcal{C}=\frac{\lambda_0}{2}$$

The above equation (1.155) is known as KP equation.

Chapter 2

Integrability, breather, lump and quasi-periodic waves of non-autonomous Kadomtsev-Petviashvili equation based on Bell-polynomial approach

[1]

2.1 Introduction

Many mysterious natures of the physical world are revealed by the NLEE. The KdV equation and its variants such as the ZK equation and KP equation are the most popular models in this field. The soliton solution is an important feature of these models and a lot of studies are available in the existing literature relating to the propagation of multi-solitons [147, 152, 153, 154, 155, 156]. Recently, a new interest has grown in the study of the integrability of these equations though, a completely integrable system is not precisely defined. But it is acknowledged that the integrable system includes Lax pair, N-symmetries, Hamiltonian as well as bi-Hamiltonian structure, and bilinear Bäcklund transformation, etc. In addition to these characteristics, the Painlevé test and the exis-

[1]The research article has been published in the journal of Wave Motion (Elsevier)

tence of conservation laws are also studied. In general, inter-particle collision causes for raising of a damping effect in any medium. There are also many phenomena that cause damping in a dynamical system, for instance, the resonant energy exchange between the particles and electrostatic waves in the plasma environment may cause for producing damping. Also, some experimental works on space plasma announced the significant influence of externally applied different types of forcing components viz., hyperbolic forcing term, Gaussian forcing term (in terms of $\mathrm{sech}^2(\xi,t)$ and $\mathrm{sech}^4(\xi,t)$) and trigonometric forcing term (in terms of $\sin(\xi,t)$ and $\cos(\xi,t)$ function), on wave propagation in plasma environment [157, 158]. Motivating by such theoretical and experimental works, we seek to investigate the different characteristics of the $(2+1)$-dimensional damped forced KP equation [159] which can be expressed as, Consider the standard (2+1)-dimensional NKP equation

$$(U_\tau + AUU_\xi + BU_{\xi\xi\xi} + DU)_\xi + CU_{\eta\eta} = h_{\xi\xi} \tag{2.1}$$

On integration it against ξ and setting $h = \xi f(\tau)$, we get

$$U_\tau + AUU_\xi + BU_{\xi\xi\xi} + DU + C\int U_{\eta\eta} = f(\tau) \tag{2.2}$$

In this chapter we investigated the infinite conservation law, quasi-periodic wave, breather, lump, and characteristic of integrability via bilinear Bäcklund and lax pairs of the NKP equation (in the presence of an external force and damping). Bell-polynomial is deduced from Bäcklund transformation from which infinite conservation law for NKP equation is derived. Obtaining well-known quasi-periodic solutions is an important aspect of this investigation. A limiting procedure is used for analyzing the asymptotic behavior of multi-periodic waves. Further, some complicated solution structures of the NKP equation such as lump and breather-type solitons are explored from the bilinear form of the said equation with the appropriate choice of polynomial functions. Important characteristics of lump and breather waves in different forcing backgrounds are graphically described. Finally, the lump wave of the NKP equation is explored from the breather wave in the limiting stage. It is also confirmed from the analytical results of the relevant motions that the velocity, maximum altitude, and interacting natures of the wave quantities are all influenced by the damping and forcing terms.

2.2 Bilinear form and Bäcklund transformation for the NKP equation

We introduce the transformation

$$U = a(\tau)Q_{\xi\xi} + R(\tau) + U_0, \tag{2.3}$$

where $Q = Q(\xi, \eta, \tau)$ is a function of ξ, η, τ and setting

$$a'(\tau) + Da(\tau) = 0, \quad R'(\tau) + DR(\tau) + DU_0 = f(\tau), \quad Aa(\tau) = 6B \tag{2.4}$$

which implies

$$a(\tau) = a_0 e^{-D\tau}, \; R(\tau) = e^{-D\tau}\left(\int e^{D\tau} f(\tau) d\tau + R_0\right) - U_0, \; A = \frac{6B}{a_0} e^{D\tau}, \tag{2.5}$$

where a_0, R_0 are constants. Substituting (2.3) along with (2.4) in the Eq.(2.2) and then integrating once with respect to ξ, we have

$$Q_{\tau\xi} + \frac{Aa(\tau)}{2} Q_{2\xi}^2 + A(R(\tau) + U_0) Q_{\xi\xi} + BQ_{4\xi} + CQ_{\eta\eta} + c_0 = 0 \tag{2.6}$$

which can be expressed in P-polynomial form [160] by imposing the condition (2.4)

$$P_{\tau\xi}(Q) + A(R(\tau) + U_0) P_{2\xi}(Q) + BP_{4\xi}(Q) + CP_{\eta\eta} + c_0 = 0 \tag{2.7}$$

Under the changing in the dependent variable,

$$Q = 2 \ln \mathcal{F} \tag{2.8}$$

U becomes

$$U = 2a_0 e^{-D\tau}\left[\frac{\partial^2}{\partial \xi^2} \ln(\mathcal{F}(\xi, \eta, \tau))\right] + e^{-D\tau}\left(\int e^{D\tau} f(\tau) d\tau + R_0\right), \tag{2.9}$$

and the P-polynomial Eq. (2.7) is reduced into the bilinear form of the Eq.(2.2) as,

$$\left(D_\tau D_\xi + A(R(\tau) + U_0) D_\xi^2 + BD_{4\xi} + CD_\eta^2 + c_0\right) \mathcal{F}.\mathcal{F} = 0 \tag{2.10}$$

where c_0 is independent of ξ. For simplicity, we assume $c_0 = 0$ and get,

$$\left(D_\tau D_\xi + A(R(\tau) + U_0) D_\xi^2 + BD_{4\xi} + CD_\eta^2\right) \mathcal{F}.\mathcal{F} = 0. \tag{2.11}$$

The bilinear form of Eq.(2.2) addressed in Eq. (2.10) will be used for finding quasi-periodic solution where as, Eq. (2.11) will be utilized to acquire breather and lump type wave solutions and in either case solution will be of the form of Eq.(2.9). Set

$$E(Q) = Q_{\tau\xi} + \frac{Aa(\tau)}{2} Q_{2\xi}^2 + A(R(\tau) + U_0) Q_{\xi\xi} + BQ_{4\xi} + CQ_{\eta\eta} = 0 \tag{2.12}$$

Let $\overline{Q} = 2\ln(F)$ and $Q = 2\ln(G)$ are two different solution of the Eq.(2.12), then the two field condition can be expressed as,

$$\begin{aligned} E(\overline{Q}) - E(Q) = (\overline{Q} - Q)_{\tau\xi} + \frac{Aa(\tau)}{2}(\overline{Q} - Q)_{2\xi}(\overline{Q} + Q)_{2\xi} + (AR(\tau) + U_0)(\overline{Q} - Q)_{2\xi} \\ + B(\overline{Q} - Q)_{4\xi} + C(\overline{Q} - Q)_{\eta\eta} = 0 \end{aligned} \tag{2.13}$$

Setting $u = \frac{\overline{Q}-Q}{2}$ and $v = \frac{\overline{Q}+Q}{2}$, it can be written as

$$\begin{aligned}
&u_{\tau\xi} + Aa(\tau)u_{2\xi}v_{2\xi} + A\left(R(\tau) + U_0\right)u_{2\xi} + Bu_{4\xi} + Cu_{\eta\eta} = 0\\
&u_{\tau\xi} + Aa(\tau)u_{2\xi}v_{2\xi} + A\left(R(\tau) + U_0\right)u_{2\xi} + B\frac{\partial}{\partial\xi}(\Upsilon_{3\xi} - 3v_{2\xi}u_\xi - u_\xi^3) + Cu_{\eta\eta} = 0\\
&u_{\tau\xi} + \left(Aa(\tau) - 3B\right)u_{2\xi}v_{2\xi} - 3Bu_\xi v_{3\xi} - 3Bu_\xi^2 u_{2\xi} + A\left(R(\tau) + U_0\right)u_{2\xi}\\
&+B\frac{\partial}{\partial\xi}(\Upsilon_{3\xi}) + Cu_{\eta\eta} = 0,
\end{aligned} \tag{2.14}$$

where $\Upsilon(u, v)$ is given by [160]

$$\Upsilon_\xi = u_\xi,\ \Upsilon_{\xi,\tau} = u_\xi u_\tau + v_{\xi,\tau},\ \Upsilon_{3\xi} = u_{3\xi} + 3v_{2\xi}u_\xi + u_\xi^3. \tag{2.15}$$

On consideration of $Aa(\tau) - 3B = 3B$, Eq.(2.14) can be expressed as,

$$u_{\tau\xi} + 3B\left(u_{2\xi}v_{2\xi} - u_\xi v_{3\xi} - u_\xi^2 u_{2\xi}\right) + A\left(R(\tau) + U_0\right)u_{2\xi} + B\frac{\partial}{\partial\xi}\left(\Upsilon_{3\xi}\right) + Cu_{\eta\eta} = 0 \tag{2.16}$$

Decomposing the two field conditions into a pair of equations in the form of a binary Bell-polynomial is the next step to obtaining the bilinear Bäcklund transformation of the NKP equation. This can be achieved by imposing the following constraint,

$$B\left(v_{2\xi} + u_\xi^2\right) + \delta u_\eta = \lambda \tag{2.17}$$

where δ and λ are the given parameters.
In the light of these constraints and on the condition $3\delta^2 = BC$, the Eq.(2.12) can be written as,

$$\frac{\partial}{\partial\tau}\Upsilon_\xi + \frac{\partial}{\partial\xi}\left[3\lambda\Upsilon_\xi + A\left(R(\tau) + U_0\right)\Upsilon_\xi + B\Upsilon_{3\xi} - 3\delta\Upsilon_{\xi\eta}\right] = 0 \tag{2.18}$$

Finally, Eq.(2.17) and Eq.(2.18) construct the bilinear Bäcklund transformation in form of the binary Bell-polynomials.

2.3 Lax pair for the NKP equation

On the basis of the binary Bell-polynomials, the Lax pair for the NKP equation (2.1) is derived from the bilinear Bäcklund transformation given by the equations (2.17) and (2.18). Using the Hopf-Cole transform $u = \ln\psi$, we obtain the following relations between binary Bell-polynomial and ψ as

$$\begin{aligned}
&\Upsilon_\xi = \frac{\psi_\xi}{\psi},\ \Upsilon_\tau = \frac{\psi_\tau}{\psi},\ \Upsilon_{2\xi}(u, v) = Q_{2\xi} + \frac{\psi_{2\xi}}{\psi},\\
&\Upsilon_{3\xi}(u, v) = \frac{\psi_{3\xi}}{\psi} + 3Q_{2\xi}\frac{\psi_\xi}{\psi},\ \Upsilon_{\tau\xi}(u, v) = Q_{\xi\tau} + \frac{\psi_{\xi\tau}}{\psi}
\end{aligned} \tag{2.19}$$

Using the relations, the pairs equations (2.17) and (2.18) is reduced to a Lax pair as below,

$$\begin{aligned}
&\sigma\psi_\eta + B\psi_{2\xi} + (BQ_{2\xi} - \lambda)\,\psi = 0\\
&\psi_\tau + B\psi_{3\xi} + (3\lambda + A\,(R(\tau) + U_0) + 3BQ_{2\xi})\,\psi_\xi - 3\sigma\psi_{\xi\eta} - 3\sigma Q_{\xi\eta}\psi = 0
\end{aligned} \tag{2.20}$$

or equivalently

$$\begin{aligned}
(\sigma\partial_\eta + L_1)\,\psi = 0\\
(\partial_\tau + L_2)\,\psi = 0
\end{aligned} \tag{2.21}$$

where $L_1 = B\partial_{2\xi} + BQ_{2\xi} - \lambda$ and $L_2 = B\partial_{3\xi} + (3\lambda + A(R(\tau) + U_0) + 3B)\,\partial_\xi - 3\sigma\partial_\xi\partial_\eta - 3\sigma Q_{\xi\eta}$.

2.4 Infinite conservation law

There are numerous ways to obtain the infinite conservation laws, including the Lax pairs, the Bäcklund transformation, the scattering problem, the formal solution of eigen functions, and the trace identity. With the binary Bell-polynomials derived from the bilinear Bäcklund transformation, we derive the infinite conservation laws for a two-dimensional NKP. Now, we introduce new potential function,

$$\zeta = \overline{Q}_\xi - Q_\xi. \tag{2.22}$$

Then we have

$$u_\xi = \zeta,\ v_\xi = \zeta + Q_\xi \tag{2.23}$$

Using the above transformation, equation (2.18) can be presented as,

$$\frac{\partial}{\partial\tau}u_\xi + \frac{\partial}{\partial\xi}\left(3\lambda u_\xi + A\,(R(\tau) + U_0)\,u_\xi + B\Upsilon_{3\xi}(u,v) - 3\delta u_\xi u_\eta\right) + \frac{\partial}{\partial\eta}\left(Cu_\eta + 3\delta u_\xi^2\right) = 0 \tag{2.24}$$

Replacing, (2.23) in the equations (2.17) and (2.24), we get

$$B\left(\zeta_\xi + Q_{2\xi} + \zeta^2\right) + \delta\int\zeta_\eta = \lambda \tag{2.25}$$

which is popularly known as Riccati equation and

$$\zeta_\tau + \frac{\partial}{\partial\xi}\left(6\lambda\zeta + A\,(R(\tau) + U_0)\,\zeta + B\zeta_{2\xi} - 6\delta\zeta\int\zeta_\eta\,d\xi - 2B\zeta^3\right) + \frac{\partial}{\partial\eta}\left(C\int\zeta_\eta\,d\xi + 3\delta\zeta^2\right) = 0 \tag{2.26}$$

which is clearly a divergence equation. Now setting $\zeta = \overline{\zeta} + \epsilon$ in the equation (2.25) and (2.26), we acquire,

$$B\left(\overline{\zeta} + Q_{2\xi} + \overline{\zeta}^2 + 2\epsilon\overline{\zeta}\right) + \delta\int\overline{\zeta}_\eta\,d\xi = 0 \tag{2.27}$$

where we choose $B\epsilon^2 = \lambda$ and

$$\overline{\zeta}_\tau + \frac{\partial}{\partial\xi}\left(A\left(R(\tau)+U_0\right)\overline{\zeta} + B\overline{\zeta}_{2\xi} - 6\delta\overline{\zeta}\int\overline{\zeta}_\eta d\xi - 6\delta\epsilon\int\overline{\zeta}_\eta d\xi - 2B\overline{\zeta}^3 - 6B\epsilon\overline{\zeta}^2\right)$$
$$+\frac{\partial}{\partial\eta}\left(C\int\overline{\zeta}_\eta d\xi + 3\delta\overline{\zeta}^2 + 6\delta\epsilon\overline{\zeta}\right) = 0 \tag{2.28}$$

Now substitute $\overline{\eta} = \sum_{n=1}^{\infty} I_n\epsilon^{-n}$ in the equation (2.27), we have

$$B\left(\sum I_n\epsilon^{-n} + Q_{2\xi} + \sum\sum I_k I_{n-k}\epsilon^{-n} + 2I_1 + 2\sum I_{n+1}\epsilon^{-n}\right) + \delta\sum\int I_{n,\eta}d\xi = 0. \tag{2.29}$$

Using equation (2.28), we derive conserved densities I_n in a recurring relation, as a result of gathering coefficients of likewise ϵ power,

$$\begin{aligned}
I_1 &= \frac{-1}{2}Q_{2x} = -\frac{U - R(\tau) - U_0}{2a(\tau)} \\
I_2 &= \frac{-1}{2B}\left[BI_1 + \delta\int I_{1,\eta}d\xi\right] = \frac{1}{4B}\left[B\frac{U - R(\tau) - U_0}{a(\tau)} + \frac{\delta}{a(\tau)}\int U_\eta d\xi\right] \\
I_3 &= \frac{-1}{8Ba(\tau)}\left[B(U - R(\tau) - U_0) + \delta\int U_\eta d\xi + \frac{B}{a(\tau)}(U - R(\tau) - U_0)^2 + \delta U_\eta + \frac{\delta^2}{B}\int U_{2\eta}d\xi\right] \\
&\cdots \\
I_{n+1} &= \frac{-1}{2B}\left[BI_n + B\sum I_k I_{n-k} + \delta\int I_{n,\eta}d\xi\right]
\end{aligned} \tag{2.30}$$

where $n = 3, 4, 5, \cdots$.

From the divergence equation (2.28), we have

$$\begin{aligned}
\sum I_{n,\tau}\epsilon^{-n} \quad & +\frac{\partial}{\partial\xi}(A(R(\tau)+U_0)\sum I_n\epsilon^{-n} + B\sum I_{n,2\xi}\epsilon^{-n} - 6\delta\sum\sum I_k\int I_{n-k,\eta}d\xi \\
& -6\delta\sum\int I_{n+1,\eta} - 2B\sum\sum I_i I_j I_k\epsilon^{-n} - 6B\epsilon\sum\sum I_k I_{n+1-k}\epsilon^n) \\
& +\frac{\partial}{\partial\eta}\left[C\sum\int I_{n,\eta}d\xi\epsilon^{-n} + 3\delta\sum\sum I_k I_{n-k}\epsilon^{-n} + 6\delta\sum I_{n+1}\epsilon^{-n}\right] = 0
\end{aligned} \tag{2.31}$$

which presents an infinite consequence of conservation laws as below,

$$I_{n,\tau} + \mathcal{F}_{n,\xi} + \mathcal{G}_{n,\eta} = 0 \tag{2.32}$$

for $n = 1, 2, 3, \cdots$

where the first fluxes $\mathcal{F}_n$'s are given by the recursion formulas

$$\begin{aligned}
\mathcal{F}_1 &= A\left(R(\tau)+U_0\right) I_1 + B I_{1,2\xi} - 6B I_1^2 - 6\delta \int I_{2,\eta}\, d\xi - A\left(R(\tau)+U_0\right)\frac{U - R(\tau) - U_0}{2a(\tau)} \\
&= -\frac{B U_{2\xi}}{2a(\tau)} - 6B\left(\frac{U - R(\tau) - U_0}{2a(\tau)}\right)^2 - \frac{6\delta}{4B}\int\left[\frac{B U_\eta}{a(\tau)} + \frac{\delta}{a(\tau)}\int U_{2\eta}\, d\xi\right] \\
\mathcal{F}_2 &= A\left(R(\tau)+U_0\right) I_2 + B I_{2,2\xi} - 6\delta I_1 \int I_{1,\eta}\, d\xi - 6\delta \int I_{3,\eta}\, d\xi \\
&= \frac{A\left(R(\tau)+U_0\right)}{4Ba(\tau)}\left[B(U - R(\tau) - U_0) + \delta\int U_\eta\, d\xi\right] - \frac{6\delta}{4a^2(\tau)}(U - R(\tau) - U_0)\int U_\eta\, d\xi + \frac{B U_{2\xi}}{4a(\tau)} \\
&\quad + \frac{\delta U_{\xi\eta}}{4a(\tau)} + \frac{3\delta}{4Ba(\tau)}\int\left[B U_\eta + \delta\int U_{2\eta}\, d\xi + \frac{2B}{a(\tau)}(U - R(\tau) - U_0)U_\eta + \delta U_\eta + \frac{\delta^2}{B}\int U_{2\eta}\, d\xi\right] d\xi \\
&\quad \cdots \\
\mathcal{F}_n &= A\left(R(\tau)+U_0\right) I_n + B I_{n,2x} - 2B \sum_{i+j+k=n} I_i I_j I_k - 6B\sum I_k I_{n+1-k} \\
&\quad -6\delta\sum I_k \int I_{n-k}\, d\xi - 6\delta\int I_{n+1,\eta}\, d\xi
\end{aligned} \tag{2.33}$$

where $n = 3, 4, \cdots$.

The second fluxes $\mathcal{G}_n$'s are given by

$$\begin{aligned}
\mathcal{G}_1 &= C\int I_{1,\eta}\, d\xi + 6\delta I_2 = \frac{3\delta}{2a(\tau)}(U - R(\tau) - U_0) \\
\mathcal{G}_2 &= C\int I_{2,\eta}\, d\xi + 3\delta I_1^2 + 6\delta I_3 \\
&= \frac{C\delta}{4Ba(\tau)}\int\int U_{2\eta}\, d\xi - \frac{3\delta}{4Ba(\tau)}\left[B(U - R(\tau)) + \delta U_\eta + \frac{\delta^2}{B}\int U_{2\eta}\, d\xi\right] \\
&\cdots \\
\mathcal{G}_n &= C\int I_{n,\eta}\, d\xi + 3\delta\sum I_k I_{n-k} + 6\delta I_{n+1}.
\end{aligned} \tag{2.34}$$

where $n = 3, 4, 5, \cdots$

Finally, we construct an infinite conservation laws with the help of the recursion formulas addressed in the equations (2.34),(2.33) and (2.31). For $n = 1$, the first conservation law is

$$\begin{aligned}
I_{1,\tau} + \mathcal{F}_{1,\xi} + \mathcal{G}_{1,\eta} &= -\frac{U_\tau}{2a(\tau)} + \frac{U a'(\tau)}{2a^2(\tau)} + \frac{R'(\tau)}{2a(\tau)} - \frac{R(\tau)a'(\tau)}{2a^2(\tau)} - \frac{B}{2a(\tau)}U_{3\xi} - \frac{3\delta}{2a(\tau)}U_\eta - \\
&\quad \frac{3\delta^2}{2Ba(\tau)}\int U_{2\eta}\, d\xi - \frac{3B}{a^2(\tau)}U U_\xi + \frac{3\delta}{2a(\tau)}U_\eta \\
&= -\frac{1}{2a(\tau)}\left[U_\tau + DU - f(\tau) + B U_{3\xi} + C\int U_{2\eta}\, d\xi + A U U_\xi\right]
\end{aligned} \tag{2.35}$$

which is exactly the the NKP equation (2.2). For our NKP equation (2.2), the expressions (2.33) and (2.34) indicate that conserved densities $\mathcal{F}_n$'s and the fluxes $\mathcal{G}_n$'s are all local. Therefore, the NKP equation is completely integrable in the sense that it admits bilinear Bäcklund transformation, Lax pair and local infinite conservation laws.

2.5 Solutions for NKP equation

The present section is divided into three parts. Firstly, the Quasi-periodic solutions of the NKP Equation are derived and in the limiting stage, the Quasi-periodic solutions are reduced into the soliton solutions. Secondly, we present the lump-type solutions for Eq.(2.2). In the third subsection, the breather wave of the said equation is constructed. The wave solution together with its novel features is discussed in this section in detail. Under the compatibility condition $A = \frac{6B}{a_0}e^{D\tau}$, using results $a(\tau) = a_0e^{-D\tau}$ and $R(\tau) = e^{-D\tau}\left(\int e^{D\tau}f(\tau)d\tau + R_0\right) - U_0$, obtained from Eq.(2.4), the perturbation method is employed to explore different types of solutions for the NKP equation via the bilinear equation (2.10).

2.5.1 Quasi-periodic wave solutions

For producing the multi-periodic wave solutions, initially we consider N-dimensional Riemann theta function defined as,

$$\mathcal{V} = \mathcal{V}(\Theta) = \mathcal{V}(\Theta, \rho) = \sum_{g \in Z^N} exp(\pi i\langle \rho g\ ,\ g\rangle + 2\pi i\langle \Theta\ ,\ g\rangle). \tag{2.36}$$

Here, $g = (g_1, g_2, \cdots, g_N)^T$, $\Theta = (\Theta_1, \Theta_2, \cdots, \Theta_N)^T$, $\Theta_i = \mu_i\xi + \nu_i\eta + \Omega_i\tau + \delta_i$, $i = 1, 2, \cdots, N$, and $\rho = [\rho_{ij}]_{N\times N}$ is symmetric matrix where $Im(\rho) > 0$, and $\langle\ ,\ \rangle$ denotes the inner product defined by $\langle a\ ,\ b\rangle = a_1b_1 + a_2b_2 + ... + a_Nb_N$, for two vectors $a = (a_1, a_2, \cdots, a_N)^T, b = (b_1, b_2, \cdots, b_N)^T$.

2.5.1.1 One-periodic wave solution

To generate one-periodic solution, we put $N = 1$ in Riemann-theta function and get,

$$\mathcal{V} = \mathcal{V}(\Theta) = \mathcal{V}(\Theta, \rho) = \sum_{g=-\infty}^{\infty} exp(\pi i g^2\rho + 2\pi i g\Theta). \tag{2.37}$$

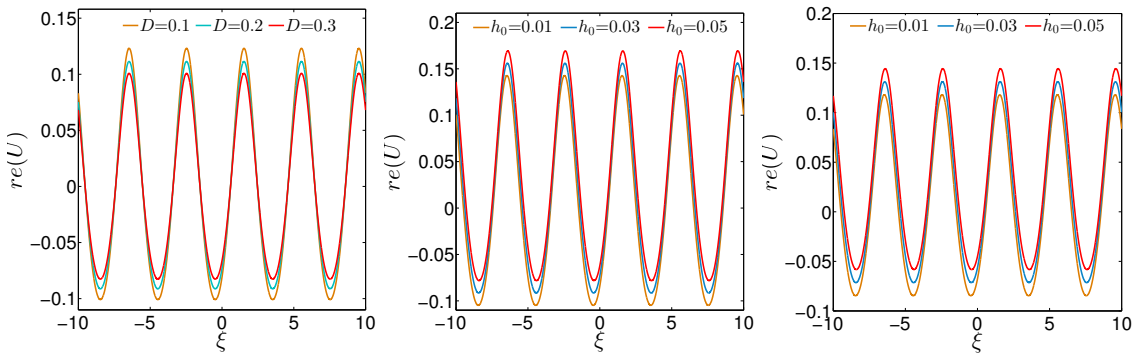

(a) (b) (c)

Figure 2.1: 2D Plots of quasiperiodic solution for (2.50), by taking $\mathrm{f}(\tau) = \mathrm{h}_0 \cos(\omega\tau)$, $\mu = 0.5$, $\nu = -0.5$, $\mathrm{A} = 2$, $\mathrm{B} = 1$, $\rho = 2.5\mathrm{i}$, $\eta = 1$, $\mathrm{C} = 2$, $\tau = 1$; and (a) for $\mathrm{h}_0 = 0$, (b) for $\mathrm{D} = 0$, (c) for $\mathrm{D} = 0.2$.

Now, putting Eq.(2.37) into the bilinear equation (2.10) we get,

$$\begin{aligned}
\mathcal{J}(\mathrm{D}_\xi, \mathrm{D}_\eta, \mathrm{D}_\tau)\mathcal{V}(\Theta)\cdot\mathcal{V}(\Theta) &= \mathcal{J}(\mathrm{D}_\xi, \mathrm{D}_\eta, \mathrm{D}_\tau)\sum_{g=-\infty}^{\infty} exp(\pi i g^2\rho + 2\pi i g\Theta)\cdot\sum_{m=-\infty}^{\infty} exp(\pi i m^2\rho + 2\pi i m\Theta)\\
&= \sum_{g=-\infty}^{\infty}\sum_{m=-\infty}^{\infty}\mathcal{J}(\mathrm{D}_\xi, \mathrm{D}_\eta, \mathrm{D}_\tau)exp(\pi i g^2\rho + 2\pi i g\Theta)\cdot exp(\pi i m^2\rho + 2\pi i m\Theta)\\
&= \sum_{g=-\infty}^{\infty}\sum_{m=-\infty}^{\infty}\mathcal{J}(2\pi i(g-m)\mu, 2\pi i(g-m)\nu, 2\pi i(g-m)\Omega)\\
&\quad exp(\pi i(g^2+m^2)\rho + 2\pi i(g+m)\Theta)\\
&= \sum_{g=-\infty}^{\infty}\sum_{m=-\infty}^{\infty}\mathcal{J}(2\pi i(2g-(g+m))\mu, 2\pi i(2g-(g+m))\nu,\\
&\quad 2\pi i(g-(g+m))\Omega)exp(\pi i(g^2+(g-(g+m))^2)\rho + 2\pi i(g+m)\Theta)\\
&= \sum_{m'=-\infty}^{\infty}\{\sum_{g=-\infty}^{\infty}\mathcal{J}(2\pi i(2g-m')\mu, 2\pi i(2g-m')\nu, 2\pi i(2g-m')\Omega)\\
&\quad exp(\pi i(g^2+(g-m')^2)\rho)\}exp(2\pi i m'\Theta), m' = m+g\\
&= \sum_{m'=-\infty}^{\infty}\overline{\mathcal{J}}(m')exp(2\pi i m'\Theta) \qquad (2.38)
\end{aligned}$$

where

$$\overline{\mathcal{J}}(m') = \sum_{g=-\infty}^{\infty}\mathcal{J}(2\pi i(2g-m')\mu, 2\pi i(2g-m')\nu, 2\pi i(2g-m')\Omega)exp(\pi i(g^2+(g-m')^2)\rho) \quad (2.39)$$

Now by making $g' = g - 1$, $\overline{\jmath}(m')$ can be expressed as

$$\begin{aligned}
\overline{\jmath}(m') &= \sum_{g'=-\infty}^{\infty} \jmath(2\pi i[2g' - (m'-2)]\mu, 2\pi i[2g' - (m'-2)]\nu, 2\pi i[2g' - (m'-2)]\Omega) \\
&\quad \exp(\pi i(g'^2 + [g' - (m'-2)]^2)\rho) \cdot \exp(2\pi i(m'-1)\rho) \\
&= \overline{\jmath}(m'-2)\exp(2\pi i(m'-1)\rho) \\
&= \cdots \\
&= \overline{\jmath}(0)\exp(\pi i m'\rho), \quad m' \text{ is even} \\
&\quad \overline{\jmath}(1)\exp(2\pi i(m'-1)\rho), \quad m' \text{ is odd.}
\end{aligned} \tag{2.40}$$

Thus, we have seen from (2.40) that the NKP approves one-periodic wave solution only when, $\overline{\jmath}(0) = 0$ and $\overline{\jmath}(1) = 0$, therefore we have

$$\sum_{g=-\infty}^{\infty} \jmath[4\pi g i\mu, 4\pi g i\nu, 4\pi g i\Omega]\exp(2\pi i g^2\rho) = 0 \tag{2.41}$$

$$\sum_{g=-\infty}^{\infty} \jmath[2\pi(2g-1)i\mu, 2\pi(2g-1)i\nu, 2\pi(2g-1)i\Omega]\exp(\pi i(2g^2 - 2g + 1)\rho) = 0 \tag{2.42}$$

Utilizing the above conditions along with the bilinear form (2.10) we get,

$$\begin{aligned}
\overline{\jmath}(0) = \sum_{g=-\infty}^{\infty} &(-16g^2\pi^2\mu\Omega - 16AR(\tau)g^2\pi^2\mu^2 - 16Cg^2\pi^2\nu^2 + 256Bg^4\pi^4\mu^4 \\
&- 16AU_0g^2\pi^2\mu^2 + c_0)\exp(2\pi i g^2\rho) = 0
\end{aligned} \tag{2.43}$$

$$\begin{aligned}
\overline{\jmath}(1) = \sum_{g=-\infty}^{\infty} &(-4(2g-1)^2\pi^2\mu\Omega - 4AR(\tau)(2g-1)^2\pi^2\mu^2 - 4C(2g-1)^2\pi^2\nu^2 + 16B(2g-1)^4\pi^4\mu^4 \\
&- 4AU_0(2g-1)^2\pi^2\mu^2 + c_0)\exp((2g^2 - 2g + 1)\pi i\rho) = 0
\end{aligned} \tag{2.44}$$

Now, Eq.(2.43) and Eq.(2.44) can be written in a linear system of Ω and c_0 as,

$$\begin{pmatrix} e_{11} & e_{12} \\ e_{21} & e_{22} \end{pmatrix} \begin{pmatrix} \Omega \\ c_0 \end{pmatrix} = \begin{pmatrix} e_{13} \\ e_{23} \end{pmatrix} \tag{2.45}$$

where

$$e_{11} = -\sum_{g=-\infty}^{\infty} 16g^2\pi^2\mu\, \exp(2\pi i g^2\rho), \quad e_{12} = \sum_{g=-\infty}^{\infty} \exp(2\pi i g^2\rho)$$

$$e_{21} = -\sum_{g=-\infty}^{\infty} 4(2g-1)^2\pi^2\mu\, \exp((2g^2-2g+1)\pi i\rho), \quad e_{22} = \sum_{g=-\infty}^{\infty} \exp((2g^2-2g+1)\pi i\rho)$$

$$e_{13} = \sum_{g=-\infty}^{\infty} (16AR(\tau)g^2\pi^2\mu^2 + 16Cg^2\pi^2\nu^2 - 256Bg^4\pi^4\mu^4 + 16AU_0g^2\pi^2\mu^2)\exp(2\pi i g^2\rho)$$

$$e_{23} = \sum_{g=-\infty}^{\infty} (4AR(\tau)(2g-1)^2\pi^2\mu^2 + 4C(2g-1)^2\pi^2\nu^2 - 16B(2g-1)^4\pi^4\mu^4 + 4AU_0(2g-1)^2\pi^2\mu^2)$$
$$\exp((2g^2-2g+1)\pi i\rho). \tag{2.46}$$

Now solving the linear system (2.45) we have

$$\Omega = \frac{e_{13}e_{22} - e_{12}e_{23}}{e_{11}e_{22} - e_{12}e_{21}}, \quad c_0 = \frac{e_{21}e_{13} - e_{11}e_{23}}{e_{12}e_{21} - e_{11}e_{22}}, \tag{2.47}$$

provided $e_{11}e_{22} - e_{12}e_{21} = A_1\mu \neq 0$, where

$$\begin{aligned} A_1 \;=\; & -16\pi^2 \sum_{g=-\infty}^{\infty} g^2 \exp(2\pi i g^2\rho) \sum_{g=-\infty}^{\infty} \exp((2g^2-2g+1)\pi i\rho) \\ & +4\pi^2 \sum_{g=-\infty}^{\infty} \exp(2\pi i g^2\rho) \sum_{g=-\infty}^{\infty} (2g-1)^2 \exp((2g^2-2g+1)\pi i\rho) \end{aligned} \tag{2.48}$$

Assuming real part of $\rho = 0$ and using mathematica software we compute $A_1 \approx 2.79847$ for $\rho = 0.2i$; $A_1 \approx 12.4452$ for $\rho = 0.5i$; $A_1 \approx 0.708949$ for $\rho = 1.5i$; $A_1 \approx 0.0306513$ for $\rho = 2.5i$, and thus, $A_1\mu \neq 0$ for non-zero μ. So, Eq. (2.47) has real solution, and therefore, we will get the one-periodic wave solution of NKP equation as

$$U = 2a_0 e^{-D\tau}\left[\frac{\partial^2}{\partial\xi^2}\ln\left(\sum_{g=-\infty}^{\infty}\exp(\pi i g^2\rho + 2\pi i g\Theta)\right)\right] + e^{-D\tau}\left(\int e^{D\tau} f(\tau)d\tau + R_0\right), \tag{2.49}$$

which gives

$$\begin{aligned} U = -2a_0 e^{-D\tau}\Bigg[& \frac{\sum_{g=-\infty}^{\infty} 4\pi^2 g^2\mu^2 \exp(\pi i g^2\rho + 2\pi i g\Theta)}{\sum_{g=-\infty}^{\infty}\exp(\pi i g^2\rho + 2\pi i g\Theta)} + \frac{\left(\sum_{g=-\infty}^{\infty} 2\pi i g\mu\, \exp(\pi i g^2\rho + 2\pi i g\Theta)\right)^2}{\left(\sum_{g=-\infty}^{\infty}\exp(\pi i g^2\rho + 2\pi i g\Theta)\right)^2}\Bigg] \\ & + e^{-D\tau}\left(\int e^{D\tau} f(\tau)d\tau + R_0\right) \end{aligned} \tag{2.50}$$

with Ω, c_0 given by Eq.(2.47) while other parameters are free.

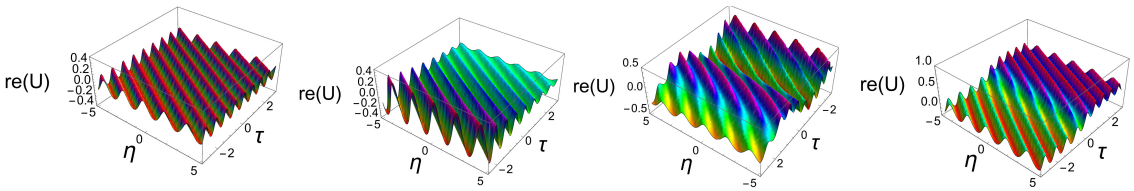

(a) (b) (c) (d)

Figure 2.2: 3D Plots of quasiperiodic solution for (2.50), by taking $f(\tau) = h_0 \cos(\omega\tau)$, $\mu = 0.5$, $\nu = -0.5$, $A = 2$, $B = 1$, $\rho = 2.5i$, $\eta = 1$, $C = 2$, $\tau = 1$ and (a) for $h_0 = 0$, (b) for $D = 0$, (c) for $D = 0.1$; (d) for $f(\tau) = h_0\, sech^2(\omega\tau)$, $h_0 = 0 = 0.1$, $D = 0.05$.

2.5.1.2 Two-periodic wave solution

To construct two-periodic solution, we choose $N = 2$ in Riemann-theta function and thus, we get

$$\mathcal{V} = \mathcal{V}(\Theta, \rho) = \mathcal{V}(\Theta_1, \Theta_2, \rho) = \sum_{g \in Z^2} exp(\pi i\langle \rho g\ ,\ g\rangle + 2\pi i\langle \Theta\ ,\ g\rangle) \tag{2.51}$$

where $g = (g_1, g_2)^T \in Z^2$, $\Theta = (\Theta_1, \Theta_2)^T \in C^2$, $\Theta_i = \mu_i\xi + \nu_i\eta + \Omega_i\tau + \delta_i$, $i = 1, 2$ and $\rho = \begin{pmatrix} \rho_{11} & \rho_{12} \\ \rho_{12} & \rho_{22} \end{pmatrix}$,
$Im(\rho_{11}) > 0$, $Im(\rho_{22}) > 0$, $\rho_{11}\rho_{22} - \rho_{12}^2 < 0$. We set $m = (m_1, m_2)^T$, $\mu = (\mu_1, \mu_2)^T$, $\nu = (\nu_1, \nu_2)^T$, $\Omega = (\Omega_1, \Omega_2)^T$, $\delta = (\delta_1, \delta_2)^T$. In order to find sufficient conditions for NKP's two-periodic solution, we need to convert Eq.(2.1) into the bilinear equation (2.10), as follows:

$$\begin{aligned}
\mathcal{J}(D_\xi, D_\eta, D_\tau)\mathcal{V}\cdot\mathcal{V} &= \sum_{m,g\in Z^2} \mathcal{J}(D_\xi, D_\eta, D_\tau) exp(\pi i\langle g\rho\ ,\ g\rangle + 2\pi i\langle \Theta\ ,\ g\rangle) \\
&\quad exp(\pi i\langle m\rho\ ,\ m\rangle + 2\pi i\langle \Theta\ ,\ m\rangle) \\
&= \sum_{m,g\in Z^2} \mathcal{J}(2\pi i\langle g - m\ ,\ \mu\rangle, 2\pi i\langle g - m\ ,\ \nu\rangle, 2\pi i\langle g - m\ ,\ \Omega\rangle) \\
&\quad exp(2\pi i\langle \Theta\ , g + m\rangle + \pi i\langle m\rho\ ,\ m\rangle + \pi i\langle g\rho\ ,\ g\rangle) \\
&= \sum_{m'\in Z^2} \{ \sum_{g\in Z^2} \mathcal{J}(2\pi i\langle 2g - m'\ ,\ \mu\rangle, 2\pi i\langle 2g - m'\ ,\ \nu\rangle, 2\pi i\langle 2g - m'\ ,\ \Omega\rangle) \\
&\quad exp(\pi i[\langle (g - m')\rho\ ,\ g - m'\rangle + \langle g\rho\ ,\ g\rangle])\} exp(2\pi i\langle \Theta\ ,\ m'\rangle), m' = m + g \\
&= \sum_{m'\in Z^2} \bar{\mathcal{J}}(m_1', m_2') exp(2\pi i\langle \Theta\ ,\ m'\rangle)
\end{aligned} \tag{2.52}$$

Now by transferring the index g as $g = g' - \epsilon_{ij}$, and putting $j = 1, 2$, we get

$$\begin{aligned}
\overline{\jmath}(m_1', m_2') &= \sum_{g\in Z^2} \jmath(2\pi i\langle 2g - m' \ , \ \mu\rangle, 2\pi i\langle 2g - m' \ , \ \nu\rangle, 2\pi i\langle 2g - m' \ , \ \Omega\rangle) \\
&\quad exp(\pi i[\langle (g - m')\rho \ , \ g - m'\rangle + \langle g\rho \ , \ g\rangle]) \\
&= \sum_{g\in Z^2} \jmath(2\pi i \sum_{i=1}^{2}[2g_i' - (m_i' - 2\epsilon_{ij})]\mu_i, 2\pi i \sum_{i=1}^{2}[2g_i' - (m_i' - 2\epsilon_{ij})]\nu_i, \\
&\quad 2\pi i \sum_{i=1}^{2}[2g_i' - (m_i' - 2\epsilon_{ij})]\Omega_i) exp(\pi i \sum_{i,k=1}^{2}[(g_i' + \epsilon_{ij})(g_k' + \epsilon_{kj}) \\
&\quad + (m_i' - g_i' - \epsilon_{ij})(m_k' - g_k' - \epsilon_{kj})]\rho_{ik}) \\
&= \begin{cases} \overline{\jmath}(m_1' - 2, m_2') exp(2\pi i(m_1' - 1)\rho_{11} + 2\pi i m_2'\rho_{12}), & j = 1, \\ \overline{\jmath}(m_1', m_2' - 2) exp(2\pi i(m_2' - 1)\rho_{22} + 2\pi i m_1'\rho_{12}), & j = 2, . \end{cases}
\end{aligned} \tag{2.53}$$

Thus, we have observed from (2.53) that the NKP approves a solution presenting two-periodic wave structure if $\overline{\jmath}(0,0) = 0$, $\overline{\jmath}(1,0) = 0$, $\overline{\jmath}(0,1) = 0$ and $\overline{\jmath}(1,1) = 0$, therefore we have

$$\sum_{g\in Z^2} \jmath(2\pi i\langle 2g-\phi_1 \ , \ \mu\rangle, 2\pi i\langle 2g-\phi_1 \ , \ \nu\rangle, 2\pi i\langle 2g-\phi_1 \ , \ \Omega\rangle) exp(\pi i[\langle (g-\phi_1)\rho \ , \ g-\phi_1\rangle + \langle g\rho \ , \ g\rangle]) = 0 \tag{2.54}$$

$$\sum_{g\in Z^2} \jmath(2\pi i\langle 2g-\phi_2 \ , \ \mu\rangle, 2\pi i\langle 2g-\phi_2 \ , \ \nu\rangle, 2\pi i\langle 2g-\phi_2 \ , \ \Omega\rangle) exp(\pi i[\langle (g-\phi_2)\rho \ , \ g-\phi_2\rangle + \langle g\rho \ , \ g\rangle]) = 0 \tag{2.55}$$

$$\sum_{g\in Z^2} \jmath(2\pi i\langle 2g-\phi_3 \ , \ \mu\rangle, 2\pi i\langle 2g-\phi_3 \ , \ \nu\rangle, 2\pi i\langle 2g-\phi_3 \ , \ \Omega\rangle) exp(\pi i[\langle (g-\phi_3)\rho \ , \ g-\phi_3\rangle + \langle g\rho \ , \ g\rangle]) = 0 \tag{2.56}$$

$$\sum_{g\in Z^2} \jmath(2\pi i\langle 2g-\phi_4 \ , \ \mu\rangle, 2\pi i\langle 2g-\phi_4 \ , \ \nu\rangle, 2\pi i\langle 2g-\phi_4 \ , \ \Omega\rangle) exp(\pi i[\langle (g-\phi_4)\rho \ , \ g-\phi_4\rangle + \langle g\rho \ , \ g\rangle]) = 0 \tag{2.57}$$

$$where \quad \phi_i = (\phi_i^1, \phi_i^2)^T, \phi_1 = (0,0)^T, \phi_2 = (1,0)^T, \phi_3 = (0,1)^T, \phi_4 = (1,1)^T, i = 1,2,3,4.$$

Now, combining Eq.(2.10) and Eqs.(2.54)-(2.57) we get

$$\begin{aligned}
&\sum_{g\in Z^2} \jmath(-4\pi^2\langle 2g - \phi_i, \mu\rangle\langle 2g - \phi_i, \Omega\rangle - 4AR(\tau)\pi^2\langle 2g - \phi_i, \mu\rangle^2 - 4C\pi^2\langle 2g - \phi_i, \nu\rangle^2 + 16B\pi^4 \times \\
&\langle 2g - \phi_i, \mu\rangle^4 - 4AU_0\pi^2\langle 2g - \phi_i \ , \ \mu\rangle^2 + c_0) exp(\pi i[\langle (g - \phi_i)\rho \ , \ g - \phi_i\rangle + \langle g\rho \ , g\rangle]) = 0.
\end{aligned} \tag{2.58}$$

Let $P = (p_{ij})$, i,j=1,2,3,4 and $r = (r_1, r_2, r_3, r_4)^T$ then, Eq.(2.58) can be written as linear system as

$$\begin{pmatrix} p_{11} & p_{12} & p_{13} & p_{14} \\ p_{21} & p_{22} & p_{23} & p_{24} \\ p_{31} & p_{32} & p_{33} & p_{34} \\ p_{41} & p_{42} & p_{43} & p_{44} \end{pmatrix} \begin{pmatrix} \Omega_1 \\ \Omega_2 \\ U_0 \\ c_0 \end{pmatrix} = \begin{pmatrix} r_1 \\ r_2 \\ r_3 \\ r_4 \end{pmatrix} \tag{2.59}$$

where

$$p_{i1} = -4\pi^2 \sum_{(g_1,g_2)\in Z^2} \langle 2g-\phi_i\ ,\ \mu\rangle(2g_1-\phi_i^1)exp(\pi i\rho_{11}[(g_1-\phi_i^1)^2+g_1^2]+\pi i\rho_{22}$$
$$[(g_2-\phi_i^2)^2+g_2^2]+2\pi i\rho_{12}[(g_1-\phi_i^1)(g_2-\phi_i^2)+g_1g_2]), \tag{2.60}$$

$$p_{i2} = -4\pi^2 \sum_{(g_1,g_2)\in Z^2} \langle 2g-\phi_i\ ,\ \mu\rangle(2g_2-\phi_i^2)exp(\pi i\rho_{11}[(g_1-\phi_i^1)^2+g_1^2]+\pi i\rho_{22}$$
$$[(g_2-\phi_i^2)^2+g_2^2]+2\pi i\rho_{12}[(g_1-\phi_i^1)(g_2-\phi_i^2)+g_1g_2]), \tag{2.61}$$

$$p_{i3} = -4A\pi^2 \sum_{(g_1,g_2)\in Z^2} \langle 2g-\phi_i\ ,\ \mu\rangle^2 exp(\pi i\rho_{11}[(g_1-\phi_i^1)^2+g_1^2]+\pi i\rho_{22}$$
$$[(g_2-\phi_i^2)^2+g_2^2]+2\pi i\rho_{12}[(g_1-\phi_i^1)(g_2-\phi_i^2)+g_1g_2]), \tag{2.62}$$

$$p_{i4} = \sum_{(g_1,g_2)\in Z^2} exp(\pi i\rho_{11}[(g_1-\phi_i^1)^2+g_1^2]+\pi i\rho_{22}$$
$$[(g_2-\phi_i^2)^2+g_2^2]+2\pi i\rho_{12}[(g_1-\phi_i^1)(g_2-\phi_i^2)+g_1g_2]), \tag{2.63}$$

$$r_i = \sum_{(g_1,g_2)\in Z^2} (4AR(\tau)\pi^2\langle 2g-\phi_i\ ,\ \mu\rangle^2+4C\pi^2\langle 2g-\phi_i\ ,\ \nu\rangle^2-16B\pi^4\langle 2g-\phi_i\ ,\ \mu\rangle^4)exp(\pi i\rho_{11}$$
$$[(g_1-\phi_i^1)^2+g_1^2]+\pi i\rho_{22}[(g_2-\phi_i^2)^2+g_2^2]+2\pi i\rho_{12}[(g_1-\phi_i^1)(g_2-\phi_i^2)+g_1g_2]), \tag{2.64}$$
$$\text{for}\ \ i=1,2,3,4.$$

Now by solving the linear system (2.59), we will obtain two-periodic wave solution of NKP as

$$U = 2a_0e^{-D\tau}\left[\frac{\partial^2}{\partial\xi^2}ln\left(\sum_{g\in Z^2} exp(\pi i\langle\rho g\ ,\ g\rangle+2\pi i\langle\Theta\ ,\ g\rangle)\right)\right]+e^{-D\tau}\left(\int e^{D\tau}f(\tau)d\tau+R_0\right), \tag{2.65}$$

which written as

$$U = 2a_0e^{-D\tau}\left[\frac{\partial^2}{\partial\xi^2}ln\left(\sum_{g_1,g_2\in Z} exp\{\pi i(\rho_{11}g_1^2+2\rho_{12}g_1g_2+\rho_{22}g_2^2)+2\pi i(\Theta_1g_1+\Theta_2g_2)\}\right)\right]$$
$$+e^{-D\tau}\left(\int e^{D\tau}f(\tau)d\tau+R_0\right), \tag{2.66}$$

with $\Omega_1,\Omega_2,U_0,c_0$ given by Eq.(2.59), while other parameters are free.

Now, we express some numerical discussions on the impact of forcing and damping terms in quasi-periodic waves. Figure 2.1, Figure 2.2 are devoted for describing the propagation characteristics of one-periodic wave via solution (2.73). The other parameters s, l,δ_i and τ are free. Figure 2.1(a)

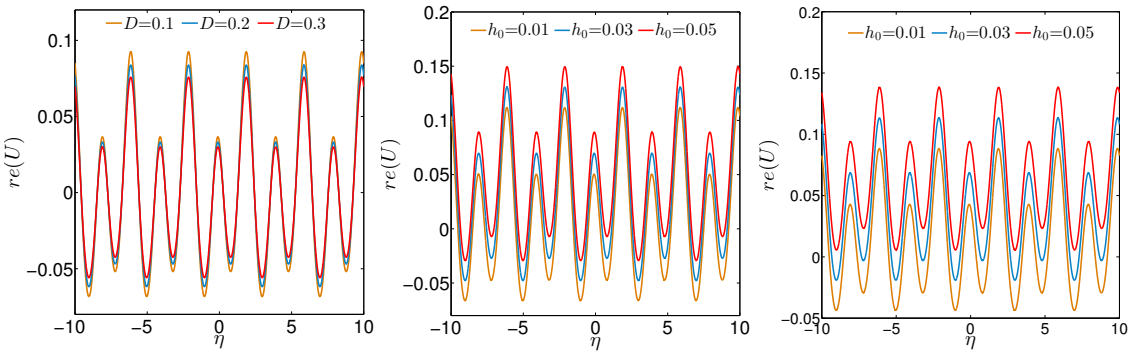

(a) (b) (c)

Figure 2.3: 2D Profiles of 2-periodic solution, when $f(\tau) = h_0 \cos(\omega\tau)$, $\mu_1 = -0.25$, $\mu_2 = 0.25$, $\nu_1 = 0.5$, $\nu_2 = 0.5$, $\xi = 1$, $A = 3$, $B = 1$, $\nu = 0; \omega = 1$, $C = 2$, $\rho_{11} = 2.5i$, $\rho_{22} = 2.5i$, $\tau = 0.5$, $a_0 = 1, R_0 = 0$ and (a) for $h_0 = 0$, (b) for $D = 0$, (c) for $D = 0.2$

depicts the diminishing effect of damping when there is no externally applied forcing ($f(\tau) = 0$) in the system. Figure 2.1(b) illuminates the effect of forcing (in the absence of damping) which causes to increase in the amplitude of the periodic wave. However, Figure 2.1(c) presents the effect of the strength of forcing when damping also associates ($D = 0.1$) in the system. Here, we see the comparatively smaller amplitude of periodic wave in Figure 2.1(b) than that of Figure 2.1(c), as a major role is played here by the negatively exponential function associated with the damping term. Figure 2.2(a) beautifully presents the propagation of one-periodic wave U in η-τ-plane, when there are no forcing and damping ($D = 0$, $f(\tau) = 0$). The one-periodic wave can be viewed as a parallel superposition of overlapping one-soliton waves, placed one period apart. Figure 2.2(b) shows the shape of the one-periodic wave U in the presence of damping. Here, the periodic wave strictly diminishes due to the act of damping. Figure 2.2(c) exhibits the propagation of one-periodic wave U the influence of the trigonometric forcing term. The background of wave structure in Figure 2.2(c) appears to be periodic due to the act of periodic force. Again, The kink periodic type wave structure has been found in Figure 2.2(d). This type of structure forms because of the acting of hyperbolic force.

From Figure 2.3, we can observe that the two-periodic wave is a direct generalization of the one-periodic wave, but it is not necessarily periodic in both the ξ and η directions during the propagation. Figure 2.3(a)-Figure 2.3(c) show that effects of damping and forcing on the two-periodic wave. We see the similar effects of damping and forcing terms in two-periodic waves as seen in one periodic wave. Figure 2.4(a)-Figure 2.4(c) exhibit three dimensional views of two periodic waves in both the η and τ directions. Figure 2.4(b) and Figure 2.4(c) respectively show the propagation of two periodic waves when periodic and hyperbolic forcing components are externally applied.

2.5.1.3 Asymptotic property of one-periodic wave solutions

In this subsection, we intend to present the asymptotic property of one-periodic wave. We introduce a new exponential transformation as $\beta = \exp(\pi i \rho)$, and thus, (2.44) can be improved in a series of β. Initially, we start with the computations as follows,

$$\begin{aligned}
e_{11} &= -\sum_{g=-\infty}^{\infty} 16g^2\pi^2\mu\, \exp(2\pi i g^2\rho) \\
&= -32\pi^2\mu(\beta^2 + 4\beta^8 + 9\beta^{18} + \cdots), \\
e_{12} &= \sum_{g=-\infty}^{\infty} \exp(2\pi i g^2\rho), \\
&= 1 + 2\beta^2 + 2\beta^8 + 2\beta^{18} + \cdots, \\
e_{21} &= -\sum_{g=-\infty}^{\infty} 4(2g-1)^2\pi^2\mu\, \exp((2g^2-2g+1)\pi i\rho), \\
&= -8\pi^2\mu(\beta + 9\beta^5 + 25\beta^{13} + \cdots), \qquad (2.67) \\
e_{22} &= \sum_{g=-\infty}^{\infty} \exp((2g^2-2g+1)\pi i\rho), \\
&= 2\beta + 2\beta^5 + 2\beta^{13} + \cdots, \\
e_{13} &= \sum_{g=-\infty}^{\infty} (16AR(\tau)g^2\pi^2\mu^2 + 16Cg^2\pi^2\nu^2 - 256Bg^4\pi^4\mu^4 + 16AU_0g^2\pi^2\mu^2)\, \exp(2\pi i g^2\rho) \\
&= 32\pi^2(AR(\tau)\mu^2 + C\nu^2 - 16B\pi^2\mu^4 + AU_0\mu^2)\beta^2 + 128\pi^2(AR(\tau)\mu^2 + C\nu^2 - 64B\pi^2\mu^4 \\
&\qquad + AU_0\mu^2)\beta^8 + 288\pi^2(AR(\tau)\mu^2 + C\nu^2 - 144B\pi^2\mu^4 + AU_0\mu^2)\beta^{18} + \cdots, \\
e_{23} &= \sum_{g=-\infty}^{\infty} (4AR(\tau)(2g-1)^2\pi^2\mu^2 + 4C(2g-1)^2\pi^2\nu^2 - 16B(2g-1)^4\pi^4\mu^4 + 4AU_0(2g-1)^2\pi^2\mu^2) \\
&\qquad \exp((2g^2-2g+1)\pi i\rho), \\
&= 8\pi^2(AR(\tau)\mu^2 + C\nu^2 - 4B\pi^2\mu^4 + AU_0\mu^2)\beta + 72\pi^2(AR(\tau)\mu^2 + C\nu^2 - 36B\pi^2\mu^4 + AU_0\mu^2)\beta^5 \\
&\qquad + 200\pi^2(AR(\tau)\mu^2 + C\nu^2 - 100B\pi^2\mu^4 + AU_0\mu^2)\beta^{13} + \cdots,
\end{aligned}$$

Now from (2.67) we have

$$\begin{aligned}
e_{11}e_{22} - e_{12}e_{21} &= 8\pi^2\mu\beta + o(\beta), \\
e_{13}e_{22} - e_{23}e_{12} &= 8\pi^2(AR(\tau)\mu^2 + C\nu^2 - 4B\pi^2\mu^4 + AU_0\mu^2)\beta + o(\beta), \qquad (2.68) \\
-e_{13}e_{21} + e_{23}e_{11} &= o(\beta)
\end{aligned}$$

Let

$$U_0 = 0,\ \mu = \frac{s}{2\pi i},\ \nu = \frac{l}{2\pi i},\ \delta = \frac{\sigma - \pi i\rho}{2\pi i}, \qquad (2.69)$$

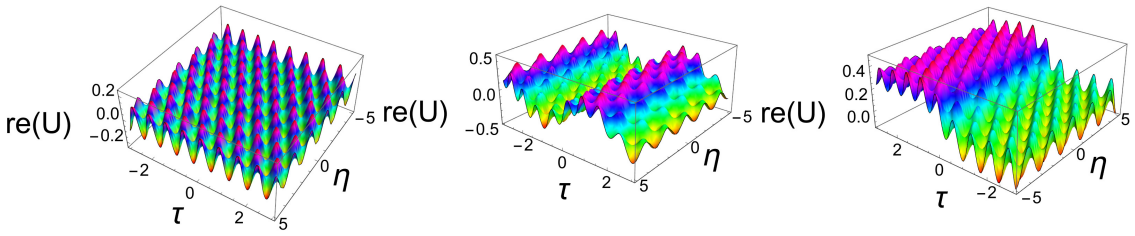

(a) (b) (c)

Figure 2.4: 3D Profiles of 2-periodic solution, when $f(\tau) = h_0\,\mathrm{cos}(\omega\tau)$, $\mu_1 = -0.25$, $\mu_2 = 0.25$, $\nu_1 = 0.5$, $\nu_2 = 0.5$, $\xi = 1$, $A = 3$, $B = 1$, $\nu = 0; \omega = 1$, $C = 2$, $\rho_{11} = 2.5i$, $\rho_{22} = 2.5i$, $\tau = 0.5$, $a_0 = 1$ and (a) for $h_0 = 0$, $D = 0.1$, (b) for $D = 0.1$, $h_0 = 0.05$, (c) for $f(\tau) = h_0\,\mathrm{sech}^2(\omega\tau)$ and $D = 0.2$, $h_0 = 0.1$.

then by using (2.47) we have $2\pi i\Omega \to -(AR(\tau)k + \frac{Cl^2+Bk^4}{k})$ and $c_0 \to 0$ as $\beta \to 0$

$$\begin{aligned} \mathcal{V}(\Theta,\rho) &= 1 + (\exp(2\pi i\Theta) + \exp(-2\pi i\Theta))\beta + (\exp(4\pi i\Theta) + \exp(-4\pi i\Theta))\beta^4 + \cdots, \\ &= 1 + \exp(\bar{\Theta}) + (\exp(-\bar{\Theta}) + \exp(2\bar{\Theta}))\beta^2 + (\exp(-2\bar{\Theta}) + \exp(3\bar{\Theta}))\beta^6 + \cdots, \\ &\to 1 + \exp(\bar{\Theta}) \quad \text{as} \quad \beta \to 0. \end{aligned} \tag{2.70}$$

Where

$$\begin{aligned} \bar{\Theta} = 2\pi i\Theta + \pi i\rho &= s\xi + l\eta + 2\pi i\Omega t + \sigma \\ &\to s\xi + l\eta - (AR(\tau)s + \frac{Cl^2 + Bs^4}{s})t + \sigma = \Psi \quad \text{as} \quad \beta \to 0. \end{aligned} \tag{2.71}$$

Thus, when $\beta \to 0$, we further derive

$$\mathcal{V}(\Theta,\rho) \to 1 + \exp(\Psi) \tag{2.72}$$

which confirms that periodic-wave Solutions (2.49) are prone to become one-solution solutions, when $\beta \to 0$.

Therefore, using transformation

$$U = 2a_0 e^{-D\tau}\left[\frac{\partial^2}{\partial\xi^2} ln(1 + \exp(\Psi))\right] + R(\tau) \tag{2.73}$$

finally, we acquire the one soliton solution of NKP equation as,

$$U(\xi,\eta,\tau) = \frac{1}{2}a_0 s^2 e^{-D\tau}\,\mathrm{sech}^2\left(\frac{\Psi}{2}\right) + R(\tau) \tag{2.74}$$

$$\text{where} \quad \Psi = s\xi + l\eta - \left(\frac{Cl^2 + Bs^4}{s} + AR(\tau)s\right)\tau \tag{2.75}$$

The characteristic wedge for any soliton defined by (2.74) is expressed as,

$$\xi + \frac{l}{s}\eta + \frac{\sigma}{s} = \frac{1}{s^2}\left(Cl^2 + AR(\tau)s^2 + Bs^4\right)\tau. \tag{2.76}$$

We consider $f(\tau) = h_0\ \cos(\omega\tau)$, then, the characteristic curve can be acquired from the following result

$$\xi + \frac{l}{s}\eta + \frac{\sigma}{s} = \left(\frac{Cl^2 + Bs^4}{s^2} + Ah_0\frac{D\cos(\omega\tau) + \omega\sin(\omega\tau)}{D^2+\omega^2} + AR_0e^{-D\tau}\right)\tau \tag{2.77}$$

and the velocity of the solitary wave in two spatial direction are represented as,

$$V = \left(\frac{Cl^2 + Bs^4}{s^2} + A(R'(\tau)\tau + R(\tau)), \frac{Cl^2 + Bs^4}{sl} + As(R'(\tau)\tau + R(\tau))/l\right) \tag{2.78}$$

where

$$\tau R'(\tau) + R(\tau) = \frac{h_0}{D^2+\omega^2}\{(D+\omega^2\tau)\cos(\omega\tau) + \omega(1-D\tau)\sin(\omega\tau)\} + R_0e^{-D\tau}(1-D\tau) \tag{2.79}$$

and the amplitude of the soliton defined by (2.74) is presented as,

$$Amp_1 = \frac{a_0}{2}s^2e^{-D\tau} + \frac{h_0}{D^2+\omega^2}\left(D\cos(\omega\tau) + \omega\sin(\omega\tau)\right) + R_0e^{-D\tau}. \tag{2.80}$$

It is clear from the above results that the characteristic curve of the soliton exhibits a periodic oscillation if $f(\tau)$ is considered as a trigonometric periodic function such as, $\sin(\tau)$ or $\cos(\tau)$. Thus, the choice of function $f(\tau)$ has a keen ability to modify the propagating velocity of the soliton. For instant, we observe the tracing of sine-cosine-type propagation of soliton-like solution corresponding to $f(\tau) = \cos(\tau)$. Even, if τ approaches zero, i.e. $\cos(\tau) >> \tau$ then, the trajectory also follows a periodic oscillation in the background of the soliton. Below, we see this type of behavior in many figures for the same role of forcing terms.

2.5.1.4 Asymptotic property of two-periodic wave solutions

In this subsection, the convergence of two-periodic solution is demonstrated. We choose $\beta_1 = \exp(\pi i\rho_{11})$, $\beta_2 = \exp(\pi i\rho_{22})$, $\beta_3 = \exp(2\pi i\rho_{12})$, and thus, the result (2.59) expresses P, r and

$(\Omega_1, \Omega_2, U_0, c_0)^T$ as,

$$
\begin{aligned}
P = & \begin{pmatrix} 0 & 0 & 0 & 1 \\ 0 & 0 & 0 & 0 \\ 0 & 0 & 0 & 0 \\ 0 & 0 & 0 & 0 \end{pmatrix} + \begin{pmatrix} 0 & 0 & 0 & 1 \\ -8\pi^2\mu_1 & 0 & -8A\pi^2\mu_1^2 & 2 \\ 0 & 0 & 0 & 0 \\ 0 & 0 & 0 & 0 \end{pmatrix} \beta_1 + \begin{pmatrix} 0 & 0 & 0 & 0 \\ 0 & 0 & 0 & 0 \\ -8\pi^2\mu_2 & 0 & -8A\pi^2\mu_2^2 & 2 \\ 0 & 0 & 0 & 0 \end{pmatrix} \beta_2 + \\
& \begin{pmatrix} -32\pi^2\mu_1 & 0 & -32A\pi^2\mu_1^2 & 2 \\ 0 & 0 & 0 & 0 \\ 0 & 0 & 0 & 0 \\ 0 & 0 & 0 & 0 \end{pmatrix} \beta_1^2 + \begin{pmatrix} -32\pi^2\mu_2 & 0 & -32A\pi^2\mu_2^2 & 2 \\ 0 & 0 & 0 & 0 \\ 0 & 0 & 0 & 0 \\ 0 & 0 & 0 & 0 \end{pmatrix} \beta_2^2 + \\
& \begin{pmatrix} 0 & 0 & 0 & 0 \\ 0 & 0 & 0 & 0 \\ 0 & 0 & 0 & 0 \\ -8\pi^2(\mu_1-\mu_2) & 8\pi^2(\mu_1-\mu_2) & -8A\pi^2(\mu_1-\mu_2)^2 & 2 \end{pmatrix} \beta_1\beta_2 + o(\beta_1\beta_2) \qquad (2.81)
\end{aligned}
$$

$$
\begin{aligned}
r = & \begin{pmatrix} 0 \\ 8\pi^2(AR(\tau)\mu_1^2 + C\nu_1^2 - 4B\pi^2\mu_1^4) \\ 0 \\ 0 \end{pmatrix} \beta_1 + \begin{pmatrix} 0 \\ 0 \\ 8\pi^2(AR(\tau)\mu_2^2 + C\nu_2^2 - 4B\pi^2\mu_2^4) \\ 0 \end{pmatrix} \beta_2 + \\
& \begin{pmatrix} 32\pi^2(AR(\tau)\mu_1^2 + C\nu_1^2 - 16B\pi^2\mu_1^4) \\ 0 \\ 0 \\ 0 \end{pmatrix} \beta_1^2 + \begin{pmatrix} 0 \\ 32\pi^2(AR(\tau)\mu_2^2 + C\nu_2^2 - 16B\pi^2\mu_2^4) \\ 0 \\ 0 \end{pmatrix} \beta_2^2 + \\
& \begin{pmatrix} 0 \\ 0 \\ 0 \\ 8\pi^2(AR(\tau)(\mu_1-\mu_2)^2 + C(\nu_1-\nu_2)^2 - 4B\pi^2(\mu_1-\mu_2)^4) \end{pmatrix} \beta_1\beta_2 + o(\beta_1\beta_2) \qquad (2.82)
\end{aligned}
$$

$$
\begin{aligned}
\begin{pmatrix} \Omega_1 \\ \Omega_2 \\ U_0 \\ c_0 \end{pmatrix} = & \begin{pmatrix} \Omega_1^{(00)} \\ \Omega_2^{(00)} \\ U_0^{(00)} \\ c_0^{(00)} \end{pmatrix} + \begin{pmatrix} \Omega_1^{(11)} \\ \Omega_2^{(11)} \\ U_0^{(11)} \\ c_0^{(11)} \end{pmatrix} \beta_1 + \begin{pmatrix} \Omega_1^{(21)} \\ \Omega_2^{(21)} \\ U_0^{(21)} \\ c_0^{(21)} \end{pmatrix} \beta_2 + \begin{pmatrix} \Omega_1^{(12)} \\ \Omega_2^{(12)} \\ U_0^{(12)} \\ c_0^{(12)} \end{pmatrix} \beta_1^2 + \\
& \begin{pmatrix} \Omega_1^{(22)} \\ \Omega_2^{(22)} \\ U_0^{(22)} \\ c_0^{(22)} \end{pmatrix} \beta_2^2 + \begin{pmatrix} \Omega_1^{(2)} \\ \Omega_2^{(2)} \\ U_0^{(2)} \\ c_0^{(2)} \end{pmatrix} \beta_1\beta_2 + o(\beta_1\beta_2) \qquad (2.83)
\end{aligned}
$$

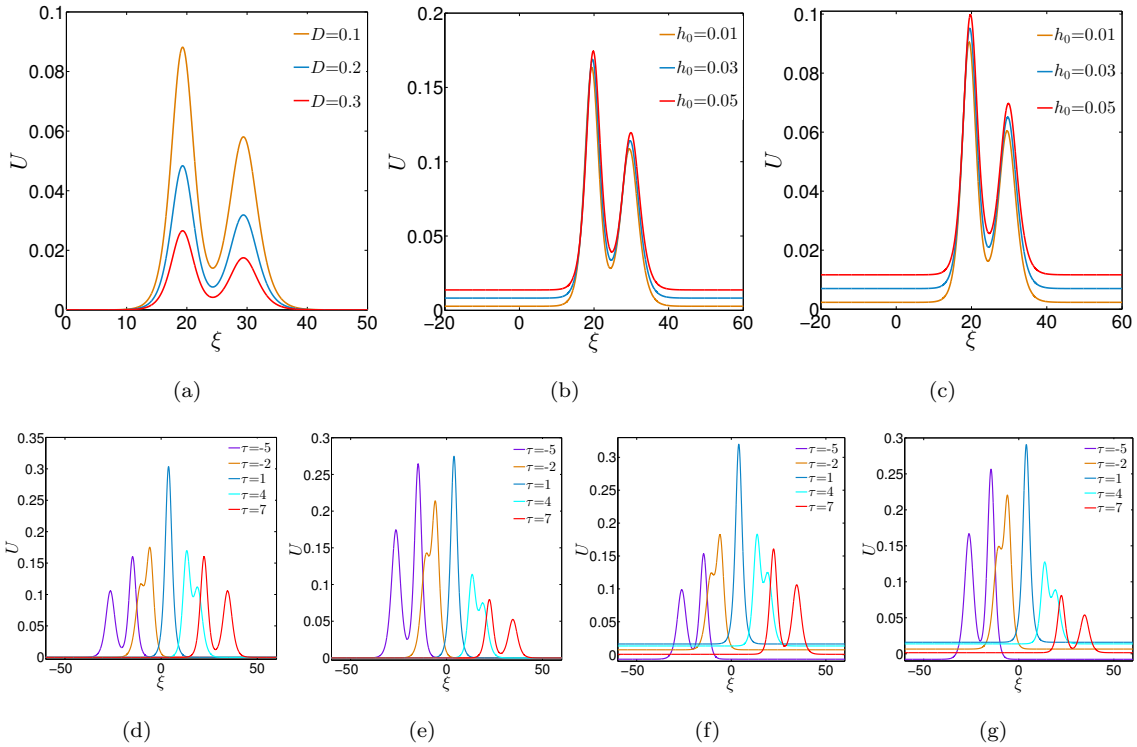

(a) (b) (c)

(d) (e) (f) (g)

Figure 2.5: 2D Plots of interaction 2-soliton solution for (2.89), by taking $\mathsf{f}(\tau) = \mathsf{h}_0\ \mathsf{cos}(\omega\tau)$, $\mathsf{s}_1 = 0.65$, $\mathsf{s}_2 = -0.8$, $\mathsf{l}_1 = 1$, $\mathsf{l}_2 = 3.5/4$, $\mathsf{A} = 6$, $\mathsf{B} = 1$, $\omega = 1.5$, $\mathsf{C} = 2$, $\mathfrak{a} = 1$, $\eta = 1$, $\tau = 6$ and (a) for $\mathsf{h}_0 = 0$, (b) for $\mathsf{D} = 0$, (c) for $\mathsf{D} = 0.1$, (d) $\mathsf{D} = 0$, $\mathsf{h}_0 = 0$, (e) for $\mathsf{D} = 0.1$, $\mathsf{h}_0 = 0$, (f) for $\mathsf{D} = 0, \mathsf{h}_0 = 0.03$, (g) for $\mathsf{D} = 0.1, \mathsf{h}_0 = 0.03$.

Let

$$U_0^{(00)} = 0,\ \mu_i = \frac{s_i}{2\pi i},\ \nu_i = \frac{l_i}{2\pi i},\ \delta_i = \frac{\sigma_i - \pi i \rho_{ii}}{2\pi i},\ \rho_{12} = \frac{A_{12}}{2\pi i}, \tag{2.84}$$

where $A_{12} = \frac{3B(s_1-s_2)^2 s_1^2 s_2^2 - C(l_1 s_2 - l_2 s_1)^2}{3B(s_1+s_2)^2 l_1^2 l_2^2 - C(l_1 s_2 - l_2 s_1)^2}$ and i=1,2. Then we have

$$\begin{aligned} U_0 &\to 0 \\ c_0 &\to 0 \\ 2\pi i \Omega_1 &\to -(AR(\tau)s_1 + \frac{Cl_1^2 + Bs_1^4}{s_1}) \\ 2\pi i \Omega_2 &\to -(AR(\tau)s_2 + \frac{Cl_2^2 + Bs_2^4}{s_2}), \quad {}_{as}\ \ \beta_1, \beta_2 \to 0. \end{aligned} \tag{2.85}$$

$$\begin{aligned} \mathcal{V}(\Theta_1, \Theta_2, \rho) &= 1 + (\exp(2\pi i \Theta_1) + \exp(-2\pi i \Theta_1))\beta_1 + (\exp(2\pi i \Theta_2) + \exp(-2\pi i \Theta_2))\beta_2 + \\ &\quad (\exp(2\pi i(\Theta_1 + \Theta_2)) + \exp(-2\pi i(\Theta_1 + \Theta_2)))\beta_1\beta_2\beta_3 + \cdots, \\ &= 1 + \exp(\bar{\Theta}_1) + \exp(\bar{\Theta}_2) + \exp(\bar{\Theta}_1 + \bar{\Theta}_2 - 2\pi i \rho_{12}) + \exp(-\bar{\Theta}_1)\beta_1^2 + \exp(-\bar{\Theta}_2)\beta_2^2 + \\ &\quad \exp(\bar{\Theta}_1 + \bar{\Theta}_2 - 2\pi i \rho_{12})\beta_1^2\beta_2^2 + \cdots, \\ &\to 1 + \exp(\bar{\Theta}_1) + \exp(\bar{\Theta}_2) + \exp(\bar{\Theta}_1 + \bar{\Theta}_2 - 2\pi i \rho_{12}) \quad {}_{as}\ \ \beta_1, \beta_2 \to 0. \end{aligned} \tag{2.86}$$

Where

$$\begin{aligned} \bar{\Theta}_i = 2\pi i \Theta_i + \pi i \rho_{ii} &= s_i \xi + l_i \eta + 2\pi i \Omega_i t + \sigma_i \\ &\to s_i \xi + l_i \eta - (AR(\tau)s_i + \frac{Cl_i^2 + Bs_i^4}{s_i})t + \sigma_i = \theta_i, \quad i = 1, 2 \quad {}_{as}\ \ \beta_1, \beta_2 \to 0 \end{aligned} \tag{2.87}$$

Thus, when $\beta_1, \beta_2 \to 0$, we further derive

$$\mathcal{V}(\Theta_1, \Theta_2, \rho) \to 1 + \exp(\Psi_1) + \exp(\Psi_2) + \exp(\Psi_1 + \Psi_2 + A_{12}) \tag{2.88}$$

which assures that periodic-wave solutions reduces to two-Soliton Solutions when $\beta_1, \beta_2 \to 0$. Finally, we get the two-soliton-like solutions of Eq.(2.2) as follows:

$$U = 2a_0 e^{-D\tau}\left[\frac{\partial^2}{\partial \xi^2} \ln(1 + \exp(\Psi_1) + \exp(\Psi_2) + \exp(\Psi_1 + \Psi_2 + A_{12}))\right] + R(\tau) \tag{2.89}$$

$$\begin{aligned} &= 2a_0 e^{-D\tau} \frac{A_{12}(s_1 + s_2)^2 e^{\Psi_1 + \Psi_2} + s_1^2 e^{\Psi_1} + s_2^2 e^{\Psi_2}}{(A_{12} e^{\Psi_1 + \Psi_2} + e^{(\Psi_1)} + e^{(\Psi_2)} + 1)} + R(\tau) \\ &\quad -2a_0 e^{-D\tau} \frac{(A_{12}(s_1 + s_2)e^{\Psi_1 + \Psi_2} + s_1 e^{\Psi_1} + s_2 e^{\Psi_2})^2}{(A_{12} e^{\Psi_1 + \Psi_2} + e^{\Psi_1} + e^{\Psi_2} + 1)^2} \end{aligned} \tag{2.90}$$

where

$$\Psi_i = s_i \xi + l_i \eta - \left(\frac{Cl_i^2 + Bs_i^4}{s_i} + AR(\tau)s_i\right)\tau + \sigma_i,\ i = 1, 2. \tag{2.91}$$

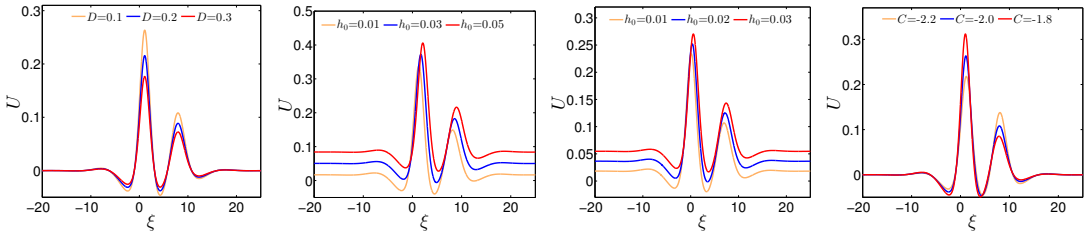

(a) (b) (c) (d)

Figure 2.6: 2D Plots of Breather wave (2.96), by taking $f(\tau) = h_0 \cos(\omega\tau)$, $q_1 = 0.65$, $q_2 = -1$, $p_1 = 0.4$, $p_2 = 0.6$, $\delta_1 = -2$, $A = 6$, $B = 1$, $\omega = 1.5$, $\eta = 1$, $C = -2$, $U_0 = -0.1$, $\tau = 2$ and (a) for $h_0 = 0$, (b) for $D = 0$, (c) for $D = 0.2$, (d) all the paprameters are same except C.

with s_1, s_2, l_1 and l_2 as the real constants and the characteristic wedge for each solitary wave in (2.89) can be defined by

$$\xi + \frac{l_i}{s_i}\eta + \frac{\sigma_i}{s_i} = \frac{1}{s_i^2}\left(Cl_i^2 + AR(\tau)s_i^2 + Bs_i^4\right)\tau \tag{2.92}$$

$$A_{12} = \frac{3B(s_1 - s_2)^2 s_1^2 s_2^2 - C(l_1 s_2 - l_2 s_1)^2}{3B(s_1 + s_2)^2 l_1^2 l_2^2 - C(l_1 s_2 - l_2 s_1)^2} \tag{2.93}$$

Figure 2.5(a)-Figure 2.5(c) illustrate solitary propagation of bi-soliton in an exciting system due to forcing and damping. Figure 2.5(a) clearly shows the negative effect of damping for a positive time in the solitary propagation, however, a rising of the wave background due to the enhancement of strength of external forces follows in Figure 2.5(b) and Figure 2.5(c). Figure 2.5(d)-Figure 2.5(f) are drawn for presenting propagation of soliton over different time interval under various physical situations. In Figure 2.5(d), we see the symmetrical wave propagation in the absence of damping and force. Figure 2.5(e) exhibits the negatively acting damping effect in wave structures and it can be anticipated from this figure that the soliton finally, completely dies out over time due to the damping. Figure 2.5(f) shows the rising of the soliton background due to the impact of forcing term, however, it is interesting to mention that soliton keeps their symmetric structures over time. In Figure 2.5(g), we see the combing effect of forcing and damping on soliton structures over time. Though, the background of the soliton rises above, but, the soliton tends to vanish over time losing its symmetry. For positive τ, damping (in the form of $e^{-D\tau}$) causes an exponentially positive boost, whereas, for negative τ, damping cannot create such a positive boost. For a positive time, this type of phenomenon occurs due to the loss of velocity, while for a negative time, soliton rises due to the augmentation of velocity. In contrast, enhancing forcing term causes the entire solitary structure to rise above. The fact that two solitons appear almost as one soliton (in Figure 2.5(d)-Figure 2.5(g)) in the interacting zone at $\tau = 1$ is interesting.

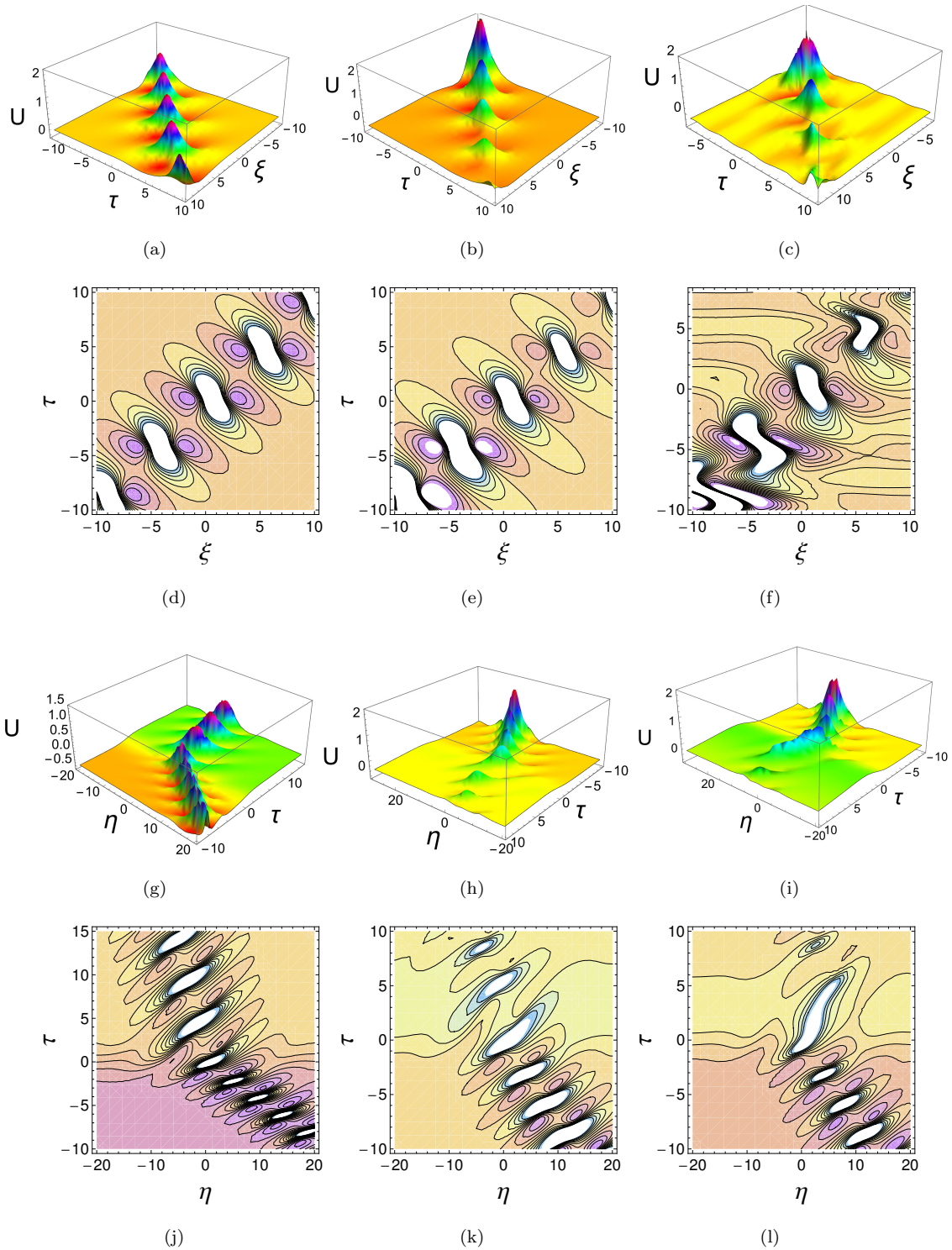

Figure 2.7: Profiles of Breather waves for solution (2.96), when $f(\tau) = h_0 \cos(\omega\tau)$ and $q_1 = 0.65$, $q_2 = -1$, $p_1 = 0.4$, $p_2 = 0.6$, $\delta_1 = -1$, $A = 6$, $B = 1$, $\omega = 1.5$, $\eta = 1$, $C = -2$, $U_0 = -1$, and (a) $D = 0$, $h_0 = 0$, (b) $D = 0.1$, $h_0 = 0$, (c) $D = 0$, $h_0 = 0.1$, (d), (e) and (f) are Contour plots of the corresponding Figure 2.7(a), Figure 2.7(b) and Figure 2.7(c); (g) when $f(\tau) = h_0\, sech^2(\omega\tau)$ and $\omega = 0.5$, $C = -1.5, D = 0$, $h_0 = 0$, (h) for $\omega = 0.5$, $C = -1.5, D = 0.1$, $h_0 = 0.05$, (i) for $\omega = 0.5$, $C = -1.5, D = 0.1$, $h_0 = 0.1$, (j), (k) and (l) are Contour plots of the corresponding Figure 2.7(g), Figure 2.7(h) and Figure 2.7(i).

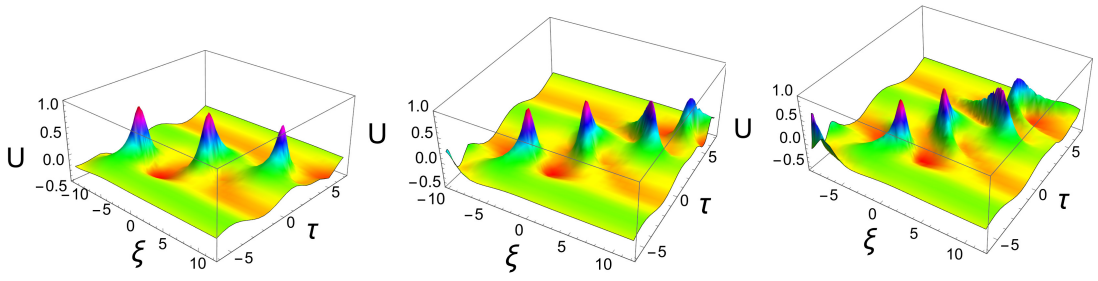

Figure 2.8: Profiles of Breather waves for solution (2.96), when $f(\tau) = h_0\cos(\omega\tau)$ and $q_1 = 0.6$, $q_2 = -1.5$, $p_1 = 0.4$, $p_2 = 0.6$, $\delta_1 = -2$, $B = 1.5$, $\omega = 1$, $\eta = 1$, $C = -1.5$, $U_0 = -0.2$, $D = 0.05$, $h_0 = 0.1$ and (a) $A = 2$, (b) $A = 5$ and (c) $A = 8$.

2.5.2 Breather wave

In order to do it, suppose that $\mathcal{F}$ has the following form:

$$\mathcal{F} = \delta_2 e^{\zeta_1} + \delta_1\cos(\zeta_2) + e^{-\zeta_1}, \quad \zeta_1 = p_1(\xi + q_1\eta + d_1\tau),\ \zeta_2 = p_2(\xi + q_2\eta + d_2\tau) \tag{2.94}$$

Now, inserting $\mathcal{F}$ in Eq.(2.11), that leads us the subsequent result on parameters. To solve these equations, one can get the parameter relations as follows

$$\begin{aligned}
d_1 &= -\frac{(Bp_1^4 - 4Bp_1^2p_2^2 - Bp_2^4 + Cp_1^2q_1^2 + 2Cp_2^2q_1q_2 - Cp_2^2q_2^2}{p_1^2 + p_2^2} \\
&\quad + \frac{AR(\tau)p_1^2 + AR(\tau)p_2^2 + Ap_1^2U_0 + Ap_2^2U_0)}{p_1^2 + p_2^2}, \\
d_2 &= -\frac{(Bp_1^4 + 4Bp_1^2p_2^2 - Bp_2^4 - Cp_1^2q_1^2 + 2Cp_1^2q_1q_2 + Cp_2^2q_2^2}{p_1^2 + p_2^2} \\
&\quad + \frac{AR(\tau)p_1^2 + AR(\tau)p_2^2 + Ap_1^2U_0 + Ap_2^2U_0)}{p_1^2 + p_2^2}, \\
\delta_2 &= -\frac{p_2^2\delta_1^2(Bp_1^4 + 6Bp_1^2p_2^2 + Bp_2^4 - Cp_1^2q_1^2 + 2Cp_1^2q_1q_2 - Cp_1^2q_2^2)}{4p_1^2(2Bp_1^4 + 7Bp_1^2p_2^2 + Bp_2^4 + Cp_2^2q_1^2 - 2Cp_2^2q_1q_2 + Cp_2^2q_2^2)}, q_1 = q_1, q_2 = q_2
\end{aligned} \tag{2.95}$$

This set of parameters generates mixed function solution defined by Eq.(2.94), yields Breather solution,

$$\begin{aligned}
U_{br} &= 2a_0e^{-dt}\left(\frac{2p_1^2\sqrt{\delta_2}\cosh(\zeta_1) + \ln(\sqrt{\delta_2}) - \delta_1p_2^2\cos(\zeta_2)}{2\sqrt{\delta_2}\cosh(\zeta_1) + \ln(\sqrt{\delta_2}) + \delta_1\cos(\zeta_2)}\right) + e^{-D\tau}\left(\int e^{D\tau}f(\tau)d\tau + R_0\right) \\
&\quad -2a_0e^{-dt}\left(\frac{(p_1\sqrt{\delta_2}\sinh(\zeta_1) + \ln(\sqrt{\delta_2}) - \delta_1p_2\sin(\zeta_2))^2}{(2\sqrt{\delta_2}\cosh(\zeta_1) + \ln(\sqrt{\delta_2}) + \delta_1\cos(\zeta_2))^2}\right).
\end{aligned} \tag{2.96}$$

To generate the lump solution from the breather solution for Eq.(2.2), we choose $p_1 = m$, $p_2 = m$ and $\delta_1 = -2$ in (2.96). Thus, the solution (2.96) is expressed as,

$$\begin{aligned} U_{br} &= 2a_0 e^{-dt}\left(\frac{m^2\sqrt{P}\cosh(\zeta_1)+\ln(\sqrt{P})+m^2\cos(\zeta_2)}{\sqrt{P}\cosh(\zeta_1)+\ln(\sqrt{P})-\cos(\zeta_2)}\right)+e^{-D\tau}\left(\int e^{D\tau}f(\tau)d\tau+R_0\right) \\ &\quad +2a_0 e^{-dt}\left(-\frac{m^2(\sqrt{P}\sinh(\zeta_1)+\ln(\sqrt{P})+\sin(\zeta_2))^2}{(\sqrt{P}\cosh(\zeta_1)+\ln(\sqrt{P})-\cos(\zeta_2))^2}\right). \end{aligned} \tag{2.97}$$

where

$$P = \frac{C(q_1-q_2)^2-8Bm^2}{C(q_1-q_2)^2+10Bm^2}$$

$$\begin{aligned} \zeta_1 &= m(\xi+q_1\eta-\left(\frac{2AR(\tau)+2AU_0+C(q_1^2-q_2^2+2q_1q_2)}{2}-2Bm^2\right)\tau) \\ &, \\ \zeta_2 &= m(\xi+q_2\eta-\left(\frac{2AR(\tau)+2AU_0-C(q_1^2-q_2^2-2q_1q_2)}{2}+2Bm^2\right)\tau) \end{aligned}$$

We noticed from Eq.(2.97) that

$$P = \frac{C(q_1-q_2)^2-8Bm^2}{C(q_1-q_2)^2+10Bm^2} \to 1,$$

when $m \to 0$. Thus, if $m \to 0$ in Eq.(2.97), the lump solution may expressed as:

$$U_{lump} = -2a_0 e^{-dt}\left(\frac{8\Gamma_1\Gamma_2+\frac{72B}{C(q_1-q_2)^2}}{(\Gamma_1^2+\Gamma_2^2-\frac{18B}{C(q_1-q_2)^2})^2}\right)+e^{-D\tau}\left(\int e^{D\tau}f(\tau)d\tau+R_0\right). \tag{2.98}$$

where

$$\begin{aligned} \Gamma_1 &= \xi+q_1\eta-\left(\frac{2AR(\tau)+2AU_0+C(q_1^2-q_2^2+2q_1q_2)}{2}\right)\tau \\ &, \\ \Gamma_2 &= \xi+q_2\eta-\left(\frac{2AR(\tau)+2AU_0-C(q_1^2-q_2^2-2q_1q_2)}{2}\right)\tau \end{aligned}$$

To get the amplitude of the lump solution, we choose $U_\xi = 0$, $U_\eta = 0$. Then, the critical point is represented as,

$$(\xi,\eta) = \left(\frac{(w_1(\tau)q_2-w_2(\tau)q_1)\tau}{q_1-q_2}, \frac{(w_1(\tau)-w_2(\tau))\tau}{q_1-q_2}\right), \tag{2.99}$$

where $w_1(\tau) = -\left(\frac{2AR(\tau)+2AU_0+C(q_1^2-q_2^2+2q_1q_2)}{2}\right)$ and $w_2(\tau) = -\left(\frac{2AR(\tau)+2AU_0-C(q_1^2-q_2^2-2q_1q_2)}{2}\right)$.

The rational solution (2.98) presents a permanent lump which moves with the velocity

$$V_\xi = \frac{(w_1(\tau)+w_1'(\tau)\tau)q_2-(w_2(\tau)+w_2'(\tau)\tau)q_1}{q_1-q_2}, V_\eta = \frac{(w_1(\tau)+w_1'(\tau)\tau)-(w_2(\tau)+w_2'(\tau)\tau)}{q_1-q_2} \tag{2.100}$$

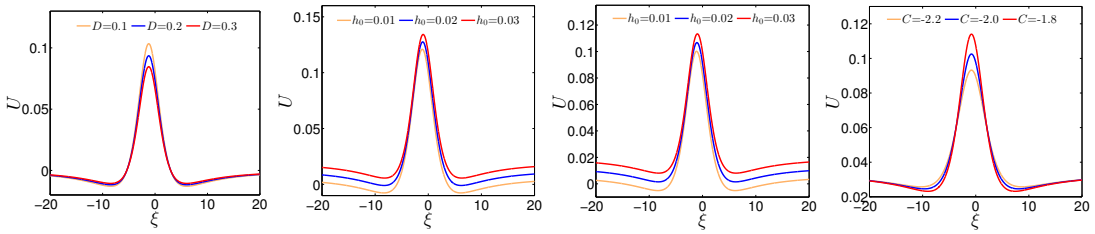

(a) (b) (c) (d)

Figure 2.9: 2D Plots of lump solution for (2.98), when $f(\tau) = h_0\ \cos(\omega\tau)$ and $U_0 = -0.1$, $C = -0.5$, $B = 1$, $A = 6$, $\omega = 1.5$, $h_0 = 0.05$, $D = 0.1$, $b_1 = 1$, $b_2 = -1$, (a) when $h_0 = 0$, $\tau = 1$, (b) when $D = 0$, $\tau = 1$ and (c) $D = 0.2$, $\tau = 1$; (d) all the paprameters are same except C.

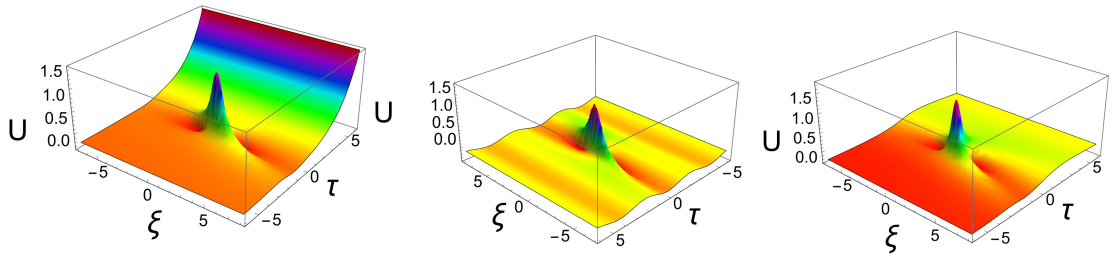

(a) (b) (c)

Figure 2.10: 3D Plots of lump solution for (2.98), when $U_0 = -0.2$, $C = -0.5$, $B = 1$, $A = 6$, $\omega = 1.5$, $q_1 = 1$, $q_2 = -1$ and (a) for $f(\tau) = h_0\ \exp(\omega\tau)\, h_0 = 0.1$, $D = 0.1$, (b) for $f(\tau) = h_0\ \sin(\omega\tau)$, $h_0 = 0.1$, $D = 0.1$, and (c) $f(\tau) = h_0\ \mathrm{sech}^2(\omega\tau)$, $h_0 = 0.1$, $D = 0.1$.

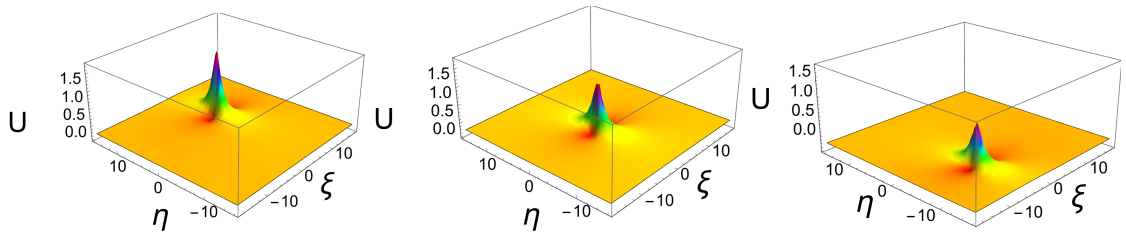

(a) (b) (c)

Figure 2.11: 3D Plots of lump solution for (2.98), when $f(\tau) = h_0 \cos(\omega\tau)$ and $U_0 = -0.1$, $C = -0.5$, $B = 1$, $A = 6$, $\omega = 1.5$, $h_0 = 0.05$, $D = 0.1$, $b_1 = 1$, $b_2 = -1$, $\tau = 2$, (a) when $D = 0.15$, $\tau = -2$, (b) when $D = 0.15$, $\tau = 0$ and (c) $D = 0.15$, $\tau = 2$.

where $(')$ is the derivative with respect to τ and $q_1 \neq q_2$. At the critical point (see the result (2.99)) for $h(\tau) = h_0 \cos(\omega\tau)$, $q_1 = 1.5$, $q_2 = 1$, $A = 6$, $B = 1$, $\omega = 1.5$, $C = -0.5$, the second order derivative and Hessian matrix [161] satisfy the following relations

$$H = \frac{\partial^2}{\partial \xi^2} U(\xi, \eta, \tau) < 0, \; M = \begin{vmatrix} \frac{\partial^2}{\partial \xi^2} U(\xi, \eta, \tau) & \frac{\partial^2}{\partial \xi \partial \eta} U(\xi, \eta, \tau) \\ \frac{\partial^2}{\partial \xi \partial \eta} U(\xi, \eta, \tau) & \frac{\partial^2}{\partial \eta^2} U(\xi, \eta, \tau) \end{vmatrix} > 0, \tag{2.101}$$

It is clear from above that the sign of H and M are solely decided by the parameters. Now, utilizing the extreme value theory of function with several variables, we estimate two cases: (a) At, $\tau = 0$, U_{lump} is in general, maximum and (b) However, if $\tau < 0$ the value of U_{lump} is higher than that of case (a) because the presence of the term $e^{-D\tau}$ causes a positive impact on amplitude. Considering the above analysis, it is understood that U_{lump} assumes its maximum value at the point (2.99). Through the simple computation, we obtain the maximum amplitude as,

$$Amp_{max} = \frac{9R(\tau)B + 9U_0B - 4Ce^{-D\tau}(q_1 - q_2)^2}{9B}. \tag{2.102}$$

For the present system, the amplitude and trajectory of the breather significantly depend on damping and forcing terms, and Figure 2.6(a)-Figure 2.6(d) are drawn for a clear presentation of the act of damping and forcing term in breather wave. In Figure 2.6(a), we see that the width and amplitude of the breather are significantly reduced when strong damping is applied. From Figure 2.6(b), it is clear that the background of the lump wave enhances due to the enhancement of the magnitude of the forcing term, and enhancing forcing increases the periodicity of the background. Figure 2.6(c) demonstrates the combined effect of the forcing and damping components and it shows that the forcing component plays a dominating role in the damping term. Overall, damping causes for diminishing of the breather whereas, forcing rises the wave background. Finally, the significant impact of the parameter C is shown in Figure 2.6(d) where the breather wave is sufficiently improved due to the variation of C. Figure 2.7(a)-Figure 2.7(c) present the propagation of homoclinic breather

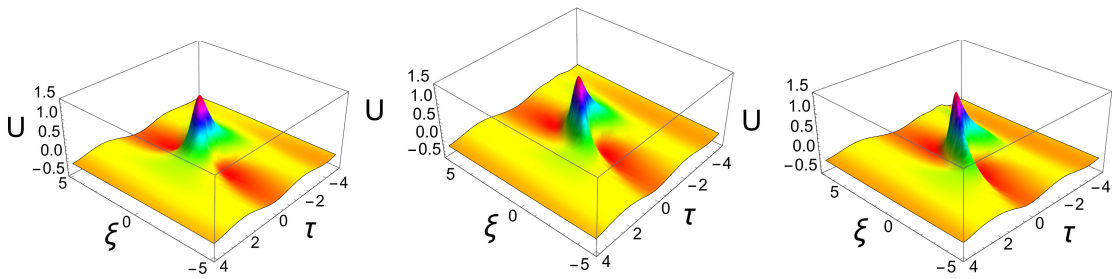

(a) (b) (c)

Figure 2.12: 3D Plots of lump solution for (2.98), when $U_0 = -0.2$, $C = -1$, $B = 1$, $\omega = 1.5$, $q_1 = 1$, $q_2 = -1.5$ and $f(\tau) = h_0 \sin(\omega\tau)$, $h_0 = 0.1$, $D = 0.1$, and (a) $A = 2$, (b) $A = 5$ and (c) $A = 8$.

waves for periodic forcing component ($f(\tau) = h_0 \cos(\omega\tau)$) and their graphical presentation express that they are by nature singular breather, that is, periodically described in a locally time-space zone. In Figure 2.7(a), we see that U_{br} evolves across a line which makes a constant angle with ξ and τ axes in the absence of damping and forcing ($D = 0, f(\tau) = 0$). Thus, it is confirmed from the graphical presentation that the breather is space periodic as well as time periodic also. Again, as expected Figure 2.7(b) shows the continuous decrement in amplitude due to the act of damping. Figure 2.7(c) is drawn for exhibiting the evolution of breather in ξ and τ plane in the presence of both damping and forcing terms. Here, the enchantment of force creates a periodic background, whereas, damping diminishes their amplitudes. The corresponding contours of the above-mentioned figures are presented in Figure 2.7(d)-Figure 2.7(f) which help to understand the significant effect of damping and periodic forcing in the dispersed media.

In Figure 2.7(g)-Figure 2.7(i), we study a special type of periodic breather which propagates in compact kink type background under the action of hyperbolic forcing term ($f(\tau) = h_0 \operatorname{sech}^2(\omega\tau)$). In the absence of damping, Figure 2.7(g) shows the kinkly breather type wave. Again, Figure 2.7(h) shows the drastic effect of damping under the influence of negligible forcing. In Figure 2.7(i), we see the combined impact of damping and forcing term, where the breather is finally, destructed after a while. A similar type of observation also follows in Figure 2.7(c) but the only difference is that the breather in the hyperbolic forcing zone strongly variates their direction in the η-τ plane. The complicated nonlinear phenomena of a breather in the hyperbolic forcing domain are also cleared from the contours plotted in Figure 2.7(j) - Figure 2.7(l).

The significant effects of the nonlinear term A in breather of the NKP system are illustrated in Figure 2.8(a)-Figure 2.8(c). The moderate periodic breather is observed in Figure 2.8(a) for comparatively lower values of A however, enhancing A boosts the nonlinearity of the system and hence, the shape and size of the breather improve sufficiently. In Figure 2.8(b), we see that the periodic breather tends to be a horseshoe-type breather. Finally, prominent pairwise horseshoe breather

structures are found in Figure 2.8(c).

Now we discuss the lump wave features of the NKP equation and the plots of these solutions are expressed in the following manners. Figure 2.9(a)-Figure 2.9(d) are depicted to present the acts of damping and forcing term in lump wave. The amplitude of the lump soliton is significantly reduced when strong damping is applied (see Figure 2.9(a)). From Figure 2.9(b), it is clear that the the background of lump wave enhances due to the enhancement of the magnitude of the forcing term. Figure 2.9(c) demonstrates the combined effect of the forcing and damping component, where we see that the amplitude of the lump enhances as the damping component is dominated by the forcing term. The significant rising impact from the parameter C is found in Figure 2.9(d). Figure 2.10(a)-Figure 2.10(c) are depicted for presenting different types wave background (exponential, periodic or kink type) of lump wave for various types of forcing terms. Figure 2.10(a), Figure 2.10(b) and Figure 2.10(c) respectively show exponential, periodical and hyperbolic backgrounds of lump waves. In Figure 2.11(a)-Figure 2.11(c), we observe that the lump moves in the space-time zone and its amplitude significantly diminishes due course of time. It is evident from the figures that the lump asymptotically vanishes over time. Actually, the lump declines due to the act of damping. The most interesting nonlinear phenomena are found in lump waves when the values of nonlinear coefficient A are enhanced moderately. In Figure 2.12(a), a simple lump wave is observed on a periodical background. But, the enhancing effect of the nonlinear term causes an enormous impact on the structure of the lump wave. An increase in the nonlinear coefficient A makes the lump wider (Figure 2.12(b)). We see the interesting horseshoe-type structure in Figure 2.12(c) for sufficiently large values of A.

2.6 Conclusion

In this article, we have introduced a Bäcklund transformation and a Lax pair of the system to highlight the integrability of the NKP equation under certain compatibility conditions. The algebra-geometrical approach presents quasi-periodic solutions to the NKP equation, which under a certain limit, converge to the classical soliton solution. A set of new analytical solutions to the NKP equation are presented here, including lump, breather, and rough waves. As a result of the investigations, the following main conclusions were reached:

a. The present investigation introduces Bäcklund transformation and a Lax pair of the NKP equation, which suggests the integrability of the said equation under some suitable compatibility conditions.

b. For the first time, the infinite conservation laws of the NKP equation are explicitly presented with the help of binary Bell-polynomial derived from bilinear Bäcklund transformation.

c. The quasi-periodic solutions are derived from the Bell-polynomial of the NKP equation using

the Riemann theta function and the significant impact of forcing and damping terms in the quasi-periodic waves are clearly presented through numerical graphs and figures.

d. One of the most important parts of the investigation is the asymptotic analysis of the quasi-periodic solution, from which single soliton and bi-soliton solutions are explored from the one and two periodic solutions of the NKP equation. Thus, it is anticipated that periodic solutions may tend to soliton or multi-soliton according to the periodicity of the quasi-periodic solution.

e. Detailed studies on the breather wave of the NKP equation have been carried out under the variations in forcing components. It is found that several backgrounds of the wave quantities forms due to the act of different types of forcing components, in addition to the diminishing effect in the breather wave from the damping term is also observed.

f. The finding of a lump soliton in the asymptotic aspect of the breather wave is an interesting part of this investigation. The effect in the formation of a background of the lump from the forcing term is analyzed in detail. The massive impact of the damping is also shown from a numerical standpoint. Finally, the maximum possible altitude of a lump is calculated in an analytical understanding.

g. Another important observation in the present studies is that the horseshoe-type lump, as well as breather, may occur due to the act of externally applied force term.

A number of investigations have been performed on the KP equation utilizing various approaches, however, the KP model with damping and external force is more realistic as damping is found everywhere whereas, the major effects of externally applied forces are available in many Astronomical and space objects. As a result of this work, the combination of the bilinear approach, bilinear Bäcklund transformation, and Bell-polynomial has proven to be an efficient mathematical tool for solving more general class of nonlinear evolution equations in the fields of mathematics, physics, and engineering. Our results may provide an improved understanding of the dynamical behavior of quasi-periodic wave, multi-soliton, breather, and lump-type wave solutions. We present the first works that discuss and show various results for NKP equations in a non-autonomous (2+1)-dimensional space. Depending on the physical background it represents, it may explain a nonlinear phenomenon.

Chapter 3

Characteristic of integrability of nonautonomous KP-modified KP equation and its qualitative studies: soliton, shock, periodic waves, breather, positons and soliton interactions

[1]

3.1 Introduction

Nonlinear evolution equations arise in almost all the physical systems and so their study is a field of active research. The qualitative and analytic study of these equations reveal complex phenomena in the several fields of application such as elasticity [162], plasticity, circuit theory [163], plasma dynamics [164], water wave phenomena [165], laser and optical fibers [166, 167], etc. KdV equation is one such common equation which arises in the study of shallow water waves in one

[1]The research article has been published in the journal of Nonlinear Dynamics (Springer)

dimension [168]. A generalization of this equation to two spatial dimension is the KP equation [86],

$$\frac{\partial}{\partial\xi}\left[\frac{\partial\phi}{\partial\tau}+Q\phi\frac{\partial\phi}{\partial\xi}+R\frac{\partial^3\phi}{\partial\xi^3}\right]+T\frac{\partial^2\phi}{\partial\eta^2}=0 \tag{3.1}$$

The modified KP (mKP) equation [169, 170] is obtained by adding cubic nonlinearity as,

$$\frac{\partial}{\partial\xi}\left[\frac{\partial\phi}{\partial\tau}+Q\phi^2\frac{\partial\phi}{\partial\xi}+R\frac{\partial^3\phi}{\partial\xi^3}\right]+T\frac{\partial^2\phi}{\partial\eta^2}=0 \tag{3.2}$$

By adopting the KP and mKP equations, the KP equation can again be extended to the KP-mKP equation [109],

$$\frac{\partial}{\partial\xi}\left[\frac{\partial\phi}{\partial\tau}+P\phi\frac{\partial\phi}{\partial\xi}+Q\phi^2\frac{\partial\phi}{\partial\xi}+R\frac{\partial^3\phi}{\partial\xi^3}\right]+T\frac{\partial^2\phi}{\partial\eta^2}=0 \tag{3.3}$$

In the present investigation, we investigate the nonautonomous KP-mKP equation, which can be stated as, in light of the effectiveness of the damping and forcing terms,

$$\frac{\partial}{\partial\xi}\left[\frac{\partial\phi}{\partial\tau}+P\phi\frac{\partial\phi}{\partial\xi}+Q\phi^2\frac{\partial\phi}{\partial\xi}+R\frac{\partial^3\phi}{\partial\xi^3}+S\phi\right]+T\frac{\partial^2\phi}{\partial\eta^2}=R\frac{\partial^2 f_2}{\partial\xi^2} \tag{3.4}$$

where the additional terms S and $f_2(\xi,\tau)$ express the damped and external force terms respectively. The nonautonomous part of the standard evolution equation in earlier research produces a variety of intriguing outcomes, which encourages us to select the source term $f_2(\xi,\tau)=\frac{\xi B(\tau)}{R}$ in the current context, resulting in the reduction of Eq.(3.4) to

$$\frac{\partial\phi}{\partial\tau}+P\phi\frac{\partial\phi}{\partial\xi}+Q\phi^2\frac{\partial\phi}{\partial\xi}+R\frac{\partial^3\phi}{\partial\xi^3}+S\phi+T\int\frac{\partial^2\phi}{\partial\eta^2}d\xi=B(\tau). \tag{3.5}$$

This chapter demonstrates the characteristic of integrability of the nonautonomous KP-mKP equation through Painlevé analysis, bilinear Bäcklund and lax pairs. The nonautonomous KP-mKP equation is converted into the Bell polynomial form which bilinear Bäcklund is constructed and lax pair of the said equation is generated. Further, multi-solitons, smooth positon, breather, and their interaction are fabricated using Hirota's bilinear approach. Besides, a qualitative analysis of the nonautonomous KP-mKP equation using bifurcation theory is carried out. The deformation of the periodic to quasiperiodic orbit signifying instability of the said system due to damping is observed. Additionally, the external periodic force perturbs the nonautonomous system's low and high-energy orbits, resulting in a chaotic structure via the path of intermittency, implying the presence of turbulent flow.

3.2 The Painlevé analysis for the nonautonomous KP-mKP equation

Many mysterious nonlinear features of nature are described by the integrable equations however, a completely integrable system is not always possible to define precisely. The most popular way to check integrability is to introduce the Painlevé property. According to Ablowitz and

colleagues [171], all accurate reductions of a nonlinear partial differential equation to ordinary differential equations must satisfy the Painlevé property for the equation to be integrable. This strategy presents clear operational challenges. Without considering any similarity reductions, Weiss et al. [68] defined the Painlevé property for PDE and introduced a method for assessing a common form of moveable singularity. Three main steps make up the Painlevé test: the leading order analysis, the resonances determination, and the verification of the resonances conditions, or figuring out the requirements of compatibility. Utilizing the Weiss-Tabor-Carnevale algorithm [68] as well as Kruskal's simplification technique [133], the Painlevé property of Eq.(3.3) is analyzed below. We present the solution of Eq.(3.3) in a generalized Laurent expansion as

$$\phi(\xi,\eta,\tau) = \Phi^{-\gamma}(\xi,\eta,\tau)\sum_{j=0}^{\infty}\phi_j(\xi,\eta,\tau)\Phi^j(\xi,\eta,\tau), \tag{3.6}$$

in the neighborhood of a noncharacteristic movable singularity manifold defined by $\Phi(\xi,\eta,\tau)=0$ where $\phi_j(\xi,\eta,\tau)$'s are assumed to be analytic functions and the positive integer γ is to be evaluated. To evaluate the leading order term of the series (3.6), we set

$$\phi(\xi,\eta,\tau) = \phi_0(\xi,\eta,\tau)\Phi^{-\gamma}(\xi,\eta,\tau) \tag{3.7}$$

where $\phi_0 \neq 0$. Substituting (3.7) into Eq.(3.4) and balancing the highest order derivative with the nonlinear terms to achieve $\gamma = 1$ and $\phi_0 = \sqrt{-\frac{6R}{Q}}\Phi_\xi$.
We take in this case Kruskal anasatz [133] of singular manifold [68] for simplicity. So, we consider as,

$$\Phi(\xi,\eta,\tau) = \xi + \eta - \chi(\tau), \tag{3.8}$$

where, $\chi(\tau)$ is analytic function chosen arbitrarily. Substitution of (3.6) and (3.8) into Eq.(3.4), yields

$$j=0 \quad : \quad \phi_0 = \sqrt{-\frac{6R}{Q}}, \tag{3.9}$$

$$j=1 \quad : \quad \phi_1 = -\frac{P}{2Q}, \tag{3.10}$$

$$j=2 \quad : \quad \phi_2 = -\frac{1}{2Q}\sqrt{-\frac{Q}{6R}}\left(T - \frac{P^2}{4Q} - \chi_\tau\right), \tag{3.11}$$

$$j=3 \quad : \quad (\phi_0)_\tau + S\phi_0 = 0, \tag{3.12}$$

$$j=4 \quad : \quad 0.\phi_4 = 0, \tag{3.13}$$

Using Eqs.(3.9)-(3.11), ϕ_0, ϕ_1 and ϕ_2 can be accquired explicitely. Eq.(3.12) and Eq.(3.13), show that ϕ_3 and ϕ_4 can not be determined uniquely, and so $j = 3, 4$ are the resonances. Hence, the resonances appears at $j = -1, 3, 4$. Clearly, the compatibility conditions at $j = 3, 4$ are satisfied for

arbitrarily considered ϕ_3 and ϕ_4. From expression (3.12), we directly get,

$$6R - Qr_0^2 e^{-2S\tau} = 0, \quad \textit{where} \;\; r_0 \;\; \textit{is chosen as a integrating constant term.} \tag{3.14}$$

Under consideration of the resonances, we choose

$$\phi(\xi, \eta, \tau) \approx \phi_0 \Phi^{-1} + \phi_j \Phi^{j-1}, \; j \geqslant 1 \tag{3.15}$$

Replacing Eq.(3.15) to Eq.(3.4) and accumulation of the lowest power terms of Φ lead

$$(j+1)(j-3)(j-4)(j-4)R\Phi_\xi^4 \phi_j = F_j(\phi_0, \phi_1, \cdots, \phi_{j-1}). \tag{3.16}$$

Here, ϕ_j appears arbitrarily for $j = -1,\ 3,\ 4$. Hence, two requirements are necessary for compatibility at $j = 3$ and $j = 4$. Utilizing the values of ϕ_0, ϕ_1, and ϕ_2 from Eqs.(3.9)-(3.11) in Eq.(3.12) the compatibility condition at the resonance $j = 3$ is not identically met. Instead, we arrived at the following variable constraint Eq.(3.14).

The compatibility conditions at $j = 4$ are not identically met. Additionally, if we set the arbitrary functions $\phi_3 = 0$, $\phi_4 = 0$ to be zero that is $\phi_3 = 0$, $\phi_4 = 0$, then we arrived at the following constraint equation of arbitrary function χ and the variables,

$$S^2 \left(T - \frac{P^2}{4Q} - \chi_\tau \right)^2 + 24R^3 Q \left(\frac{\partial^2 f_2}{\partial \xi^2} \right)^2 = 0 \tag{3.17}$$

By vanishing subsequent coefficient terms of Φ, we report that the number of arbitrary functions (χ, ϕ_3, ϕ_4) is equal to the number of resonances $(-1, 3, 4)$. It is significant to remember that Eq.(3.4) confirms the sufficiency of numbers of arbitrary functions. Hence, Eq.(3.4) meets the Painlevé test and Eq.(3.4) is necessarily integrable.

3.3 Bilinear formation, Bilinear Bäcklund transformation and Lax pair of nonautonomous KP-mKP equation

Obtaining several solutions to the evolution equation gets crucial to understanding nonlinearity. The Hirota technique [27] is used in the current situation to obtain the multi-soliton of the nonautonomous KP-mKP equation.

3.3.1 Bilinear formation :

Eq.(3.5) is converted into the binary-Bell-polynomial form by setting

$$\phi(\xi, \eta, \tau) = N(\tau) \; (_{\ln}[\nu(\xi, \eta, \tau)])_\xi + G(\tau) \tag{3.18}$$

We construct the binary-Bell-polynomial form of Eq.(3.5) using the binary Bell polynomial expressions ([139, 172, 173]) as follows:

$$Y_\tau(v) + M(\tau)Y_\xi(v) + RY_{3\xi}(v,w) = 0, \tag{3.19}$$

$$Y_\eta(v) = \lambda Y_\xi(v), \tag{3.20}$$

$$Y_{2\xi}(v,w) = 0. \tag{3.21}$$

Here $M(\tau) = PG(\tau) + QG(\tau)^2 + T\lambda^2$, along with the relation $QN(\tau)^2 + 6R = 0, P + 2QG(\tau) = 0$ where $N(\tau) = N_0 e^{-S\tau}$, $G(\tau) = e^{-S\tau}\left(\int e^{S\tau}B(\tau)d\tau + G_0\right)$, N_0 and G_0 are taking as integrating constants. Using the identity ([139, 172, 173])

$$Y_{n_1x_1,\cdots,n_lx_l}\left(v = \ln(\frac{\mathcal{H}}{\mathcal{G}}), w = \ln(\mathcal{H}\mathcal{G})\right) = (\mathcal{H}\mathcal{G})^{-1}\mathcal{D}_{x_1}^{n_1}\mathcal{D}_{x_2}^{n_2}\cdots, \mathcal{D}_{x_l}^{n_l}\mathcal{H}\cdot\mathcal{G} \tag{3.22}$$

and chosing $v = \ln(\frac{\mathcal{H}}{\mathcal{G}})$ and $w = \ln(\mathcal{H}\mathcal{G})$, where $\mathcal{H}$ and $\mathcal{G}$ being the functions of ξ, η and τ, we obtain the bilinear form for Eq.(3.5):

$$\begin{aligned}
&(\mathcal{D}_\tau + M(\tau)\mathcal{D}_\xi + R\mathcal{D}_\xi^3)\mathcal{H}\cdot\mathcal{G} = 0,\\
&(\mathcal{D}_\eta - \lambda\mathcal{D}_\xi)\mathcal{H}\cdot\mathcal{G} = 0,\\
&\mathcal{D}_{\xi\xi}\mathcal{H}\cdot\mathcal{G} = 0,
\end{aligned} \tag{3.23}$$

Now using $\mathcal{H} = g + ih, \quad \mathcal{G} = g - ih$, bilinear Eqs.(3.23) reduced to

$$\begin{aligned}
&(\mathcal{D}_\tau + M(\tau)\mathcal{D}_\xi + R\mathcal{D}_\xi^3)h\cdot g = 0,\\
&(\mathcal{D}_\eta - \lambda\mathcal{D}_\xi)h\cdot g = 0,\\
&\mathcal{D}_{\xi\xi}(h\cdot h + g\cdot g) = 0,
\end{aligned} \tag{3.24}$$

and the variable transformation (3.18) leads to

$$\phi(\xi,\eta,\tau) = 2iN_0e^{-S\tau}\left[\frac{\partial}{\partial\xi}\tan^{-1}\left(\frac{h(\xi,\eta,\tau)}{g(\xi,\eta,\tau)}\right)\right] + e^{-S\tau}\left(\int e^{S\tau}B(\tau)d\tau + G_0\right) \tag{3.25}$$

3.3.2 The Bilinear Bäcklund Transformation :

Let (v', w') and (v, w) are two distinct solutions of the Eq.(3.5) respectively, where $v' = \ln(\frac{\mathcal{H}'}{\mathcal{G}'})$, $w' = \ln(\mathcal{H}'\mathcal{G}')$, $v = \ln(\frac{\mathcal{H}}{\mathcal{G}})$ and $w = \ln(\mathcal{H}\mathcal{G})$. Now, let's assume some new mixed variables

$$\begin{aligned}
&v_1 = \ln(\frac{\mathcal{G}'}{\mathcal{G}}),\ v_2 = \ln(\frac{\mathcal{H}'}{\mathcal{H}}),\ v_3 = \ln(\frac{\mathcal{G}'}{\mathcal{H}}),\ v_4 = \ln(\frac{\mathcal{H}'}{\mathcal{G}})\\
&w_1 = \ln(\mathcal{G}\mathcal{G}'),\ w_2 = \ln(\mathcal{H}'\mathcal{H}),\ w_3 = \ln(\mathcal{H}\mathcal{G}'),\ w_4 = \ln(\mathcal{H}'\mathcal{G}).
\end{aligned} \tag{3.26}$$

Next, we have the relationships shown below,

$$\begin{aligned}
&v' - v = v_2 - v_1,\ v' + v = v_4 - v_3,\ w' - w = v_3 + v_4,\\
&w' + w = w_1 + w_2 = w_3 + w_4.
\end{aligned} \tag{3.27}$$

Considering the following two field conditions,

$$Y_{2\xi}(\nu', w') - Y_{2\xi}(\nu, w) = 0 \tag{3.28}$$

$$Y_{\tau}(\nu') - Y_{\tau}(\nu) + M(\tau)\left[Y_{\xi}(\nu') - Y_{\xi}(\nu)\right] + R\left[Y_{3\xi}(\nu', w') - Y_{3\xi}(\nu, w)\right] = 0, \tag{3.29}$$

the expression for the Eq.(3.28) is

$$(\nu_3 + \nu_4)_{2\xi} + (\nu_2 - \nu_1)_{\xi}(\nu_4 - \nu_3)_{\xi} = 0. \tag{3.30}$$

By decoupling the above equation we get,

$$(\nu_4)_{\xi} = c_1 e^{\nu_1 - \nu_2}, \qquad (\nu_3)_{\xi} = c_2 e^{\nu_2 - \nu_1} \tag{3.31}$$

Using the mixed variable to decouple the Eq.(3.29), one can obtain

$$Y_{\tau}(\nu_1) + M(\tau)Y_{\xi}(\nu_1) + 6Rc_1c_2Y_{\xi}(\nu_1) + RY_{3\xi}(\nu_1, w_1) = 0 \tag{3.32}$$

$$Y_{\tau}(\nu_2) + M(\tau)Y_{\xi}(\nu_2) + 6Rc_1c_2Y_{\xi}(\nu_2) + RY_{3\xi}(\nu_2, w_2) = 0 \tag{3.33}$$

and one can obtain from the Eq.(3.20),

$$Y_{\eta}(\nu_1) = \lambda Y_{\xi}(\nu_1), \qquad Y_{\eta}(\nu_2) = \lambda Y_{\xi}(\nu_2) \tag{3.34}$$

Thus using Hirota's operators ([139, 172, 173]) and relations (3.22), the Eqs.(3.31)-(3.34) can be represented the bilinear Bäcklund transformation for Eq.(3.5) as bellow:

$$\left[\mathcal{D}_{\eta} - \lambda\mathcal{D}_{\xi}\right]\mathcal{G}' \cdot \mathcal{G} = 0 \tag{3.35a}$$

$$\left[\mathcal{D}_{\eta} - \lambda\mathcal{D}_{\xi}\right]\mathcal{H}' \cdot \mathcal{H} = 0 \tag{3.35b}$$

$$\mathcal{D}_{\xi}\mathcal{H}' \cdot \mathcal{G} = c_1\mathcal{H} \cdot \mathcal{G}' \tag{3.35c}$$

$$\mathcal{D}_{\xi}\mathcal{G}' \cdot \mathcal{H} = c_2\mathcal{G} \cdot \mathcal{H}' \tag{3.35d}$$

$$\left[\mathcal{D}_{\tau} + \left(M(\tau) + 6Rc_1c_2\right)\mathcal{D}_{\xi} + R\mathcal{D}_{\xi}^3\right]\mathcal{G}' \cdot \mathcal{G} = 0 \tag{3.35e}$$

$$\left[\mathcal{D}_{\tau} + \left(M(\tau) + 6Rc_1c_2\right)\mathcal{D}_{\xi} + R\mathcal{D}_{\xi}^3\right]\mathcal{H}' \cdot \mathcal{H} = 0 \tag{3.35f}$$

3.3.3 Lax pair :

Using $\nu = \ln(\frac{\mathcal{H}}{\mathcal{G}}) = \nu_1 - \nu_3 = \nu_4 - \nu_2$, we can remove ν_3 and ν_4 from the Eq.(3.31). Taking $\nu_1 = \ln(\psi_1)$ and $\nu_2 = \ln(\psi_2)$, we get,

$$(\psi_1)_{\eta} = c_2\lambda\psi_2 + \lambda\nu_{\xi}\psi_1 \tag{3.36}$$

$$(\psi_2)_{\eta} = c_1\lambda\psi_1 - \lambda\nu_{\xi}\psi_2 \tag{3.37}$$

Utilizing Eqs.(3.32) and (3.33), we find

$$(\psi_1)_\tau = A_1\psi_1 + A_2\psi_2, \tag{3.38}$$

$$(\psi_2)_\tau = A_3\psi_1 + A_4\psi_2. \tag{3.39}$$

The relations can presented in matrix form as,

$$\begin{aligned} &\psi_\eta = \mathcal{M}\psi, \qquad \psi_\tau = \mathcal{N}\psi,\ \psi = (\psi_1, \psi_2)', \\ &\mathcal{M} = \begin{pmatrix} \lambda\frac{\phi - G(\tau)}{N(\tau)} & \lambda c_2 \\ c_1\lambda & -\lambda\frac{\phi - G(\tau)}{N(\tau)} \end{pmatrix}, \qquad \mathcal{N} = \begin{pmatrix} A_1 & A_2 \\ A_3 & A_4 \end{pmatrix}, \end{aligned} \tag{3.40}$$

where

$$\begin{aligned} A_1 &= -\left[M(\tau)v_\xi + 4Rc_1c_2v_\xi + RY_{3\xi}(v,w)\right] \\ A_2 &= -c_2\left[M(\tau) + 4Rc_1c_2 + RY_{2\xi}(v,w) + 2RP_{2\xi}(w-v))\right] \\ A_3 &= -c_1\left[M(\tau) + 4Rc_1c_2 + RY_{2\xi}(v,w) + 2RP_{2\xi}(w+v)\right] \\ A_4 &= -A_3. \end{aligned} \tag{3.41}$$

This meets the compatibility requirement, $\mathcal{M}_\tau - \mathcal{N}_\eta + \mathcal{M}\mathcal{N} - \mathcal{N}\mathcal{M} = 0$. On consideration $Y_{2\xi}(v,w) = 0$ and we finally, obtained

$$\begin{aligned} A_1 &= -\left[(M(\tau) + 4Rc_1c_2)\frac{\phi - G(\tau)}{N(\tau)} + R\frac{\phi_{\xi\xi}}{N(\tau)} - 2R\frac{(\phi - G(\tau))^2}{N(\tau)^2}\right] \\ A_2 &= -c_2\left[M(\tau) + 4Rc_1c_2 - 2R\left(\frac{\phi_\xi}{N(\tau)} + \frac{(\phi - G(\tau))^2}{N(\tau)^2}\right)\right] \\ A_3 &= -c_1\left[M(\tau) + 4Rc_1c_2 + 2R\frac{\phi_{\xi\xi}}{N(\tau)} - 2R\frac{(\phi - G(\tau))^2}{N(\tau)^2}\right] \\ A_4 &= -A_3 \end{aligned} \tag{3.42}$$

According to the transformation $\psi_1 = \frac{1}{2}(\phi_1 + \phi_2)$ and $\psi_2 = \frac{1}{2}(\phi_1 - \phi_2)$ and $c_1 = c_2 = c$, one can obtain a natural Lax pair of Eq.(3.5) as shown below,

$$\begin{pmatrix}\phi_1\\ \phi_2\end{pmatrix}_\eta = \begin{pmatrix} \lambda c & \lambda\frac{\phi - G(\tau)}{N(\tau)} \\ -\lambda\frac{\phi - G(\tau)}{N(\tau)} & -\lambda c \end{pmatrix}\begin{pmatrix}\phi_1\\ \phi_2\end{pmatrix}, \qquad \begin{pmatrix}\phi_1\\ \phi_2\end{pmatrix}_\tau = \begin{pmatrix} \mathcal{A} & \mathcal{B} \\ \mathcal{C} & -\mathcal{A} \end{pmatrix}\begin{pmatrix}\phi_1\\ \phi_2\end{pmatrix}, \tag{3.43}$$

where

$$\begin{aligned} \mathcal{A} &= -4Rc^3 - c\left[M(\tau) - 2R\left(\frac{\phi - G(\tau)}{N(\tau)}\right)^2\right], \\ \mathcal{B} &= -4Rc^2\frac{\phi - G(\tau)}{N(\tau)} - 2Rc\frac{\phi_\xi}{N(\tau)} - M(\tau)\frac{\phi - G(\tau)}{N(\tau)} - R\frac{\phi_{2\xi}}{N(\tau)} + 2R\left(\frac{\phi - G(\tau)}{N(\tau)}\right)^2, \\ \mathcal{C} &= -4Rc^2\frac{\phi - G(\tau)}{N(\tau)} + 2Rc\frac{\phi_\xi}{N(\tau)} - M(\tau)\frac{\phi - G(\tau)}{N(\tau)} - R\frac{\phi_{2\xi}}{N(\tau)} + 2R\left(\frac{\phi - G(\tau)}{N(\tau)}\right)^2. \end{aligned}$$

3.4 Soliton, smooth positon, breather and their interaction solutions

The K-soliton solutions of the nonautonomous KP-mKP equation (3.5), founded on the framework of Hirota's bilinear approach from the bilinear equations (3.24), are as follows.

$$\phi_K(\xi,\eta,\tau) = 2iN_0e^{-S\tau}\left[\frac{\partial}{\partial\xi}tan^{-1}\left(\frac{h_K(\xi,\eta,\tau)}{g_K(\xi,\eta,\tau)}\right)\right]+e^{-S\tau}\left(\int e^{S\tau}B(\tau)d\tau+G_0\right) \tag{3.44}$$

$$h_K = \sum_{d=0,1}(-1)^{\sum_r d_r}\exp\left(\sum_{r<s}^{K}d_rd_s\mathcal{M}_{rs}+\sum_{r=1}^{K}d_r(\psi_r+M_r)\right), \tag{3.45a}$$

$$g_K = \sum_{d=0,1}\exp\left(\sum_{r<s}^{K}d_rd_s\mathcal{M}_{rs}+\sum_{r=1}^{K}d_r(\psi_r+N_r)\right), \tag{3.45b}$$

where

$$\psi_r = \mathcal{A}_r(\xi+\lambda\eta)-(M(\tau)\mathcal{A}_r+R\mathcal{A}_r^3)\tau+\psi_r^0,\ r=1,\cdots,K \tag{3.46}$$

with

$$exp(M_r)=m_r,\ exp(N_r)=n_r,\ m_r=-n_r, \tag{3.47}$$

$$e^{\mathcal{M}_{rs}}=\mathcal{B}_{rs}=-\frac{(m_rm_s+n_rn_s)}{2}\frac{(\mathcal{A}_r-\mathcal{A}_s)^2}{(\mathcal{A}_r+\mathcal{A}_s)^2}. \tag{3.48}$$

The phase constant is ψ_r^0, and r,s take the values $1,2,\cdots,K$, where K denotes the soliton numbers. Here, $\sum_{d=0,1}$ and $\sum_{r<s}$ express the summation of the conceivable combinations of these values. $d=0,1\,(r,s=1,2,\cdots,K)$ are real constants that are picked at random.

Now, we conider $P=6,Q=-6,R=1,T=1,S=0,B(t)=0,\lambda=0,N_0=2,\ m_r=1,n_r=-1$, then the solutions (3.44)–(3.48) become identical as the multisoliton solution of the Gardner-KP or KP-mKP equation obtained by Wazwaz in Refs. [109]. When $P=a,\ Q=b,R=c,S=m,B(\tau)=H,n=0,T=0,\lambda=0$, and $N_0=-\frac{i}{\mu}$, the solution shown for the Nonautonomous Extended Forced Korteweg-de Vries equation with variable coefficients in Refs. [174] is the same as the multi soliton solutions (3.44)-(3.48). Given the following: $P=A,\ Q=B,R=C,S=L,B(\tau)=\Delta,T=0,\lambda=0N_0=s_0$, the above solution set (3.44)-(3.48) in the current literature, become same as the multisoliton solution for the non-autonomous Gardner equation derived by Raut et al. in the Refs. [175]. Considering $m_r=-1,n_r=1,(r=1,\cdots,K)$, the K-soliton solution for the model follows as,

$$\phi_K(\xi,\eta,\tau) = 2iN_0e^{-S\tau}\left[\frac{\partial}{\partial\xi}tan^{-1}\left(\frac{h_K(\xi,\eta,\tau)}{g_K(\xi,\eta,\tau)}\right)\right]+e^{-S\tau}\left(\int e^{S\tau}B(\tau)d\tau+G_0\right) \tag{3.49}$$

where

$$h_K = \sum_{d=0,1} (-1)^{\sum_r d_r} \exp\left(\sum_{r<s}^{K} d_r d_s \mathcal{M}_{rs} + \sum_{r=1}^{K} d_r \psi_r\right) \tag{3.50a}$$

$$g_K = \sum_{d=0,1} \exp\left(\sum_{r<s}^{K} d_r d_s \mathcal{M}_{rs} + \sum_{r=1}^{K} d_r \psi_r\right) \tag{3.50b}$$

with

$$\psi_r = \mathcal{A}_r(\xi + \lambda\eta) - (M(\tau)\mathcal{A}_r + R\mathcal{A}_r^3)\tau + \psi_r^0,\ r = 1, \cdots, K \tag{3.51}$$

$$e^{\mathcal{M}_{rs}} = \mathcal{B}_{rs} = -\frac{(\mathcal{A}_r - \mathcal{A}_s)^2}{(\mathcal{A}_r + \mathcal{A}_s)^2} \tag{3.52}$$

The phase constant is ψ_r^0, and r, s take the values $1, 2, \cdots, K$, where K denotes the soliton numbers. Here, $\sum_{d=0,1}$ and $\sum_{r<s}$ express the summation of the conceivable combinations of these values. $d = 0, 1\,(r, s = 1, 2, \cdots, K)$ are real constants that are picked at random.

3.4.1 1-soliton solution

When $K = 1$, we get

$$\begin{aligned} h_1 &= 1 - e^{\psi_1},\ g_1 = 1 + e^{\psi_1} \\ \psi_1 &= \mathcal{A}_1(\xi + \lambda\eta) - (M(\tau)\mathcal{A}_1 + R\mathcal{A}_1^3)\tau + \psi_1^0 \end{aligned} \tag{3.53}$$

For the set of real constant parameters $\mathcal{A}_1$, ψ_1^0, the 1-solitons represent the one-order solution. We obtain the single soliton solution by substituting the functions from transformation (3.49) with those from (3.53). The solitary waves' characteristic face is described as,

$$\xi + \lambda\eta = (M(\tau) + R\mathcal{A}_1^2)\tau - \frac{\psi_1^0}{\mathcal{A}_1} \tag{3.54}$$

and the wave velocity can be expressed as, respectively, in the direction of the ξ and η axes,

$$(V_\xi, V_\eta) = \left((M(\tau) + \tau M'(\tau) + R\mathcal{A}_1^2), \frac{1}{\lambda}(M(\tau) + \tau M'(\tau) + R\mathcal{A}_1^2)\right). \tag{3.55}$$

The speed of a single wave, denoted as (V_ξ, V_η) expresses both the strength and the direction of each spatial direction. By regulating the wave's velocities and orientation, the magnitude and signature of the velocity play significant roles in governing motion.

3.4.2 2-soliton solution

The 2-soliton solution for the nonautonomous KP-mKP Eq.(3.5) is given by the Eqs.(3.49)-(3.50) for $K = 2$ as,

$$h_2 = 1 - e^{\psi_1} - e^{\psi_2} + \mathcal{B}_{12} e^{\psi_1+\psi_2} \tag{3.56}$$

$$g_2 = 1 + e^{\psi_1} + e^{\psi_2} + \mathcal{B}_{12} e^{\psi_1+\psi_2} \tag{3.57}$$

where $\psi_j = \mathcal{A}_j(\xi + \lambda\eta) - \{M(\tau)\mathcal{A}_j + R\mathcal{A}_j^3\}\tau + \psi_j^0$, $j = 1, 2$ and $\mathcal{B}_{12} = -\frac{(\mathcal{A}_1-\mathcal{A}_2)^2}{(\mathcal{A}_1+\mathcal{A}_2)^2}$. The 2-soliton solution can be derived by inserting the functions (3.56)-(3.57) into Eq.(3.49) if all the parameters $\mathcal{A}_1$, $\mathcal{A}_2$, ψ_1^0 and ψ_2^0 are specified as real constants.

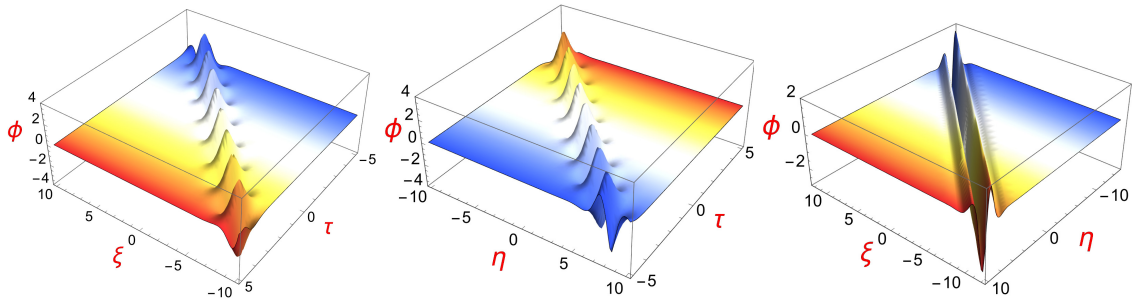

(a) (b) (c)

Figure 3.1: (a), (b) and (c) are the 3D graphs of 1-order breather solution (3.63), by considering $a_1 = 1.5$, $b_1 = 1.85$, $G_0 = 0$, $N_0 = i$, $S = 0.0$, $T = 0.15$, $\lambda = 1$, $B(\tau) = 0$, $Q = 1.5$, $\Omega = 1$ in (ξ, τ)-plane, (η, τ)-plane and (ξ, η)-plane respectively.

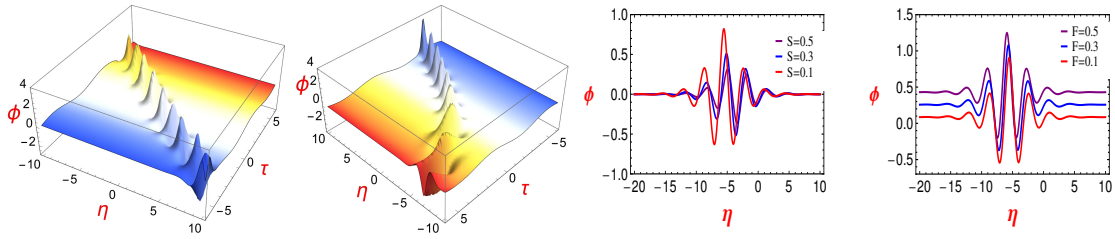

(a) (b) (c) (d)

Figure 3.2: The 3D graphs of 1-order breather solution (3.63), by considering $B(\tau) = F\cos(\Omega\tau)$, $a_1 = 1.5$, $b_1 = 1.85$, $M_0 = 0$, $N_0 = i$, $T = 0.15$, $\lambda = 1$, $Q = 1.5$, $\Omega = 1$ in (η, τ)-plane and (a) when $F = 0.3$, $S = 0$, (b) when $F = 0.3$, $S = 0.05$; (c) when $S = 0$ and (d) when $S = 0.05$.

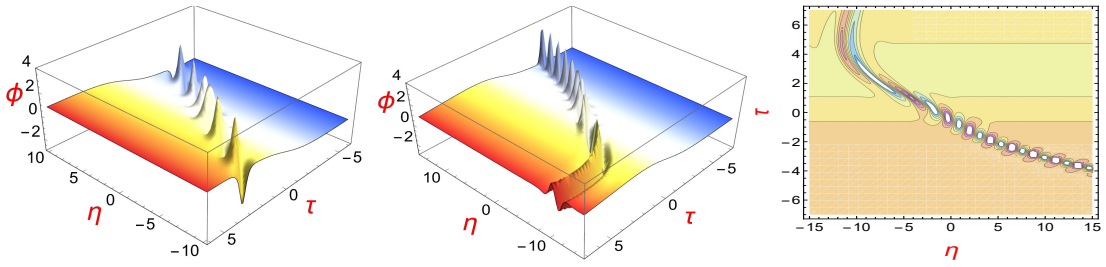

(a) (b) (c)

Figure 3.3: The 3D graphs of 1-order breather sol.(3.63), by considering $B(\tau) = F\ sech^2(\Omega\tau)$, $a_1 = 1.5$, $b_1 = 1.85$, $G_0 = 0$, $N_0 = i$, $T = 0.15$, $\lambda = 1$, $Q = 1.5$, $\Omega = 1$ in (η, τ)-plane and (a) when $F = 0.4$, $S = 0$, (b) when $F = 0.4$, $S = 0.05$ and (c) Contour plots of the corresponding Figure 3.3(b).

3.4.2.1 1-order breather solution

From the two soliton solution, formulate the 1-order breather solution of Eq.(3.5) the parameters can be choosen as,

$$\mathcal{A}_1 = a_1 + ib_1,\ \mathcal{A}_2 = a_1 - ib_1,\ \psi_1^0 = \psi_{11}^0 + i\psi_{12}^0,\ \psi_2^0 = \psi_{11}^0 - i\psi_{12}^0 \tag{3.58}$$

The function h_2 and g_2 in Eq.(3.56) can be presented as

$$h_2 = 1 - 2e^{\psi_{11}}\cos(\psi_{12}) + \frac{b_1^2}{a_1^2}e^{2\psi_{11}} \tag{3.59}$$

$$g_2 = 1 + 2e^{\psi_{11}}\cos(\psi_{12}) + \frac{b_1^2}{a_1^2}e^{2\psi_{11}} \tag{3.60}$$

where

$$\psi_{11} = a_1(\xi + \lambda\eta) - \{M(\tau)a_1 + R(a_1^3 - 3a_1b_1^2)\}\tau + \psi_{11}^0, \tag{3.61}$$

$$\psi_{12} = b_1(\xi + \lambda\eta) - \{M(\tau)b_1 + R(3a_1^2b_1 - b_1^3)\}\tau + \psi_{12}^0, \tag{3.62}$$

and ψ_{11}^0, ψ_{12}^0 are real constants. Then, 1-order breather solution is available as

$$\phi = 2iN_0e^{-S\tau}\left[\frac{\partial}{\partial\xi}\tan^{-1}\left(\frac{h_2}{g_2}\right)\right] + e^{-S\tau}\left(\int e^{S\tau}B(\tau)d\tau + G_0\right) \tag{3.63}$$

where (3.59) and (3.60) determine h_2 and g_2, respectively. The breather solution Eq.(3.63) depicts an oscillating periodically localised wave moving along ξ, and η axes the breather waves' characteristic face is expressed as,

$$\xi + \lambda\eta = \{M(\tau) + R(3a_1^2 - b_1^2)\}\tau - \frac{\psi_{12}^0}{b_1}, \tag{3.64}$$

and the velocity can be represented, respectively, in the directions of ξ and η as,

$$(V_\xi,\ V_\eta) = \left([M(\tau) + \tau M'(\tau) + R(3a_1^2 - b_1^2)],\ \frac{1}{\lambda}[M(\tau) + \tau M'(\tau) + R(3a_1^2 - b_1^2)]\right). \tag{3.65}$$

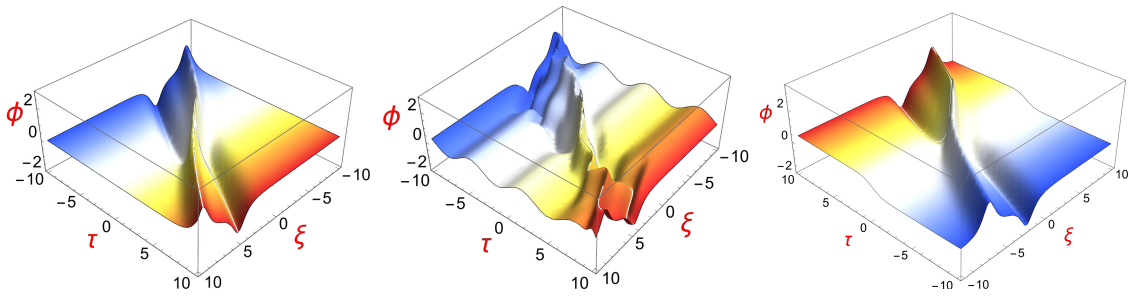

(a) (b) (c)

Figure 3.4: The 3D graphs of 2-order smooth positon sol.(3.67), by considering $B(\tau) = F\cos(\Omega\tau)$, $A_1 = 1.5$, $G_0 = 0$, $N_0 = i$, $T = 0.15$, $\lambda = 1$, $Q = 1.5$, $\Omega = 1$, $\alpha = 0.5$ in (η, τ)-plane and (a) when $F = 0$, $S = 0$, (b) when $F = 0.4$, $S = 0.0$ and (c) when $B(\tau) = F\,\mathrm{sech}^2(\Omega\tau)$ and $F = 0.4$, $S = 0.0$.

3.4.2.2 2-order smooth positon solution

For identifying a 2-order smooth position from a 2-soliton solution, we now apply the following proposition.

Proposition 1 *Setting some parameters of the relation* (3.51) *to*

$$\mathcal{A}_2 = \mathcal{A}_1 + \delta,\ \psi_1^0 = \ln(-\frac{\beta}{\delta}) + \zeta_1^0,\ \psi_2^0 = \ln\left(\frac{\beta}{\delta}\right) + \zeta_1^0 \tag{3.66}$$

and taking limit as $\delta \to 0$, *the 2-order smooth position solution to the non-autonomous KP-mKP equation* (3.5) *is yielded as:*

$$\phi_{2sp} = 2iN_0 e^{-S\tau}\left[\frac{\partial}{\partial\xi}\tan^{-1}\left(\frac{h_2}{g_2}\right)\right] + e^{-S\tau}\left(\int e^{S\tau}B(\tau)d\tau + G_0\right) \tag{3.67}$$

where

$$\begin{aligned} h_2 &= 1 - \beta\Psi_{11}e^{\Psi_1} + \frac{\beta^2}{4\mathcal{A}_1^2}e^{2\Psi_1},\ g_2 = 1 + \beta\Psi_{11}e^{\Psi_1} + \frac{\beta^2}{4\mathcal{A}_1^2}e^{2\Psi_1} \\ \Psi_1 &= \mathcal{A}_1(\xi + \lambda\eta) - \{M(\tau)\mathcal{A}_1 + R\mathcal{A}_1^3\}\tau + \zeta_1^0 \\ \Psi_{11} &= (\xi + \lambda\eta) - \{M(\tau) + 3R\mathcal{A}_1^2\}\tau. \end{aligned} \tag{3.68}$$

Proof. Utilizing Eq.(3.66), h_2 in Eq.(3.56) is presented as

$$\begin{aligned} h_2 \;=\; & 1 + \frac{\beta}{\delta}\left(1 - e^{(\xi+\lambda\eta-\tau M(\tau)-3R\mathcal{A}_1^2\tau)\delta-3R\mathcal{A}_1\tau\delta^2-R\tau\delta^3}\right)e^{\Psi_1} \\ & + \frac{\beta^2}{(2\mathcal{A}_1+\delta)^2}e^{2\Psi_1+(\xi+\lambda\eta-\tau M(\tau)-3R\mathcal{A}_1^2\tau)\delta-3R\mathcal{A}_1\tau\delta^2-R\tau\delta^3}, \end{aligned} \tag{3.69}$$

where $\Psi_1 = \mathcal{A}_1(\xi+\lambda\eta) - \{M(\tau)\mathcal{A}_1 + R\mathcal{A}_1^3\}\tau + \zeta_1^0$, which represents the semi-rational expression, when $\delta \to 0$:

$$h_2 = 1 - \beta\Psi_{11}e^{\Psi_1} + \frac{\beta^2}{4\mathcal{A}_1^2}e^{2\Psi_1}, \tag{3.70}$$

where $\Psi_{11} = (\xi + \lambda\eta) - \{M(\tau) + 3\mathcal{R}\mathcal{A}_1^2\}\tau$. In a similar manner, g_2 in Eq.(3.57) is transformed to

$$g_2 = 1 + \beta\Psi_{11}e^{\Psi_1} + \frac{\beta^2}{4\mathcal{A}_1^2}e^{2\Psi_1}. \tag{3.71}$$

Hence, Eq.(3.67) is simply verified.

Here, it is very important to mention one interesting observation. In, Refs. [176, 177], the authors only present bright smooth positons for $(1+1)$-dimesional equation when $\beta > 0$; however, for $\beta < 0$, they do not obtain even a dark degenerate solution using the degenerate Darboux transformation. In the current solution set, one can obtain bright or dark smooth positons for both the (1+1)-dimesional equation and the $(2+1)$-dimesional equation by appropriately choosing β.

3.4.3 3-soliton solution

When $K = 3$, from Eqs.(3.49)-(3.52), we get a triple soliton solution as well as different types of solitary interaction structures. Through analysis and calculations, different interactive structure is also found. For the 3rd-order solution, there are three different sorts of combinations. Below, we discuss three typical problems: Subsection 3.4.3.1 presenting 1-order breather and 1-soliton solution, Subsection 3.4.3.2 exploring 3-order smooth positon solution, and Subsection 3.4.3.3 exhibiting 2-order smooth positon and 1-soliton solution.

3.4.3.1 Interaction of 1-order breather and 1-soliton solution

The interaction of 1-order breather and 1-soliton solution for the Eq.(3.5) is shown from 3-soliton solution by setting the parameters

$$\mathcal{A}_1 = a_1 + ib_1,\ \mathcal{A}_2 = a_1 - ib_1,\ \psi_1^0 = \psi_{11}^0 + i\psi_{12}^0,\ \psi_2^0 = \psi_{11}^0 - i\psi_{12}^0 \quad \text{and} \quad \mathcal{A}_3 = (\text{a constant}) \tag{3.72}$$

Substitute this in the Eq.(3.50), one can obtained the interaction of 1-order breather and 1-soliton solution for Eq.(3.5) as

$$\phi = 2iN_0e^{-S\tau}\left[\frac{\partial}{\partial\xi}\tan^{-1}\left(\frac{h_3}{g_3}\right)\right] + e^{-S\tau}\left(\int e^{S\tau}B(\tau)d\tau + G_0\right) \tag{3.73}$$

where

$$\begin{aligned} h_3 = {} & 1 - 2e^{\psi_{11}}\cos(\psi_{12}) - e^{\psi_3} + \frac{b_1^2}{a_1^2}e^{2\psi_{11}} - 2\frac{\left((a_1^2-\mathcal{A}_3^2+b_1^2)^2-4b_1^2\mathcal{A}_3^2\right)}{\left[(a_1+\mathcal{A}_3)^2+b_1^2\right]^2}\cos(\psi_{12})e^{\psi_3+\psi_{11}} \\ & + \frac{8b_1\mathcal{A}_3(a_1^2-\mathcal{A}_3^2+b_1^2)}{\left[(a_1+\mathcal{A}_3)^2+b_1^2\right]^2}\sin(\psi_{12})e^{\psi_3+\psi_{11}} - \frac{b_1^2}{a_1^2}\frac{\left[(a_1^2-\mathcal{A}_3^2+b_1^2)^2+4b_1^2\mathcal{A}_3^2\right]^2}{\left[(a_1+\mathcal{A}_3)^2+b_1^2\right]^4}e^{2\psi_{11}+\psi_3} \end{aligned} \tag{3.74}$$

$$\begin{aligned} g_3 = {} & 1 + 2e^{\psi_{11}}\cos(\psi_{12}) + e^{\psi_3} + \frac{b_1^2}{a_1^2}e^{2\psi_{11}} - 2\frac{\left((a_1^2-\mathcal{A}_3^2+b_1^2)^2-4b_1^2\mathcal{A}_3^2\right)}{\left[(a_1+\mathcal{A}_3)^2+b_1^2\right]^2}\cos(\psi_{12})e^{\psi_3+\psi_{11}} \\ & + \frac{8b_1\mathcal{A}_3(a_1^2-\mathcal{A}_3^2+b_1^2)}{\left[(a_1+\mathcal{A}_3)^2+b_1^2\right]^2}\sin(\psi_{12})e^{\psi_3+\psi_{11}} + \frac{b_1^2}{a_1^2}\frac{\left[(a_1^2-\mathcal{A}_3^2+b_1^2)^2+4b_1^2\mathcal{A}_3^2\right]^2}{\left[(a_1+\mathcal{A}_3)^2+b_1^2\right]^4}e^{2\psi_{11}+\psi_3} \end{aligned} \tag{3.75}$$

with ψ_{11}^0, ψ_{12}^0 are constants and

$$\psi_{11} = a_1(\xi + \lambda\eta) - \{M(\tau)a_1 + R(a_1^3 - 3a_1b_1^2)\}\tau + \psi_{11}^0,$$
$$\psi_{12} = b_1(\xi + \lambda\eta) - \{M(\tau)b_1 + R(3a_1^2b_1 - b_1^3)\}\tau + \psi_{12}^0,$$
$$\psi_3 = \mathcal{A}_3(\xi + \lambda\eta) - \{M(\tau)\mathcal{A}_3 + R\mathcal{A}_3^3\}\tau + \psi_3^0.$$

3.4.3.2 3-order smooth positon solution

To obtain a 3-order smooth positon, we can show the following proposition by a similar argument to Proposition (1).

Proposition 2 *On consideration of the parameteric relation* (3.51), $\psi_1^0 = \zeta_1^0 + \ln(\frac{\beta}{\delta^2})$, $\psi_2^0 = \zeta_1^0 + \ln(-\frac{2\beta}{\delta^2})$, $\psi_3^0 = \zeta_1^0 + \ln(\frac{\beta}{\delta^2})$, $\mathcal{A}_2 = \mathcal{A}_1 + \delta$, $\mathcal{A}_3 = \mathcal{A}_1 + 2\delta$ *and on account of the limit* $\delta \to 0$, *yields a smooth 3-order position solution:*

$$\phi = 2iN_0e^{-S\tau}\left[\frac{\partial}{\partial\xi}\tan^{-1}\left(\frac{h_3}{g_3}\right)\right] + e^{-S\tau}\left(\int e^{S\tau}B(\tau)d\tau + G_0\right) \tag{3.76}$$

where

$$\begin{aligned} h_3 &= 1 - \beta(\Psi_{11}^2 + \Psi_{22})e^{\Psi_1} - \frac{8\beta^3}{(2\mathcal{A}_1)^6}e^{3\Psi_1} \\ &\quad -\beta^2\left(\frac{1}{2\mathcal{A}_1^4} + \frac{1}{\mathcal{A}_1^3}\Psi_{11} - \frac{1}{2\mathcal{A}_1^2}\Psi_{11}^2 + \frac{1}{2\mathcal{A}_1^2}\Psi_{22}\right)e^{2\Psi_1} \end{aligned} \tag{3.77}$$

$$\begin{aligned} g_3 &= 1 + \beta(\Psi_{11}^2 + \Psi_{22})e^{\Psi_1} + \frac{8\beta^3}{(2\mathcal{A}_1)^6}e^{3\Psi_1} \\ &\quad -\beta^2\left(\frac{1}{2\mathcal{A}_1^4} + \frac{1}{\mathcal{A}_1^3}\Psi_{11} - \frac{1}{2\mathcal{A}_1^2}\Psi_{11}^2 + \frac{1}{2\mathcal{A}_1^2}\Psi_{22}\right)e^{2\Psi_1} \end{aligned} \tag{3.78}$$

with

$\Psi_1 = \mathcal{A}_1(\xi + \lambda\eta) - \{M(\tau)\mathcal{A}_1 + R\mathcal{A}_1^3\}\tau + \zeta_1^0$, $\Psi_{11} = (\xi + \lambda\eta) - \{M(\tau) + 3R\mathcal{A}_1^2\}\tau$, $\Psi_{22} = -6R\mathcal{A}_1\tau$.

3.4.3.3 Interaction of 2-order smooth positon and 1-soliton solution

Proposition 3 *By setting the parameters* $\psi_1^0 = \ln(-\frac{\beta}{\delta}) + \zeta_1^0$, $\psi_2^0 = \ln\left(\frac{\beta}{\delta}\right) + \zeta_1^0$ *and* $\mathcal{A}_2 = \mathcal{A}_1 + \delta$ *and using the limit as* $\delta \to 0$, *we obtain the corresponding interaction solution between a 2-order smooth positon and a 1-soliton:*

$$\phi = 2iN_0e^{-S\tau}\left[\frac{\partial}{\partial\xi}\tan^{-1}\left(\frac{h_3}{g_3}\right)\right] + e^{-S\tau}\left(\int e^{S\tau}B(\tau)d\tau + G_0\right) \tag{3.79}$$

where

$$h_3 = 1 - \beta\Psi_{11}e^{\Psi_1} - e^{\psi_3} + \frac{\beta^2}{4\mathcal{A}_1^2}e^{2\Psi_1} + \beta e^{\psi_3+\Psi_1}\left[\frac{\partial\mathcal{B}_{13}}{\partial\mathcal{A}_1} + \mathcal{B}_{13}\Psi_{11}\right] - \frac{\beta^2}{4\mathcal{A}_1^2}\mathcal{B}_{13}^2e^{2\Psi_1+\psi_3} \tag{3.80}$$

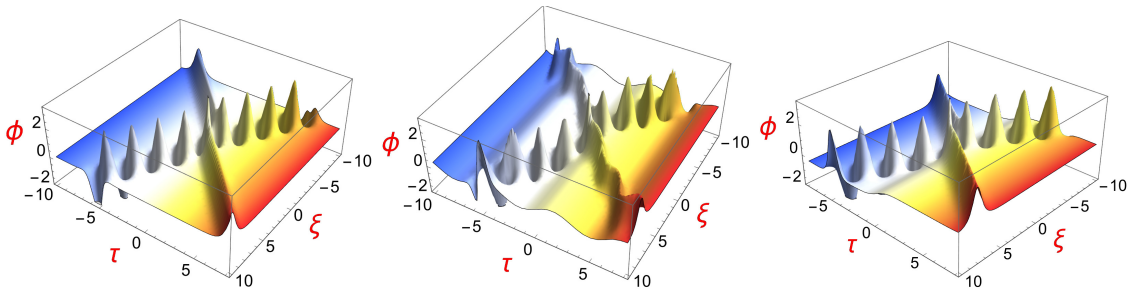

(a) (b) (c)

Figure 3.5: The 3D graphs of 1-order breather and 1-soliton sol.(3.73), by considering $B(\tau) = F\cos(\Omega\tau)$, $a_1 = 1.5, b_1 = 1.85, \mathcal{A}_3 = 2$, $G_0 = 0$, $N_0 = i$, $T = 0.15$, $\lambda = 1$, $Q = 1.5$, $\Omega = 1$, $\alpha = 0.5$ in (η, τ)-plane and (a) when $F = 0$, $S = 0$, (b) when $F = 0.4$, $S = 0.0$ and (c) when $B(\tau) = F\,\mathrm{sech}^2(\Omega\tau)$ and $F = 0.4$, $S = 0.0$.

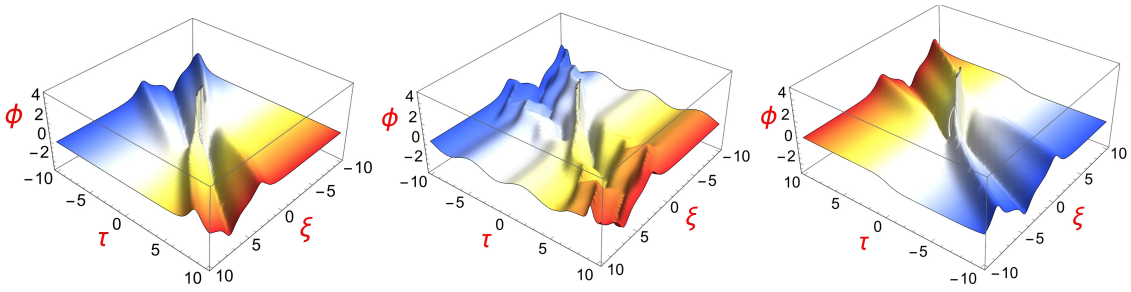

(a) (b) (c)

Figure 3.6: The 3D graphs of 3-order smooth positon sol.(3.76), by considering $B(\tau) = F\cos(\Omega\tau)$, $\mathcal{A}_1 = 1.5$, $G_0 = 0$, $N_0 = i$, $T = 0.15$, $\lambda = 1$, $Q = 1.5$, $\Omega = 1$, $\beta = 0.5$ in (η, τ)-plane and (a) when $F = 0$, $S = 0$, (b) when $F = 0.4$, $S = 0.0$ and (c) when $B(\tau) = F\,\mathrm{sech}^2(\Omega\tau)$ and $F = 0.4$, $S = 0.0$.

$$g_3 = 1 + \beta\Psi_{11}e^{\Psi_1} + e^{\psi_3} + \frac{\beta^2}{4\mathcal{A}_1^2}e^{2\Psi_1} + \beta e^{\psi_3+\Psi_1}\left[\frac{\partial\mathcal{B}_{13}}{\partial\mathcal{A}_1} + \mathcal{B}_{13}\Psi_{11}\right] + \frac{\beta^2}{4\mathcal{A}_1^2}\mathcal{B}_{13}^2 e^{2\Psi_1+\psi_3} \quad (3.81)$$

with

$$\Psi_1 = \mathcal{A}_1(\xi + \lambda\eta) - \{M(\tau)\mathcal{A}_1 + R\mathcal{A}_1^3\}\tau + \zeta_1^0,\ \Psi_{11} = \xi + \lambda\eta - \{M(\tau) + 3R\mathcal{A}_1^2\}\tau,$$
$$\psi_3 = \mathcal{A}_3(\xi + \lambda\eta) - \{M(\tau)\mathcal{A}_3 + R\mathcal{A}_3^3\}\tau + \psi_3^0,\ \mathcal{B}_{13} = -\frac{(\mathcal{A}_1 - \mathcal{A}_3)^2}{(\mathcal{A}_1 + \mathcal{A}_3)^2}. \quad (3.82)$$

With the exception of the computation step, the argument for Proposition (3) is nearly identical to that for Proposition (1). Summarizing Proposition (1) and Proposition (2), the following conjecture is addressed through mathematical induction:

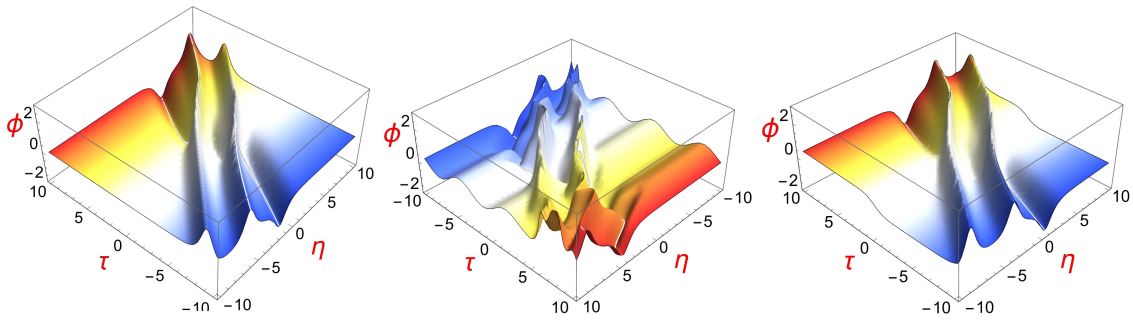

(a) (b) (c)

Figure 3.7: The 3D graphs of 2-order positon and 1-soliton sol.(3.79), by considering $B(\tau) = F\cos(\Omega\tau)$, $\mathcal{A}_1 = 1.5$, $\mathcal{A}_3 = 1.85$, $G_0 = 0$, $N_0 = i$, $T = 0.15$, $\lambda = 1$, $Q = 1.5$, $\Omega = 1.5$, $\alpha = 0.5$ in (η, τ)-plane and (a) when $F = 0$, $S = 0$, (b) when $F = 0.4$, $S = 0.0$ and (c) when $B(\tau) = F\,\mathrm{sech}^2(\Omega\tau)$ and $F = 0.4$, $S = 0.0$.

Inference 1 *If some of the parameters in Eq.*(3.49) *are taken as,*

$$\begin{aligned}
&\mathcal{A}_2 = \mathcal{A}_1 + \delta,\ \mathcal{A}_3 = \mathcal{A}_1 + 2\delta,\ \mathcal{A}_4 = \mathcal{A}_1 + 3\delta, \cdots, \mathcal{A}_K = \mathcal{A}_1 + (K-1)\delta,\\
&\psi_1^0 = \zeta_1^0 + \ln\frac{(-1)^{K+1}C_0^{K-1}\beta}{\delta^{K-1}},\ \psi_2^0 = \zeta_1^0 + \ln\frac{(-1)^{K+2}C_1^{K-1}\beta}{\delta^{K-1}},\\
&\psi_3^0 = \zeta_1^0 + \ln\frac{(-1)^{K+3}C_2^{K-1}\beta}{\delta^{K-1}}, \cdots, \psi_K^0 = \zeta_1^0 + \ln\frac{(-1)^{2K}C_{K-1}^{K-1}\beta}{\delta^{K-1}},
\end{aligned} \tag{3.83}$$

then, a Kth-order smooth positon ϕ_{K-sp} *can be derived from the K-soliton solution on consideration of* $\delta \to 0$.

Here, our present investigation is unique since multiple-pole solutions or degenerate solutions are derived in a number of creative approaches, including Propositions (1), (2), and Inference (1). The method introduced by Inference (1) is more straightforward and practical when compared to classical techniques like inverse scattering and Darboux transformation [178, 179, 180].

3.4.4 Interaction structures between solitons and breathers with $K \geqslant 4$

In this section, from the solution (3.49)-(3.50) and for $K = 4$, using various types of breather-solitons interacting with solitons, we are able to generate several brand-new interaction structures. For the 4-soliton solution, there are three different sorts of combinations. Below, we discuss three typical problems: Subsection 3.4.4.1 presenting 2-order breather solution, Subsection 3.4.4.2 exploring 1-order breather and 2-soliton solution, and finally Subsection 3.4.4.3 exhibiting 2-order breather positon solution.

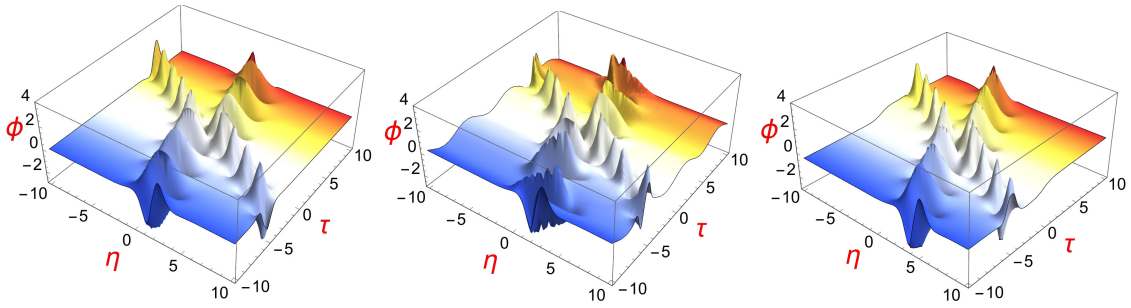

(a) (b) (c)

Figure 3.8: The 3D graphs of 2-order breather sol.(3.85), by considering $B(\tau) = F\cos(\Omega\tau)$, $a_1 = 1.5$, $b_1 = 1.75$, $a_2 = 1.55$, $b_2 = 1.15$, $G_0 = 0$, $N_0 = i$, $T = 0.15$, $\lambda = 1$, $Q = 1.5$, $\Omega = 1$ in (η, τ)-plane and (a) when $F = 0$, $S = 0$, (b) when $F = 0.4$, $S = 0.0$ and (c) when $B(\tau) = F\,sech^2(\Omega\tau)$ and $F = 0.4$, $S = 0.0$.

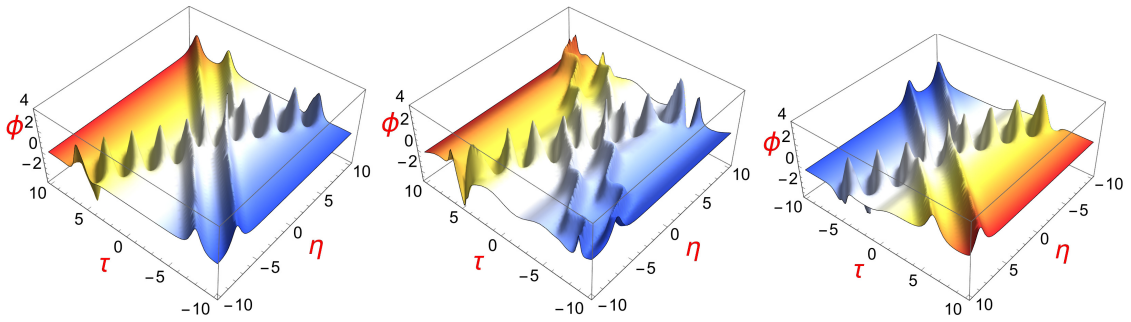

(a) (b) (c)

Figure 3.9: The 3D graphs of 1-order breather and 2-soliton sol.(3.86), by considering $B(\tau) = F\cos(\Omega\tau)$, $a_1 = 1.5$, $b_1 = 1.75$, $\mathcal{A}_3 = 2, \mathcal{A}_4 = 1.9$, $G_0 = 0$, $N_0 = i$, $T = 0.15$, $\lambda = 1$, $Q = 1.5$, $\Omega = 1$ in (η, τ)-plane and (a) when $F = 0$, $S = 0$, (b) when $F = 0.4$, $S = 0.0$ and (c) when $B(\tau) = F\,sech^2(\Omega\tau)$ and $F = 0.4$, $S = 0.0$.

3.4.4.1 2-order breather solution

The two breather wave can be directly constructed from the four soliton (when $K = 4$) solution (3.49) and the fixed restrictive conditions are fulfilled, is similar to (3.58) by taking advantage of the substitution of

$$\begin{aligned} &\mathcal{A}_1 = a_1 + ib_1,\ \mathcal{A}_1 = \mathcal{A}_2^*,\ \mathcal{A}_3 = a_2 + ib_2,\ \mathcal{A}_3 = \mathcal{A}_4^*, \\ &\psi_1^0 = \psi_{11}^0 + i\psi_{12}^0, \psi_1^0 = \psi_2^{0*}, \psi_3^0 = \psi_{31}^0 + i\psi_{32}^0,\ \psi_3^0 = \psi_4^{0*}, \end{aligned} \tag{3.84}$$

in Eqs.(3.50)-(3.51), we obtained the 2-order breather solution for the Eq.(3.5) as

$$\phi = 2iN_0 e^{-S\tau}\left[\frac{\partial}{\partial\xi}\tan^{-1}\left(\frac{h_4}{g_4}\right)\right] + e^{-S\tau}\left(\int e^{S\tau}B(\tau)d\tau + G_0\right) \tag{3.85}$$

3.4.4.2 Interaction of 1-order breather and 2-soliton solution

The interaction of 1-order breather and 2-soliton solution for the nonautonomous KP-mKP Eq.(3.5) is shown by choosing $\mathcal{A}_1 = a_1 + ib_1$, $\mathcal{A}_2 = a_1 - ib_1$. Now we get 1-order breather and 2-soliton solution by substituting h_4, g_4 in the equation given below

$$\phi = 2iN_0 e^{-S\tau}\left[\frac{\partial}{\partial\xi}\tan^{-1}\left(\frac{h_4}{g_4}\right)\right] + e^{-S\tau}\left(\int e^{S\tau}B(\tau)d\tau + G_0\right) \tag{3.86}$$

where

$$\begin{aligned} h_4 &= 1 - 2e^{\psi_{11}}\cos(\psi_{12}) - e^{\psi_3} - e^{\psi_4} + \frac{b_1^2}{a_1^2}e^{2\psi_{11}} + \mathcal{B}_{34}e^{\psi_3+\psi_4} - e^{\psi_{11}+\psi_3}[2\mathcal{B}_{131}\cos(\psi_{12}) \\ &-2\mathcal{B}_{132}\sin(\psi_{12})] - e^{\psi_{11}+\psi_4}[2\mathcal{B}_{141}\cos(\psi_{12}) - 2\mathcal{B}_{142}\sin(\psi_{12})] - \frac{b_1^2}{a_1^2}[(\mathcal{B}_{131}^2 + \mathcal{B}_{132}^2)e^{2\psi_{11}+\psi_3} \\ &+(\mathcal{B}_{141}^2 + \mathcal{B}_{142}^2)e^{2\psi_{11}+\psi_4}] - \mathcal{B}_{34}e^{\psi_{11}+\psi_3+\psi_4}[2(\mathcal{B}_{131}\mathcal{B}_{141} - \mathcal{B}_{132}\mathcal{B}_{142})\cos(\psi_{12}) - \\ &2(\mathcal{B}_{131}\mathcal{B}_{142} + \mathcal{B}_{132}\mathcal{B}_{141})\sin(\psi_{12})] + \frac{b_1^2}{a_1^2}\mathcal{B}_{34}(\mathcal{B}_{131}^2 + \mathcal{B}_{132}^2)(\mathcal{B}_{141}^2 + \mathcal{B}_{142}^2)e^{2\psi_{11}+\psi_3+\psi_4} \end{aligned} \tag{3.87}$$

$$\begin{aligned} g_4 &= 1 + 2e^{\psi_{11}}\cos(\psi_{12}) + e^{\psi_3} + e^{\psi_4} + \frac{b_1^2}{a_1^2}e^{2\psi_{11}} + \mathcal{B}_{34}e^{\psi_3+\psi_4} - e^{\psi_{11}+\psi_3}[2\mathcal{B}_{131}\cos(\psi_{12}) \\ &-2\mathcal{B}_{132}\sin(\psi_{12})] - e^{\psi_{11}+\psi_4}[2\mathcal{B}_{141}\cos(\psi_{12}) - 2\mathcal{B}_{142}\sin(\psi_{12})] + \frac{b_1^2}{a_1^2}[(\mathcal{B}_{131}^2 + \mathcal{B}_{132}^2)e^{2\psi_{11}+\psi_3} \\ &+(\mathcal{B}_{141}^2 + \mathcal{B}_{142}^2)e^{2\psi_{11}+\psi_4}t] + \mathcal{B}_{34}e^{\psi_{11}+\psi_3+\psi_4}[2(\mathcal{B}_{131}\mathcal{B}_{141} - \mathcal{B}_{132}\mathcal{B}_{142})\cos(\psi_{12}) - 2(\mathcal{B}_{131}\mathcal{B}_{142} \\ &+\mathcal{B}_{132}\mathcal{B}_{141})\sin(\psi_{12})] + \frac{b_1^2}{a_1^2}\mathcal{B}_{34}(\mathcal{B}_{131}^2 + \mathcal{B}_{132}^2)(\mathcal{B}_{141}^2 + \mathcal{B}_{142}^2)e^{2\psi_{11}+\psi_3+\psi_4} \end{aligned} \tag{3.88}$$

where

$$\mathcal{B}_{34} = -\frac{(\mathcal{A}_3 - \mathcal{A}_4)^2}{(\mathcal{A}_3 + \mathcal{A}_4)^2},\ \mathcal{B}_{131} = \frac{(a_1^2 - \mathcal{A}_3^2 + b_1^2)^2 - 4b_1^2\mathcal{A}_3^2}{[(a_1 + \mathcal{A}_3)^2 + b_1^2]^2},\ \mathcal{B}_{141} = \frac{(a_1^2 - \mathcal{A}_4^2 + b_1^2)^2 - 4b_1^2\mathcal{A}_4^2}{[(a_1 + \mathcal{A}_4)^2 + b_1^2]^2},$$
$$\mathcal{B}_{132} = \frac{4b_1\mathcal{A}_3(a_1^2 - \mathcal{A}_3^2 + b_1^2)}{[(a_1 + \mathcal{A}_3)^2 + b_1^2]^2},\ \mathcal{B}_{142} = \frac{4b_1\mathcal{A}_4(a_1^2 - \mathcal{A}_4^2 + b_1^2)}{[(a_1 + \mathcal{A}_4)^2 + b_1^2]^2},$$

and

$$\begin{aligned} \psi_{11} &= a_1(\xi + \lambda\eta) - \{M(\tau)a_1 + R(a_1^3 - 3a_1b_1^2)\}\tau + \psi_{11}^0, \\ \psi_{12} &= b_1(\xi + \lambda\eta) - \{M(\tau)b_1 + R(3a_1^2b_1 - b_1^3)\}\tau + \psi_{12}^0, \\ \psi_3 &= \mathcal{A}_3(\xi + \lambda\eta) - \{M(\tau)\mathcal{A}_3 + R\mathcal{A}_3^3\}\tau + \psi_3^0, \\ \psi_4 &= \mathcal{A}_4(\xi + \lambda\eta) - \{M(\tau)\mathcal{A}_4 + R\mathcal{A}_4^3\}\tau + \psi_4^0. \end{aligned}$$

3.4.4.3 2-order breather positon solution

Through degenerate Darboux transformation, Breather positons with a nonzero background for $(1+1)$-dimensional equations, can be derived from the plane wave solution when the

spectral parameters λ_{2j-1} tend to a specific value λ_1 [181]. Ref. [182] describes another mechanism for generating breather positons with a zero background using module resonance conditions. In fact, there have been some well-developed schemes for constructing breather positons for $(1+1)$-dimensional equations via degenerate Darboux transformation. A quick and easy way to obtain breather positons resting on a zero background from Eq.(3.49) is provided in this section. To obtain a 2-order breather-positon solution from the 4-soliton solution, we use the following proposition:

Proposition 4 *On consideration of some certain parameteric relation* (3.51) *as*

$$\begin{aligned}
&K = 4,\ \mathcal{A}_2 = \mathcal{A}_1 + \delta,\ \mathcal{A}_4 = \mathcal{A}_3 + \delta,\ \psi_1^0 = \zeta_1^0 + \ln\left(-\frac{\beta}{\delta}\right),\ \psi_2^0 = \zeta_1^0 + \ln\left(\frac{\beta}{\delta}\right),\\
&\psi_3^0 = \zeta_3^0 + \ln\left(-\frac{\beta}{\delta}\right),\ \psi_4^0 = \zeta_3^0 + \ln\left(\frac{\beta}{\delta}\right),\ \mathcal{A}_1 = \mathcal{A}_3^*,\ \zeta_1^0 = \zeta_3^{0*}
\end{aligned} \tag{3.89}$$

and on account of the limit, $\delta \to 0$, a 2-order breather-positon solution to the non-autonomous KP-mKP equation is drawn as follows:

$$\phi = 2iN_0 e^{-S\tau}\left[\frac{\partial}{\partial\xi}\tan^{-1}\left(\frac{h_4}{g_4}\right)\right] + e^{-S\tau}\left(\int e^{S\tau}B(\tau)d\tau + G_0\right) \tag{3.90}$$

where

$$\begin{aligned}
h_4 \;=\;& 1 - \beta\Psi_{11}e^{\Psi_1} - \beta\Psi_{33}e^{\Psi_3} + \frac{\beta^2}{4\mathcal{A}_1^2}e^{2\Psi_1} + \frac{\beta^2}{4\mathcal{A}_3^2}e^{2\Psi_3} + \\
&\beta^2\left[\frac{\partial}{\partial\mathcal{A}_1}\frac{\partial\mathcal{B}_{13}}{\partial\mathcal{A}_3} - \frac{\partial\mathcal{B}_{13}}{\partial\mathcal{A}_3}\Psi_{11} + \frac{\partial\mathcal{B}_{13}}{\partial\mathcal{A}_1}\Psi_{33} + \mathcal{B}_{13}\Psi_{11}\Psi_{33}\right]e^{\Psi_1+\Psi_3} - \\
&\frac{\beta^3\mathcal{B}_{13}^2}{4\mathcal{A}_1^2}\left(\frac{4}{(\mathcal{A}_1+\mathcal{A}_3)} - \Psi_{33}\right)e^{2\Psi_1+\Psi_3} - \\
&\frac{\beta^3\mathcal{B}_{13}^2}{4\mathcal{A}_3^2}\left(\frac{4}{(\mathcal{A}_1+\mathcal{A}_3)} - \Psi_{11}\right)e^{\Psi_1+2\Psi_3} + \\
&\frac{\beta^4}{16\mathcal{A}_1^2\mathcal{A}_3^2}\mathcal{B}_{13}^4 e^{2\Psi_1+2\Psi_3}
\end{aligned} \tag{3.91}$$

$$\begin{aligned}
g_4 \;=\;& 1 + \beta\Psi_{11}e^{\Psi_1} + \beta\Psi_{33}e^{\Psi_3} + \frac{\beta^2}{4\mathcal{A}_1^2}e^{2\Psi_1} + \frac{\beta^2}{4\mathcal{A}_3^2}e^{2\Psi_3} + \\
&\beta^2\left[\frac{\partial}{\partial\mathcal{A}_1}\frac{\partial\mathcal{B}_{13}}{\partial\mathcal{A}_3} - \frac{\partial\mathcal{B}_{13}}{\partial\mathcal{A}_3}\Psi_{11} + \frac{\partial\mathcal{B}_{13}}{\partial\mathcal{A}_1}\Psi_{33} + \mathcal{B}_{13}\Psi_{11}\Psi_{33}\right]e^{\Psi_1+\Psi_3} + \\
&\frac{\beta^3\mathcal{B}_{13}^2}{4\mathcal{A}_1^2}\left(\frac{4}{(\mathcal{A}_1+\mathcal{A}_3)} - \Psi_{33}\right)e^{2\Psi_1+\Psi_3} + \\
&\frac{\beta^3\mathcal{B}_{13}^2}{4\mathcal{A}_3^2}\left(\frac{4}{(\mathcal{A}_1+\mathcal{A}_3)} - \Psi_{11}\right)e^{\Psi_1+2\Psi_3} + \\
&\frac{\beta^4}{16\mathcal{A}_1^2\mathcal{A}_3^2}\mathcal{B}_{13}^4 e^{2\Psi_1+2\Psi_3}
\end{aligned} \tag{3.92}$$

with

$$\Psi_1 = \mathcal{A}_1(\xi + \lambda\eta) - \{M(\tau)\mathcal{A}_1 + R\mathcal{A}_1^3\}\tau + \zeta_1^0,\ \Psi_3 = \mathcal{A}_3(\xi + \lambda\eta) - \{M(\tau)\mathcal{A}_3 + R\mathcal{A}_3^3\}\tau + \zeta_3^0,$$
$$\Psi_{11} = (\xi + \lambda\eta) - \{M(\tau) + 3R\mathcal{A}_1^2\}\tau,\ \Psi_{33} = (\xi + \lambda\eta) - \{M(\tau) + 3R\mathcal{A}_3^2\}\tau,\ \mathcal{B}_{13} = -\frac{(\mathcal{A}_1 - \mathcal{A}_3)^2}{(\mathcal{A}_1 + \mathcal{A}_3)^2}.$$

It is pointed out that the proof for Proposition (4) is almost identical to that of Proposition (1), and is omitted here.

From the above results, we assert through mathematical induction that the following is true:

Inference 2 *The* K*-soliton solution* (3.49) *can be used to construct the high-order breather solution by keeping the parameters in complex conjugate relations. If the parameters satisfy the following constraint criteria, the* K*-soliton solution* (3.49) *specifies the* m*-order breather solution.*

$$K = 2m,\ A_i = A_{i+1}^*,\ \psi_i^0 = \psi_{i+1}^{0*}, i = 1, \cdots, K. \tag{3.93}$$

Then, the K*-soliton solution turns into the* m*-order breather solution.*

Inference 3 *Interactive solutions between* m*-order breather and* k*-soliton can be obtained by permitting*

$$K = 2m + k, A_{2m} = A_{2m-1}^*,\ \psi_{2m}^0 = \psi_{2m-1}^{0*}. \tag{3.94}$$

In the above declaration, the real constants $A_{2m+j}, \psi_{2m+j}^0, j = 1, 2, \cdots, k$ *are taken arbitrarily, in the expression of* K*-soliton solution* (3.49).

The following inference provides a quick and easy method to extract breather positons laying on a zero background from Eq.(3.49), much like Proposition (4).

Inference 4 *If the following assignments are made to some of the parameters in Eq.*(3.49)*:*

$$\begin{aligned}
&\mathcal{A}_2 = \mathcal{A}_1 + \delta, \mathcal{A}_3 = \mathcal{A}_1 + 2\delta, \cdots, \mathcal{A}_m = \mathcal{A}_1 + (m-1)\delta, \mathcal{A}_{m+2} = \mathcal{A}_{m+1} + \delta, \mathcal{A}_{m+3} = \mathcal{A}_{m+1} + 2\delta, \cdots,\\
&\mathcal{A}_{2m} = \mathcal{A}_{m+1} + (m-1)\delta, \psi_1^0 = \zeta_1^0 + \ln\frac{(-1)^{m+1}C_0^{m-1}\beta}{\delta^{m-1}}, \psi_2^0 = \zeta_1^0 + \ln\frac{(-1)^{m+2}C_1^{m-1}\beta}{\delta^{m-1}}, \cdots, K = 2m,\\
&\psi_m^0 = \zeta_1^0 + \ln\frac{(-1)^{2m}C_{m-1}^{m-1}\beta}{\delta^{m-1}}, \psi_{m+1}^0 = \zeta_{m+1}^0 + \ln\frac{(-1)^{m+1}C_0^{m-1}\beta}{\delta^{m-1}}, \mathcal{A}_1 = \mathcal{A}_{m+1}^*, \zeta_1^0 = \zeta_{m+1}^{0*}\\
&\psi_{2m}^0 = \zeta_{m+1}^0 + \ln\frac{(-1)^{2m}C_{m-1}^{m-1}\beta}{\delta^{m-1}}, \psi_{m+2}^0 = \zeta_{m+1}^0 + \ln\frac{(-1)^{m+2}C_1^{m-1}\beta}{\delta^{m-1}}, \cdots,
\end{aligned} \tag{3.95}$$

then a mth-order breather positon ϕ_{m-bp} *will be extracted from the* $2m$*-soliton solution on consideration of* $\delta \to 0$.

3.4.5 Results and Discussion

(i) **1-order breather**: If the parameters are properly set, we may obtain the one-breath solution of the nonautonomous KP-mKP when $\mathfrak{a}_1 \neq 0$ and $\exp(\mathcal{B}_{12}) > 1$ in Eq.(3.5). Additionally, a general breather is possible, as seen in Figure 3.1 in the (ξ, τ), (η, τ), and (ξ, η)-plane. The graphical description, which describes them as happening frequently in a local time-space zone, indicates that they are naturally single breathers. The graphical representation thus shows that the breather is both spatially and temporally periodic. When $\tau = 1$ is low enough, the breather wave exhibits the line structure, as seen in Figure 3.1(c). Although the periodic line waves are parallel and independent of one another, time τ consistently affects how they behave. We refer to the periodic line wave as the line breather because the basic line rogue wave can be thought of as a specific instance of the period line wave. With the same parameters as above in varying damping, and forcing values, the breathers (Figure 3.2) exhibit a range of behavioral traits without sacrificing generality. A locally oscillating wave travelling in a straight line at the speed defined by (3.65), is seen in the breather solution Eq.(3.63). For small values of S, the moderate periodic breather is found in Figure 3.2(a). However, when the forcing component $\mathsf{B}(\tau) = \mathsf{F}\,\mathsf{cos}(\beta\tau)$ is taken into account, the periodicity of the system is increased. The shape and size of the breather sufficiently improve. Finally, the periodic breather tends to be a horseshoe-type breather due to the presence of $\mathsf{B}(\tau)$ in the velocity part. When both damping and forcing impacts occur at the same time, the breather wave's amplitude is significantly reduced, and the polarity of the breather shifts (see Figure 3.2(b)). The damping term S has a noticeable effect on the 1-order breather's amplitude, as shown in Figure 3.2(c). Actually, damping has a detrimental effect on all dynamic systems, causing their potential energy to decrease. Therefore, the fading of a breather is depicted in Figure 3.2(c). As can be observed in Figure 3.2(d), the forcing term's rising magnitude causes the amplitude of breather waves to increase. This paper examines the kinky-breather, a special sort of breather (Figure 3.3) in the (η, τ)-plane that occurs when a forced term has the formula $\mathsf{B}(\tau) = \mathsf{F}\,\mathsf{sech}^2(\omega\tau)$. We can see the interaction between a breather wave and a kink wave, sometimes known as a kinky-breather wave solution, in Figure 3.3(a) and Figure 3.3(b). During contact, a breather wave is seen to move along the bend portion of a kink wave. These 3-dimensional views unmistakably show the existence of periodic lump waves known as kinky-breather waves. The periodic lump waves are clear from the superposition of the single lump waves. These graphs show that the speed, amplitude, and width of kinky-breather waves remain constant throughout their entire propagation. Due to the significant influence of S over $\mathsf{B}(\tau)$, the kink wave's amplitude lowers whenever S increases in value (see Figure 3.3(b), Figure 3.3(c)).

(ii) **2-order smooth positon**: A bright 2-order smooth positon composed of two bright parts will be derived, as shown in Figure 3.4(a) when damped and forced terms are taken to be zero. In a spatial dimension, a positon attains a singularity in its neighboring zone. After the mutual

interaction of two positons, they remain unaltered as before their interactions. Figure 3.4(b) depicts the situation for $B(\tau) = 0.4\,\cos(\tau)$, the two order smooth positon wave has one peak and two valleys, and the two valleys have the same depth, but the peak has been stretched to a periodic shape which is different from those of autonomous NLEEs. When we take hyperbolic functions for the forced term, we will obtain kinky-positon waves as shown in Figure 3.4(c).

(iii) **1-order breather and 1-soliton**: Three different types of hybrid solutions are depicted in Figure 3.5 by selecting appropriate parameters. However, if we choose the parameters $B(\tau) = F\,\cos(\Omega\tau)$, $a_1 = 1.5, b_1 = 1.85, \mathcal{A}_3 = 2$, $G_0 = 0$, $N_0 = i$, $T = 0.15$, $\lambda = 1$, $Q = 1.5$, $\Omega = 1$, $\alpha = 0.5$ and $F = 0$, $S = 0$, we discover that the breather in the hybrid solution intersects the stripe soliton at a specific angle, as shown in Figure 3.5(a). The hybrid solution shown in Figure 3.5(b) is made up an interaction of a horseshoe-type breather and a periodic soliton moving in the opposite direction. A hybrid solution made up of a kinky-breather and a parabolic soliton is shown in Figure 3.5(c) (for $B(\tau) = F\,\mathrm{sech}^2(\Omega\tau)$ and $F = 0.4$, $S = 0$).

(iv) **3-order smooth positon**: When $\mathcal{A}_1 = 1.5$, $G_0 = 0$, $N_0 = i$, $T = 0.15$, $\lambda = 1$, $Q = 1.5$, $\Omega = 1$, $\beta = 0.5$ and $F = 0$, $S = 0$, a bright 3-order smooth positon composed of two bright parts and one dark part will be derived, as shown in Figure 3.6(a). Figure 3.6(b) depicts the situation for $B(\tau) = F\,\cos(\Omega\tau)$ and $F = 0.4$, $S = 0.0$, the the peak of the 3-order smooth positon wave has been stretched to a periodic shape that is different from those of the 3-order smooth positon for the autonomous KP-mKP equation. For $B(\tau) = F\,\mathrm{sech}^2(\Omega\tau)$ and $F = 0.4$, $S = 0.0$, 3-order smooth positon converted to 3-order kinky-positon waves as shown in Figure 3.6(c).

(v) **2-order smooth positon and 1-soliton**: When $\mathcal{A}_1 = 1.5$, $\mathcal{A}_3 = 1.85$, $G_0 = 0$, $N_0 = i$, $T = 0.15$, $\lambda = 1$, $Q = 1.5$, $\Omega = 1.5$, $\alpha = 0.5$ and $F = 0$, $S = 0$, a bright 2-order smooth positon and one-soliton shown in Figure 3.7(a). Figure 3.7(b) depicts the situation for $B(\tau) = F\,\cos(\Omega\tau)$, and $F = 0.4$, $S = 0.0$, the two order smooth positon wave has one peak and two valleys, have the same depth, but the peak has been stretched to a parabolic shape together with parabolic soliton which is different from Figure 3.7(a). When we take $B(\tau) = F\,\mathrm{sech}^2(\Omega\tau)$ and $F = 0.4$, $S = 0.0$, we will obtain kinky-positon-soliton waves as shown in Figure 3.7(c).

(vi) **2-order breather**: The spreading of 2-order breathers, which is the interaction between two types of breathers, those periodic in η and those periodic in τ, is depicted in Figure 3.8. The configurations of the breathers have varied with numerous values of P, Q, R, S, $B(\tau)$ at each period. 2-order breather solutions are shown in Figure 3.8(a) for zero values of damped and forced terms. Due to the breather's consistency in terms of waveforms, amplitudes, and pulse widths, the interactions are likewise elastic. When considered a periodic force, the 2-order breather solutions turn out to be two horseshoe-type breather solutions (Figure 3.8(b)). From Figure 3.8(c) it is clear that when choosing a hyperbolic forcing, 2-order kinky-breathers change their polarity in interacting breathers.

(vii) **1-order breather and 2-soliton**: The interaction of a breather and 2-solitons is shown

in Figure 3.9(a) with the appropriate paragraphs. Due to the breather's form, amplitude, and pulse width invariance, the interactions are also elastic. When $B(\tau) = F\cos(\Omega\tau)$, $a_1 = 1.5$, $b_1 = 1.75$, $\mathcal{A}_3 = 2, \mathcal{A}_4 = 1.9$, $G_0 = 0$, $N_0 = i$, $T = 0.15$, $\lambda = 1$, $Q = 1.5$, $\Omega = 1$, $\alpha = 0.5$ and $F = 0.4$, $S = 0.0$, the interaction of breather and two-soliton solutions turn to be horseshoe-type breather and snake-like soliton solution (Figure 3.9(b)). From Figure 3.9(c) it is clear that when $B(\tau) = F\,sech^2(\Omega\tau)$ and $F = 0.4$, $S = 0.0$, the interaction of breather and 2-soliton solutions turn to be kinky-breather and Light refraction-like phenomena appear in the soliton's propagation. Additionally, we observe how an external force causes a tight kink structure to emerge in the backdrop. After colliding, the solitons naturally migrate apart.

3.5 The stability analysis

In this section, the concept of linear stability analysis [183, 184, 185] will be applied to study the stability analysis for the giving equation Eq.(3.4). The perturbed solution of the nonautonomous KP-mKP equation given by

$$\phi(\xi,\eta,\tau) = N(\tau)V(\xi,\eta,\tau) + G(\tau) \tag{3.96}$$

in above the relation: (i) when $S \neq 0$ and $B(\tau) \neq 0$, $N(\tau)$ and $G(\tau)$ are given by $N(\tau) = N_0 e^{-S\tau}$, $G(\tau) = e^{-S\tau}\int e^{S\tau}B(\tau)d\tau$; (ii) when $S = 0$ and $B(\tau) = 0$, N is considered as a constant and G is steady state solution for the KP-mKP equation. Here we choose the nonautonomous case. Substituting (3.96) into Eq.(3.4), one can obtain

$$\left(N\frac{\partial V}{\partial\tau} + PN^2V\frac{\partial V}{\partial\xi} + PNG\frac{\partial V}{\partial\xi} + QNG^2\frac{\partial V}{\partial\xi} + QN^3V^2\frac{\partial V}{\partial\xi} + 2QN^2GV\frac{\partial V}{\partial\xi} + RN\frac{\partial^3 V}{\partial\xi^3}\right)_\xi$$
$$+TN\frac{\partial^2 V}{\partial\eta^2} = 0. \tag{3.97}$$

By linerization Eq.(3.97), we get

$$\left(\frac{\partial V}{\partial\tau} + PG\frac{\partial V}{\partial\xi} + QG^2\frac{\partial V}{\partial\xi} + R\frac{\partial^3 V}{\partial\xi^3}\right)_\xi + T\frac{\partial^2 V}{\partial\eta^2} = 0, \tag{3.98}$$

assuming the above Eq.(3.98) has a solution in form of

$$V(\xi,\eta,\tau) = e^{i(A_0\xi + B_0\eta - W\tau)}. \tag{3.99}$$

Here A_0, and B_0 are normalized wave numbers and W is the frequency of perturbation. Now inserting Eq.(3.99) into Eq.(3.98) and solving for W, yields the result

$$W(A_0,B_0) = \frac{(PG + QG^2)A_0^2 - RA_0^4 + TB_0^2}{A_0}. \tag{3.100}$$

The sign of $W(A_0, B_0)$ recommeneds that the solution is expected to either decrease or grow over time. Group velocity dispersion, self-phase modulation, and stimulated Raman scattering all contribute to the steady-state stability of the dispersion relation Eq.(3.100). Furthermore, it is easy to show that modulation stability happens when $A_0 \neq 0$. Any superposition of solutions of the form $e^{i(A_0\xi + B_0\eta - W\tau)}$ will come to decay when the sign of $W(A_0, B_0)$ is negative for all values of A_0. At this point, the steady state is stable. The steady state is unstable if, for some values of A_0, the term $W(A_0, B_0)$ is positive. This is because some components of a superposition will get larger with time. The dispersion is referred to as marginally stable if the maximum of $W(A_0, B_0)$ is precisely 0. The relations for the propagation in Eq.(3.100) is examined and the corresponding plots are depicted in Figure 3.10. It is clear from Figure 3.10(a)-Figure 3.10(c) that, for all values of A_0, the variation of $W(A_0, B_0)$ is positive, negative, and 0. Specifically, when A_0 resides in $(-0.65, 0) \cup (0.65, k_0)$, where k_0 is a finite constant, $W(A_0, B_0)$ is negative for the following values: $Q = 1, P = 6, S = 0.1, R = 0.5, T = 0.15, F = 0.1, \tau = 5, B_0 = 0.5, \Omega = 1.5$. From Figure 3.10(a)-Figure 3.10(c) it also cleared that variation of F, B_0 and R significantly effects on the variation of stable state domain. The velocity dispersion default for all normalised wave numbers A_0 and B_0 is real. Therefore, the stable state remains stable in the face of wave number perturbations.

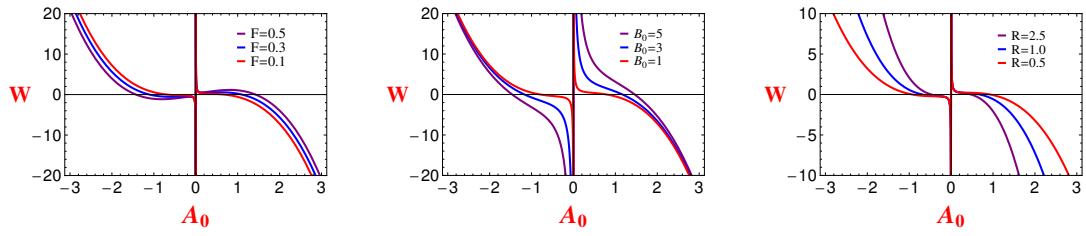

(a) (b) (c)

Figure 3.10: The dispersion relation between frequency $W(A_0, B_0)$ and wave number A_0, by considering $B(\tau) = F\cos(\Omega\tau)$, and (a) for $Q = 1$, $P = 6$, $S = 0.1$, $R = 0.5$, $T = 0.15$, $\tau = 5$, $B_0 = 0.5$, $\Omega = 1.5$, (b) for $Q = 1$, $P = 6$, $S = 0.1$, $R = 0.5$, $T = 0.15$, $F = 0.1$, $\tau = 5$, $\Omega = 1.5$ and (c) for $Q = 1$, $P = 6$, $S = 0.1$, $T = 0.15$, $F = 0.1$, $\tau = 5$, $B_0 = 0.5, \Omega = 1.5$.

3.6 Study of Phase Plane

It is well established that different biological and physical phenomena are well described by evolution equations. However, solving evolution equations analytically becomes very hard in many times and sometimes it becomes impossible. Examining the dynamics of a system that controls the nonlinear evolution equation, encourages geometric and qualitative techniques. To comprehend the geometrical characteristics and behavior of solutions, we explore the dynamical system of the KP-

mKP model in this part. The examination of phase pictures reveals that alterations in the plasma parameters operating in the system alter the geometric patterns of the solution profiles.
By combining the actual variables ξ, η, and τ, a new variable s is created, such as,

$$\phi(\xi,\eta,\tau)=\theta_1(s),\quad s=l_1\xi+l_2\eta-\alpha\tau \tag{3.101}$$

where $l_1^2+l_2^2=1$ and α represents the wave's speed, in Eq.(3.3) we get

$$-\alpha l_1\theta_1''+Pl_1^2((\theta_1')^2+\theta_1\theta_1'')+Ql_1^2(\theta_1^2\theta_1''+2\theta_1(\theta_1')^2)+Rl_1^4\theta_1''''+Tl_2^2\theta_1''=0, \tag{3.102}$$

which on integration gives

$$-\alpha l_1\theta_1'+Pl_1^2\theta_1\theta_1'+Ql_1^2\theta_1^2\theta_1'+Rl_1^4\theta_1'''+Tl_2^2\theta_1'=0. \tag{3.103}$$

Again integrating we get

$$-\alpha l_1\theta_1+\frac{1}{2}Pl_1^2\theta_1^2+\frac{1}{3}Ql_1^2\theta_1^3+Rl_1^4\theta_1''+Tl_2^2\theta_1=0. \tag{3.104}$$

Now Eq.(3.104) is equivalent to the autonomous system

$$\begin{aligned}\frac{d\theta_1}{ds}&=\theta_2\\ \frac{d\theta_2}{ds}&=\frac{1}{Rl_1^4}\left[[\alpha l_1-T(1-l_1^2)]\theta_1-l_1^2\left(\frac{P}{2}\theta_1^2+\frac{Q}{3}\theta_1^3\right)\right].\end{aligned} \tag{3.105}$$

The first integral to this system is given by

$$H=Rl_1^4\theta_2^2-(\alpha l_1-T(1-l_1^2))\theta_1^2+l_1^2\left(\frac{P}{3}\theta_1^3+\frac{Q}{6}\theta_1^4\right)=h\ \ (say). \tag{3.106}$$

The system (3.105) has three equilibrium point, namely $A_1=(x_{A_1},0)$, $A_2=(x_{A_2},0)$ and $A_3=(x_{A_3},0)$, when its discriminant

$$\Delta_0=\frac{l_1^2}{4}\left[P^2l_1^2+\frac{16}{3}Q(\alpha l_1-T(1-l_1^2))\right]>0, \tag{3.107}$$

where

$$x_{A_1}=0,\ x_{A_{2,3}}=\frac{3}{4Ql_1^2}\left(-Pl_1^2\pm2\sqrt{\Delta_0}\right)=\frac{3}{4Ql_1}\left(-Pl_1\pm\sqrt{P^2l_1^2+\frac{16}{3}Q(\alpha l_1-T(1-l_1^2))}\right). \tag{3.108}$$

Otherwise it has only one equilibrium point $A_1=(0,0)$. Now, we draw the coefficient matrix of the linearized system of (3.105) at the point (θ_1,θ_2) as $M(\theta_1,\theta_2)$. Let, the elements of the matrix are $J_A=\det(M(\theta_1,\theta_2))$, $T_A^{(1)}=\mathrm{Tr}(M(\theta_1,\theta_2))$ and $T_A^{(2)}=(\mathrm{Tr}(M(\theta_1,\theta_2)))^2$ and so,

$$M(\theta_1,\theta_2)=\begin{pmatrix}0 & 1\\ \frac{1}{Rl_1^4}[\alpha l_1-T(1-l_1^2)-Pl_1^2\theta_1-Ql_1^2\theta_1^2] & 0\end{pmatrix}$$

Now, we investigate the phase plane (θ_1, θ_2) for the system (3.105) varying the values of P, Q, R, T, α, l_1.

Case 1. When $P^2l_1^2 + \frac{16}{3}Q(\alpha l_1 - T(1-l_1^2)) > 0$ and $R(\alpha l_1 - T(1-l_1^2)) < 0$. The equilibrium point A_3 becomes saddle because at that point $J_A < 0, T_A^{(2)} - 4J_A > 0$ and the equilibrium points A_1 and A_2 become center because for these points $J_A > 0, T_A^{(1)} = 0$. Thus a couple of homoclinic orbits are there through A_3 encircling the centers A_1 and A_2 on both sides of the saddle point A_3 (see Figure 3.11(a)).

Case 2. When $P^2l_1^2 + \frac{16}{3}Q(\alpha l_1 - T(1-l_1^2)) > 0$, $R(\alpha l_1 - T(1-l_1^2)) > 0$. The equilibrium point A_3 becomes center because at that point $J_A > 0, T_A^{(1)} = 0$ and the equilibrium points A_1 and A_2 becomes saddle because for these points $J_A < 0, T_A^{(2)} - 4J_A > 0$. Thus, a pair of heteroclinic paths are found joining two saddle points A_1 and A_2 connecting the center A_3 (see Figure 3.11(b)).

Case 3. When $P^2l_1^2 + \frac{16}{3}Q(\alpha l_1 - T(1-l_1^2)) < 0$ and $R(\alpha l_1 - T(1-l_1^2)) < 0$. The equilibrium point A_1 becomes center because at that point $J_A > 0, T_A^{(1)} = 0$. Thus we observed a periodic orbit about A_1 (see Figure 3.11(c)).

Case 4. When $P^2l_1^2 + \frac{16}{3}Q(\alpha l_1 - T(1-l_1^2)) < 0$ and $R(\alpha l_1 - T(1-l_1^2)) > 0$. The equilibrium point A_1 becomes saddle because for these points $J_A < 0, T_A^{(2)} - 4J_A > 0$ (see Figure 3.11(d)).

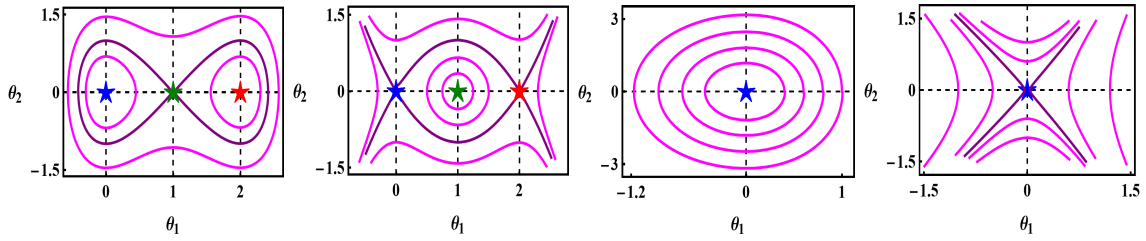

(a) (b) (c) (d)

Figure 3.11: 2D profiles of phase portraits of the dynamical system (3.105), (a) when $P^2l_1^2 + \frac{16}{3}Q(\alpha l_1 - T(1-l_1^2)) > 0$ and $R(\alpha l_1 - T(1-l_1^2)) < 0$, (b) when $P^2l_1^2 + \frac{16}{3}Q(\alpha l_1 - T(1-l_1^2)) > 0$ and $R(\alpha l_1 - T(1-l_1^2)) > 0$, (c) when $P^2l_1^2 + \frac{16}{3}Q(\alpha l_1 - T(1-l_1^2)) < 0$ and $R(\alpha l_1 - T(1-l_1^2)) < 0$, (d) when $P^2l_1^2 + \frac{16}{3}Q(\alpha l_1 - T(1-l_1^2)) < 0$ and $R(\alpha l_1 - T(1-l_1^2)) > 0$.

3.7 Classification of all travelling wave solutions and Parametric Representations of the solutions to the KP-mKP equation

The existence of shock, solitary, and periodic solutions in the present system is already confirmed. Now, we show that effective solutions can not be only acquired by analytical technique but can be attained also by utilizing the qualitative analysis of the system. Now, we will find

traveling wave solutions of Eq.(3.105) using the integral bifurcation method. We write Eq.(3.106) as

$$\theta_2^2 = \frac{1}{Rl_1^4}(h + [\alpha l_1 - T(1-l_1^2)]\theta_1^2 - \frac{Pl_1^2}{3}\theta_1^3 - \frac{Ql_1^2}{6}\theta_1^4) \tag{3.109}$$

Now, integrating along the level curves mentioned as $H(\theta_1, \theta_2) = h$ gives

$$s = \int \frac{d\theta_1}{\sqrt{\frac{1}{Rl_1^4}\left[h + [\alpha l_1 - T(1-l_1^2)]\theta_1^2 - l_1^2(\frac{P}{3}\theta_1^3 + \frac{Q}{6}\theta_1^4)\right]}}. \tag{3.110}$$

3.7.1 Solitary wave solutions

When $P^2l_1^2 + \frac{16}{3}Q(\alpha l_1 - T(1-l_1^2)) > 0$ and $R(\alpha l_1 - T(1-l_1^2)) < 0$, for the level $h = 0$, there exist two homoclinic orbits belonging to left and right side of phase plane joining the origin which is a saddle point and back again. Each orbit of this family cuts the θ_1 axis in three points (see Figure 3.11(a)). Then we can write Eq.(3.110) as

$$\sqrt{\frac{1}{Rl_1^4}}s = \int \frac{d\theta_1}{\theta_1\sqrt{[\alpha l_1 - T(1-l_1^2)] - \frac{Pl_1^2}{3}\theta_1 - \frac{Ql_1^2}{6}\theta_1^2}}. \tag{3.111}$$

By integrating we obtain the parametric representation of solitary wave solutions of Eq.(3.105) as

$$\theta_1(s) = \frac{6[\alpha l_1 - T(1-l_1^2)]}{\sqrt{P^2l_1^4 - 6Ql_1^2[\alpha l_1 - T(1-l_1^2)]}\cosh(\sqrt{\frac{1}{Rl_1^4}}s) + Pl_1^2}. \tag{3.112}$$

Thus we obtain the solitary wave solutions of Eq.(3.3) as

$$\phi(\xi,\eta,\tau) = \frac{6[\alpha l_1 - T(1-l_1^2)]}{\sqrt{P^2l_1^4 - 6Ql_1^2[\alpha l_1 - T(1-l_1^2)]}\cosh[\sqrt{\frac{1}{Rl_1^4}}(l_1\xi + l_2\eta - \alpha\tau)] + Pl_1^2}. \tag{3.113}$$

3.7.2 Shock wave solutions

When $P^2l_1^2 + \frac{16}{3}Q(\alpha l_1 - T(1-l_1^2)) > 0$, $R(\alpha l_1 - T(1-l_1^2)) > 0$, for the level $h = -\frac{3(\alpha l_1 - T(1-l_1^2))^2}{2Ql_1^2}$, there exist heteroclinic orbits joining two saddle point. Each orbit of this family cuts the θ_1 axis in two saddle point (see Figure 3.11(b)). Thus we can express the Eq.(3.110) as

$$\sqrt{\frac{Q}{6Rl_1^2}}s = \int \frac{d\theta_1}{([\alpha l_1 - T(1-l_1^2)]\frac{3}{Ql_1^2} - \theta_1^2)}. \tag{3.114}$$

Integrating we obtain the parametric representation of shock wave solution of Eq.(3.105) as

$$\theta_1(s) = \sqrt{\frac{3[\alpha l_1 - T(1-l_1^2)]}{Ql_1^2}}\tanh\left(\sqrt{\frac{[\alpha l_1 - T(1-l_1^2)]}{2Rl_1^4}}s\right). \tag{3.115}$$

Thus we get the shock wave solutions of Eq.(3.3) as

$$\phi(\xi,\eta,\tau) = \sqrt{\frac{3[\alpha l_1 - T(1-l_1^2)]}{Ql_1^2}}\tanh\left(\sqrt{\frac{[\alpha l_1 - T(1-l_1^2)]}{2Rl_1^4}}(l_1\xi + l_2\eta - \alpha\tau)\right). \tag{3.116}$$

3.7.3 Periodic wave solutions

When $P^2l_1^2 + \frac{16}{3}Q(\alpha l_1 - T(1-l_1^2)) < 0$ and $R(\alpha l_1 - T(1-l_1^2)) < 0$, for the level $h > 0$, there exist a periodic orbit centered at the origin and the orbit cuts the θ_1 axis in two points (see Figure 3.11(c)). So we can express Eq.(3.110) as

$$\sqrt{\frac{Q}{6Rl_1^2}}s = \int \frac{d\theta_1}{\sqrt{(\Theta_1-\theta_1)(\theta_1-\Theta_2)((\theta_1-\mu)^2+\nu^2)}}, \tag{3.117}$$

where $\Theta_2 < \theta_1 < \Theta_1$. We obtain periodic wave solution of system (3.105) in parametric form as

$$\theta_1(s) = \frac{\Theta_2 x_1(1+cn(\lambda_1 s, m_1)) + \Theta_1 x_2(1-cn(\lambda_1 s, m_1))}{x_1(1+cn(\lambda_1 s, m_1)) + x_2(1-cn(\lambda_1 s, m_1))}, \tag{3.118}$$

where $x_1^2 = (\Theta_1-\mu)^2+\nu^2$, $x_2^2 = (\Theta_2-\mu)^2+\nu^2$, $m_1^2 = \frac{(\Theta_1-\Theta_2)^2-(x_1-x_2)^2}{4x_1x_2}$, $\lambda_1 = \sqrt{\frac{x_1x_2Q}{6Rl_1^2}}$.
Then we get the periodic wave solution of Eq.(3.3) as

$$\phi(\xi,\eta,\tau) = \frac{\Theta_2 x_1(1+cn(\lambda_1(l_1\xi+l_2\eta-\alpha\tau), m_1)) + \Theta_1 x_2(1-cn(\lambda_1(l_1\xi+l_2\eta-\alpha\tau), m_1))}{x_1(1+cn(\lambda_1(l_1\xi+l_2\eta-\alpha\tau), m_1)) + x_2(1-cn(\lambda_1(l_1\xi+l_2\eta-\alpha\tau), m_1))}. \tag{3.119}$$

3.8 Qualitative Study of Damped KP-mKP Equation under External Periodic Force

In this section, we are trying to investigate the qualitative behavior of the system constructed from Eq. (3.4). The system is, therefore, studied using qualitative analysis to explore its nature and dependence on the damping coefficient and the external force. The system (3.4) is converted to a nonlinear ordinary differential equation (ODE)

$$-\alpha l_1\theta_1''(s) + Pl_1^2\frac{d}{ds}(\theta_1\theta_1') + Ql_1^2\frac{d}{ds}\left(\theta_1^2\theta_1'\right) + Rl_1^4\theta_1''''(s) + Sl_1\theta_1'(s) + T\left(1-l_1^2\right)\theta_1''(s) = Rl_1^2f_2''(s) \tag{3.120}$$

under the transformation (3.101) and

$$f_2(s) = F\sin(\omega\, s) \tag{3.121}$$

where ω designates the frequency of the external force. On integration with respect to s and vanishing the constant of integration we get the ODE

$$Rl_1^4\theta_1''' + l_1^2\left(P\theta_1 + Q\theta_1^2\right)\theta_1' + \left[T\left(1-l_1^2\right) - \alpha l_1\right]\theta_1' + Sl_1\theta_1 = Rl_1^2f_2' \tag{3.122}$$

which can be transformed to the non-autonomous system

$$\frac{d\theta_1}{ds} = \theta_2 \tag{3.123a}$$

$$\frac{d\theta_2}{ds} = \theta_3 \tag{3.123b}$$

$$\frac{d\theta_3}{ds} = \frac{1}{Rl_1^4}\left[-P_1 l_1^2\left(P\theta_1 + Q\theta_1^2\right)\theta_2 + \left[\alpha l_1 - T\left(1-l_1^2\right)\right]\theta_2 - Sl_1\theta_1\right] + \frac{f_2'}{l_1^2}. \tag{3.123c}$$

The ODE (3.122) with vanishing damping terms S and f_2 is nothing but the system (3.103) which is an integrable system the Hamiltonian of which, with little abuse of notation, is given by

$$H = \frac{\theta_2^2}{2} - \frac{1}{Rl_1^4}\left[\left[\alpha l_1 - T\left(1-l_1^2\right)\right]\frac{\theta_1^2}{2} - P_1 l_1^2\left(P\frac{\theta_1^3}{6} + Q\frac{\theta_1^4}{12}\right)\right]. \tag{3.124}$$

The Hamiltonian representing the total energy of the system is proportional to the first integral h given by Eq.(3.106) which is used to identify the parameters generating solitary, shock, and periodic wave solutions as discussed in section 3.6. On the other hand, the non-autonomous system (3.123) is not integrable but its detailed qualitative analysis reveals much more rich behavior, viz. intermittency, and chaos, of the system (3.4). In the following subsection, we elaborately study the system (3.105) again and subsequently explore the nature of the non-integrable system (3.122) in a systematic manner.

3.8.1 The KP-mKP System without Damping and External Periodic Force

The KP-mKP system (3.3) without damping and external periodic force is reduced to the autonomous system (3.105) which is integrable having Hamiltonian given by Eq.(3.106). We recall that the system has three equilibrium points $A_i = (x_{A_i}, 0)$, $i = 1, 2, 3$ when the discriminant Δ_0 given by Eq.(3.107) is positive and one equilibrium point $A_1 = (x_{A_1}, 0)$ when $\Delta_0 < 0$. Further, if $\Delta_0 = 0$, then the equilibrium points A_2 and A_3 coincide. Assuming

$$\frac{P}{Q} = r,\ Q = 1,\ R = 1,\ \alpha = 1 \text{ so that } T = 4^{-1/3} \tag{3.125}$$

we plot x_{A_k} given by Eq.(3.108) for $k = 1, 2, 3$ in Figure 3.12 and find that a bifurcation takes place against r for different values of l_1. When Δ_0 increases from negative to positive through the value $\Delta_0 = 0$ we find that the number of fixed points changes from one to three. In Figure 3.12 we elaborately study the change in position and nature of the equilibrium points $A_{1,2,3}$ represented by blue, red, and green colors respectively. In Figure 3.12(a) choosing $l_1 = 0.35$ we observe that two fixed points (represented by blue and green colors) suddenly vanish at $r = r_L = -2.98$ as r increases. Again two extra fixed points (blue and green) arise out of the clear blue sky at $r = r_R = 2.98$ as r increases. Thus, we encounter *fold bifurcation* at $r = r_L$ and $r = r_R$. In the regime $r_L < r < r_R$

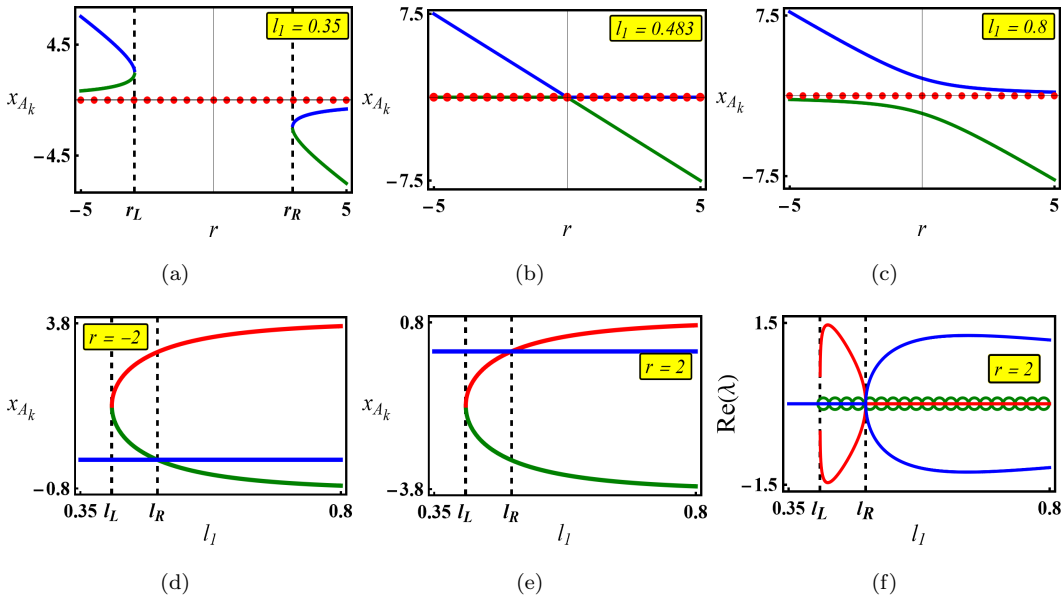

Figure 3.12: Bifurcation diagrams of x_{A_k} against the parameter r for (a) $l_1 = 0.35$, (b) $l_1 = 0.483$, (c) $l_1 = 0.8$. Bifurcation diagrams of x_{A_k} against the parameter l_1 for (d) $r = -2$, (e) $r = 2$. Real parts of the eigen values of the linearised system corresponding to the system (3.105) at the points $A_{1,2,3}$ are plotted in (f) against the parameter l_1 for $r = 2$. In all these figures blue, red and green lines refer to the equilibrium points A_1, A_2 and A_3 respectively.

we have $\Delta_0 < 0$ so that only one equilibrium point is there. However, for $r \leqslant r_L$ or $r \geqslant r_R$ we have $\Delta_0 > 0$ so that three equilibrium points are generated. The Figure 3.12(b) shows that same bifurcation arises only at $r = 0$ where $l_1 = 0.483$. Interestingly, taking $l_1 = 0.8$ we do not get any such bifurcation as evident from the Figure 3.12(c). In this case Δ_0 is always positive. In order to have a clear idea about the influence of the parameter l_1 on the system we study the bifurcation diagrams of x_{A_k} for $k = 1, 2, 3$ against l_1 for fixed values of r. In Figure 3.12(d) we choose $r = -2$ and observe that two new fixed points (represented by green and red color) evolve out of nowhere at $l_1 = l_L = 0.404$ resembling *fold bifurcation*. Such phenomena arise because of the fact that Δ_0 changes its sign from negative to positive as l_1 increases through $l_1 = l_L$. Two fixed points cross each other at $l_1 = l_R = 0.483$. A similar nature is seen for $r = 2$ in Figure 3.12(e). In order to study the nature of the fixed points elaborately for the last case where $r = 2$ we draw the bifurcation diagram of the real part of the eigenvalues of the corresponding linearized systems at the points $A_{1,2,3}$ and present them in Figure 3.12(f). This figure can be decomposed into three segments where $l_1 < l_L = 0.404$, $l_L \leqslant l_1 < l_R = 0.483$ and $l_1 \geqslant l_R$. The blue solid line shows that at the fixed point A_1 the system has purely imaginary eigenvalues for $l_1 < l_R$. Thus, A_1 remains a center for $l_1 < l_R$. This blue line bifurcates into two lines at $l_1 = l_R$ in which one is positive and the other is negative

showing that center A_1 converts into a node for $l_1 > l_L$. Here, we find that at $l_1 = l_L$ two new fixed points $A_{2,3}$ emerge. Two solid red lines starting from $l_1 = l_R$ represent positive and negative real parts of the eigenvalues showing that point A_2 is a node for $l_L \leqslant l_1 < l_R$. These eigenvalues become purely imaginary for $l_1 \geqslant l_R$ and so A_2 becomes a center. The green circled line shows that the eigenvalues of A_3 are purely imaginary implying a center for $l_1 \geqslant l_L$.

The Figure 3.13 show how the phase portrait change for $r = 2$ as l_1 increases. We observe that the red node A_2 approaches towards the blue center A_1 as l_1 increases for $l_1 \leqslant l_R$ and is shown in Figure 3.12(e). The point A_2 coincides with the point A_1 for $l_1 = l_R$ as shown in Figure 3.13(c) through a bicolour pentagram. This bicolor pentagram consisting of red and blue have been used in order to highlight the fact that the red point A_2 coincides with the blue point A_1 at $l_1 = l_R = 0.483$. This equilibrium point represents a node and a homoclinic orbit passes through this node surrounding the center A_3. Further, as l_1 increases the point A_2 crosses A_1 and interchanging their nature the equilibrium point A_2 becomes a center and A_1 becomes a node. This change of nature of the stability of A_1 and A_2 at $r = 2$, $l_1 = l_R$ represent a *transcritical bifurcation*. The values of the Hamiltonian are shown in Figure 3.13(d) along different phase paths for $l_1 = 0.8 > l_R$. The separatrix is given by $H = 0$ as shown in this figure. The Figure 3.13(d) shows that this separatrix is a homoclinic orbit surrounding the centers A_2 and A_3. The coexistence of various periodic, homoclinic orbits in these phase diagrams implies the multistability of the system which in turn indicates the dependence of the solution on the parameters r and l_1. Thus, for a single set of parameter values various periodic, soliton solutions may coexist for different initial conditions. We shall now check how external periodic perturbation deforms these orbits.

3.8.2 The KP-mKP System under External Periodic Force

The KP-mKP system (3.4) without damping under the influence of the external periodic force (3.121) can be written using the transformations (3.101) as the non-autonomous system

$$\frac{d\theta_1}{ds} = \theta_2 \tag{3.126a}$$

$$\frac{d\theta_2}{ds} = \frac{1}{Rl_1^4}\left[\left[\alpha l_1 - T\left(1 - l_1^2\right)\right]\theta_1 - P_1 l_1^2\left(P\frac{\theta_1^2}{2} + Q\frac{\theta_1^3}{3}\right)\right] + \frac{F}{l_1^2}\sin\left(\omega\ s\right). \tag{3.126b}$$

We now study the deformation of the phase portrait of this non-integrable system and investigate the influence of the amplitude F of the external periodic force. Under the light of the study conducted in the previous subsection we choose the following values of the parameters to start the investigation about the system (3.126) along with the values of the other parameters given by Eq.(3.125). Under

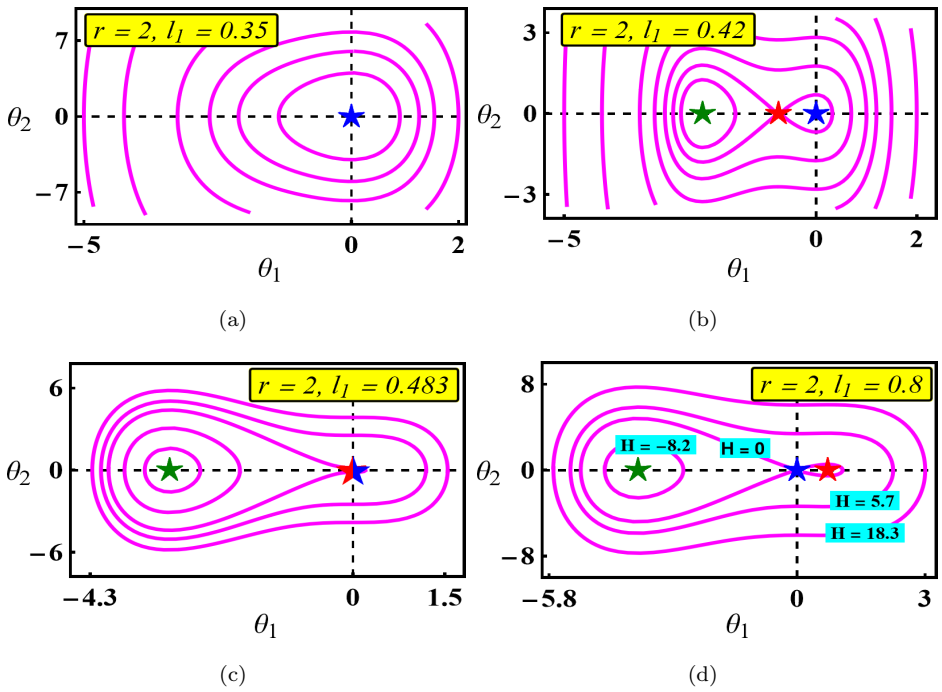

Figure 3.13: Phase diagram of the system (3.105) for different values of $\mathfrak{l}_1$ keeping $\mathfrak{r} = 2$. The values of the other parameters are given by Eq.(3.125).

the light of the previous subsection we choose

$$\mathfrak{r} = 2,\ \mathfrak{l}_1 = 0.35 \tag{3.127a}$$

$$\mathfrak{r} = 2,\ \mathfrak{l}_1 = 0.42 \tag{3.127b}$$

$$\mathfrak{r} = 2,\ \mathfrak{l}_1 = 0.483 \tag{3.127c}$$

$$\mathfrak{r} = 2,\ \mathfrak{l}_1 = 0.8 \tag{3.127d}$$

and elaborate the behaviour of the system (3.126) for each of the above cases. We find that the system behaves in a very much similar manner for values of the parameters given by Eq.(3.127b) and Eq.(3.127c) and so we do not explicitly present the detail study for Eq.(3.127c) and confine ourselves in the cases (3.127a), (3.127b) and (3.127c).

3.8.2.1 Study of Deformation of the Phase Portrait under $\mathfrak{r} = 2,\ \mathfrak{l}_1 = 0.35$

In this case $\Delta_0 < 0$ and the corresponding unperturbed system (3.105) has only one equilibrium point A_1 (represented by blue line in Figure 3.12(f) and blue star in Figure 3.13(a)) which is a center and so all the solutions are periodic. We choose $\omega = 1$ and investigate how the periodic

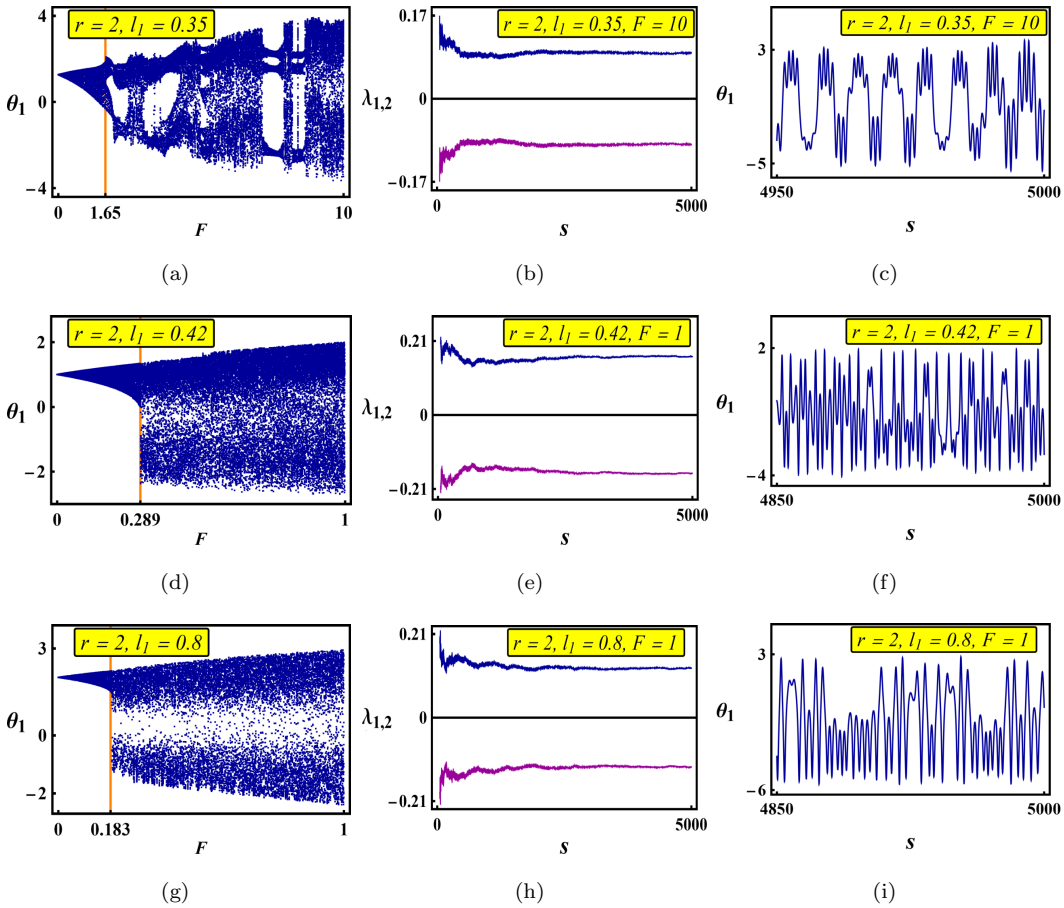

Figure 3.14: (a) The bifurcation diagram of θ_1 against F for the system (3.126) when $r = 2,\ l_1 = 0.35$. (b) Corresponding sprectra of LCE for $F = 10$ and (c) the solution $\theta_1(s)$ of the system (3.126). (d) The bifurcation diagram of θ_1 against F for the system (3.126) when $r = 2,\ l_1 = 0.42$. (e) Corresponding sprectra of LCE for $F = 1$ and (f) the solution $\theta_1(s)$ of the system (3.126). (g) The bifurcation diagram of θ_1 against F for the system (3.126) when $r = 2,\ l_1 = 0.8$. (h) Corresponding sprectra of LCE for $F = 1$ and (i) the solution $\theta_1(s)$ of the system (3.126).

orbit starting from the initial condition

$$\mathrm{IC}_1 : \theta_1(0) = 0,\ \theta_2(0) = 6 \tag{3.128}$$

deform as we increase the value of F. The bifurcation diagram of θ_1 against F is displayed in Figure 3.14(a) showing that the periodic orbit becomes quasiperiodic followed by a much irregular pattern when F increases through $0 \leqslant F \leqslant 10$. The onset of intermittency is visible at $F = 1.65$ which ultimately leads to a chaotic orbit as F increases further. The intermittency can be seen in this bifurcation diagram for different regimes of F. The bifurcation diagram of θ_2, although not shown here explicitly, has similar irregularity as F increases. In order to confirm the chaotic behavior

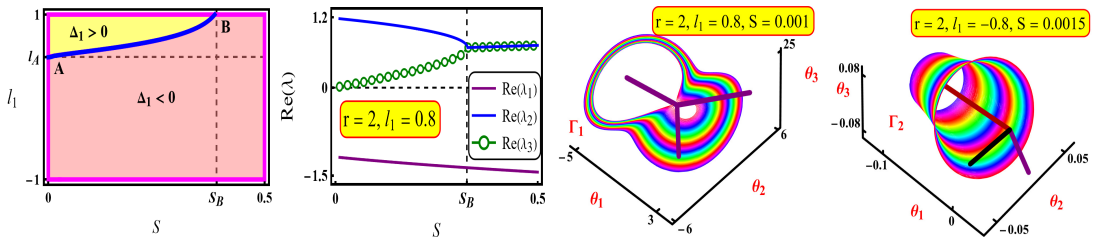

(a) (b) (c) (d)

Figure 3.15: (a) The S, l_1 parametric plane showing regions $\Delta_1 > 0$ in yellow, $\Delta_1 < 0$ in pink and the curve $\Delta_1 = 0$ in blue. (b) Real parts of the eigen values $\lambda_{1,2,3}$ are plotted against the damping coefficient S. (c) The solution orbit Γ_1 of the damped system (3.131) under the initial condition IC_5 given by Eq.(3.135) for which $\Delta_1 > 0$. (d) The solution orbit Γ_2 of the damped system (3.131) under the initial condition IC_6 given by Eq.(3.137) for which $\Delta_1 < 0$. The values of the parameters r, l_1 and S are specified in the respective figures. The remaining parameters are given by Eq.(3.125) in all these figures.

we draw the spectrum of the Lyapunov characteristic exponent (LCE) for the system (3.126) for $F = 10$ in Figure 3.14(b). The largest LCE is clearly positive implying that the solution is chaotic for $F = 10$. The corresponding solution of the system (3.126) for $F = 10$ is shown in Figure 3.14(c).

3.8.2.2 Study of Deformation of the Phase Portrait under $r = 2,\ l_1 = 0.42$

In this case $\Delta_0 > 0$ and we find three equilibrium points of the unperturbed system (3.105) out of which two points A_1 and A_3 (represented by blue and green color respectively in Figure 3.12(f) and 3.13(b)) centers and the third point A_2 (represented by red color in Figure 3.12(f) and 3.13(b)) is a node. The low-energy orbits encircle the centers and two homoclinic orbits surrounding these centers meet at the node. The Hamiltonian at the points on these low energy orbits have negative or small positive values. The value of the Hamiltonian gradually increases as we move away far from these centers and ultimately assumes a critical value where the homoclinic orbits are formed. Further, considering an initial condition

$$IC_2 : \theta_1(0) = 1,\ \theta_2(0) = 0 \tag{3.129}$$

far away from these centers, we obtain periodic orbit, at each point of which the Hamiltonian or energy function assumes relatively high values, in the phase plane surrounding all the equilibrium points $A_{1,2,3}$ and the homoclinic orbit when the external force F is not present. In order to find the deformation of such high energy periodic orbit in the presence of F we plot the bifurcation diagram of θ_1 for $0 \leqslant F \leqslant 1$ in the Figure 3.14(d) where we observe that the intermittency arises near $F = 0.289$ and this orbit becomes chaotic for larger values of F. In order to confirm the chaotic nature of the solution with the initial condition IC_2 we plot the spectra of the LCE for $F = 1$ as shown in the

Figure 3.14(e). The positive maximum LCE implies that the solution orbit is chaotic for $\mathsf{F} = 1$. The corresponding solution of the system (3.126) for $\mathsf{F} = 1$ is shown in Figure 3.14(f).
The deformation of the low energy periodic orbits as F increases is similar to the previous case given by Eq.(3.127a) and so its explicit study is omitted in order to avoid the repetitions. Although the deformation of the orbits is not shown here explicitly when $\mathsf{r} = 2$ and $\mathsf{l}_1 = 0.483$ given by Eq.(3.127c), one may observe similar behavior of the orbits as discussed here. In this context, we should recall that the equilibrium points A_1 and A_2 coincide in the absence of external force F as shown in the Figure 3.13(c) and a cusp is formed at that point where the reversal of the direction of the orbits can be observed in the phase plane.

3.8.2.3 Study of Deformation of the Phase Portrait under $\mathsf{r} = 2,\ \mathsf{l}_1 = 0.8$

In case $\Delta_0 > 0$ and we find high energy periodic orbits for unperturbed system (3.105) surrounding all the three equilibrium points $\mathsf{A}_{1,2,3}$ (see Figure 3.13(d)) and the homoclinic orbit. As the external force F increases we find that such periodic orbit with initial condition

$$\mathrm{IC}_3 : \theta_1(0) = 2,\ \theta_2(0) = 0 \tag{3.130}$$

deforms to a quasiperiodic orbit for $0 \leqslant \mathsf{F} \leqslant 0.183$ and finally produces a chaotic orbit through the route of intermittency as F increases further. The bifurcation diagram of θ_1 for $0 \leqslant \mathsf{F} \leqslant 1$ is shown in Figure 3.14(g). The spectra of LCE for $\mathsf{F} = 1$ are drawn in Figure 3.14(h) in which one positive LCE is found confirming the chaotic nature of the solution of the perturbed system. The corresponding solution of the system (3.126) is presented in Figure 3.14(i). In the above discussion, we have studied the deformation of different low and high-energy periodic orbits of the perturbed system (3.126) as the amplitude F of the external periodic force increases. It is observed that the low energy orbits are much more stable and less sensitive to external perturbation and large amplitude, such as $\mathsf{F} = 10$, of the external periodic disturbance is required to generate chaotic behavior in such orbits. The high-energy orbits, on the other hand, are less stable and much more sensitive to external force. Relatively small amplitude, such as $\mathsf{F} = 1$, of the external periodic perturbation produces chaotic behavior in such orbits. Thus, the inherent energy of the system in an orbit plays a key role in the deformation of the orbits as the external perturbation increases. We now study the effect of damping on the system and check if it enables the system to gain some stability against external disturbances. We first explore the effect of damping without external periodic perturbation in the following subsection.

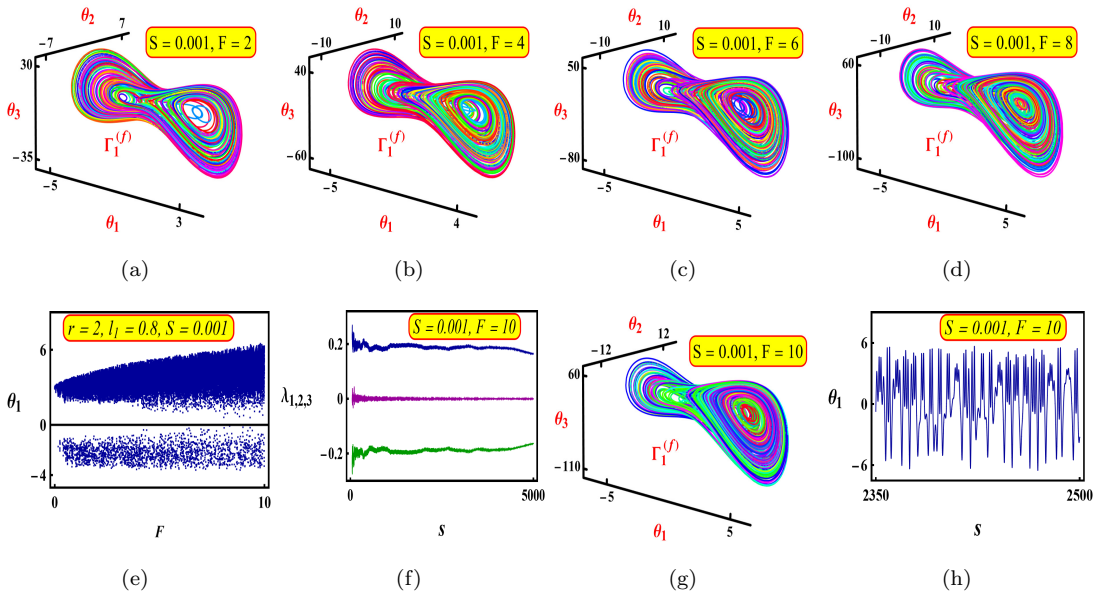

Figure 3.16: (a) – (d) : The phase diagram of $\Gamma_1^{(f)}$ for $S = 0.001$, $l_1 = 0.8$ and for different F. (e) : The bifurcation diagram of θ_1 against F corresponding to $\Gamma_1^{(f)}$. (f) : The spectrum of LCE of $\Gamma_1^{(f)}$ for $S = 0.001$ and $F = 10$. (g) : The phase diagram of $\Gamma_1^{(f)}$ for $S = 0.001$ and $F = 10$. (h) : The solution θ_1 plotted against s corresponding to $\Gamma_1^{(f)}$.

3.8.3 The Damped KP-mKP System without External Force

The damped KP-mKP system (3.4) without external force can be written under the transformation (3.101) as

$$\frac{d\theta_1}{ds} = \theta_2 \tag{3.131a}$$

$$\frac{d\theta_2}{ds} = \theta_3 \tag{3.131b}$$

$$\frac{d\theta_3}{ds} = \frac{1}{Rl_1^4}\left[-l_1^2\left(P\theta_1 + Q\theta_1^2\right)\theta_2 + \left[\alpha l_1 - T\left(1 - l_1^2\right)\right]\theta_2 - Sl_1\theta_1\right] \tag{3.131c}$$

which has only one fixed point at $O(0,0,0)$ in the phase space. We linearize the system and find the characteristic equation of the Jacobian of the linearized system at O as

$$\lambda^3 - \frac{\left(\alpha l_1 + l_1^2 T - T\right)}{l_1^4 R}\lambda + \frac{S}{l_1^3 R} = 0 \tag{3.132}$$

which is a depressed cubic equation having discriminant

$$\Delta_1 = -\left(-4\frac{\left(\alpha l_1 + l_1^2 T - T\right)^3}{l_1^{12} R^3} + 27\frac{S^2}{l_1^6 R^2}\right) = \frac{4\left(\alpha l_1 + l_1^2 T - T\right)^3 - 27S^2 l_1^6 R}{l_1^{12} R^3}. \tag{3.133}$$

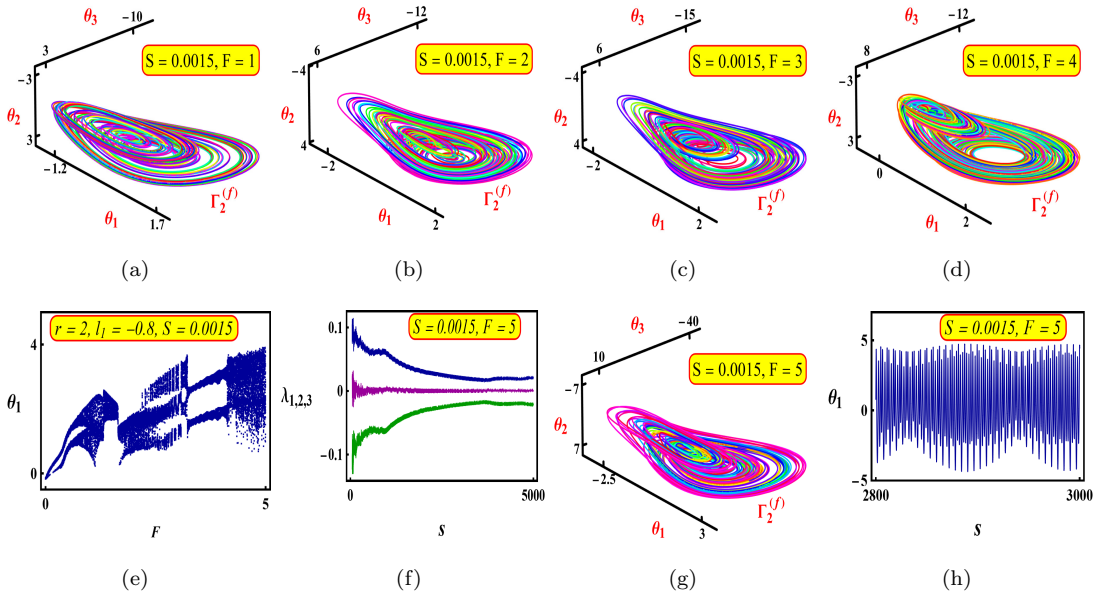

Figure 3.17: $(a)-(d)$: The phase diagram of $\Gamma_2^{(f)}$ for $S = 0.0015$, $l_1 = -0.8$ and for different F. (e) : The bifurcation diagram of θ_1 against F corresponding to $\Gamma_2^{(f)}$. (f) : The spectrum of LCE of $\Gamma_2^{(f)}$ for $S = 0.0015$ and $F = 5$. (g) : The phase diagram of $\Gamma_2^{(f)}$ for $S = 0.0015$ and $F = 5$. (h) : The solution θ_1 plotted against s corresponding to $\Gamma_2^{(f)}$.

Therefore, the Eq.(3.132) has three real roots when $\Delta_1 \geqslant 0$ and one real along with two complex conjugate roots when $\Delta_1 < 0$. We assume the values of the parameters given by Eq.(3.125) under which Δ_1 becomes the function of the parameters l_1 and S. The regions $\Delta_1 > 0$ and $\Delta_1 < 0$ are presented in the Figure 3.15(a). It is interesting to observe that the characteristic equation (3.132) and its discriminant Δ_1 do not depend on the parameter r which being the ratio of coefficients P and Q of KP and mKP terms implies that the eigenvalues of the linearized system remain invariant for these two coefficients. The boundary of these two regions are given by the blue curve AB having endpoints $A\,(0, l_A)$ and $B\,(S_B, 0.8)$ in the S, l_1 parametric plane where $l_A = 0.485$, $S_B = 0.325$. It is clear that the cubic equation (3.132) has only one real root for $l_1 \leqslant l_A$. It may have three real roots only when $l_1 > l_A$. In order to have a clear idea regarding the nature of the equilibrium point O we choose $l_1 = 0.8$ and plot the real parts of the eigenvalues of the linearized system against S in the Figure 3.15(b). In the light of these two figures, it is clear that one eigenvalue λ_1 always remains real and negative. Other two eigenvalues $\lambda_{2,3}$ are real-valued and positive for $S < S_B$ showing that the equilibrium point O is a node in this regime. These eigenvalues change to complex numbers with positive real parts as S increases and becomes $S \geqslant S_B$ implying that the solution orbits near the equilibrium point O will spirally move away from O towards the direction of the eigen vector

corresponding to λ_1. A similar effect is observed if we decrease $\mathfrak{l}_1$ keeping S fixed. These two cases are illustrated below considering two sets of values of the parameters $\mathfrak{l}_1$ and S for which $\Delta_1 > 0$ and $\Delta_1 < 0$ respectively. Choosing

$$\mathsf{r} = 2,\ \mathfrak{l}_1 = 0.8,\ \mathsf{S} = 0.001 \tag{3.134}$$

so that $\Delta_1 = 10.9629 > 0$ and consequently all the eigen values of the Jacobian matrix of the linearized system being real, the phase diagram of the damped system (3.131) under the initial condition

$$\mathrm{IC}_5 : \theta_1(0) = -0.1,\ \theta_2(0) = -0.1,\ \theta_3(0) = 0.1 \tag{3.135}$$

is displayed in the Figure 3.15(c). The orbit Γ_1 moves away spirally from the equilibrium point O. We can compare it with Figure 3.13(d) where similar values of the parameters have been chosen with the special case when there was no damping term, i.e., $\mathsf{S} = 0$ and two homoclinic orbits were passing through the equilibrium point. It is clear from the Figure 3.15(c) that these homoclinic orbits have been deformed to an unstable spiral in the presence of the damping term. The line of action of the eigenvectors $\vec{\mathfrak{e}}_{1,2,3}$ are shown here in solid purple color. Next, keeping the damping term S small we choose

$$\mathsf{r} = 2,\ \mathfrak{l}_1 = -0.8,\ \mathsf{S} = 0.0015 \tag{3.136}$$

for which $\Delta_1 = -63.0117 < 0$ and the initial condition

$$\mathrm{IC}_6 : \theta_1(0) = -0.05,\ \theta_2(0) = 0.05,\ \theta_3(0) = 0.05 \tag{3.137}$$

leads to the solution orbit Γ_2 of the damped system (3.131) as displayed in the Figure 3.15(d). Here the linearized system has one real eigen value and two complex conjugate eigen values given by

$$\lambda_1 = 0.00116869,\ \lambda_2 = -0.000584347 + 1.58329\ \mathfrak{i},\ \lambda_3 = -0.000584347 - 1.58329\ \mathfrak{i} \tag{3.138}$$

and the corresponding eigen vectors are

$$\vec{\mathfrak{e}}_4 = (0.000235901, -0.505999, 0)\,, \tag{3.139a}$$

$$\vec{\mathfrak{e}}_5 = (0.801142,\ -0.319587 + 0.000235901\ \mathfrak{i},\ -0.00018675 - 0.505999\ \mathfrak{i})\,, \tag{3.139b}$$

$$\vec{\mathfrak{e}}_6 = (0.801142,\ -0.319587 - 0.000235901\ \mathfrak{i},\ -0.00018675 + 0.505999\ \mathfrak{i})\,. \tag{3.139c}$$

We chose $\vec{\mathfrak{e}}_7 = \mathrm{Re}(\vec{\mathfrak{e}}_5)$ and $\vec{\mathfrak{e}}_8 = \mathrm{Im}(\vec{\mathfrak{e}}_5)$ and draw the line of action of the real vectors $\vec{\mathfrak{e}}_{4,7,8}$ by red, purple and black colours in this figure and observe that solution orbit Γ_2 moves spirally around the line of action of the vector $\vec{\mathfrak{e}}_4$. It is evident that the damping term disturbs the stability of the KP-mKP system and generate an unstable quasiperiodic solution in the absence of external periodic force. We shall now study how the external periodic disturbance make its impact and deform the solution orbits Γ_1 and Γ_2 in the next section.

3.8.4 The Damped KP-mKP System with External Periodic Force

The damped KP-mKP system (3.4) with external periodic force (3.121) can be written under the transformation (3.101) as the non-autonomous system (3.123). In this section, we explore how the solutions Γ_1 and Γ_2 of the damped system (3.131) deform due to the external force. These two deformed orbits under the external periodic disturbance are denoted by $\Gamma_1^{(f)}$ and $\Gamma_2^{(f)}$ respectively. The phase diagram of the orbit $\Gamma_1^{(f)}$ with $F = 2,\ 4,\ 6,\ 8$ under the initial condition IC_5 are plotted for $0 \leqslant s \leqslant 400$ in the Figure 3.16(a)-3.16(d) each of which look chaotic where different colors represent different intervals of s. In order to confirm the chaotic nature of the solution we first draw the bifurcation diagram of θ_1 against F for $0 \leqslant F \leqslant 10$ as displayed in the Figure 3.16(e) in which we observe the onset of intermittency character for moderate values of F and the irregularities become more prominent as F increases. Secondly, we draw the spectrum of Lyapunov characteristic exponent (LCE) of the orbit $\Gamma_1^{(f)}$ for a longer range $0 \leqslant s \leqslant 5000$ with $F = 10$ as shown in the Figure 3.16(f) and observe that the largest LCE is positive confirming the chaotic nature of the solution orbit which is itself displayed in Figure 3.16(g). The solution θ_1 is plotted against s in the Figure 3.16(h) showing intermittency character.
We next study the phase diagram of the orbit $\Gamma_2^{(f)}$ with $F = 1,\ 2,\ 3,\ 4$ under the initial condition IC_6 and find very much irregular orbit for $0 \leqslant s \leqslant 400$ as displayed in the Figure 3.17(a)-3.17(d). The irregular nature of the solution becomes clear from the bifurcation diagram of the solution θ_1 for $0 \leqslant F \leqslant 5$ in Figure 3.17(e) where one may observe the inception of intermittency for moderate values of F and find that the irregularity increases with the increase of F. We present the spectrum of the LCE in the Figure 3.17(f) for a longer range $0 \leqslant s \leqslant 5000$ with $F = 5$ and find a positive LCE confirming that the corresponding orbit is chaotic which itself is shown in Figure 3.17(g). The corresponding solution θ_1 is plotted against s in the Figure 3.17(h) displaying intermittency character. Thus, the external periodic force deforms the quasiperiodic solution, arising as the effect of damping, to the solution with intermittency. Further, larger values of the amplitude of the external force produce chaotic solutions through the route of intermittency which indicates the generation of turbulence.

3.9 Conclusion

The newly built analytic multi-soliton is used to determine the breather and positons shape solutions for the Eq.(3.3) and Eq.(3.4) while including the qualitative characterization of the system. The key findings of the evaluations are stated as follows:

i. It is determined that the Painlevé integrability of the non-autonomous KP-mKP equation is restricted, and a new Painlevé sense integrability criterion that is exactly the same as the

prerequisite for the creation of the Bilinear equation is also established.

ii. We are able to create two-component Lax systems and a four-filed bilinear Bäcklund transformation with the aid of these mixing variables.

iii. By applying the correct parameter restrictions and using the long wave limiting process, it is also possible to design other types of solutions based on the K-soliton solutions, including $\mathfrak{m}$-breather (for $\mathsf{K} = 2\mathfrak{m}$) solutions, hybrid ones made up of breathers and solitons (for $\mathsf{K} = 2\mathfrak{m}+\mathsf{k}$), K-order smooth positons and $\mathfrak{m}$th-order breather positons. To confirm their existence, all of the solutions identified are also incorporated into the equation.

iv. The refinements and summaries of our approach in deriving solutions are found in Inference (1) and Inference (4). The advantages of this method over the degenerate Darboux transformation method are its simplicity and quickness. However, unlike the Darboux transformation method, this approach is unable to get the general mathematical expression of nth smooth positions. We have also made numerous attempts: either Inference (4) shows that the result lacks a general law, or our lack of skill makes it difficult to find the general formula. It is our expectation that this issue will be resolved and the limit method presented in this study will be developed shortly into a complete system by specialists in the field.

v. For the current system, various types of complex solution structures have been built in the appropriate parametric zones, including kinky-breather, double kinky-breather, horseshoe-shaped breather, periodic positon, kinky-breather-positon, horseshoe-shaped breather-positon, horseshoe-type breather parabolic, double horseshoe-type breather, etc.

vi. Modulation instability is used to discuss the stability of the obtained solutions. Travelling wave solutions, which enable the study of the wave dispersion phenomena, are also used to explain the relationship between the wave's phase velocity and wave number.

vii. The qualitative analysis of the system shows the existence of multistability and dependence of the solution on various parameters. The multistability indicates the coexistence of various categories of solutions such as periodic, soliton, and shock solutions for different sets of initial conditions.

viii. As far as we know, no research has been done on the three-dimensional phase portrait analysis of the nonautonomous KP-mKP framework. It is most often observed that the dynamics of nonhomogenous evolution equations are described only in two dimensions, but choosing a three-dimensional framework allows the presence of a damping coefficient to have a significant impact on dynamic movement.

ix. The damping term alone has the strength to generate different quasiperiodic orbits in the phase diagram. Various unstable spirals in the phase space indicate the increase in internal energy manifesting the instability of the solutions. The increase of the magnitude of the external periodic force further leads to a chaotic solution. The generation of chaos through the path of intermittency signifies the existence of turbulence.

x. This study reveals that a large amplitude of the external force is required to generate instability and chaos using the deformation of the low-energy orbits. On the other hand, a relatively small amplitude of the external force generates intermittency and chaos by the deformation of high-energy orbits. Thus, the system in low total energy is much more stable under external disturbance relative to that in the state of high energy.

Our results may provide an improved understanding of the qualitative dynamical behavior of the non-autonomous KP-mKP system and its non-autonomous soliton, breather, and mixed-type wave solutions. Besides the generation of chaotic solutions through the route of intermittency may refer to turbulence [186]. Explosive instability, multistability [187], coexistence [188] of many quasi-periodic, self-exited, hidden [189] attractors and various other complex behavior are uncovered by many researchers. Therefore, the study of these systems has manifold practical applications in real-world problems.

Chapter 4

The classification of the exact single travelling wave solutions to the constant coefficient KP-mKP equation employing complete discrimination system for polynomial method

[1]

4.1 Introduction

Nonlinear evolution equations are the real treasure of the modern scientific world because various complex physical phenomena that appeared in the natural system are well described by NLEEs and so, these evolutions are applied to almost all branches of science such as physics, chemistry, biology, Astronomy, plasma dynamics, water-wave phenomena, ocean engineering, etc [1, 2, 3, 4, 5, 7]. Among the various NLEEs the KdV is the basic and most popular equation dis-

[1]The research article has been published in the journal of Computational and Mathematical Methods (Wiley-Hindawi)

covered by Diederik Johannes Korteweg and his pupil Gustav De Vries to describe shallow-water waves. But the KdV model can be used to study the theory of soliton in one dimension only. To overcame the restriction for studying wave dynamics in absolutely one-dimensional ZK and KP model arise. So, to study soliton theory in two dimension system KP equation is a widely used model[190, 191, 192]. However, as with the KdV model, there are situations in which the nonlinear coefficient of the KP equation disappears, at which point it will result in a singularity of infinite amplitude, which is unrealistic. Soliton in finite-amplitude requires strong nonlinearity, which is achieved by incorporating dual nonlinearities into the KP model. The KP-mKP equation is developed to provide soliton in finite-amplitude. In this article, we intend to study the KP-mKP equation in the following form:

$$\frac{\partial}{\partial x}\left[\frac{\partial v}{\partial \tau}+Pv\frac{\partial v}{\partial x}+Qv^2\frac{\partial v}{\partial x}+R\frac{\partial^3 v}{\partial x^3}\right]+S\frac{\partial^2 v}{\partial y^2}=0. \tag{4.1}$$

This equation contains quadratic and cubic nonlinear terms along with a third order dispersive term. Different types of complex physical phenomena in diverse field, such as strong nonlinear internal waves on the ocean shelf in two dimension [111], propagation of dust acoustic waves in plasma environment [118], are well described by the KP-mKP model.

In order to explore all the exact travelling wave solutions for a nonlinear system Liu introduced a new approach which is termed as complete discrimination system for polynomial method (CDSPM) [193, 194]. It is found that if a NLEE can be turned into an integral form then all possible exact solutions can be derived by this CDSPM [195]. The purpose of this chapter is to explore different types of solutions for the KP-mKP equation which is termed as KP-Gardner equation. Introducing Liu's approach regarding the complete discrimination system for polynomial and the trial equation technique, a set of new solutions to the KP-mKP equation containing Jacobi elliptic function have been derived. It is found that these analytical solutions numerically exhibit different nonlinear structures such as solitary waves, shock waves, periodic wave profiles, etc. The reliability and effectiveness are confirmed from the numerical graphs of the solutions. Finally, the existence and validity of the various topological structures of the solutions are confirmed from the phase portrait of the dynamical system. Based on this investigation, it is confirmed that the method is not only suited for obtaining the classification of the solutions, but also for qualitative analysis, which means that it can also be extended to other fields of application.

4.2 All travelling wave solutions to KP-mKP equation

In this section we investigate all travelling wave solutions of constant co-efficient KP-mKP equation (4.1). Substituting the transform (1.55) in equation (4.1) we have

$$-ck_1\phi''+Pk_1^2((\phi')^2+\phi\phi'')+Qk_1^2(\phi^2\phi''+2\phi(\phi')^2)+Rk_1^4\phi''''+Sk_2^2\phi''=0, \tag{4.2}$$

integrating and taking integrating constant to be zero we have

$$-ck_1\phi' + Pk_1^2\phi\phi' + Qk_1^2\phi^2\phi' + Rk_1^4\phi''' + Sk_2^2\phi' = 0, \tag{4.3}$$

again integrating we have

$$-ck_1\phi + \frac{1}{2}Pk_1^2\phi^2 + \frac{1}{3}Qk_1^2\phi^3 + Rk_1^4\phi'' + Sk_2^2\phi = \frac{1}{2}c_1, \tag{4.4}$$

where c_1 is an integrating constant. Multiplying both sides by $2\phi'$ and then integrating we have

$$-ck_1\phi^2 + \frac{1}{3}Pk_1^2\phi^3 + \frac{1}{6}Qk_1^2\phi^4 + Rk_1^4\phi'^2 + Sk_2^2\phi^2 = c_1\phi + c_2, \tag{4.5}$$

where c_2 is an integrating constant. The above equation can be written as

$$(\phi')^2 = \frac{1}{Rk_1^4}\left[-\frac{1}{6}Qk_1^2\phi^4 - \frac{1}{3}Pk_1^2\phi^3 + (ck_1 - Sk_2^2)\phi^2 + c_1\phi + c_2\right], \tag{4.6}$$

or

$$(\phi')^2 = \alpha_4\phi^4 + \alpha_3\phi^3 + \alpha_2\phi^2 + \alpha_1\phi + \alpha_0, \tag{4.7}$$

$\implies$

$$\pm(\zeta - \zeta_0) = \int \frac{d\phi}{\sqrt{\alpha_4\phi^4 + \alpha_3\phi^3 + \alpha_2\phi^2 + \alpha_1\phi + \alpha_0}}, \tag{4.8}$$

where $\alpha_4 = -\frac{Q}{6Rk_1^2}$, $\alpha_3 = -\frac{P}{3Rk_1^2}$, $\alpha_2 = \frac{ck_1 - Sk_2^2}{Rk_1^4}$, $\alpha_1 = \frac{c_1}{Rk_1^4}$, $\alpha_0 = \frac{c_2}{Rk_1^4}$.
For $\alpha_4 > 0$, let $\Psi = (\alpha_4)^{\frac{1}{4}}(\phi + \frac{\alpha_3}{4\alpha_4})$ and $\zeta_1 = (\alpha_4)^{\frac{1}{4}}\zeta$, then (4.7) changes to

$$\Psi_{\zeta_1}^2 = \Psi^4 + p\Psi^2 + q\Psi + r, \tag{4.9}$$

and (4.8) becomes

$$\pm(\zeta_1 - \zeta_0) = \int \frac{d\Psi}{\sqrt{\Psi^4 + p\Psi^2 + q\Psi + r}}, \tag{4.10}$$

where $p = -\frac{3\alpha_3^2}{8\alpha_4\sqrt{\alpha_4}} + \frac{\alpha_2}{\sqrt{\alpha_4}}$, $q = \frac{\alpha_3^4}{8\alpha_4^2\sqrt[4]{\alpha_4}} - \frac{\alpha_3\alpha_2}{2\alpha_4\sqrt[4]{\alpha_4}} + \frac{\alpha_1}{\sqrt[4]{\alpha_4}}$, $r = \alpha_0 - \frac{3\alpha_3^4}{256\alpha_4^3} + \frac{\alpha_3^2\alpha_2}{16\alpha_4^2} - \frac{3\alpha_3\alpha_1}{4\alpha_4}$.
For $\alpha_4 < 0$, let $\Psi = (-\alpha_4)^{\frac{1}{4}}(\phi + \frac{\alpha_3}{4\alpha_4})$ and $\zeta_1 = (-\alpha_4)^{\frac{1}{4}}\zeta$, then (4.7) changes to

$$\Psi_{\zeta_1}^2 = -(\Psi^4 + p\Psi^2 + q\Psi + r), \tag{4.11}$$

and (4.8) becomes

$$\pm(\zeta_1 - \zeta_0) = \int \frac{d\Psi}{\sqrt{-(\Psi^4 + p\Psi^2 + q\Psi + r)}}, \tag{4.12}$$

where $p = \frac{3\alpha_3^2}{8\alpha_4\sqrt{-\alpha_4}} - \frac{\alpha_2}{\sqrt{-\alpha_4}}$, $q = -\frac{\alpha_3^4}{8\alpha_4^2\sqrt[4]{-\alpha_4}} + \frac{\alpha_3\alpha_2}{2\alpha_4\sqrt[4]{-\alpha_4}} - \frac{\alpha_1}{\sqrt[4]{-\alpha_4}}$, $r = -\alpha_0 + \frac{3\alpha_3^4}{256\alpha_4^3} - \frac{\alpha_3^2\alpha_2}{16\alpha_4^2} + \frac{3\alpha_3\alpha_1}{4\alpha_4}$.
Let $H(\Psi) = \Psi^4 + p\Psi^2 + q\Psi + r$, then its complete discrimination system can be expressed as [196]

$$D_1 = 4,\ D_2 = -p,\ D_3 = -2p^3 + 8pr - 9q^2, E_2 = 9p^2 - 32pr,$$
$$D_4 = -p^3q^2 + 4p^4r + 36pq^2r - 32p^2r^2 - \frac{27}{4}q^4 + 64r^3. \tag{4.13}$$

Table 4.1: Stable and unstable region

Stable region	Relative unstable region	Absolute unstable region
$D_i < 0 \cup D_i > 0 \cup E_2 > 0$ $i = 1, 2, 3, 4$	$D_i = 0 \cup E_2 = 0 \backslash (0, 0, 0)$ $i = 1, 2, 3, 4$	$(0, 0, 0)$ $i = 1, 2, 3, 4$

Again, to make the study effective and reliable, it is very necessary to find the stable and unstable region of the solution for different values of discriminant quantities of the polynomial $H(\Psi)$. The stable and unstable parametric zones of the system are given in Table 1 [197]. According to the complete discrimination system for the polynomial of order four has total nine cases and to obtain solution of (4.10) and (4.8), we discussed all the cases separately as follows:

case1. When $D_4 = 0, \quad D_3 = 0, \quad D_2 = 0$, $H(\Psi)$ has only one root zero of multiplicity four. Then $H(\Psi)$ becomes

$$H(\Psi) = \Psi^4, \tag{4.14}$$

for $\alpha_4 > 0$, from (4.10) we have

$$\zeta_1 - \zeta_0 = \int \frac{d\Psi}{\Psi^2} = -\Psi^{-1}, \tag{4.15}$$

where ζ_0 is an integral constant. So, the solutions of equation (4.7) is of the form

$$\phi(\zeta) = \mp \alpha_4^{-1/4} (\alpha_4^{1/4} \zeta - \zeta_0)^{-1} - \frac{\alpha_3}{4\alpha_4}, \tag{4.16}$$

which is a rational function solution. For example, when $P = 3$, $Q = 6$, $R = -1$, $S = \frac{11}{8}$, $c_1 = 0$, $c_2 = 0$, $k_1 = 1$, $k_2 = 1$, $c = 1$, $\zeta_0 = 0$, then we get rational function solution of (4.1) as (see Figure 4.1.(a)),

$$v(x, y, \tau) = -(x + y - \tau)^{-1} - \frac{1}{4}. \tag{4.17}$$

case2. When $D_4 = 0, \quad D_3 = 0, \quad D_2 > 0$ and $E_2 = 0$, $H(\Psi)$ has two real roots of multiplicities three and one. Then $H(\Psi)$ can be written in the following form as

$$H(\Psi) = (\Psi - r_1)^3 (\Psi - r_2), \tag{4.18}$$

therefore when $\alpha_4 > 0$ from (4.10) we have

$$\pm\zeta_1 - \zeta_0 = \int \frac{d\Psi}{(\Psi - r_1)\sqrt{(\Psi - r_1)(\Psi - r_2)}} = \frac{2}{r_2 - r_1} \sqrt{\frac{\Psi - r_2}{\Psi - r_1}}, \tag{4.19}$$

when $\Psi > r_1$, $\Psi > r_2$ or $\Psi < r_1$, $\Psi < r_2$, the solution of (4.10) is of the form

$$\Psi = \frac{4(r_1 - r_2)}{(r_2 - r_1)^2 (\zeta_1 - \zeta_0)^2 - 4} + r_1, \tag{4.20}$$

$$\phi(\zeta) = \pm \alpha_4^{-\frac{1}{4}} \left[\frac{4(r_1 - r_2)}{(r_2 - r_1)^2 (\alpha_4^{\frac{1}{4}} \zeta - \zeta_0)^2 - 4} + r_1 \right] - \frac{\alpha_3}{4\alpha_4}. \tag{4.21}$$

When $P = 12$, $Q = 6$, $R = -1$, $S = 1$, $c_1 = 24$, $c_2 = 72$, $k_1 = 1$, $k_2 = 1$, $c = 1$, $\zeta_0 = 0$, then $r_1 = 1$ and $r_2 = -3$, we get rational function solution of (4.1) as

$$\nu(x, y, \tau) = \frac{4}{4(x + y - \tau)^2 - 1}. \tag{4.22}$$

When $\alpha_4 < 0$ from (4.12) we have

$$\pm\zeta_1 - \zeta_0 = \int \frac{d\Psi}{(\Psi - r_1)\sqrt{(\Psi - r_1)(\Psi - r_2)}} = \frac{2}{r_1 - r_2}\sqrt{\frac{r_2 - \Psi}{\Psi - r_1}}. \tag{4.23}$$

When $\Psi > r_1$, $\Psi < r_2$ or $\Psi < r_1$, $\Psi > r_2$, the solution of (4.12) is of the form

$$\Psi = \frac{4(r_1 - r_2)}{-(r_2 - r_1)^2(\zeta_1 - \zeta_0)^2 - 4} + r_1, \tag{4.24}$$

$$\phi(\zeta) = \pm(-\alpha_4)^{-\frac{1}{4}}\left[\frac{4(r_1 - r_2)}{-(r_2 - r_1)^2((-\alpha_4)^{\frac{1}{4}}\zeta - \zeta_0)^2 - 4} + r_1\right] - \frac{\alpha_3}{4\alpha_4}. \tag{4.25}$$

case3. When $D_4 = 0$, $D_3 = 0$, $D_2 < 0$, $H(\Psi)$ has a pair of complex conjugate roots of multiplicities two. Then $H(\Psi)$ can be expressed as in the following form as

$$H(\Psi) = ((\Psi - \gamma)^2 + \delta^2)^2, \tag{4.26}$$

where $\delta > 0$, if $\alpha_4 > 0$ then from (4.10) we obtain

$$\zeta_1 - \zeta_0 = \int \frac{d\Psi}{(\Psi - \gamma)^2 + \delta^2} = \frac{1}{\delta}\arctan\frac{\Psi - \gamma}{\delta}, \tag{4.27}$$

then we get

$$\Psi = \delta\tan(\delta(\zeta_1 - \zeta_0)) + \gamma. \tag{4.28}$$

We obtain solution as

$$\phi(\zeta) = \pm\alpha_4^{-\frac{1}{4}}\delta\tan(\delta(\alpha_4^{\frac{1}{4}}\zeta - \zeta_0)) + \gamma - \frac{\alpha_3}{4\alpha_4}. \tag{4.29}$$

When $P = 12$, $Q = 6$, $R = -1$, $S = 5$, $c_1 = 4$, $c_2 = 7$, $k_1 = 1$, $k_2 = 1$, $c = 1$, $\zeta_0 = 0$, then $\gamma = 0$ and $\delta = 2$, we get solution of original equation (4.1) as (see Figure 4.1.(b)),

$$\nu(x, y, \tau) = 2\tan(2(x + y - \tau)) - 1. \tag{4.30}$$

case4. When $D_4 > 0$, $D_3 > 0$, and $D_2 > 0$, then $H(\Psi)$ has four distinct real roots. In this case we write

$$H(\Psi) = (\Psi - r_1)(\Psi - r_2)(\Psi - r_3)(\Psi - r_4), \tag{4.31}$$

where r_1, r_2, r_3, and r_4 are all real numbers and let $r_1 > r_2 > r_3 > r_4$. When $a_4 > 0$, if $\Psi > r_1$ or $\Psi < r_4$, then we take the following transformation

$$\Psi = \frac{r_2(r_1 - r_4)\sin^2\theta - r_1(r_2 - r_4)}{(r_1 - r_4)\sin^2\theta - (r_2 - r_4)}, \tag{4.32}$$

if $r_3 < \Psi < r_2$, then we take the following transformation

$$\Psi = \frac{r_4(r_2 - r_3)\sin^2\theta - r_3(r_2 - r_4)}{(r_2 - r_3)\sin^2\theta - (r_2 - r_4)}. \tag{4.33}$$

Combining (4.32) or (4.33) with (4.10) we get

$$\zeta_1 - \zeta_0 = \int \frac{d\Psi}{\sqrt{(\Psi - r_1)(\Psi - r_2)(\Psi - r_3)(\Psi - r_4)}} = \frac{2}{(r_1 - r_3)(r_2 - r_4)} \int \frac{d\theta}{\sqrt{1 - m^2\sin^2\theta}}, \tag{4.34}$$

where $m^2 = \frac{(r_1 - r_4)(r_2 - r_3)}{(r_1 - r_3)(r_2 - r_4)}$, also from the definition of jacobi elliptic sine function we get

$$\sin\theta = sn\left(\frac{\sqrt{(r_1 - r_3)(r_2 - r_4)}}{2}(\zeta_1 - \zeta_0), m\right). \tag{4.35}$$

Combining (4.35) with (4.32) we obtain solution of (4.10) as

$$\Psi = \frac{r_2(r_1 - r_4)sn^2\left(\frac{\sqrt{(r_1 - r_3)(r_2 - r_4)}}{2}(\zeta_1 - \zeta_0), m\right) - r_1(r_2 - r_4)}{(r_1 - r_4)sn^2\left(\frac{\sqrt{(r_1 - r_3)(r_2 - r_4)}}{2}(\zeta_1 - \zeta_0), m\right) - (r_2 - r_4)}, \tag{4.36}$$

and we can get elliptic function double solutions of equation (4.7) as

$$\phi(\zeta) = \frac{\alpha_4^{-\frac{1}{4}}[r_2(r_1 - r_4)sn^2\left(\frac{\sqrt{(r_1 - r_3)(r_2 - r_4)}}{2}(\alpha_4^{\frac{1}{4}}\zeta - \zeta_0), m\right) - r_1(r_2 - r_4)]}{(r_1 - r_4)sn^2\left(\frac{\sqrt{(r_1 - r_3)(r_2 - r_4)}}{2}(\alpha_4^{\frac{1}{4}}\zeta - \zeta_0), m\right) - (r_2 - r_4)} - \frac{\alpha_3}{4\alpha_4}. \tag{4.37}$$

Combining (4.35) with (4.34) we obtain solution of (4.10) as

$$\Psi = \frac{r_4(r_2 - r_3)sn^2\left(\frac{\sqrt{(r_1 - r_3)(r_2 - r_4)}}{2}(\zeta_1 - \zeta_0), m\right) - r_3(r_2 - r_4)}{(r_2 - r_3)sn^2\left(\frac{\sqrt{(r_1 - r_3)(r_2 - r_4)}}{2}(\zeta_1 - \zeta_0), m\right) - (r_2 - r_4)}, \tag{4.38}$$

and solutions of (4.7) as

$$\phi(\zeta) = \frac{\alpha_4^{-\frac{1}{4}}[r_4(r_2 - r_3)sn^2\left(\frac{\sqrt{(r_1 - r_3)(r_2 - r_4)}}{2}(\alpha_4^{\frac{1}{4}}\zeta - \zeta_0), m\right) - r_3(r_2 - r_4)]}{(r_2 - r_3)sn^2\left(\frac{\sqrt{(r_1 - r_3)(r_2 - r_4)}}{2}(\alpha_4^{\frac{1}{4}}\zeta - \zeta_0), m\right) - (r_2 - r_4)} - \frac{\alpha_3}{4\alpha_4}. \tag{4.39}$$

The expressions (4.37) and (4.39) are elliptic functions double periodic solutions. For instance, when $P = 0$, $Q = 6$, $R = -1$, $S = 4$, $c_1 = 0$, $c_2 = -4$, $k_1 = 1$, $k_2 = 1$, $c = 1$, $\zeta_0 = 0$, then $r_1 = 2$, $r_2 = 1$, $r_3 = -1$, $r_4 = -2$. So if $\Psi > r_1$ or $\Psi < r_4$ we get the elliptic function solution of (4.1) as (see Figure 4.1.(c)),

$$v(x, y, \tau) = \frac{4sn^2\left(\frac{3}{2}(x + y - \tau), \frac{8}{9}\right) - 6}{4sn^2\left(\frac{3}{2}(x + y - \tau), \frac{8}{9}\right) - 3}. \tag{4.40}$$

For $\alpha_4 < 0$, if $r_1 > \Psi > r_2$, then we consider the following transformation

$$\Psi = \frac{r_3(r_1 - r_2)\sin^2\theta - r_2(r_1 - r_3)}{(r_1 - r_2)\sin^2\theta - (r_1 - r_3)}, \tag{4.41}$$

and if $r_4 < \Psi < r_3$, then we consider the following transformation

$$\Psi = \frac{r_1(r_3 - r_4)\sin^2\theta - r_4(r_3 - r_1)}{(r_3 - r_4)\sin^2\theta - (r_3 - r_1)}. \tag{4.42}$$

Similarly from (4.12) we have

$$\Psi = \frac{r_3(r_1 - r_2)sn^2\left(\frac{\sqrt{(r_1-r_3)(r_2-r_4)}}{2}(\zeta_1 - \zeta_0), m\right) - r_2(r_1 - r_3)}{(r_1 - r_2)sn^2\left(\frac{\sqrt{(r_1-r_3)(r_2-r_4)}}{2}(\zeta_1 - \zeta_0), m\right) - (r_1 - r_3)}, \tag{4.43}$$

$$\phi(\zeta) = \frac{(-\alpha_4)^{-\frac{1}{4}}[r_3(r_1 - r_2)sn^2\left(\frac{\sqrt{(r_1-r_3)(r_2-r_4)}}{2}((-\alpha_4)^{\frac{1}{4}}\zeta - \zeta_0), m\right) - r_2(r_1 - r_3)]}{(r_1 - r_2)sn^2\left(\frac{\sqrt{(r_1-r_3)(r_2-r_4)}}{2}((-\alpha_4)^{\frac{1}{4}}\zeta - \zeta_0), m\right) - (r_1 - r_3)} - \frac{\alpha_3}{4\alpha_4}, \tag{4.44}$$

$$\Psi = \frac{r_1(r_3 - r_4)sn^2\left(\frac{\sqrt{(r_1-r_3)(r_2-r_4)}}{2}(\zeta_1 - \zeta_0), m\right) - r_4(r_3 - r_1)}{(r_3 - r_4)sn^2\left(\frac{\sqrt{(r_1-r_3)(r_2-r_4)}}{2}(\zeta_1 - \zeta_0), m\right) - (r_3 - r_1)}, \tag{4.45}$$

$$\phi(\zeta) = \frac{(-\alpha_4)^{-\frac{1}{4}}[r_1(r_3 - r_4)sn^2\left(\frac{\sqrt{(r_1-r_3)(r_2-r_4)}}{2}((-\alpha_4)^{\frac{1}{4}}\zeta - \zeta_0), m\right) - r_4(r_3 - r_1)]}{(r_3 - r_4)sn^2\left(\frac{\sqrt{(r_1-r_3)(r_2-r_4)}}{2}((-\alpha_4)^{\frac{1}{4}}\zeta - \zeta_0), m\right) - (r_3 - r_1)} - \frac{\alpha_3}{4\alpha_4}, \tag{4.46}$$

where $m^2 = \frac{(r_1-r_2)(r_3-r_4)}{(r_1-r_3)(r_2-r_4)}$.

case5. When $D_4 < 0$ and $D_2D_3 \geqslant 0$, $H(\Psi)$ has a pair of complex conjugate roots and two distinct real roots. Then $H(\Psi)$ can be presented as

$$H(\Psi) = (\Psi - r_1)(\Psi - r_2)[(\Psi - \gamma)^2 + \delta^2], \tag{4.47}$$

where r_1, r_2, γ and δ are numbers also $r_1 > r_2$ and $\delta > 0$. we consider the following transformation

$$\Psi = \frac{e_1\cos\theta + e_2}{e_3\cos\theta + e_4}, \tag{4.48}$$

where

$$\begin{aligned}
e_1 &= \frac{1}{2}(r_1+r_2)e_3 - \frac{1}{2}(r_1-r_2)e_4,\\
e_2 &= \frac{1}{2}(r_1+r_2)e_4 - \frac{1}{2}(r_1-r_2)e_3,\\
e_3 &= r_1 - \gamma - \frac{\delta}{f},\\
e_4 &= r_1 - \gamma - \delta f,\\
f &= g \pm \sqrt{g^2+1},\\
g &= \frac{\delta^2 + (r_1-\gamma)(r_2-\gamma)}{\delta(r_1-r_2)}.
\end{aligned} \tag{4.49}$$

Using (4.10) and the transformation (4.48) we get

$$\zeta_1 - \zeta_0 = \int \frac{d\Psi}{\sqrt{\pm(\Psi-r_1)(\Psi-r_2)[(\Psi-\gamma)^2+\delta^2]}} = \frac{2fm}{\sqrt{\mp 2f\delta(r_1-r_2)}} \int \frac{d\theta}{\sqrt{1-m^2\sin^2\theta}}, \tag{4.50}$$

where $m^2 = \frac{1}{1+f^2}$. Using (4.50) and jacobi elliptic cosine function we obtain

$$\cos\theta = cn\left(\frac{\sqrt{\mp 2f\delta(r_1-r_2)}}{2fm}(\zeta_1-\zeta_0), m\right). \tag{4.51}$$

Now combining (4.50) and (4.50) we gain solution of (4.10) as

$$\Psi = \frac{e_1 cn\left(\frac{\sqrt{\mp 2f\delta(r_1-r_2)}}{2fm}(\zeta_1-\zeta_0), m\right) + e_2}{e_3 cn\left(\frac{\sqrt{\mp 2f\delta(r_1-r_2)}}{2fm}(\zeta_1-\zeta_0), m\right) + e_4}. \tag{4.52}$$

Therefore the solution of (4.7) is

$$\phi(\zeta) = \frac{\alpha_4^{-\frac{1}{4}}[e_1 cn\left(\frac{\sqrt{\mp 2f\delta(r_1-r_2)}}{2fm}(\alpha_4^{\frac{1}{4}}\zeta-\zeta_0), m\right) + e_2]}{e_3 cn\left(\frac{\sqrt{\mp 2f\delta(r_1-r_2)}}{2fm}(\alpha_4^{\frac{1}{4}}\zeta-\zeta_0), m\right) + e_4} - \frac{\alpha_3}{4\alpha_4}, \tag{4.53}$$

which is an jacobi elliptic function double periodic solution. Particularly, When $P=-24$, $Q=-12$, $R=2$, $S=-5$, $c_1=52$, $c_2=148$, $k_1=1$, $k_2=1$, $c=1$, $\zeta_0=0$, then $r_1=2$, $r_2=-2$, $\gamma=0$, $\delta=1$, $f=\frac{1}{2}$, $e_1=-3$, $e_2=0$, $e_3=0$, $e_4=\frac{3}{2}$, and $m=\frac{4}{5}$, then we obtain jacobi elliptic function solution of (4.1) as (see Figure 4.1.(d)),

$$v(x,y,\tau) = -2cn\left(\frac{5}{2}(x+y-\tau), \frac{4}{5}\right) - 1. \tag{4.54}$$

case6. When $D_4 > 0$ and $D_2D_3 \leqslant 0$, then $H(\Psi)$ has two pairs of complex conjugate roots and this case we write $H(\Psi)$ as

$$H(\Psi) = [(\Psi-\gamma_1)^2 + \delta_1^2][(\Psi-\gamma_2)^2 + \delta_2^2], \tag{4.55}$$

where γ_1, γ_2, δ_1 and δ_2 are real numbers and $\delta_1 \geqslant \delta_2 > 0$. For $a_4 > 0$, we take the following transformation

$$\Psi = \frac{e_1 \tan\theta + e_2}{e_3 \tan\theta + e_4}, \tag{4.56}$$

where

$$\begin{aligned} e_1 &= \gamma_1 e_3 + \delta_1 e_4, \\ e_2 &= \gamma_1 e_4 - \delta_1 e_3, \\ e_3 &= -\delta_1 - \frac{\delta_2}{f}, \\ e_4 &= \gamma_1 - \gamma_2, \\ f &= g + \sqrt{g^2 - 1} \\ g &= \frac{(\gamma_1 - \gamma_2)^2 + \delta_1^2 + \delta_2^2}{2\delta_1\delta_2}. \end{aligned} \tag{4.57}$$

Then from (4.10) we get

$$\zeta_1 - \zeta_0 = \int \frac{d\Psi}{\sqrt{((\Psi - \gamma_1)^2 + \delta_1^2)((\Psi - \gamma_2)^2 + \delta_2^2)}} = \frac{e_3^2 + e_4^2}{\delta_2\sqrt{(e_3^2 + e_4^2)(f^2 e_3^2 + e_4^2)}} \int \frac{d\theta}{\sqrt{1 - m^2 \sin^2\theta}}, \tag{4.58}$$

where $m = \frac{f^2 - 1}{f^2}$. By using (4.58) and the definition of jacobi elliptic functions [198], we get

$$\sin\theta = sn\left(\frac{\delta_2\sqrt{(e_3^2 + e_4^2)(f^2 e_3^2 + e_4^2)}}{e_3^2 + e_4^2}(\zeta_1 - \zeta_0), m\right), \tag{4.59}$$

$$\cos\theta = cn\left(\frac{\delta_2\sqrt{(e_3^2 + e_4^2)(f^2 e_3^2 + e_4^2)}}{e_3^2 + e_4^2}(\zeta_1 - \zeta_0), m\right). \tag{4.60}$$

Combining (4.59) and (4.60) with (4.56) we have elliptic function double periodic solution as

$$\Psi = \frac{e_1 sn(\xi(\zeta_1 - \zeta_0), m) + e_2 cn(\xi(\zeta_1 - \zeta_0), m)}{e_3 sn(\xi(\zeta_1 - \zeta_0), m) + e_4 cn(\xi(\zeta_1 - \zeta_0), m)}, \tag{4.61}$$

and

$$\phi(\zeta) = \frac{\alpha_4^{-\frac{1}{4}}[e_1 sn(\xi(a_4^{\frac{1}{4}}\zeta - \zeta_0), m) + e_2 cn(\xi(\alpha_4^{\frac{1}{4}}\zeta - \zeta_0), m)]}{e_3 sn(\xi(a_4^{\frac{1}{4}}\zeta - \zeta_0), m) + e_4 cn(\xi\alpha_4^{\frac{1}{4}}\zeta - \zeta_0), m)} - \frac{\alpha_3}{4\alpha_4}, \tag{4.62}$$

where

$$\xi = \frac{\delta_2\sqrt{(e_3^2 + e_4^2)(f^2 e_3^2 + e_4^2)}}{e_3^2 + e_4^2}. \tag{4.63}$$

For example, when $P = -12$, $Q = -6$, $R = 1$, $S = -10$, $c_1 = -10$, $c_2 = -34$, $k_1 = 1$, $k_2 = 1$, $c = 1$, $\zeta_0 = 0$, then $\gamma_1 = 0$, $\delta_1 = 2$, $\gamma_2 = 0$, $\delta_2 = 1$, $f = 2$, $e_1 = 0$, $e_2 = 5$, $e_3 = -\frac{5}{4}$, $e_4 = 0$, and $\zeta = 2$, then we obtain jacobi elliptic function solution of (4.1) as

$$v(x, y, \tau) = -\frac{2cn(2(x + y - \tau), \frac{3}{4})}{sn(2(x + y - \tau), \frac{3}{4})} - \frac{1}{4}. \tag{4.64}$$

case7. When $D_4 = 0$, $D_3 > 0$ and $D_2 > 0$, $H(\Psi)$ has a real root of multiplicities two and two single real roots. Then $H(\Psi)$ is of the following form

$$H(\Psi) = (\Psi - r_1)^2(\Psi - r_2)(\Psi - r_3), \tag{4.65}$$

where r_1, r_2 and r_3 are real numbers and $r_2 > r_3$, $r_1 = -\frac{r_2+r_3}{2}$. When $\Psi > r_2$, $r_2 > r_1 > r_3$, we obtain the solution of (4.10) and (4.7) respectively as

$$\Psi = \frac{2(r_1 - r_2)(r_1 - r_3)}{\pm(r_2 - r_3)\sin[\sqrt{-(r_1 - r_2)(r_1 - r_3)}(\zeta_1 - \zeta_0)] - (2r_1 - r_2 - r_3)}, \tag{4.66}$$

$$\phi(\zeta) = \frac{2\alpha_4^{-\frac{1}{4}}(r_1 - r_2)(r_1 - r_3)}{\pm(r_2 - r_3)\sin[\sqrt{-(r_1 - r_2)(r_1 - r_3)}(\alpha_4^{\frac{1}{4}}\zeta - \zeta_0)] - (2r_1 - r_2 - r_3)} - \frac{\alpha_3}{4\alpha_4}. \tag{4.67}$$

When $r_1 > r_2$ or $r_1 < r_3$, we obtain the solution of (4.10) and (4.7) respectively as

$$\Psi = \frac{2(r_1 - r_2)(r_1 - r_3)}{(r_2 - r_3)\cosh[\sqrt{(r_1 - r_2)(r_1 - r_3)}(\zeta_1 - \zeta_0)] - (2r_1 - r_2 - r_3)}, \tag{4.68}$$

$$\phi(\zeta) = \frac{2\alpha_4^{-\frac{1}{4}}(r_1 - r_2)(r_1 - r_3)}{(r_2 - r_3)\cosh[\sqrt{(r_1 - r_2)(r_1 - r_3)}(\alpha_4^{\frac{1}{4}}\zeta - \zeta_0)] - (2r_1 - r_2 - r_3)} - \frac{\alpha_3}{4\alpha_4}. \tag{4.69}$$

The expression (4.67) and (4.69) are solitary wave solutions. For instance, when $P = 12$, $Q = 6$, $R = -1$, $S = -12$, $c_1 = 64$, $c_2 = 104$, $k_1 = 1$, $k_2 = 1$, $c = 1$, $\zeta_0 = 0$, then $r_1 = -3$, $r_2 = 4$, $r_3 = 2$,we can get solitary solution of (4.1) as (see Figure 4.1.(e)),

$$u(x, y, \tau) = \frac{35}{\cosh[\sqrt{35}(x + y - \tau)] + 6} - 1. \tag{4.70}$$

case8. When $D_4 = 0$, $D_3D_2 < 0$, $H(\Psi)$ has a pair of complex conjugate roots and a real root of multiplicity two. Then we can write $H(\Psi)$ as

$$H(\Psi) = (\Psi - r_1)^2[(\Psi - \gamma)^2 + \delta^2], \tag{4.71}$$

where r_1, γ and δ all are real numbers and $\delta \neq 0$. Then from (4.10) we have

$$\begin{aligned} \pm\zeta_1 - \zeta_0 &= \int \frac{d\Psi}{(\Psi - r_1)\sqrt{(\Psi - \gamma)^2 + \delta^2}} \\ &= \frac{1}{\sqrt{(r_1 - \gamma)^2 + \delta^2}} \ln \mid \frac{\xi_1\Psi + \xi_2 - \sqrt{(\Psi - \gamma)^2 + \delta^2}}{\Psi - r_1} \mid, \end{aligned} \tag{4.72}$$

where

$$\begin{aligned} \xi_1 &= \frac{r_1 - 2\gamma}{\sqrt{(r_1 - \gamma)^2 + \delta^2}} \\ \xi_2 &= \sqrt{(r_1 - \gamma)^2 + \delta^2} - \frac{r_1(r_1 - 2\gamma)}{\sqrt{(r_1 - \gamma)^2 + \delta^2}}. \end{aligned} \tag{4.73}$$

Then the solution of (4.10)

$$\Psi = \frac{(e^{\pm\sqrt{(r_1-\gamma)^2+\delta^2}(\zeta_1-\zeta_0)} - \xi_1) + \sqrt{(r_1-\gamma)^2+\delta^2}(2-\xi_1)}{(e^{\pm\sqrt{(r_1-\gamma)^2+\delta^2}(\zeta_1-\zeta_0)} - \xi_1)^2 - 1}, \tag{4.74}$$

hence

$$\phi(\zeta) = \frac{\alpha_4^{-\frac{1}{4}}[(e^{\pm\sqrt{(r_1-\gamma)^2+\delta^2}(\alpha_4^{\frac{1}{4}}\zeta-\zeta_0)} - \xi_1) + \sqrt{(r_1-\gamma)^2+\delta^2}(2-\xi_1)]}{(e^{\pm\sqrt{(r_1-\gamma)^2+\delta^2}(\alpha_4^{\frac{1}{4}}\zeta-\zeta_0)} - \xi_1)^2 - 1} - \frac{\alpha_3}{4\alpha_4}. \tag{4.75}$$

For instance, when $P = 12$, $Q = 6$, $R = -1$, $S = 9$, $c_1 = 24$, $c_2 = 72$, $k_1 = 1$, $k_2 = 1$, $c = 1$, $\zeta_0 = 0$, then $r_1 = 1$, $\gamma = -1$, $\delta = 2$, we can obtain solution of (4.1) as

$$v(x,y,\tau) = \frac{(e^{\pm 2\sqrt{2}(x+y-\tau)} - \frac{3}{2\sqrt{2}}) + 2\sqrt{2}(2 - \frac{3}{2\sqrt{2}})}{(e^{\pm 2\sqrt{2}(x+y-\tau)} - \frac{3}{2\sqrt{2}})^2 - 1} - 1. \tag{4.76}$$

case9. When $D_4 = 0$, $D_3 = 0$, $D_2 > 0$ and $E_2 > 0$, $H(\Psi)$ has two real roots of multiplicity two. Then we can express $H(\Psi)$ as follows

$$H(\Psi) = (\Psi - r_1)^2(\Psi - r_2)^2, \tag{4.77}$$

where r_1 and r_2 are real numbers and $r_1 > r_2$. Therefore from (4.10) we have

$$\begin{aligned} \pm\zeta_1 - \zeta_0 &= \int \frac{d\Psi}{(\Psi - r_1)(\Psi - r_2)} \\ &= \frac{1}{r_1 - r_2} \ln \mid \frac{\Psi - r_1}{\Psi - r_2} \mid . \end{aligned} \tag{4.78}$$

When $\Psi > r_1$ or $\Psi < r_2$, the solution of (4.10)

$$\begin{aligned} \Psi &= \frac{r_2 - r_1}{e^{(r_1-r_2)(\zeta_1-\zeta_0)-1}} + r_2 \\ &= \frac{r_2 - r_1}{2}[\coth\frac{(r_1 - r_2)(\zeta_1 - \zeta_0)}{2} - 1] + r_2, \end{aligned} \tag{4.79}$$

and solution of (4.7) is given by

$$\phi(\zeta) = \alpha_4^{-\frac{1}{4}}\left[\frac{r_2 - r_1}{2}[\coth\frac{(r_1 - r_2)(\alpha_4^{\frac{1}{4}}\zeta - \zeta_0)}{2} - 1] + r_2\right] - \frac{\alpha_3}{4\alpha_4}. \tag{4.80}$$

When $r_1 > \Psi > r_2$, the solution of (4.10)

$$\begin{aligned} \Psi &= \frac{r_2 - r_1}{-e^{(r_1-r_2)(\zeta_1-\zeta_0)-1}} + r_2 \\ &= \frac{r_2 - r_1}{2}[\tanh\frac{(r_1 - r_2)(\zeta_1 - \zeta_0)}{2} - 1] + r_2, \end{aligned} \tag{4.81}$$

and of (4.7)

$$\phi(\zeta) = \alpha_4^{-\frac{1}{4}}\left[\frac{r_2 - r_1}{2}[\tanh\frac{(r_1 - r_2)(\alpha_4^{\frac{1}{4}}\zeta - \zeta_0)}{2} - 1] + r_2\right] - \frac{\alpha_3}{4\alpha_4}. \tag{4.82}$$

So for this case, we have obtain hyperbolic solution (4.82) and (4.80) of (4.7). For instance, when $P = 12, Q = 6, R = -1, S = \frac{13}{2}, c_1 = 21, c_2 = \frac{1047}{16}, k_1 = 1, k_2 = 1, c = 1, \zeta_0 = 0$, then $r_1 = \frac{1}{2}, r_2 = -\frac{1}{2}$ and $-1 < \Psi < 1$, we get shock wave solution of Eq.(4.1) as (see Figure 4.1.(f)),

$$\nu(x, y, \tau) = -\frac{1}{2}\tanh[\frac{1}{2}(x + y - \tau)] - 1. \tag{4.83}$$

4.3 Dynamic Properties

Now, we observe the dynamical properties of KP-mKP Eq.(4.1) through the CDSPM. Analyzing the phase portraits of the dynamic system[199, 200], it is observed that the topological structures of the solution profiles are changed due to the variations of the parameters involved in the system. Thus, the CDSPM is not only effective for acquiring various types of solutions but could also be utilized to conduct the qualitative analysis of the solutions. Applying the theory of dynamical system [199, 200], Eq.(4.4) is stated equivalently to the following system

$$\begin{aligned} \frac{d\phi}{d\zeta} &= z \\ \frac{dz}{d\zeta} &= \frac{1}{Rk_1^4}[\frac{1}{2}c_1 + (ck_1 - Sk_2^2)\phi - \frac{1}{2}Pk_1^2\phi^2 - \frac{1}{3}Qk_1^2\phi^3]. \end{aligned} \tag{4.84}$$

and it is equivalent to

$$\begin{aligned} \frac{d\phi}{d\zeta} &= z \\ \frac{dz}{d\zeta} &= \beta_3\phi^3 + \beta_2\phi^2 + \beta_1\phi + \beta_0, \end{aligned} \tag{4.85}$$

where $\beta_3 = -\frac{Q}{3Rk_1^2}, \quad \beta_2 = -\frac{P}{2Rk_1^2}, \quad \beta_1 = \frac{(ck_1 - Sk_2^2)}{Rk_1^4}, \beta_0 = \frac{c_1}{2Rk_1^4}$.
The existence of a homoclinic orbit in phase portrait, in general corresponds to a solitary wave profile whereas the kink (anti-kink) wave solution is recognized by a heteroclinic orbit. Again a periodic orbit confirms the presence of a periodic traveling wave solution. Varying the values of different parameters β_0, β_1, β_2, and β_3 involved in the system, we determine all homoclinic orbits, heteroclinic orbits and periodic orbits of (4.85). Thus, the existence of solitary waves, kink (or anti-kink) waves and periodic waves of Eq.(4.1) are confirmed. The Hamiltonian function corresponding to the dynamical system (4.85) is defined as

$$H_2(\phi, z) = \frac{z^2}{2} - (\frac{\beta_3}{4}\phi^4 + \frac{\beta_2}{3}\phi^3 + \frac{\beta_1}{2}\phi^2 + \beta_0\phi + c_2), \tag{4.86}$$

which satisfies

$$\begin{aligned} \frac{\partial H_2}{\partial z} &= \frac{d\phi}{d\zeta} \\ \frac{\partial H_2}{\partial \phi} &= -\frac{dz}{d\zeta}. \end{aligned} \tag{4.87}$$

Now, we call $M(a,0)$ as the coefficient matrix of the system (4.85) and denote J as the determinant of $M(a,0)$ at the equilibrium point $(a,0)$. We take $T = trace(M(a,0))$ and $N = T^2 - 4J$.
Let $L(\phi) = \beta_3\phi^3 + \beta_2\phi^2 + \beta_1\phi + \beta_0$, whose complete discrimination system follows as

$$\Delta = \beta_2^2\beta_1^2 - 27\beta_3^2\beta_0^2 - 4\beta_1^3\beta_3 - 4\beta_2^3\beta_0 - 18\beta_3\beta_2\beta_1\beta_0. \tag{4.88}$$

Case 1. $\Delta = 0$, $L(\phi)$ has a single real root together with another real root of multiplicity two, then

$$L(\phi) = \beta_3(\phi - a_1)^2(\phi - a_2), \tag{4.89}$$

then the $(a,0)$ and $(b,0)$ are the equilibrium points of the system (4.85). For example when $\beta_3 = -2$, $\beta_2 = 0$, $\beta_1 = 6$ and $\beta_0 = 4$, we have $a_1 = -1$ and $a_2 = 2$. For the equilibrium point $(2,0)$ we have $J = 18 > 0$, $T = 0$ and $N = -72 < 0$, so $(2,0)$ is a centre. Thus, it is confirmed that there exist a family of periodic orbits about $(2,0)$. And at the equilibrium point $(-1,0)$, we have $J = 0$, $T = 0$, so $(-1,0)$ is a cusp (see Figure 4.2.(a)).
Case 2. $\Delta > 0$, $L(\phi)$ has three distinct single real root, then

$$L(\phi) = \beta_3(\phi - a_1)(\phi - a_2)(\phi - a_3), \tag{4.90}$$

then $(a_1 - 0)$, $(a_2 - 0)$ and $(a_3 - 0)$ become the three equilibrium points of the system. In particular when $\beta_3 = -2$, $\beta_2 = 6$, $\beta_1 = -4$ and $\beta_0 = 0$, we have $a_1 = 0$, $a_2 = 1$ and $a_3 = 2$. At the equilibrium point $(0,0)$ we find $J = 4 > 0$, $T = 0$ and $N = -16 < 0$, thus, naturally $(0,0)$ becomes a centre. On the other hand, at $(1,0)$ we have $J = -2 < 0$, $T = 0$ and $N = 8 > 0$, so $(1,0)$ becomes saddle point. On the another equilibrium point $(2,0)$ we compute $J = 4 > 0$, $T = 0$ and $N = -16 < 0$, so $(2,0)$ is a centre. More over, a couple of homoclinic orbits to $(1,0)$ encircling the centers $(0,0)$ and $(2,0)$ on both sides of the saddle point $(1,0)$ are found (see Figure 4.2.(b)).
But, if $\beta_3 = 1$, $\beta_2 = -3$, $\beta_1 = -1$ and $\beta_0 = 3$, we acquire $a_1 = 1$, $a_2 = 3$ and $a_3 = -1$. The equilibrium point $(1,0)$ becomes centre, as we see $J > 0$, $T = 0, N < 0$. Again, at the equilibrium point $(3,0)$, we get $J < 0$, $N > 0$, and at $(-1,0)$, we find $J < 0$, $N > 0$, for the same values of the parameter. Thus, $(3,0)$ and $(-1,0)$ become saddle. And a pair of nonlinear heteroclinic orbits are observed joining two saddle points $(3,0)$ and $(-1,0)$ enfolding the center $(1,0)$ (see Figure 4.2.(c))
Case 3. $\Delta < 0$, $L(\phi)$ contains a real root as well as a pair of conjugate complex root, then

$$L(\phi) = \beta_3(\phi - a_1)[(\phi - \gamma)^2 + \delta^2]. \tag{4.91}$$

Thus, $(a,0)$ is the only equilibrium point of the system and when $\beta_3 = -2, \beta_2 = 4$, $\beta_1 = -2$ and $\beta_0 = 4$, we find $a_1 = 2$. In that case we have $J = 10 > 0$, $T = 0$ and $N = -40 < 0$, and thus, the point $(2,0)$ becomes a centre. Then a family of periodic orbits exist near about $(2,0)$ (see Figure 4.2.(d)).
From the above analysis, we observe that the CDSPM might be possibly utilized to analyze the characteristic of the equilibrium points, and hence, the topological properties of the solution of the

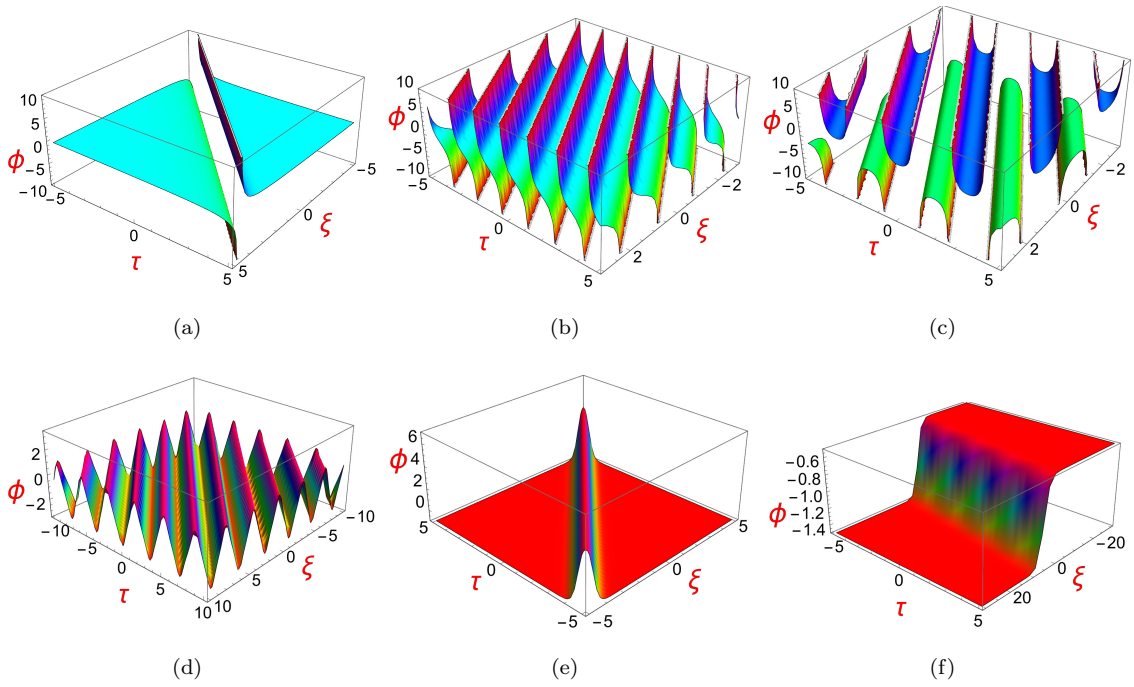

Figure 4.1: (a) 3D plot of Sol.(4.17), when $P = 3$, $Q = 6$, $R = -1$, $S = \frac{11}{8}$, $c_1 = 0$, $c_2 = 0$, $k_1 = 1$, $k_2 = 1$, $c = 1$, $\zeta_0 = 0$, (b) 3D plot of Sol.(4.30) when $P = 12$, $Q = 6$, $R = -1$, $S = 5$, $c_1 = 24$, $c_2 = 72$, $k_1 = 1$, $k_2 = 1$, $c = 1$, $\zeta_0 = 0$, (c) 3D plot of Sol.(4.40), when $P = 0$, $Q = 6$, $R = -1$, $S = 4$, $c_1 = -10$, $c_2 = -34$, $k_1 = 1$, $k_2 = 1$, $c = 1$, $\zeta_0 = 0$, (d) 3D plot of Sol.(4.54), when $P = -24$, $Q = -12$, $R = 2$, $S = -5$, $c_1 = 52$, $c_2 = 148$, $k_1 = 1$, $k_2 = 1$, $c = 1$, $\zeta_0 = 0$, (e) 3D plot of Sol.(4.70), when $P = 12$, $Q = 6$, $R = -1$, $S = -12$, $c_1 = 64$, $c_2 = 104$, $k_1 = 1$, $k_2 = 1$, $c = 1$, $\zeta_0 = 0$, (f) 3D plot of Sol.(4.83) when $P = 12$, $Q = 6$, $R = -1$, $S = \frac{13}{2}$, $c_1 = 21$, $c_2 = \frac{1047}{16}$, $k_1 = 1$, $k_2 = 1$, $c = 1$, $\zeta_0 = 0$

original equation could also be studied. Thus, we claim that if an equation is possibly presented in an integral form similar to (4.4), then different characteristics of the said equation may be determined by the corresponding complete discrimination.

4.4 Conclusion

In this present investigation, employing the idea of the CDSPM, special kinds of exact analytical solutions for the KP-mKP equation are derived. Various wave features, such as solitary wave solution (Figure 4.1.(e)), kink wave solution (Figure 4.1.(f)), rational function solution (Figure 4.1.(a)), singular wave solution (Figure 4.1.(b)), hyperbolic wave solution (Figure 4.1.(e)), and periodic wave solution (Figure 4.1.(c) and Figure 4.1.(d)) are explored from the KP-mKP equation. All these types of solutions in a combined manner could be scarcely acquired by any other technique

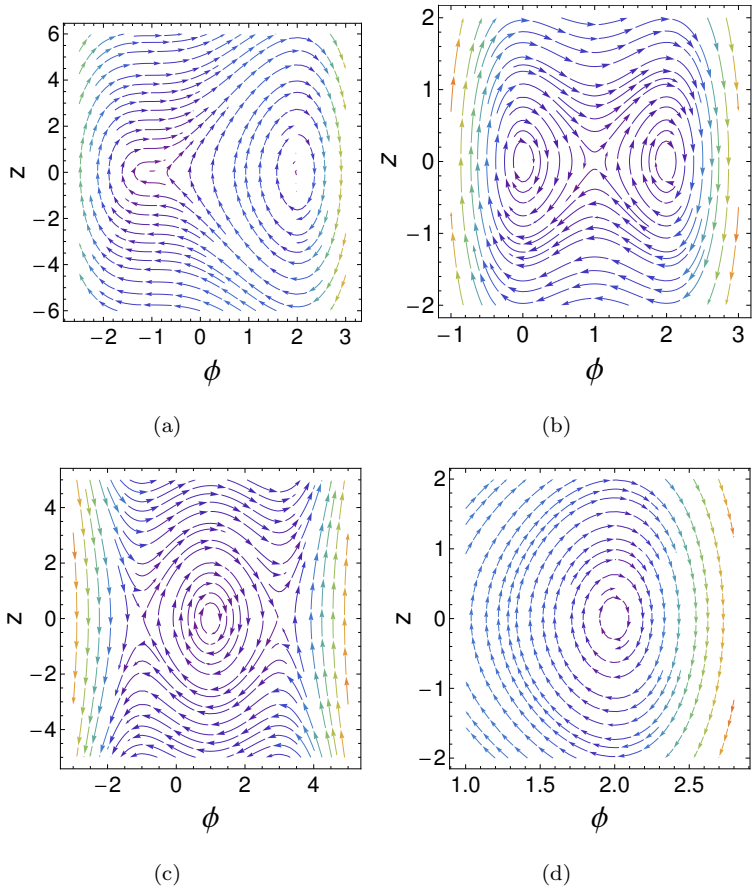

Figure 4.2: Phase portrait of dynamical dynamical system (4.84) in $(\phi, \frac{d\phi}{d\zeta} = z)$-plane, (a) when $\beta_3 = -2$, $\beta_2 = 0$, $\beta_1 = 6$ and $\beta_0 = 4$, (b) for $\beta_3 = -2$, $\beta_2 = 6$, $\beta_1 = -4$ and $\beta_0 = 0$, (c) when $\beta_3 = 1, \beta_2 = -3$, $\beta_1 = -1$ and $\beta_0 = 3$, (d) when $\beta_3 = -2, \beta_2 = 4$, $\beta_1 = -2$ and $\beta_0 = 4$.

as they include Jacobian elliptic functions. In particular, the existing popular method fail miserably in many cases to find any finite amplitude periodic solution for the evolution equation. In addition with we can also find stable ranges of the parameters involved in the equation. The qualitative properties of these solutions are analyzed through the numerical graphs which also show some new identities on Jacobian elliptic functions. More over, this article also demonstrates the strength of CDSPM in qualitative and quantitative analysis, by finding the critical domain for bifurcation and changing the type of solution, classifying the equilibrium points, and examining the phase portrait of topological characteristic. Based on this above analysis, the method can be applied not only to classify the solutions, but can also be used for qualitative analysis, which opens the door to further promotion of the method. This result confirms the effectiveness and consequence of the CDSPM in solving evolution equations and the solutions obtained in this article, could be realized through the significant applications in different scientific and engineering fields such as fluid dynamics, atmospheric phenomena, plasma science matter and elastic media, etc.

Chapter 5

Analytical Solutions of Damped Gardner-Burgers Equation Using Two Expansion Methods

[1]

5.1 Introduction

An NLEEs can be used to describe many complex physical phenomena and for that reason, NLEEs have applications in physics, chemistry, biology, astronomy, etc [144, 201, 202, 203]. For understanding a physical phenomena properly and then applying it in specific fields of science, it is always desired to obtain analytical solutions of NLEEs. In many real-world applications, besides non-linearity in wave propagation, one may need to also deal with dispersion, dissipation, and damping effects. Thus, the Gardner equation in conjunction with dissipation, and damping terms may be a better option to deal with more realistic situations than their counterpart without these terms. Inclusion of these terms in Gardner equation is referred to as damped Gardner-Burgers (dGB) equation which takes the following form

$$\frac{\partial u}{\partial \tau} + Au\frac{\partial u}{\partial \xi} + Bu^2\frac{\partial u}{\partial \xi} + C\frac{\partial^3 u}{\partial \xi^3} + D\frac{\partial^2 u}{\partial \xi^2} + Eu = 0, \tag{5.1}$$

where $u(\xi, \tau)$ is a function of two independent variable ξ-space and τ-time and $A, B, C \in \mathcal{R}$. The term $\frac{\partial u}{\partial \tau}$ denotes the time evolution of the wave propagation, $u\frac{\partial u}{\partial \xi}$, and $u^2\frac{\partial u}{\partial \xi}$ represent the nonlinear

[1]The research article has been published as a chapter of the book Nonlinear Dynamics and Applications, Springer Proceedings in Complexity (Springer)

terms which are responsible for steepening of the wave, $\frac{\partial^3 u}{\partial \xi^3}$ denotes linear dispersion term. The additional two terms $\frac{\partial^2 u}{\partial \xi^2}$ and $Eu(E > 0)$ here in Eq. (5.1) are dissipation and damping terms, respectively. To the best of our knowledge, till now, there are no effective solutions to the damped Gardner-Burgers equation given by Eq.(5.1). In this article, (G'/G)-expansion method, and Method of undetermined coefficient are employed to find the analytical solutions of damped Gardner-Burgers equation. The impact of various parameters are also shown using various surface plots.

5.2 Solutions of dGB equation through the (G'/G)- expansion method

In this section, we implement the (G'/G)-expansion method for our model problem dGB equation (5.1). We use the transformation $U(z) = u(\xi, \tau)$, $z = k\xi - c\tau$, where c is the wave speed. Then, we have,

$$-cU' + AkUU' + BkU^2U' + Ck^3U''' + Dk^2U'' + EU = 0, \tag{5.2}$$

where $'$ denotes the derivative with respect to z.
Now, we use an ansatz Eq.(1.47) for solving Eq.(5.2). Balancing the terms U^2U' and U''' in Eq.(5.2) we get $N = 1$. Thus, the solution can be of the following form

$$U(z) = P_0 + P_1 \left(\frac{G'}{G}\right). \tag{5.3}$$

Substitute Eq.(5.3) into Eq.(5.2), the left hand side transforms into polynomials in $\left(\frac{G'}{G}\right)^j$ $(j = 0, 1, \cdots, 4)$ and setting the coefficients of $\left(\frac{G'}{G}\right)^j$ $(j = 0, 1, \cdots, 4)$ to zero, we obtain the following under determined system of equations for P_0, P_1, λ, μ and c:

$$\begin{aligned}
\left(\frac{G'}{G}\right)^0 &: Dk^2P_1\lambda\mu - AkP_0P_1m u - 2Ck^3P_1\mu^2 - Ck^3P_1\lambda^2\mu + cP_1\mu + EP_0 - BkP_1\mu P_0^2 = 0,\\
\left(\frac{G'}{G}\right)^1 &: 2Dk^2P_1\mu - AkP_0P_1\lambda - Ck^3P_1\lambda^3 + EP_1 - 2BkP_1^2\mu P_0 - AkP_1^2\mu + Dk^2P_1\lambda^2\\
&\quad -BkP_1\lambda P_0^2 - 8Ck^3P_1\lambda\mu + cP_1\lambda = 0,\\
\left(\frac{G'}{G}\right)^2 &: -8Ck^3P_1\mu - 2BkP_1^2\lambda P_0 + cP_1 - AkP_1^2\lambda + 3Dk^2P_1\lambda - BkP_1^3\mu - BkP_1P_0^2 - 7Ck^3P_1\lambda^2\\
&\quad -AkP_0P_1 = 0,\\
\left(\frac{G'}{G}\right)^3 &: -BkP_1^3\lambda - 12Ck^3\lambda P_1 - 2BkP_0P_1^2 - AkP_1^2 + 2Dk^2P_1 = 0,\\
\left(\frac{G'}{G}\right)^4 &: -BkP_1^3 - 6Ck^3P_1 = 0.
\end{aligned} \tag{5.4}$$

Solving (5.4), we obtain two sets of solutions:

Set 1.

$$c = \frac{A\lambda k\sqrt{-\frac{6Ck^3\lambda^3+E}{Bk\lambda}}+E}{2\lambda}, D = \frac{6Ck^3\lambda^3+A\lambda k\sqrt{-\frac{6Ck^3\lambda^3+E}{Bk\lambda}}-E}{2k^2\lambda^2},$$
$$k = k, \mu = \lambda^2, P_0 = 0, P_1 = \frac{\sqrt{-\frac{6Ck^3\lambda^3+E}{Bk\lambda}}}{\lambda}. \tag{5.5}$$

Set 2.

$$c = -\frac{4Ck^3\lambda^3+A\lambda k\sqrt{-\frac{6Ck^3\lambda^3+E}{Bk\lambda}}+3E}{2\lambda}, D = \frac{6Ck^3\lambda^3-A\lambda k\sqrt{-\frac{6Ck^3\lambda^3+E}{Bk\lambda}}-E}{2k^2\lambda^2},$$
$$k = k, \mu = 0, P_0 = 0, P_1 = \frac{\sqrt{-\frac{6Ck^3\lambda^3+E}{Bk\lambda}}}{\lambda}. \tag{5.6}$$

Substituting the values from Eq.(5.5) into Eq.(5.3) and using the general solutions of Eq.(1.48) in different situations, multiple analytical solutions of Eq.(5.2) can be obtained.

Case 1. When $\delta = \lambda^2 - 4\mu = -3\lambda^2 < 0$, for non zero, negative and positive values of λ, the solution of the trigonometric form of Eq.(5.2) is as follows

$$u_1(\xi,\tau) = \sqrt{-\frac{18Ck^3\lambda^3+3E}{Bk\lambda}}\left(\frac{-r_1\sin(\frac{\sqrt{3}\lambda}{2}z)+r_2\cos(\frac{\sqrt{3}\lambda}{2}z)}{r_1\cos(\frac{\sqrt{3}\lambda}{2}z)+r_2\sin(\frac{\sqrt{3}\lambda}{2}z)}-\frac{\lambda}{2}\right), \tag{5.7}$$

where $z = k\xi - \frac{A\lambda k\sqrt{-\frac{6Ck^3\lambda^3+E}{Bk\lambda}}+E}{2\lambda}\tau$ and r_1 and r_2 are arbitrary constants.
These results can be simplified depending upon the conditions on the ratio of r_1 and r_2 as

$$u_1(\xi,\tau) = \sqrt{-\frac{18Ck^3\lambda^3+3E}{Bk\lambda}}\left(\cot\left(\frac{-\lambda}{2}z+\eta_0\right)-\frac{\lambda}{2}\right), \tag{5.8}$$
$$where \quad \lambda^2-4\mu<0, \quad \cot(\eta_0)=\frac{r_2}{r_1}, \quad r_1\neq 0.$$

Now using values from Eq.(5.6) in Eq.(5.3) and considering the general solutions of Eq.(1.48) in different situations, another multiple exact solutions of different types of Eq.(5.2) can be obtained.

Case 1. The solution of the hyperbolic form of Eq.(5.2) is as follows:

$$u_2(\xi,\tau) = \sqrt{-\frac{6Ck^3\lambda^3+E}{Bk\lambda}}\frac{\sqrt{\Delta}}{2}\left(\frac{r_1\cosh(\frac{\sqrt{\Delta}}{2}z)+r_2\sinh(\frac{\sqrt{\Delta}}{2}z)}{r_1\sinh(\frac{\sqrt{\Delta}}{2}z)+r_2\cosh(\frac{\sqrt{\Delta}}{2}z)}-\frac{\lambda}{2}\right), \quad \Delta=\lambda^2-4\mu>0. \tag{5.9}$$

Case 2. The solution of the trigonometric form of Eq.(5.2) is as follows

$$u_3(\xi,\tau) = \sqrt{-\frac{6Ck^3\lambda^3+E}{Bk\lambda}}\frac{\sqrt{\Delta}}{2}\left(\frac{-r_1\sin(\frac{\sqrt{-\Delta}}{2}z)+r_2\cos(\frac{\sqrt{-\Delta}}{2}z)}{r_1\cos(\frac{\sqrt{-\Delta}}{2}z)+r_2\sin(\frac{\sqrt{-\Delta}}{2}z)}-\frac{\lambda}{2}\right), \quad \Delta=\lambda^2-4\mu<0. \tag{5.10}$$

Case 3. The solution to Eq.(5.2), in rational functional form, is as follows:

$$u_4(\xi,\tau) = \sqrt{-\frac{18Ck^3\lambda^3+3E}{Bk\lambda}}\left(\frac{r_2}{r_1+r_2z}-\frac{\lambda}{2}\right), \quad \Delta=\lambda^2-4\mu=0. \tag{5.11}$$

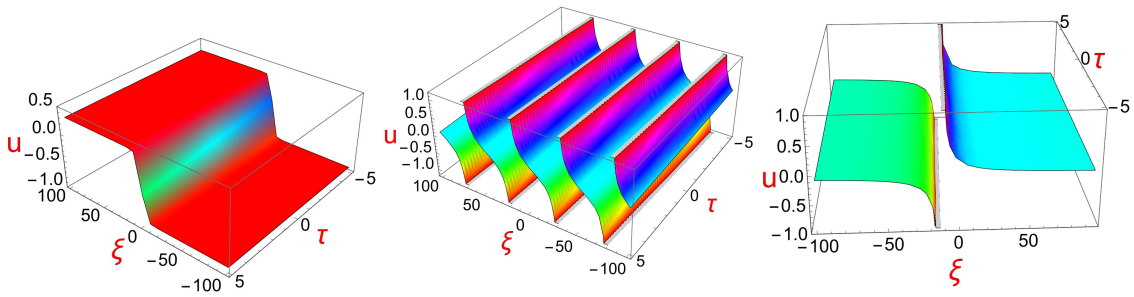

(a) (b) (c)

Figure 5.1: (a) Profiles of solution given by Eq.(5.9) for $\lambda = 1, E = 0.01, r_1 = 1; r_2 = 0; A = 0.5; B = 0.5; c = -0.5; k = 0.5; \mu = 0$. (b) Profiles of solution given by Eq.(5.10) for $\lambda = 0.5; E = 0.05; r_1 = 1; r_2 = 0.5; A = 0.5; B = -0.5; c = 0.5; k = 0.5; \mu = 0;$. (c) Profiles of solution given by Eq.(5.11) for $\lambda = 0.5; s = 0.05; r1 = 1; r2 = 5; A = 0.5; B = -0.5; c = 0.5; k = 0.5; \mu = 0;$

For all cases $z = k\xi + \frac{4Ck^3\lambda^3 + A\lambda k\sqrt{-\frac{6Ck^3\lambda^3+E}{Bk\lambda}} + 3E}{2\lambda}\tau$ and r_1 and r_2 are arbitrary constants.
These results can be simplified depending upon the conditions on the ratio of r_1 and r_2 as

$$u_{2a}(\xi,\tau) = \sqrt{-\frac{6Ck^3\lambda^3 + E}{Bk\lambda}}\frac{\sqrt{\Delta}}{2}\left(\tanh\left(\frac{\lambda}{2}z + \eta_0\right) - \frac{\lambda}{2}\right), \quad (5.12)$$
$$\text{where } \lambda^2 - 4\mu > 0, \quad \tanh(\eta_0) = \frac{r_2}{r_1}, \quad r_1 \neq 0, \quad \left|\frac{r_2}{r_1}\right| < 1.$$

$$u_{2b}(\xi,\tau) = \sqrt{-\frac{6Ck^3\lambda^3 + E}{Bk\lambda}}\frac{\sqrt{\Delta}}{2}\left(\coth\left(\frac{\lambda}{2}z + \eta_0\right) - \frac{\lambda}{2}\right), \quad (5.13)$$
$$\text{where } \lambda^2 - 4\mu > 0, \quad \coth(\eta_0) = \frac{r_2}{r_1}, \quad r_1 \neq 0, \quad \left|\frac{r_2}{r_1}\right| > 1.$$

$$u_3(\xi,\tau) = \sqrt{-\frac{6Ck^3\lambda^3 + E}{Bk\lambda}}\frac{\sqrt{\Delta}}{2}\left(\cot\left(\frac{-\lambda}{2}z + \eta_0\right) - \frac{\lambda}{2}\right), \quad (5.14)$$
$$\text{where } \lambda^2 - 4\mu < 0, \quad \cot(\eta_0) = \frac{r_2}{r_1}, \quad r_1 \neq 0.$$

where z is givem by $z = k\xi + \frac{4Ck^3\lambda^3 + A\lambda k\sqrt{-\frac{6Ck^3\lambda^3+E}{Bk\lambda}} + 3E}{2\lambda}\tau$.

5.3 Solutions of dGB equation through the method of undetermined coefficients

In this section, we apply method of undetermined coefficients to solve the damped Gardner-Burgers equation given by Eq.(5.1).

5.3.0.1 The Bright Soliton Solution:

To get the bright soliton solution of Eq.(5.2), we can take expansion given by Eq.(1.62), where λ, V are nonzero constants. From the Eq.(1.62), we obtain

$$\begin{aligned} U' &= -\lambda m\ sech^{m+1}(z)sinh(z), \\ U'' &= \lambda m^2 sech^m(z) - \lambda m(m+1)sech^{m+2}(z), \\ UU' &= -\lambda^2 m\ sech^{2m+1}(z)sinh(z), \\ U^2U' &= -\lambda^3 m\ sech^{3m+1}(z)sinh(z), \\ U''' &= -\lambda m^3 sech^{m+1}(z)sinh(z) + \lambda m(m+1)(m+2)sech^{m+3}(z)sinh(z). \end{aligned} \tag{5.15}$$

Thus, substituting the ansatz (5.15), Eq. (1.62) into Eq.(5.2), yields

$$\begin{aligned} &[V\lambda m - Ck^3\lambda m^3]sech^{m+1}(z)sinh(z) - Ak\lambda^2 m\ sech^{2m-1}(z)sinh(z) - Bk\lambda^3 m\ sech^{3m+1}(z) \\ &sinh(z) - Ck^3\lambda m(m+1)(m+2)sech^{m+3}(z)sinh(z) - Dk^2\lambda m(m+1)sech^{m+2}(z)sinh(z) \\ &+[Dk^2\lambda m^2 + E\lambda]sech^m(z) = 0. \end{aligned} \tag{5.16}$$

Equating the exponents $sech^{3m+1}(z)$ and $sech^{m+3}(z)$ gives

$$3m + 1 = m + 3 \quad \rightarrow \quad m = 1.$$

From Eq.(5.16), setting the coefficients of $sech^{3m+1}(z)$ and $sech^{m+3}(z)$ terms to zero, we obtain

$$-Bk\lambda^3 m - Ck^3\lambda m(m+1)(m+2) = 0. \tag{5.17}$$

We find, from setting the coefficients of $sech^m(z)$ terms in Eq.(5.16) to zero

$$Dk^2\lambda m^2 + E\lambda = 0. \tag{5.18}$$

We find, from setting the coefficients of $sech^{m+1}(z)$ terms in Eq.(5.16) to zero

$$V\lambda m - Ck^3\lambda m^3 = 0. \tag{5.19}$$

Considering Eqs.(5.17)-(5.18), one may easily get some certain constraint for the existence of the soliton for the present system as:

$$E = -Dk^2, C = \frac{B\lambda^2}{6k^2}. \tag{5.20}$$

From Eq.(5.19), we find

$$V = Ck^3. \tag{5.21}$$

Finally, we obtain the solitary solution as

$$u(\xi,\tau) = \lambda\ sech(k\xi - Ck^3\tau). \tag{5.22}$$

Thus, subject to some certain condition, the solution (5.22) becomes the exact solution of Eq.(5.1). Thus finally, using the values of V and λ, the solitary soliton solution of Eq.(5.1) can be re-written in the following form:

$$u(\xi,\tau) = \pm\sqrt{-\frac{6CE}{BD}}\ sech\left(\pm\sqrt{-\frac{E}{D}}\xi \pm C\left(\sqrt{-\frac{E}{D}}\right)^3\tau\right). \tag{5.23}$$

5.3.0.2 The Dark Soliton Solution

Here, we use the solution of the form Eq.(1.63), where k, λ, and V are the free parameters. From the Eq.(1.63), we obtain

$$\begin{aligned}
U' &= \lambda m(tanh^{m-1}(z) - tanh^{m+1}(z)),\\
U'' &= \lambda m[(m-1)tanh^{m-2}(z) - 2m^2 tanh^m(z) + (m+1)tanh^{m+2}(z)],\\
UU' &= \lambda^2 m\ tanh^{2m-1}(z) - \lambda^2 m\ tanh^{2m+1}(z),\\
U''' &= \lambda(m^3 - 3m^2 + 2m)tanh^{m-3}(z) - \lambda(m^3 + 3m^2 + 2m)tanh^{m+3}(z)\\
&\quad -\lambda(3m^3 - 3m^2 + 2m)tanh^{m-1}(z) + \lambda(3m^3 + 3m^2 + 2m)tanh^{m+1}(z).
\end{aligned} \tag{5.24}$$

Substituting Eq. (1.63) and Eq. (5.24) into Eq. (5.2), gives

$$\begin{aligned}
&[-V\lambda m - Ck^3\lambda m(3m^2 - 3m + 2)]tanh^{m-1}(z) + [c\lambda m - Ck^3\lambda m(3m^2 + 3m + 2)]tanh^{m+1}(z)\\
&+Ak\lambda^2 m\ tanh^{2m-1}(z) - Ak\lambda^2 m\ tanh^{2m+1}(z) + Bk\lambda^3 m\ tanh^{3m-1}(z) - Bk\lambda^3 m\ tanh^{3m+1}(z)\\
&+Ck^3\lambda m(m-1)(m-2)tanh^{m-3}(z) - Ck^3\lambda m(m+1)(m+2)tanh^{m+3}(z) + Dk^2\lambda m(m-1) \times\\
&tanh^{m-2}(z) + Dk^2\lambda m(m+1)tanh^{m+2}(z) + [E\lambda - 2D\lambda k^2 m^2]tanh^m(z) = 0.
\end{aligned} \tag{5.25}$$

Now, from Eq. (5.25), equating the exponents of $tanh^{3m+1}(z)$ and $tanh^{m+3}(z)$ gives,

$$3m + 1 \quad = \quad m + 3 \quad \rightarrow \quad m = 1.$$

Setting the coefficients of $tanh^{3m+1}(z)$ and $tanh^{m+3}(z)$ terms in Equation to zero, we have

$$-Bk\lambda^3 m - Ck^3\lambda m(m+1)(m+2) = 0. \tag{5.26}$$

Again, from Eq. (5.25) setting the coefficients of $tanh^m(z)$ terms to zero we have

$$E\lambda - 2m^2 Dk^2\lambda = 0. \tag{5.27}$$

Again, from Eq.(5.20) setting the coefficients of $\tanh^{m-1}(z)$ terms to zero

$$-\lambda m V - Ck^3\lambda(3m^3 - 3m^2 + 2m) = 0. \tag{5.28}$$

Utilizing Eqs. (5.26) and (5.27), we may find the constraint condition for the existence soliton as:

$$E = 2Dk^2,\ B = -\frac{6Ck^2}{\lambda^2} \tag{5.29}$$

Eq.(5.28), provides the result

$$V = -2Ck^3 \tag{5.30}$$

Finally, we acquires the solution as

$$u(\xi,\tau) = \lambda \tanh(k\xi + 2Ck^3\tau) \tag{5.31}$$

The solution (5.31) is the exact shock solution for Eq.(5.1) under the particular constraint condition (5.29). Thus finally, the another form of dark soliton solution for the damped Gardner-Burgers equation (5.1) is given by:

$$u(\xi,\tau) \quad = \quad \pm\sqrt{-\frac{3CE}{DB}}\tanh\left(\pm\frac{1}{2}\sqrt{\frac{2E}{D}}\xi \pm \frac{\sqrt{2}C}{2}\left(\frac{E}{D}\right)^{3/2}\tau\right). \tag{5.32}$$

5.4 Parametric Discussion

To understand and appreciate the effect of different terms, we draw surface plots corresponding to the solutions (5.23) and (5.32). Figure 5.2(a) is the three dimensional graph for the solution given by Eq.(5.23) which is drawn for different values of coefficient D with others coefficients $A = 0.01$, $B = 0.6$, $C = 0.02$ and $E = 0.06$. Figure 5.2(a) shows that the depth of the rarefactive soliton increases with respect to increase in D. The effect of damping on the solution structure given by Eq.(5.23) is shown in Figure 5.2(b). In this case other coefficients are fixed as $A = 0.01$, $B = 0.6$, $C = 0.02$ and $D = -0.02$. It is clear from Figure 5.2(b) that the depth of the rarefactive soliton increases with respect to increased damping. The profound effect of Burgers term on the kink soliton obtained from solution represented by Eq.(5.32) is shown in Figure 5.2(c). For this plot we have taken the fixed values of parameters as $A = 0.01$, $B = 0.02$, $C = -0.02$ and $E = 0.01$. It is deduced from the Figure 5.2(c) that the amplitude of the soliton diminishes for increasing burgers coefficient value. Significant impact can be noticed of damping on the solution structure obtained from the Sol.(5.32) and is shown by the Figure 5.2(d) for which other coefficients are fixed at $A = 0.01$, $B = 0.02$, $C = -0.02$ and $D = 0.3$. From the Figure 5.2(d) it is deduced that the height of the kink shape soliton is increased for an increased value of damping.

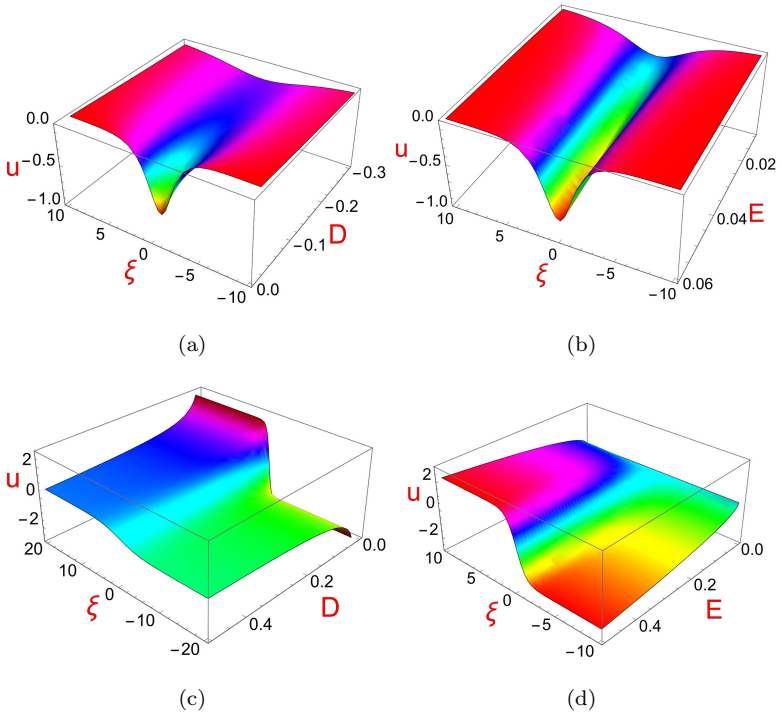

Figure 5.2: (a) Profiles of solution given by Eq. (5.23) for $A = 0.01, B = 0.6, C = 0.02, D = [-0.3, -0.02], E = -0.06$, and $\tau = 1$. (b) Profiles of solution given by Eq.(5.23) for $A = 0.01, B = 0.6, C = 0.02, D = -0.02, E = [0.01, 0.06]$ and $\tau = 1$. (c) Profiles of solution given by Eq.(5.32) for $A = 0.01, B = 0.02, C = -0.02, D = [0.02, 0.5], E = 0.05$ and $\tau = 1$. (d) Profiles of solution given by Eq.(5.32) for $A = 0.01, B = 0.02, C = -0.02, D = 0.3, E = [0, 0.5]$ and $\tau = 1$.

5.5 Conclusions

Different types of solutions such as kink soliton solution (Figure 5.1(a), Figure 5.2(c) and Figure 5.2(d)), singular periodic solution (Figure 5.1(b)), rational solution (Figure 5.1(c)), rarefactive soliton solution (Figure 5.2(a) and Figure 5.2(b)) are obtained for the dGB equation by employing (G'/G)-expansion method and Method of undetermined coefficient. Three dimensional surface plots are drawn for specific values of the parameters to depict the effect of damping term and the effect of burgers term on the physical structure of the solution. The results obtained from our observations are summarized as:

- Rarefactive soliton gets deeper for higher values of damping and burgers coefficients.
- The amplitude of the kink soliton increases with an increase in the dampness.
- Higher values of burgers coefficient can reduce the height of the kink soliton.

The obtained solutions and results may be helpful in the study of plasma physics, dynamics of soliton, fluid dynamics, and other branches.

Chapter 6

Studies on the dust acoustic shock, solitary and periodic waves in an unmagnetized viscous dusty plasma with two temperature ion

[1]

6.1 Introduction

Dusty plasma describes a particular type of ionized gas which contains electrons, positive as well as negative ions, micrometer-measured charged dust grains, neutral atoms, etc. It is abundantly appeared in different astrophysical objects viz., galactic nuclei [204], pulsar magnetosphere [205, 206, 207], solar atmosphere [208, 206], planet rings, comet tails, noctilucent clouds etc [209, 210, 211]. Several physicists conducted some laboratory experiments on waves and instabilities have been performed on different dusty plasmas [212, 85, 213, 214] and their experiments established the existence of the DAW mode. Applying some effective approaches to the plasma diagnostics, it is found that dusty plasma produces different kinds of wave modes viz. DIAWs, DAWs, dust-lattice wave, etc. [215, 216, 217] and among them, DAW is the most fundamental content in dusty plasma. Recently, DAW emerge as one of the most popular research areas in dusty plasma physics because

[1]The research article has been published in the journal of Brazilian Journal of Physics (Springer)

of its applications not only in astrophysical space studies but also in real-world applications, such as semiconductor manufacturing, nano-particle processing, film industries, etc [218, 219]. The low-frequency DAW is abundantly found in the planetary rings, comet tails, earth's mesosphere, moon, etc. [62]. The speed of research on DAWs increase a lot soon after their existence was proved through experiments. In plasma medium, solitons are the most common and convenient waves that may be generated by perturbations at low frequencies. However, shocks and periodic solutions often arise in plasma environments. Some theoretical observations also show that soliton may turn into a cnoidal wave under certain conditions [220]. It is important to mention here that a nonlinear periodic wave is presented through the form of a Jacobian elliptical function.

In this chapter we investigated the non-linear propagation of DAW in collisionless, unmagnetized, viscous dusty plasma containing Maxwellian Boltzmann distributed electrons, two temperature ions, and highly negatively charged dust grains. Following the approach of the Reductive Perturbation Technique (RPT), the KPb equation is constructed from the governing equation, and further, utilizing traveling wave transformation, the KPb equation is converted into an ordinary differential equation. Analyzing phase portraits for the KPb system varying different plasma parameters, it is found that the KPb system includes *shock, solitary* as well as *periodic solutions*. But, in case of lack of Burgers term, the system only provides the *solitary, and periodic solutions* which are directly generated from the KP equation, and further, a shock solution of the KPb equation is derived by applying (G'/G)-Expansion method. Introducing the indirect F-function method and incorporating Jacobi elliptic function, a finite-amplitude periodic solution for the KPb equation is also constructed. Finally, the impacts of the physical parameters on wave propagation in the present system are illustrated from a numerical standpoint.

6.2 Basic equation

We consider the propogation of DAWs in a collisionless, viscous, unmagnetized dusty plasma containing of highly negative charged dust grain, electrons and two temperature ions. Then the dynamics of DAWs can be characterized by the following normalized equations as

$$\frac{\partial N_d}{\partial t} + \frac{\partial (N_d U_d)}{\partial x} + \frac{\partial (N_d V_d)}{\partial y} = 0, \tag{6.1}$$

$$\frac{\partial U_d}{\partial t} + U_d \frac{\partial U_d}{\partial x} + V_d \frac{\partial U_d}{\partial y} = Z_d \frac{\partial \phi}{\partial x} - \zeta \left(\frac{\partial^2}{\partial x^2} + \frac{\partial^2}{\partial y^2} \right) U_d, \tag{6.2}$$

$$\frac{\partial V_d}{\partial t} + U_d \frac{\partial V_d}{\partial x} + V_d \frac{\partial V_d}{\partial y} = Z_d \frac{\partial \phi}{\partial y} - \zeta \left(\frac{\partial^2}{\partial x^2} + \frac{\partial^2}{\partial y^2} \right) V_d, \tag{6.3}$$

$$\frac{\partial^2 \phi}{\partial x^2} + \frac{\partial^2 \phi}{\partial y^2} = Z_d N_d - N_{il} - N_{ih} + N_e, \tag{6.4}$$

where N_d denotes the number density of dust particles in the normal state which is N_{d0}. T_e, T_{il} and T_{ih} are respectively the temperatures of electrons, low and high temperature ions. T_{ef} is the effective temperature and is given by

$$\frac{1}{T_{ef}} = \frac{1}{N_{d0}Z_{d0}}\left(\frac{N_{e0}}{T_e} + \frac{N_{il0}}{T_{il}} + \frac{N_{ih0}}{T_{ih}}\right), \tag{6.5}$$

where $N_{j0}(j = e, i)$ are the number of charge particles (electrons, ions) at equilibrium state and Z_{d0} denotes the unperturbed number of charges on the dust particles. U_d and V_d are the velocities of the dust flow along the direction of x and y axis respectively and normalized by the dust acoustic speed $c_d = (\frac{K_B T_{ef} Z_{d0}}{m_d})^{\frac{1}{2}}$ in which K_B is the Boltzman constant and m_d is the dust particles mass. ϕ is the electrostatic potential normalized by $\phi = \frac{K_B T_{ef}}{e}$. Time and space variables are scaled over the effective Debye length, $\lambda_d = \left(\frac{K_B T_{ef}}{4\pi N_{d0} Z_{d0} e^2}\right)^{\frac{1}{2}}$ and the inverse of dust plasma frequency $\omega_{pd}^{-1} = \left(\frac{m_d}{4\pi N_{d0} Z_{d0}^2 e^2}\right)^{\frac{1}{2}}$. ζ is the dust viscocity coefficient.

N_e, N_{il} and N_{ih} are the number densities for electrons, low temperature ions, high temperature ions respectively and all are assumed to be Boltzmann disribution functions and which are given by

$$N_e = \frac{N_{e0}}{N_{d0}Z_{d0}} \exp(\beta_2 s\phi), \tag{6.6}$$

$$N_{il} = \frac{N_{il0}}{N_{d0}Z_{d0}} \exp(-s\phi), \tag{6.7}$$

$$N_{ih} = \frac{N_{e0}}{N_{d0}Z_{d0}} \exp(-\beta_1 s\phi), \tag{6.8}$$

$$\text{where} \quad \beta_1 = \frac{T_{il}}{T_{ih}}, \quad \beta_2 = \frac{T_{il}}{T_e}, \quad \beta_3 = \frac{T_{ih}}{T_e}, \quad s = \frac{T_{ef}}{T_{il}}, \quad \delta_1 = \frac{N_{il0}}{N_{e0}}, \quad \delta_2 = \frac{N_{ih0}}{N_{e0}}. \tag{6.9}$$

Net charge neutrality at equilibrium yields

$$N_{e0} = N_{il0} + N_{ih0} - N_{d0}Z_{d0}, \tag{6.10}$$

where N_{il0} and N_{ih0} are the number of lower temperature ions and higher temperature ions respectively at equilibrium state. From Eq.(6.9) and Eq.(6.10) it follows

$$\delta_1 + \delta_2 \geqslant 1, \tag{6.11}$$

$$s = \frac{\delta_1 + \delta_2 - 1}{\delta_1 + \delta_2\beta_1 + \beta_2}. \tag{6.12}$$

The charge-current balance equation [221] gives the dust charge variable Q_d as

$$\left(\frac{\partial}{\partial t} + \vec{V}.\vec{\nabla}\right) Q_d = J_e + J_{il} + J_{ih}, \tag{6.13}$$

where $\overrightarrow{I} = (U_d, V_d)$ and J_{il}, J_{ih} and J_e are the lower temperature ions, higher temperature ions and electrons currents respectively. Suppose $\frac{dQ_d}{dt} << J_e, J_{il}, J_{ih}$ then the Eq.(6.13) looks [222]

$$\left(\frac{\partial}{\partial t} + \overrightarrow{I}.\overrightarrow{\nabla}\right) Q_d = J_e + J_{il} + J_{ih} \approx 0. \tag{6.14}$$

The ion and electron currents are expressed as [223].

$$J_{il} = e\pi r^2 \left(\frac{8T_{il}}{\pi m_i}\right)^{\frac{1}{2}} N_{il} \left(1 - \frac{e\Phi}{T_{il}}\right), \tag{6.15}$$

$$J_{ih} = e\pi r^2 \left(\frac{8T_{ih}}{\pi m_i}\right)^{\frac{1}{2}} N_{ih} \left(1 - \frac{e\Phi}{T_{ih}}\right), \tag{6.16}$$

$$J_e = -e\pi r^2 \left(\frac{8T_e}{\pi m_e}\right)^{\frac{1}{2}} N_e \exp\left(\frac{e\Phi}{T_e}\right), \tag{6.17}$$

where Φ is the potential of dust particles surface relative to the potential of plasma ϕ [224].
The number of dust particles charge, Z_d is gained from $Z_d = \frac{\psi}{\psi_0}$, where $\psi = \frac{\exp^{\Phi}}{T_{ef}}$, and $\psi_0 = \psi(\phi = 0)$. Expanding Z_d with respect ϕ we have [121],

$$Z_d = 1 + \gamma_1\phi + \gamma_2\phi^2 + \cdots, \tag{6.18}$$

where $\gamma_1 = \frac{1}{\psi_0}\left(\frac{d}{d\phi}\psi(\phi)\right)_{\phi=0}$ and $\gamma_2 = \frac{1}{2\psi_0}(\frac{d^2\psi(\phi)}{d\phi^2})_{\phi=0}$.

6.3 Derivation of KPb equation

To derive the KPb equation, we have used the RPT [225]. The stretching co-ordinates are given as

$$\xi = \epsilon(x - \lambda_p t),\ \eta = \epsilon^2 y,\ \tau = \epsilon^3 t, \tag{6.19}$$

where ϵ is the small parameter which characterizes the strength of the nonlinearity of the system and λ_p is the phase velocity of the wave. To obtain the KPb equation, we expand the perturbation quantities N_d, U_d, V_d, Z_d, ϕ and ζ in power series of ϵ as

$$N_d = 1 + \epsilon^2 N_{d1} + \epsilon^4 N_{d2} + \cdots, \tag{6.20}$$

$$U_d = 0 + \epsilon^2 U_{d1} + \epsilon^4 U_{d2} + \cdots, \tag{6.21}$$

$$V_d = 0 + \epsilon^3 V_{d1} + \epsilon^5 V_{d2} + \cdots, \tag{6.22}$$

$$Z_d = 1 + \epsilon^2 Z_{d1} + \epsilon^4 Z_{d2} + \cdots, \tag{6.23}$$

$$\phi = 0 + \epsilon^2\phi_1 + \epsilon^4\phi_2 + \cdots, \tag{6.24}$$

$$\zeta \approx \epsilon\zeta_0. \tag{6.25}$$

By using the RPT from Eqs. (6.1)-(6.4) and using stretching coordinates (6.19) along with state variables from Eqs. (6.20)-(6.25), we get a set of evolution equations. Collecting the coefficients of lower power of ϵ, we have gained

$$N_{d1} = -\frac{\phi_1}{\lambda_p^2}, \quad U_{d1} = -\frac{\phi_1}{\lambda_p}, \quad \lambda_p = (1+\gamma_1)^{-\frac{1}{2}}, \tag{6.26}$$

$$\lambda_p \frac{\partial V_{d1}}{\partial \xi} = -\frac{\partial \phi_1}{\partial \eta}, \tag{6.27}$$

$$\frac{\partial N_{d1}}{\partial \tau} - \lambda_p \frac{\partial N_{d2}}{\partial \xi} + \frac{\partial (N_{d1} U_{d1})}{\partial \xi} + \frac{\partial U_{d2}}{\partial \xi} + \frac{\partial V_{d1}}{\partial \eta} = 0, \tag{6.28}$$

$$\frac{\partial U_{d1}}{\partial \tau} - \lambda_p \frac{\partial U_{d2}}{\partial \xi} + U_{d1} \frac{\partial U_{d1}}{\partial \xi} = Z_{d1} \frac{\partial \phi_1}{\partial \xi} + \frac{\partial \phi_2}{\partial \xi} - \zeta_0 \frac{\partial^2 U_{d1}}{\partial \xi^2}, \tag{6.29}$$

$$\frac{\partial V_{d1}}{\partial \tau} - \lambda_p \frac{\partial V_{d2}}{\partial \xi} + U_{d1} \frac{\partial V_{d1}}{\partial \xi} = Z_{d1} \frac{\partial \phi_1}{\partial \eta} + \frac{\partial \phi_2}{\partial \eta} - \zeta_0 \frac{\partial^2 V_{d1}}{\partial \xi^2}, \tag{6.30}$$

$$\frac{\partial^2 \phi_1}{\partial \xi^2} = Z_{d2} + Z_{d1} N_{d1} + N_{d2} + \phi_2 - \frac{1}{2}(\delta_1 + \delta_2 \beta_1 - \beta_2^2) \frac{s^2}{(\delta_1 + \delta_2 - 1)} \phi_1^2. \tag{6.31}$$

Also comparing (6.18) and (6.23) we can find

$$Z_{d1} = \gamma_1 \phi_1, Z_{d2} = \gamma_1 \phi_2 + \gamma_2 \phi_1^2. \tag{6.32}$$

By eliminating N_{d2}, U_{d2}, and ϕ_2 from Eqs. (6.28)-(6.31) and letting $\phi_1 = \phi$, we obtain the KPb equation as

$$\frac{\partial}{\partial \xi}\left(\frac{\partial \phi}{\partial \tau} + A\phi \frac{\partial \phi}{\partial \xi} + B \frac{\partial^3 \phi}{\partial \xi^3} + C \frac{\partial^2 \phi}{\partial \xi^2}\right) + D \frac{\partial^2 \phi}{\partial \eta^2} = 0, \tag{6.33}$$

where

$$A = \frac{\lambda_p^3}{2}\left[(\delta_1 + \delta_2 \beta_1^2 - \beta_2^2) \frac{(\delta_1 + \delta_2 - 1)}{(\delta_1 + \delta_2 \beta_1 + \beta_2)^2} - 2\gamma_2\right] + \frac{3}{2}\gamma_1 \lambda_p - \frac{3}{2\lambda_p}, \quad B = \frac{\lambda_p^3}{2}, \quad C = \frac{\zeta_0}{2}, \quad D = \frac{\lambda_p}{2}. \tag{6.34}$$

In the absence of Burgers term Eq.(6.33) converted to standerd KP equation as

$$\frac{\partial}{\partial \xi}\left(\frac{\partial \phi}{\partial \tau} + A\phi \frac{\partial \phi}{\partial \xi} + B \frac{\partial^3 \phi}{\partial \xi^3}\right) + D \frac{\partial^2 \phi}{\partial \eta^2} = 0. \tag{6.35}$$

The nonlinear coefficient A plays the most important role in the formation of wave structure in any nonlinear field. Here, we intend to discuss the variation of the values of A due to the variation of different parameters. The effect of different parameters such as, β_1, β_2, δ_1, δ_2, etc. are explicitly described in Figure 6.1. From, Figure 6.1(a) and Figure 6.1(b), it is observed that the negativity of A strictly enhances because of the enhancement of the parameters, β_1, β_2. Thus it is confirmed that the temperature of lower-temperature ions leads to enhance in the negativity of non-linearity. As can also be seen from these figures, A is positive for small values of β_1 and β_2. The most interesting fact is found in Figure 6.1(c) where the non-linearity has a sudden hike for small values of δ_1 however, non-linearity further strictly decreases as δ_1 enhances. It is found that On the other hand, from Figure 6.1(d), it is observed that the values of A strictly enhanced due to the enhancement in δ_2. Even the values of A may attain the positive value for sufficiently large δ_2.

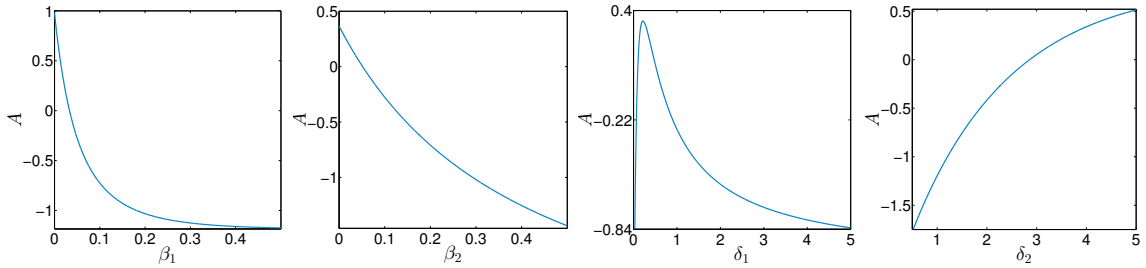

(a) (b) (c) (d)

Figure 6.1: Variation A vs various parameter, (a) for $\delta_1 = 0.3$, $\delta_2 = 3.5$, $\beta_2 = 0.1$, $\gamma_1 = 0.01$, $\gamma_2 = 0.03$, (b) for $\delta_1 = 0.3$, $\delta_2 = 3.5$, $\beta_1 = 0.05$, $\gamma_1 = 0.01$, $\gamma_2 = 0.03$, (c) for $\beta_1 = 0.02$, $\delta_2 = 3.5$, $\beta_2 = 0.1$, $\gamma_1 = 0.1$, $\gamma_2 = 0.01$, (d) for $\delta_1 = 0.3$, $\beta_2 = 0.1$, $\beta_2 = 0.05$, $\gamma_1 = 0.01$, $\gamma_2 = 0.03$.

6.4 Phase portrait analysis of the unperturbed dynamical system for the KP equation

Now, we analyze the phase portrait of the KPb equation, considering the unperturbed dynamical system and finally, by using bifurcation theory [199] the characteristic of the nonlinear propagation of the wave solutions are discussed. We choose the traveling wave transformation as,

$$\phi(\xi, \eta, \tau) = U(\theta),\ \theta = l\xi + m\eta - V\tau, \tag{6.36}$$

where V presents the wave velocity V and l, m are the constants such that $l^2 + m^2 = 1$. Thus, the Eq.(6.33) is converted into the ODE

$$(-Vl + Dm^2)U'' + Al^2(UU')' + Bl^4U^{(4)} + Cl^3U^{(3)} = 0. \tag{6.37}$$

Integration on Eq.(6.37) leades

$$(-Vl + Dm^2)U + \frac{Al^2}{2}U^2 + Bl^4U'' + Cl^3U' = 0, \tag{6.38}$$

where prime designates ordinary derivative with respect to θ. Due to the lack of Burgers term ($C = 0$ i.e., $\zeta_0 = 0$), the system turns into the form,

$$\begin{aligned} \frac{dU}{d\theta} &= z \\ \frac{dz}{d\theta} &= \frac{Vl - Dm^2}{Bl^4}U - \frac{A}{2Bl^2}U^2. \end{aligned} \tag{6.39}$$

In general, the solitary wave solution is mentioned by a homoclinic orbit; a heteroclinic orbit ensures the presence of a shock solution and a periodic orbit indicates the presents of a periodic solution. When the burgers term is unavailable, i.e. ($\zeta_0 = 0$), the Hamiltonian of (6.39) is defined as

$$\mathcal{H}(U, z) = z^2 - \frac{(Vl - Dm^2)U^2}{Bl^4} + \frac{AU^3}{3Bl^2} = h \quad (say). \tag{6.40}$$

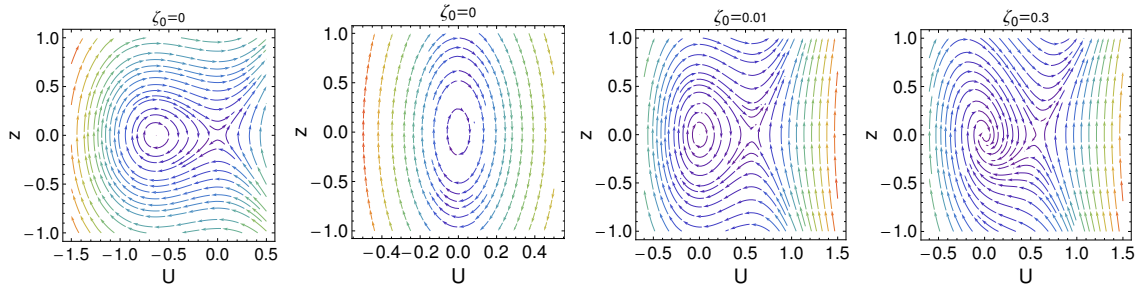

(a) (b) (c) (d)

Figure 6.2: (a) Phase portrait of dynamical system (6.39), for $l = 1/\sqrt{2}$, $m = 1/\sqrt{2}, \gamma_1 = 0.1$, $\beta_2 = 0.1$, $\beta_1 = 0.1$, $\delta_2 = 4$, $\delta_1 = 1$, $\gamma_2 = 0.1$, $V = 0.5$, and (b) for $l = 0.5$, $m = 1$, $V = 0.1$, $\gamma_1 = 0.1$, $\beta_2 = 0.1$, $\beta_1 = 0.1$, $\delta_2 = 2$, $\delta_1 = 1, \gamma_2 = 0.05$. The phase portrait of dynamical system (6.53), (c) for $l = 0.5$, $m = 0.5$, $V = 0.1$, $\gamma_1 = 0.2$, $\beta_2 = 0.1$, $\beta_1 = 0.1$, $\delta_2 = 4$, $\delta_1 = 2$, $\gamma_2 = 0.2$, (d) for all the parameter values same as (c) except ζ_0.

The system (6.39) has two equilibrium points which are stated as, $U_0(0,0)$ and $U_1(\frac{2(Vl-Dm^2)}{Al^2}, 0)$. Now, we draw the coefficient matrix of the linearized system of (6.39) at the point (U, z) as $M(U, z)$. Let, the elements of the matrix are $J_d = \det(M(U,z)), T_{r1} = \mathrm{trace}(M(U,z))$ and $T_{r2} = (\mathrm{trace}(M(U,z)))^2$ and so, $M(U,z) = \begin{pmatrix} 0 & 1 \\ \frac{Vl-Dm^2}{Bl^4} - \frac{A}{Bl^2}U & 0 \end{pmatrix}$. At $(0,0)$, $J_d = \frac{Dm^2-Vl}{Bl^4}$ and $\mathcal{H}(U,z) = 0$ whereas at $(\frac{2(Vl-Dm^2)}{Al^2}, 0)$, $J_d = \frac{Vl-Dm^2}{Bl^4}$ and $\mathcal{H}(U,z) = -\frac{4}{3}\frac{(Vl-Dm^2)^3}{A^2Bl^8}$. Now, varying the values of the different effective parameters such as, δ_1, δ_2, β_1, β_2 and V, we investigate the phase plane (U, z) for the system (6.39).

Set 1.

For $l = 1/\sqrt{2}$, $m = 1/\sqrt{2}, \gamma_1 = 0.1$, $\beta_2 = 0.1$, $\beta_1 = 0.1$, $\delta_2 = 4$, $\delta_1 = 1$, $\gamma_2 = 0.1$, $V = 0.5$, the equilibrium point $U_0(0,0)$ becomes saddle because at that point $J_d < 0$, $T_{r2} - 4J_d > 0$, and the equilibrium point $U_1(\frac{2(Vl-Dm^2)}{Al^2}, 0)$ becomes centre because at that point $J_d > 0$, $T_{r1} = 0$. Thus we get a homoclinic orbits at $U_0(0,0)$(see Figure 6.2(a)).

Set 2.

For $l = 0.5$, $m = 1$, $V = 0.1$, $\gamma_1 = 0.1$, $\beta_2 = 0.1$, $\beta_1 = 0.1$, $\delta_2 = 2$, $\delta_1 = 1, \gamma_2 = 0.05$, the equilibrium point $U_0(0,0)$ turns into a centre at that point $J_d > 0$, $T_{r1} = 0$. Thus, periodic orbits have been observed about $(0,0)$ (see Figure 6.2(b)).

6.5 An analysis of all travelling wave solutions

6.5.1 Solitary wave solutions of KP equation

In particular, a solitary wave represents the propagation of a wave packet that is localized in the sense, and in addition, the solitons do not spread their energy during propagation, and their stability allows them to move without losing their energy, shape, or momentum. Some kind of nonlinearity exists in the system to explain the existence of solitons. Solitons are formed only when nonlinearity and dispersion combine into a stable balance, forming a pulse that propagates without changing shape. To find solitary solution, we rewrite equation (6.40) as

$$z^2 = h + \frac{Vl - Dm^2}{Bl^4}U^2 - \frac{A}{3Bl^2}U^3. \tag{6.41}$$

Now, integrating along the level curves mentioned as $\mathcal{H}(U, z) = h$ gives

$$\theta = \int \frac{dU}{\sqrt{h + \frac{Vl-Dm^2}{Bl^4}U^2 - \frac{A}{3Bl^2}U^3}}. \tag{6.42}$$

Finally, (6.42) expresses the parametric representation of the exact solutions. The level curves mentioned by $\mathcal{H}(U, z) = h$, for $h = 0$, signifies a homoclinic orbit (Figure 6.2(a)) Eq.(6.42) becomes

$$\sqrt{\frac{A}{3Bl^2}}\theta = \int \frac{dU}{U\sqrt{\frac{3(Vl-Dm^2)}{Al^2} - U}}, \tag{6.43}$$

which gives the solitary solution as,

$$\phi(\xi, \eta, \tau) = \phi_0 \, \mathrm{sech}^2\left(\frac{l\xi + m\eta - V\tau}{w}\right), \tag{6.44}$$

with

$$w^2 = \frac{3Bl^2}{A\phi_0}, \quad V = \frac{Al\phi_0}{3} + \frac{m^2 D}{l}, \tag{6.45}$$

where A, B, D are defined in (6.34) and ϕ_0 is considered as the initial amplitude. The solution (6.44) is presented in a particular form for future purpose,

$$\phi(\xi, \eta, \tau) = \phi_{amp} \, \mathrm{sech}^2\left(\frac{l\xi + m\eta - V\tau}{w}\right), \tag{6.46}$$

where

$$\phi_{amp} = \frac{3(Vl - m^2 D)}{Al^2}, \; w = 2\sqrt{\frac{Bl^4}{(Vl - m^2 D)}}. \tag{6.47}$$

ϕ_{amp} and w present the amplitude and width of the soliton and l, m are the constant such that, $l^2 + m^2 = 1$.

6.5.2 Periodic wave solutions of KP equation

In order to acquire periodic wave solution of KP equation (6.35), we consider a particular type of transformation (6.36) which brings,

$$\frac{1}{2}\left(\frac{dU}{d\theta}\right)^2 + \frac{A}{6Bl^2}U^3 - \frac{Vl - Dm^2}{2Bl^4}U^2 - \frac{\Gamma}{2Bl^4} = 0, \tag{6.48}$$

where Γ is an integrating constant. If $\Gamma = \frac{2(Dm^2-Vl)^3}{3A^2l^4}$, the expression (6.48) is represented below for $A > 0$ and $A < 0$ respectively as,

$$\left(\frac{dU}{d\theta}\right)^2 = \frac{A}{3Bl^2}[(e_1 - U)(U - e_2)(U - e_3)], \tag{6.49}$$

$$\left(\frac{dU}{d\theta}\right)^2 = (-\frac{A}{3Bl^2})[(U - e_1)(e_2 - U)(e_3 - U)], \tag{6.50}$$

where

$$e_1 = (1+\sqrt{3})\frac{Vl - Dm^2}{Al^2},\ e_2 = \frac{Vl - Dm^2}{Al^2},\ e_3 = (1-\sqrt{3})\frac{Vl - Dm^2}{Al^2}. \tag{6.51}$$

In the present plasma model (6.48), B is always positive, and thus, in response to A's positivity or negativity, the term $\frac{A}{3Bl^2}$ becomes positive or negative. For consideration of positive values of $\frac{A}{3Bl^2}$, the real numbers e_1, e_2, e_3 are chosen as $e_1 > e_2 > e_3$ and $e_1 > U \geqslant e_2$. On the contrary, the real numbers e_1, e_2, e_3 are ordered as $e_1 < e_2 < e_3$ and $e_1 < U \leqslant e_2$ when $\frac{A}{3Bl^2}$ is negative. Thus, we obtain the periodic solution in the following form as,

$$\phi(\xi, \eta, \tau) = e_1 - (e_1 - e_2)sn^2\left(\frac{\sqrt{\frac{A}{3Bl^2}(e_1 - e_3)}}{2}(l\xi + m\eta - V\tau), \sqrt{\frac{e_1 - e_2}{e_1 - e_3}}\right), \tag{6.52}$$

where sn is the Jacobi elliptic function, and the terms $\frac{Dm^2}{l} + \frac{Al}{3}(e_1 + e_2 + e_3)$, $e_1 - e_2$ $(= \sqrt{3}\frac{Vl-Dm^2}{Al^2})$and $4\sqrt{\frac{3Bl^2}{A(e_1-e_3)}}S(\sqrt{\frac{e_1-e_2}{e_1-e_3}})$ respectively represent velocity, amplitude and wave length of the periodic waves. Here, the complete elliptic integral of first kind is denoted by $S(\sqrt{\frac{e_1-e_2}{e_1-e_3}})$ [226, 227, 198].

For a visual presentation, some figures are drawn in Figure 6.3. It is important to mention here that especially, two types of periodic wave profiles are found as a consequence of negative and positive values of nonlinear coefficient A. Clearly, positive A provides a positive potential periodic structure, whereas negative potential periodic structure comes into existence for negative values of A. In a three dimensional view, the positive potential and negative potential periodic structures are presented in Figure 6.3(a) and Figure 6.3(b) respectively. We consider both (positive and negative potential wave) structures and numerically observe the impacts of some parameters such as, β_1, β_2 and δ_1

in Figure 6.3(c)-Figure 6.3(e) (positive potential wave structure) and Figure 6.3(f)-Figure 6.3(h) (negative potential wave structure). Figure 6.3(c) and Figure 6.3(f) exhibits the enhancing effect of β_1. Enhancing β_1 means not only the rising of temperature of low-temperature ions but also the falling of temperature of high-temperature ions. Thus, it may be concluded from Figure 6.3(c) and Figure 6.3(f) that the increase in a temperature difference of high and low-temperature ions causes enhancement (diminishment) of the amplitude of positive (negative) potential periodic structure. Figure 6.3(d) and Figure 6.3(g) respectively show the impact of the parameter β_2 in the positive and negative potential wave structure of periodic wave. Actually, the rising temperature of lower temperature ions in comparison to that of electrons causes the enhancement of β_2. It is found from Figure 6.3(d) that the amplitude of positive potential periodic structure significantly improves because of the increase of β_2, whereas in contrary Figure 6.3(g) exhibits the diminish of the amplitude of negative potential wave structure. The parameter δ_1 represents the ratio of equilibrium values of the number densities of low-temperature ions to the unperturbed number of electrons, and it is deduced from Figure 6.3(e) and Figure 6.3(h) that with an increase in δ_1 causes for enhancement (impairment) of the amplitude of positive (negative) potential periodic structure. On the whole, the rising of temperature, as well as the mean concentration of low-temperature ions, leads to an enhancement (diminishment) in the periodic amplitude of positive (negative) potential periodic structure. Increasing $\beta_1, \beta_2, \delta_1$ means decreasing A, and A is inversely proportional to the amplitude of the periodic wave and that is why positive potential structure increases on the other hand negative potential structure decreases.

6.6 Analysis of unperturbed dynamics and phase portraits for the KPb equation

The planar dynamical system of Eq.(6.38) takes the following form as

$$\begin{aligned} \frac{dU}{d\theta} &= z \\ \frac{dz}{d\theta} &= \frac{Vl - Dm^2}{Bl^4}U - \frac{A}{2Bl^2}U^2 - \frac{Cz}{Bl}. \end{aligned} \tag{6.53}$$

Now, we study the characteristic of traveling wave solutions by analyzing the trajectory in a phase paths of the dynamic system (6.53).

Set 1.(When $C \approx 0$ that is $\zeta_0 = 0.01$) (Figure 6.2(c))

For $l = 0.5$, $m = 0.5$, $V = 0.1$, $\gamma_1 = 0.2$, $\beta_2 = 0.1$, $\beta_1 = 0.1$, $\delta_2 = 4$, $\delta_1 = 2$, $\gamma_2 = 0.2$, the equilibrium point $U_0(0,0)$ becomes saddle because at that point $J_d < 0$, $T_{r2} - 4J_d > 0$, and the equilibrium point $U_1(\frac{2(Vl-Dm^2)}{Al^2}, 0)$ becomes centre because at that point $J_d > 0$, $T_{r1} = 0$. Thus at the point $(0,0)$ we get a homoclinic orbits.

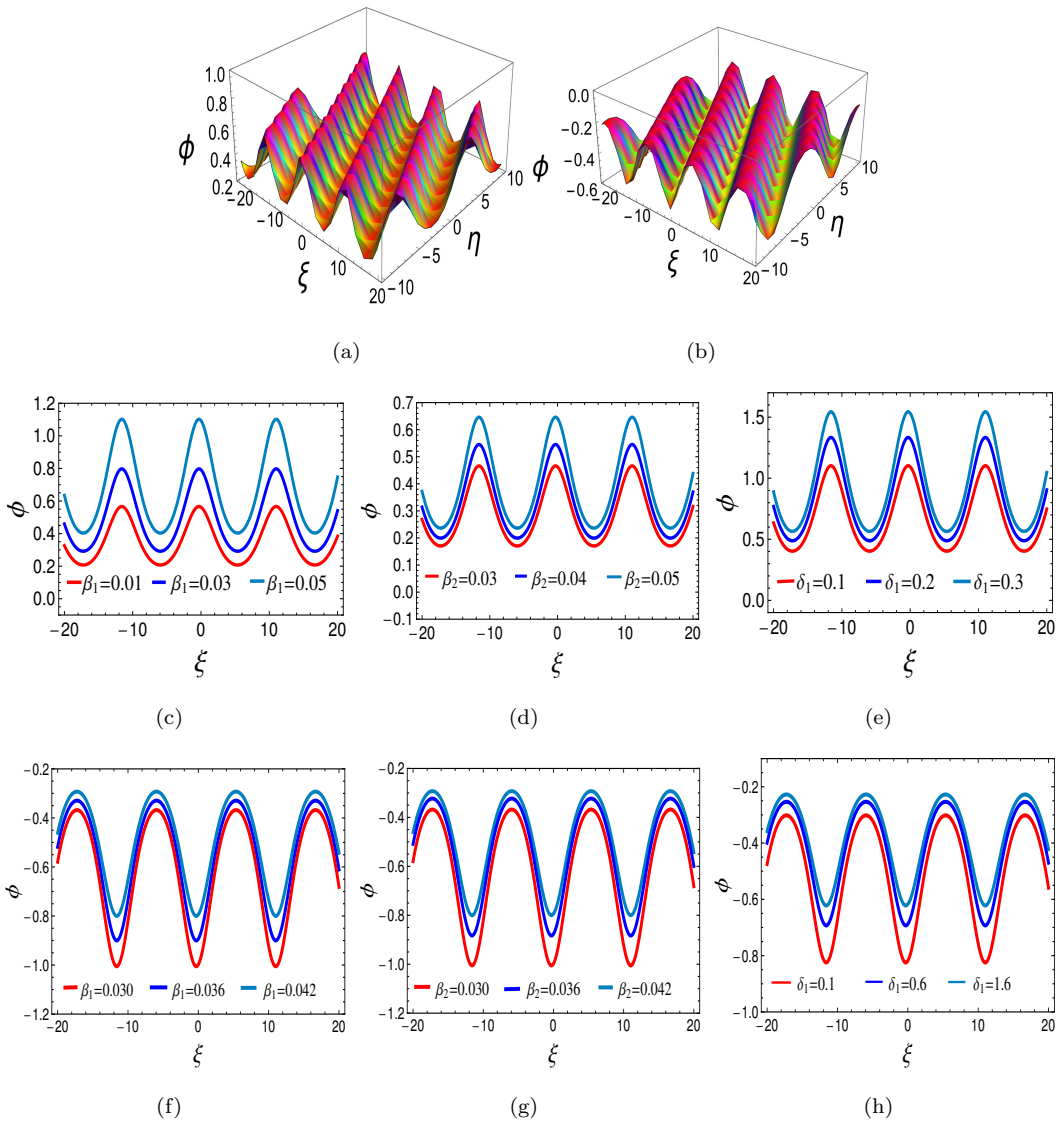

Figure 6.3: 3D and 2D Profiles of Sol.(6.52), (a) for $\gamma_1 = 0.05$, $\delta_1 = 0.2$, $\delta_2 = 3.5$, $\beta_1 = 0.04$, $\beta_2 = 0.03$, $\gamma_2 = 0.05$, $\tau = 1$, $\mathfrak{l} = \frac{1}{\sqrt{2}}$, $\mathfrak{m} = \frac{1}{\sqrt{2}}$, $V = 0.5$, (b) for $\gamma_1 = 0.01$, $\delta_1 = 5$, $\delta_2 = 1$, $\beta_1 = 0.04$, $\beta_2 = 0.1$, $\gamma_2 = 0.01$, $\tau = 1$, $\mathfrak{l} = \frac{1}{\sqrt{2}}$, $\mathfrak{m} = \frac{1}{\sqrt{2}}$, $V = 0.5$, (c) for $\gamma_1 = 0.05$, $\delta_1 = 0.2$, $\delta_2 = 3.5$, $\beta_2 = 0.03$, $\gamma_2 = 0.05$, $\tau = 1$, $\mathfrak{l} = \frac{1}{\sqrt{2}}$, $\mathfrak{m} = \frac{1}{\sqrt{2}}$, $V = 0.5$, (d) for $\gamma_1 = 0.05$, $\delta_1 = 0.2$, $\delta_2 = 3.5$, $\beta_1 = 0.04$, $\beta_2 = 0.03$, $\gamma_2 = 0.05$, $\tau = 1$, $\mathfrak{l} = \frac{1}{\sqrt{2}}$, $\mathfrak{m} = \frac{1}{\sqrt{2}}$, $V = 0.5$ and (e) for $\gamma_1 = 0.05$, $\delta_1 = 0.2$, $\delta_2 = 3.5$, $\beta_1 = 0.04$, $\beta_2 = 0.03$, $\gamma_2 = 0.05$, $\tau = 1$, $\mathfrak{l} = \frac{1}{\sqrt{2}}$, $\mathfrak{m} = \frac{1}{\sqrt{2}}$, $V = 0.5$; (f) for $\gamma_1 = 0.05$, $\delta_1 = 0.1$, $\delta_2 = 1.5$, $\beta_2 = 0.03$, $\gamma_2 = 0.05$, $\tau = 1$, $\mathfrak{l} = \frac{1}{\sqrt{2}}$, $\mathfrak{m} = \frac{1}{\sqrt{2}}$, $V = 0.5$, (g) $\gamma_1 = 0.05$, $\delta_1 = 0.1$, $\delta_2 = 1.5$, $\beta_1 = 0.042$, $\gamma_2 = 0.05$, $\tau = 1$, $\mathfrak{l} = \frac{1}{\sqrt{2}}$, $\mathfrak{m} = \frac{1}{\sqrt{2}}$, $V = 0.5$, (h) for $\gamma_1 = 0.05$, $\delta_2 = 1.5$, $\beta_2 = 0.03$, $\beta_1 = 0.04$, $\gamma_2 = 0.05$, $\tau = 1$, $\mathfrak{l} = \frac{1}{\sqrt{2}}$, $\mathfrak{m} = \frac{1}{\sqrt{2}}$, $V = 0.5$,

.

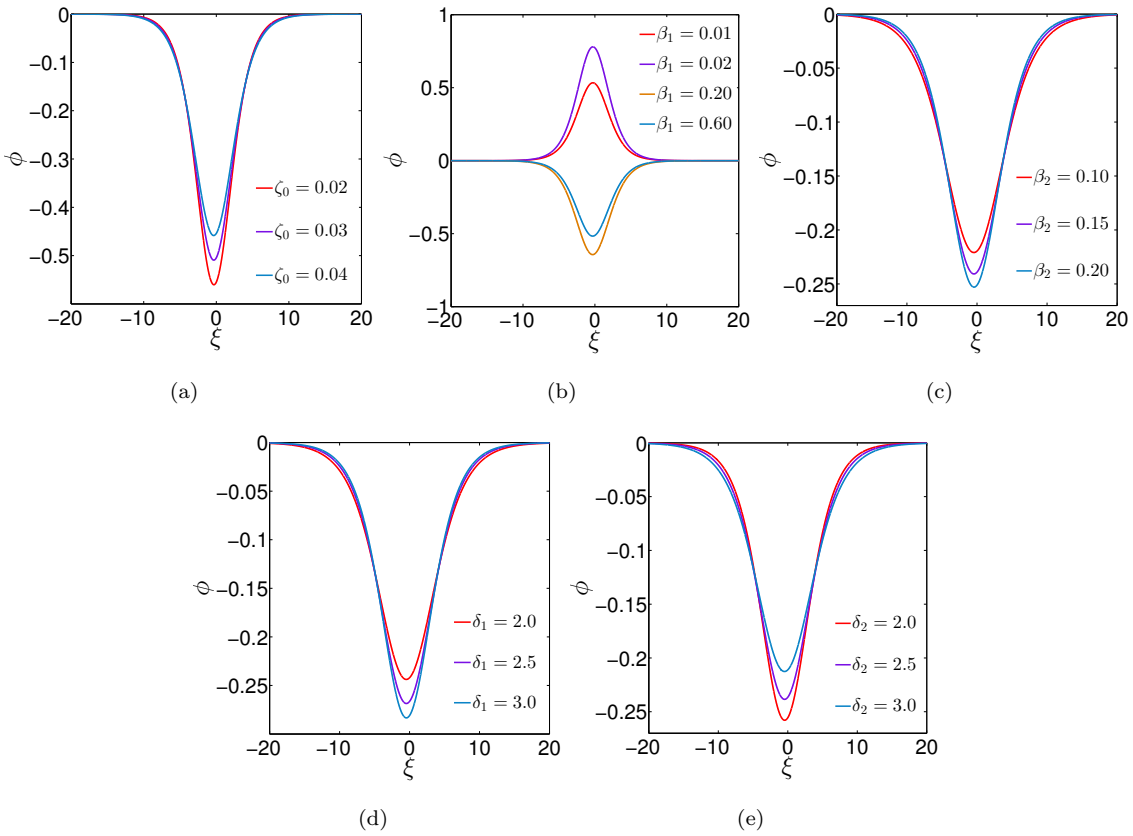

(a) (b) (c)

(d) (e)

Figure 6.4: 2D Profiles of Sol.(6.63) when $\tau = 1$, $\mathfrak{l} = \frac{1}{\sqrt{2}}$, $\mathfrak{m} = \frac{1}{\sqrt{2}}$, $V_0 = 0.5$ and (a) $\gamma_1 = 0.01$, $\beta_2 = 0.05$, $\delta_1 = 1$, $\delta_2 = 2$, $\beta_1 = 0.1$, $\gamma_2 = 0.1$; (b) $\zeta_0 = 0.01$, $\gamma_1 = 0.01$, $\beta_2 = 0.02$, $\delta_1 = 0.4$, $\delta_2 = 3.5$, $\gamma_2 = 0.02$, $\beta_2 = 0.01$; (c) $\zeta_0 = 0.07$, $\gamma_1 = 0.1$, $\delta_1 = 1$, $\delta_2 = 2$, $\beta_1 = 0.1$, $\gamma_2 = 0.01$; (d) $\zeta_0 = 0.07$, $\gamma_1 = 0.1$, $\beta_2 = 0.05$, $\delta_1 = 1$, $\delta_2 = 2$, $\beta_1 = 0.1$, $\gamma_2 = 0.01$; (e) $\zeta_0 = 0.07$, $\gamma_1 = 0.1$, $\beta_2 = 0.05$, $\delta_1 = 1$, $\beta_1 = 0.1$, $\gamma_2 = 0.01$

.

Set 2. (When $C \neq 0$ that is $\zeta_0 \neq 0$) (Figure 6.2(d))

For $\mathfrak{l} = 0.5$, $\mathfrak{m} = 0.5$, $V = 0.1$, $\gamma_1 = 0.2$, $\beta_2 = 0.1$, $\beta_1 = 0.1$, $\delta_2 = 4$, $\delta_1 = 2$, $\gamma_2 = 0.2$, the point $U_0(0, 0)$ becomes saddle because at that point $J_d < 0$, $T_{r2} - 4J_d > 0$, and the point $U_1(\frac{2(V\mathfrak{l} - D\mathfrak{m}^2)}{A\mathfrak{l}^2}, 0)$ becomes stable spiral because at that point $J_d > 0$, $T_{r2} - 4J_d < 0$. From the analysis of the system it is confirmed that the kink or anti-kink solution of the KPb equation exist.

6.7 Solutions of the (2+1)-dimensional KPb equation

We determine an approximate analytical solution for the KP-Burgers equation.

6.7.1 Analytical solitary solution for KPb equation

It is assumed that the system remains conserved for negligible values of ζ_0, and thus the KPb Eq.(6.33) is approximated as Eq.(6.35) that gives the solitary wave solution (6.46). Taking the solution (6.46) as a seed solution, the solution for the equation (6.33) can be expressed as

$$\phi(\xi,\eta,\tau) = \phi_{amp}\,\mathrm{sech}^2\left(\frac{l\xi + m\eta - V(\tau)\tau}{w}\right), \tag{6.54}$$

where

$$\phi_{amp} = \frac{3(V(\tau)l - m^2D)}{Al^2},\ w = 2\sqrt{\frac{Bl^4}{(V(\tau)l - m^2D)}}. \tag{6.55}$$

We assume that the solution of KPb equation also follows the solitary pattern like KP equation but with a small deviation due to the presence of small burgers term. For this reason amplitude, width and velocity have a small dependency on τ. Now conserved quantity for the KP equation is given by

$$I = \int_{-\infty}^{\infty} \phi^2 d\xi, \tag{6.56}$$

here I presents the soliton energy. Thus, using solution (6.54), from the energy conservation relation we find

$$I = \frac{24\sqrt{B}}{Al}(V(\tau)l - m^2D)^{3/2}. \tag{6.57}$$

Differentiating Eq.(6.57) with respect to τ, we obtain

$$\frac{dI}{d\tau} = \frac{36\sqrt{B}}{A}(V(\tau)l - m^2D)^{1/2}\frac{d}{d\tau}(V(\tau)). \tag{6.58}$$

Now, differentiating Eq.(6.56) with respect to τ and utilizing Eq.(6.14) and Eq.(6.54)-Eq.(6.55) we get,

$$\frac{dI}{d\tau} = -2D\int_{-\infty}^{\infty}\phi\left(\int\frac{\partial^2\phi}{\partial\eta^2}d\xi\right)d\xi + \frac{48C}{5A^2l^5\sqrt{B}}(V(\tau)l - m^2D)^{5/2}. \tag{6.59}$$

Now

$$\int_{-\infty}^{\infty}\phi\left(\int\frac{\partial^2\phi}{\partial\eta^2}d\xi\right)d\xi = \frac{8m^2\phi_{amp}^2}{l^2}G(\eta,\tau), \tag{6.60}$$

where $G(\eta,\tau)$ is an arbitrary function of η and τ. Taking $G(\eta,\tau) = 0$, we get from Eq.(6.59)

$$\frac{dI}{d\tau} = \frac{48C}{5A^2l^5\sqrt{B}}(V(\tau)l - m^2D)^{5/2}. \tag{6.61}$$

Combining the equations (6.58) and (6.61) we find

$$V(\tau) = \frac{4C\tau}{15Al^4B} + V_0, \tag{6.62}$$

here, $V(\tau)$ is the time dependent velocity of DAW and V_0 is the velocity at $\tau = 0$. Thus, the solution of the KPb equation is

$$\phi(\xi, \eta, \tau) = \phi_{amp}(\tau)\, sech^2\left(\frac{l\xi + m\eta - V(\tau)\tau}{w(\tau)}\right), \tag{6.63}$$

where the amplitude, width of DAW are given by

$$\phi_{amp}(\tau) = \frac{3(V(\tau)l - m^2D)}{Al^2},\ w(\tau) = 2\sqrt{\frac{Bl^4}{(V(\tau)l - m^2D)}}, \tag{6.64}$$

and $V(\tau)$ is given by Eq.(6.62).

6.7.2 Analytical shock solution for KPb equation

Waves carry energy and can propagate through media, but shock waves are characterized by abrupt, nearly discontinuous changes in pressure, temperature, and density. In contrast to solitons, shock waves dissipate relatively quickly with distance. As shock waves cause abrupt changes in the properties of the medium, they can also be viewed as phase transitions. For shock type wave solutions of KPb equation we used (G'/G)-expansion method.

6.7.2.1 Application of the (G'/G)-expansion method on KPb equation

In this sub-section (G'/G)-expansion method is employed to construct a set of exact analytic solution of KPb equation. Let us take the KPb equation in the present form described in Eq. (6.33). We consider the transformation $U(\theta) = \phi(\xi, \eta, \tau)$, $\theta = l\xi + m\eta - V\tau$, where V designates the speed of wave. Finally, we get transformed ODE from (6.33) as,

$$(-Vl + Dm^2)U + \frac{Al^2}{2}U^2 + Bl^4U'' + Cl^3U' = 0. \tag{6.65}$$

Now, we make an ansatz (1.47) as a solution of Eq.(6.65). Balancing the coefficient of the terms U'' and U^2 in Eq. (6.65) we get $N = 2$. Thus, the required solution of Eq. (6.65) can be express as

$$U(\theta) = P_0 + P_1\left(\frac{G'}{G}\right) + P_2\left(\frac{G'}{G}\right)^2. \tag{6.66}$$

Substitute Eq. (6.66) into Eq. (6.65), the left hand side of Eq. (6.65) is transformed into a polynomial $\left(\frac{G'}{G}\right)^j$ $(j = 0, 1, \cdots, 4)$ and setting the coefficients of $\left(\frac{G'}{G}\right)^j$ $(j = 0, 1, \cdots, 4)$ to zero, we

have a set of algebraic equations for P_0, P_1, λ, μ and V as,

$$\left(\frac{G'}{G}\right)^0 : \frac{1}{2}Al^2P_0^2 + Bl^4P_1\lambda\mu + 2Bl^4P_2\mu^2 - Cl^3P_1\mu + Dm^2P_0 - VlP_0 = 0, \tag{6.67}$$

$$\left(\frac{G'}{G}\right)^1 : Al^2P_0P_1 + Bl^4P_1\lambda^2 + 6Bl^4P_2\lambda\mu + 2Bl^4P_1\mu - Cl^3P_1\lambda - 2Cl^3P_2\mu + Dm^2P_1 - VlP_1 = 0, \tag{6.68}$$

$$\left(\frac{G'}{G}\right)^2 : \frac{1}{2}Al^2P_1^2 + Al^2P_0P_2 + 3Bl^4P_1\lambda + 8Bl^3P_2\mu + 4Bl^4P_2\lambda^2 - Cl^3P_1 - 2Cl^3P_2\lambda + Dm^2P_2 - VlP_2 = 0, \tag{6.69}$$

$$\left(\frac{G'}{G}\right)^3 : Al^2P_1P_2 + 2Bl^4P_1 + 10Bl^4P_2\lambda - 2Cl^3P_2 = 0, \tag{6.70}$$

$$\left(\frac{G'}{G}\right)^4 : \frac{1}{2}Al^2P_2^2 + 6Bl^4P_2 = 0, \tag{6.71}$$

Solving these equations by employing the symbolic computation system Maple, we have two sets of solutions:

$$P_0 = -\frac{AP_1^2}{48Bl^2}, \quad P_1 = P_1, \quad P_2 = -\frac{12Bl^2}{A}, \quad \lambda = -\frac{5AP_1 - 12Cl}{60Bl^2}, \quad \mu = \frac{AP_1(5AP_1 - 24Cl)}{2880B^2l^4}, \quad c = \frac{25BDm^2 - 6C^2l^2}{25B}. \tag{6.72}$$

Substituting the values from Eq. (6.72) into Eq. (6.66) and utilizing the solutions of Eq. (1.48) in different cases, different types of exact analytical solution of Eq. (6.65) can be obtained. When $\Delta = \lambda^2 - 4\mu = \left(\frac{5AP_1-12Cl}{60Bl^2}\right)^2 - \frac{AP_1(5AP_1-24Cl)}{720B^2l^4} > 0$, the hyperbolic solution of Eq. (6.65) is as follows:

$$\phi(\xi,\eta,\tau) = -\frac{AP_1^2}{48Bl^2} + P_1\frac{\sqrt{\Delta}}{2}\left(\frac{r_1\cosh(\frac{\sqrt{\Delta}}{2}\theta) + r_2\sinh(\frac{\sqrt{\Delta}}{2}\theta)}{r_1\sinh(\frac{\sqrt{\Delta}}{2}\theta) + r_2\cosh(\frac{\sqrt{\Delta}}{2}\theta)} + \frac{5AP_1 - 12Cl}{120Bl^2}\right) - \frac{12Bl^2}{A}\left(\frac{\sqrt{\Delta}}{2}\left(\frac{r_1\cosh(\frac{\sqrt{\Delta}}{2}\theta) + r_2\sinh(\frac{\sqrt{\Delta}}{2}\theta)}{r_1\sinh(\frac{\sqrt{\Delta}}{2}\theta) + r_2\cosh(\frac{\sqrt{\Delta}}{2}\theta)} + \frac{5AP_1 - 12Cl}{120Bl^2}\right)\right)^2, \tag{6.73}$$

where $\theta = l\xi + m\eta - (\frac{25BDm^2-6C^2l^2}{25B})\tau$, r_1 and r_2 are arbitrary constants. This result can further be written in some more simplified forms depending upon the conditions on the ratio of r_1 and r_2 as

$$\begin{aligned}\phi(\xi,\eta,\tau) = &-\frac{AP_1^2}{48Bl^2} + P_1\frac{\sqrt{\Delta}}{2}\left(\tanh\left(\frac{\sqrt{\Delta}}{2}\theta+\eta_0\right)+\frac{5AP_1-12Cl}{120Bl^2}\right)\\ &-\frac{12Bl^2}{A}\left(\frac{\sqrt{\Delta}}{2}\left(\tanh\left(\frac{\sqrt{\Delta}}{2}\theta+\eta_0\right)+\frac{5AP_1-12Cl}{120Bl^2}\right)\right)^2,\\ \text{with}\ \ &\lambda^2-4\mu>0,\quad \tanh(\eta_0)=\frac{r_2}{r_1},\quad r_1\neq 0,\quad \left|\frac{r_2}{r_1}\right|<1\\ \text{and}\ \ &\theta = l\xi+m\eta-\left(\frac{25BDm^2-6C^2l^2}{25B}\right)\tau.\end{aligned} \tag{6.74}$$

6.7.3 Solutions of the KPb equation by F-function method

Here we employed indirect F-function method [142] to find jacobi elliptic function solution of KPb equation. We assume that the solutions of Eq. (6.33) can be taken as

$$U(\xi,\eta,\tau) = \lambda(\tau)F^s(\zeta),\quad \zeta = l\xi+m\eta-V(\tau)\tau, \tag{6.75}$$

where parameter functions λ, V and the exponent s are to be determined. Also the function F satisfy the following differential equation

$$F'^2(\zeta) = PF^4(\zeta)+QF^2(\zeta)+R. \tag{6.76}$$

Substituting Eqs. (6.75)-(6.76) into (6.33) and equating the exponents $2s-1$ and $s+1$ in the obtained equation gives

$$s = 2. \tag{6.77}$$

Then replacing (6.77) in the remaining equation and equating the coefficients of F^s, $F^{2s-1}F'$, $F^{s-1}F'$, and $F^{s+1}F'$ equal to zero, we get:

$$\lambda'(\tau)+4Cl^3Q\lambda(\tau) = 0, \tag{6.78}$$

$$\frac{d}{d\tau}(\tau V(\tau)) = 4Bl^4Q+Dm^2, \tag{6.79}$$

$$16PBl^2+A\lambda(\tau) = 0. \tag{6.80}$$

From Eq.(6.78) and Eq.(6.79) gives

$$\lambda(\tau) = \lambda_0 e^{-4Cl^3Q\tau}, \tag{6.81}$$

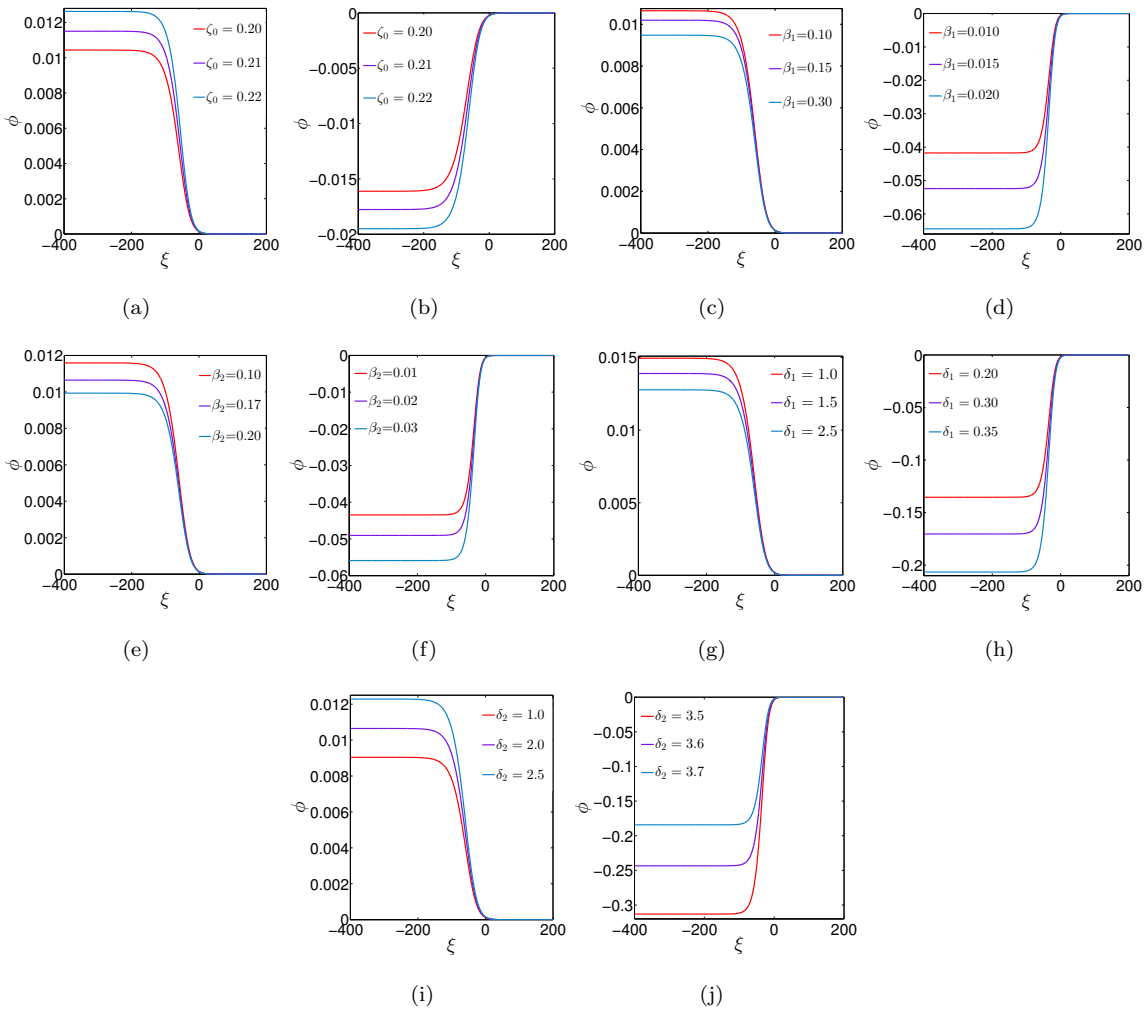

Figure 6.5: 2D Profiles of Shock Sol.(6.74), when $\tau = 1$, $\eta = 1$, $\eta_0 = 1$, $P_1 = 0.5$, $\mathfrak{l} = \frac{1}{\sqrt{2}}$, $\mathfrak{m} = \frac{1}{\sqrt{2}}$ and (a) $\delta_1 = 1$, $\delta_2 = 2$, $\beta_1 = 0.05$, $\gamma_1 = 0.1$, $\beta_2 = 0.1$, $\gamma_2 = 0.05$; (b) $\delta_1 = 0.4$, $\delta_2 = 3.5$, $\beta_1 = 0.05$, $\gamma_1 = 0.01$, $\beta_2 = 0.04$, $\gamma_2 = 0.1$; (c) $\zeta_0 = 0.2$, $\delta_1 = 1$, $\delta_2 = 2$, $\gamma_1 = 0.1$, $\beta_2 = 0.1$, $\gamma_2 = 0.05$; (d) $\delta_1 = 0.4$, $\delta_2 = 3.5$, $\zeta_0 = 0.4$, $\gamma_1 = 0.01$, $\zeta_0 = 0.4$, $\gamma_2 = 0.1$; (e) $\zeta_0 = 0.2$, $\delta_1 = 1$, $\delta_2 = 2$, $\beta_1 = 0.05$, $\gamma_1 = 0.1$, $\gamma_2 = 0.05$; (f) $\delta_1 = 0.4$, $\zeta_0 = 0.4$, $\beta_1 = 0.05$, $\gamma_1 = 0.01$, $\beta_2 = 0.04$, $\gamma_2 = 0.1$; (g) $\zeta_0 = 0.2$, $\delta_2 = 3$, $\beta_1 = 0.1$, $\gamma_1 = 0.1$, $\beta_2 = 0.05$, $\gamma_2 = 0.05$; (h) $\delta_1 = 0.4$, $\zeta_0 = 0.4$, $\beta_1 = 0.05$, $\gamma_1 = 0.01$, $\beta_2 = 0.04$, $\gamma_2 = 0.1$; (i) $\zeta_0 = 0.2$, $\delta_1 = 1$, $\beta_1 = 0.05$, $\gamma_1 = 0.1$, $\beta_2 = 0.1$, $\gamma_2 = 0.05$; (j) $\delta_1 = 0.4$, $\zeta_0 = 0.4$, $\beta_1 = 0.05$, $\gamma_1 = 0.01$, $\beta_2 = 0.04$, $\gamma_2 = 0.1$

.

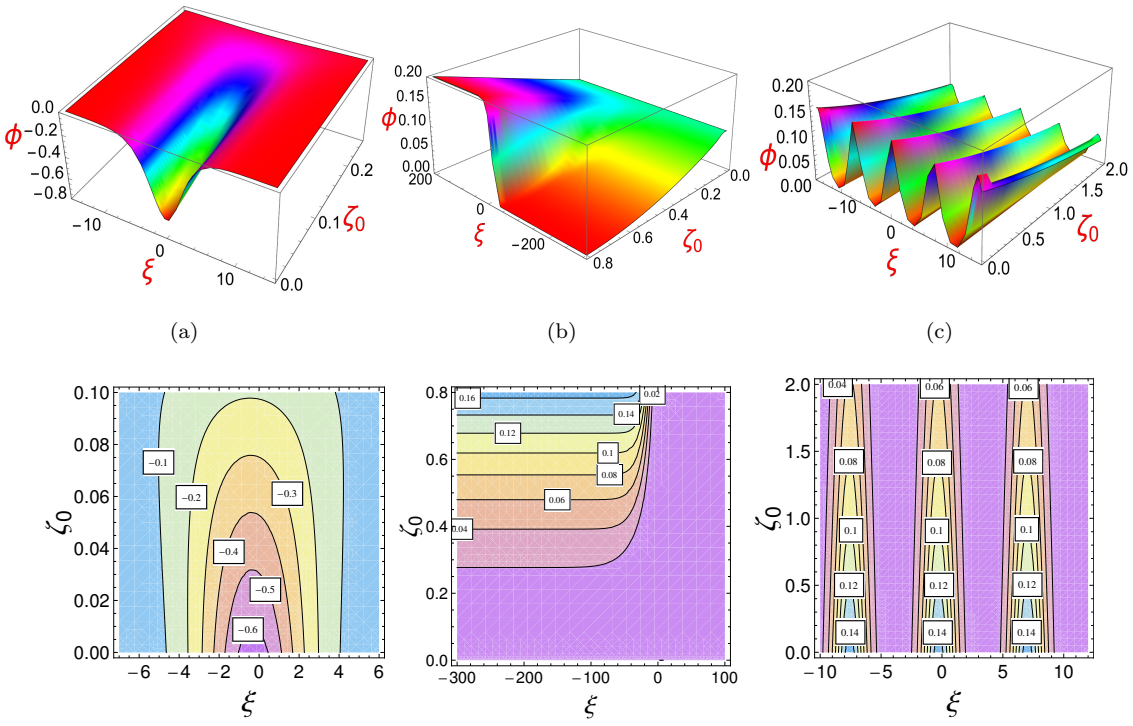

Figure 6.6: (a) 3D plot of Sol.(6.63), when $\gamma_1 = 0.01$, $\beta_2 = 0.05$, $\delta_1 = 1$, $\delta_2 = 2$, $V_0 = 0.5$, $\beta_1 = 0.1$, $\gamma_2 = 0.1$, $\tau = 1$, $l = \frac{1}{\sqrt{2}}$, $m = \frac{1}{\sqrt{2}}$; (b) 3D plot of Sol.(6.74), for $\delta_1 = 1$, $\delta_2 = 2$, $\beta_1 = 0.05$, $\gamma_1 = 0.1$, $\beta_2 = 0.1$, $\gamma_2 = 0.05$, $\tau = 1$, $\eta = 1$, $\eta_0 = 1$, $P_1 = 1$, $l = \frac{1}{\sqrt{2}}$, $m = \frac{1}{\sqrt{2}}$; (c) 3D plot of Sol.(6.89) when $\gamma_1 = 0.01$, $\beta_2 = 0.05$, $\delta_1 = 1$, $\delta_2 = 2$, $V_0 = 0.5$, $\beta_1 = 0.1$, $\gamma_2 = 0.1$, $\tau = 1$, $l = \frac{1}{\sqrt{2}}$, $m = \frac{1}{\sqrt{2}}$, $\lambda_0 = 0.15, m_1 = 0.9$; (d), (e) and (f) are Contour plots of the corresponding Figure 6.6(a), Figure 6.6(b) and Figure 6.6(c)

.

Table 6.1: Jacobi elliptic functions.

P	Q	R	F'^2=PF^4+QF^2+R	F
m_1^2	-(1+m_1^2)	1	F'^2=(1-F^2)(1-$m_1^2F^2$)	snζ,sdζ=cnζ/dnζ
-m_1^2	(2m_1^2-1)	1-m_1^2	F'^2=(1-F^2)($m_1^2F^2$+1-m_1^2)	cnζ
-1	(2-m_1^2)	m_1^2-1	F'^2=(1-F^2)(m_1^2+F^2-1)	dnζ
1	-(1+m_1^2)	m_1^2	F'^2=(1-F^2)(m_1^2-F^2)	nsζ=(snζ)$^{-1}$,dcζ=dnζ/cnζ
1-m_1^2	2m_1^2-1	-m_1^2	F'^2=(1-F^2)[(m_1^2-1)F^2-m_1^2]	ncζ=cn$^{-1}\zeta$
m_1^2-1	2-m_1^2	-1	F'^2=(1-F^2)[(1-m_1^2)F^2-1]	ndζ=dn$^{-1}\zeta$

and

$$V(\tau) = 4Bl^4Q + Dm^2, \tag{6.82}$$

where λ_0 is the initial amplitude of the soliton and considererd as the initial velocity to be zero. From Eq.(6.80) one gets an important constraint equation for the solution exist as

$$\frac{B}{A} = -\frac{\lambda}{16Pl^2}. \tag{6.83}$$

Thus, the solutions of the equation with time-dependent coefficients are given by

$$U(\zeta) = \lambda(\tau)F^2(\zeta). \tag{6.84}$$

The Relationship between the values of P, Q, R and $F(\zeta)$ in (6.76) is given in table 1.

From Table 1, if we select

$$\begin{aligned} F(\zeta) &= sn(\zeta, m_1), \quad P = m_1^2, \\ Q &= -(1 + m_1^2), \quad R = 1, \end{aligned} \tag{6.85}$$

then by choosing the relations (6.81)-(6.83), in Eq.(6.84), we gain the exact solutions to the KPb equation (6.33) is given by:

$$\phi(\xi, \eta, \tau) = \lambda_0 e^{4Cl^3(1+m_1^2)\tau} sn^2(\zeta, m_1), \tag{6.86}$$

where

$$\zeta = l\xi + m\eta + \left(4Bl^4(1 + m_1^2) - Dm^2\right)\tau, \tag{6.87}$$

From Table 1, if we select

$$\begin{aligned} F(\zeta) &= cn(\zeta, m_1), \quad P = -m_1^2, \\ Q &= (2m_1^2 - 1), \quad R = 1 - m_1^2, \end{aligned} \tag{6.88}$$

then by choosing relations (6.81)-(6.83), in Eq.(6.84), we achieve the exact solution to the KPb equation as

$$\phi(\xi,\eta,\tau) = \lambda_0 e^{-4Cl^3(2m_1^2-1)\tau} cn^2(\zeta, m_1), \tag{6.89}$$

where

$$\zeta = l\xi + m\eta - \left(4Bl^4(2m_1^2-1), +Dm^2\right)\tau, \tag{6.90}$$

From Table 1, if we select

$$\begin{aligned} F(\zeta) &= dn(\zeta, m_1), \quad P = -1, \\ Q &= (2-m_1^2), \quad R = m_1^2 - 1, \end{aligned} \tag{6.91}$$

then by choosing relations (6.81)-(6.83), in Eq.(6.84), we gain the exact solution of Eq.(6.33) as

$$\phi(\xi,\eta,\tau) = \lambda_0 e^{-4Cl^3(2-m_1^2)\tau} dn^2(\zeta, m_1), \tag{6.92}$$

where

$$\zeta = l\xi + m\eta - \left(4Bl^4(2-m_1^2) + Dm^2\right)\tau, \tag{6.93}$$

ans l, m are constant parameters in the above mentioned solutions.

6.8 Parametric discussion

Now, we discuss the impact of different physical parameters including dust kinematic viscosity (ζ_0), the ratio of low-temperature ions and high-temperature ions (β_1), the ratio of low-temperature ions to the temperature of electrons (β_2), the ratio of equilibrium values of the number densities of low-temperature ions to the unperturbed number of electrons (δ_1), the ratio of equilibrium values of the number densities of high-temperature ions to the unperturbed number densities of electrons (δ_2) on the solution structure. Generally, the nonlinear coefficient of the evolution equation may vanish for some specific group values of the parameters. In these cases, we can find the solitons with an infinite amplitude which is totally unrealistic. To overcome these hurdles some graphs are drawn in Figure 6.1(a)-Figure 6.1(d) and a suitable parametric domain is chosen accordingly to obtain finite amplitude solitary, shock, and periodic solution.

To shows the effect of different parameters, Figure 6.4 and Figure 6.5 are drawn with the help of solitary wave solution (6.63) and shock wave solution (6.74) respectively. Figure 6.4(a) is plotted for distinct values of the dust viscosity parameter ζ_0. It is cleared from Figure 6.4(a) that the amplitude of the wave substantially hangs on dust kinematic viscosity. From the graph, it can be concluded that the amplitudes of the negative potential solitary structure decrease abruptly with the

enhancement in the dust kinematic viscosity parameter ζ_0. Figure 6.4(b) is depicted for presenting the effect of the parameter β_1 on the solitary wave profile. It is important to mention here that the positive potential, as well as negative potential wave structures, are formed due to the variations in β_1. Figure 6.4(b) shows that positive potential wave structures formed if the temperature of higher temperature ions is sufficiently large than that of lower temperature ions. On the contrary, the same type of structure may observe if the temperature of lower-temperature ions is very small than that of another one. Figure 6.4(c) is depicted respectively for presenting the effect of the parameters β_2 on the solitary wave profiles. It is deduced that if the temperature of electrons significantly enhances than that of low-temperature ions, i.e. if β_2 decreases, the amplitude of negative potential soliton decrease. The effect of the negative potential solitary structure with respect to the parameter δ_1 and δ_2 are plotted in Figure 6.4(d) and Figure 6.4(e) respectively. From Figure 6.4(d), it is seen that increasing low-temperature ion concentration, results in an enhancement in the amplitude of negative potential solitary structure. On the other hand, an enhancement in higher temperature ion concentration in comparison to the electron concentration decreases the amplitude of negative potential solitary structure (see, Figure 6.4(e)).

To show the impact of Burgers term in positive and negative potential shock wave, Figure 6.5(a) and Figure 6.5(b) are plotted for distinct values of the dust viscosity parameter ζ_0. it is cleared from Figure 6.5(a) and Figure 6.5(b) that the amplitude of the wave substantially depends on dust kinematic viscosity. Enhancing ζ_0 causes rising dissipation and naturally the amplitudes of the shock enhance substantially with the enhancement in the dust kinematic viscosity ζ_0. Figure 6.5(c) and Figure 6.5(d) are depicted for presenting the effect of the parameter β_1 on the positive and negative potential shock wave profile. It is deduced that increment of two types of ion temperature ratio (β_1) results in a decrement of the amplitude of positive potential shock structure where an increment of amplitude can be observed for negative potential shock structure. In the shock propagation, we get the similar effect in the Figure 6.5(e) and Figure 6.5(f) for the parameter β_2 as like as shown in Figure 6.5(c) and Figure 6.5(d) respectively. The variation of the amplitudes of the positive and negative potential shock wave with the ratio of low-temperature ion concentration to the concentration of electron (δ_1) are plotted in Figure 6.5(g) and Figure 6.5(h). From the graph, we noticed that the decrement (increment) of the amplitude of the potentially positive (negative) shock is due to the increase of the parameter δ_1. The effect of the ratio of equilibrium values of the number densities of higher temperature ions to that of electrons (δ_2) on the potentially positive and negative wave amplitude is shown in Figure 6.5(i) and Figure 6.5(j), which shows that an increase in the value of δ_2 causes to increase (decrease) the amplitude of the potentially positive (negative) wave. That means if the concentration of higher temperature ions is significantly greater than the concentration of electrons then the amplitude of potentially negative shock will decrease whereas the amplitude of positive potential shock will increase.

Utilizing the symbolic computation system Mathematica, some three dimensional graphs of the obtained solutions of KPb medium are drawn in Figure 6.6 under the variation in dust viscosity parameter ζ_0, which includes different shaped wave profile such as bell type (Figure 6.6(a)) for the solution (6.63), kink type (Figure 6.6(b)) for the solution (6.74) and periodic features (Figure 6.6(c)) for the solution (6.89). The corresponding contour plots are drawn respectively in Figure 6.6(d), Figure 6.6(e), and Figure 6.6(f) from which the significant impact from the dust kinematic viscosity (ζ_0) on the wave propagation is well understood.

6.9 Conclusion

In order to study the propagating properties of DAW in unmagnetized, viscous dusty plasma made up of charged dust, electrons, and two temperature ions, we consider the KPb equation. Different types of solutions, as predicted by the phase portrait analysis of the corresponding system, are derived by using different nonlinear approaches. Using these solutions, the effect of dust kinematic viscosity (ζ_0), the ratio of two types of temperature ions (β_1), the ratio of low-temperature ions to the temperature of electrons (β_2), the ratio of equilibrium values of the number densities of lower temperature ions to the unperturbed number of electrons (δ_1), etc. are discussed from a numerical standpoint. The important outcomes have been observed in this theoretical research:

a. The KPb system includes kink (or anti-kink) shaped shock and solitary-type solitons. Viscosity and inter-collision of plasma particles lead to the creation of the Burgers effect in the KPb system. Due to the enhancement of the Burgers term (ζ_0) solitary type wave soliton goes downward. This is expected as enhancing ζ_0 causes to diminish the energy of the system. Again, the amplitude of kink increases with the enhancement of dissipation from enhancing ζ_0.

b. Ions temperature ratio β_1 also takes a valuable part in the emergence of the wave structure in the present system. It is noticed that the shock rises (decreases) with the increase (decrease) of β_1 whereas, enhancing β_1 causes for diminishing of the depth of solitary type wave solution. Similar observation follows from the parameter β_2. Occurrences of these types of nonlinear phenomena are expected, as the rising temperature of cold ion causes enhancement in potential energy of the nonlinear system, and the rising potential energy boosts the soliton moves upward.

c. The solitary as well shock soliton both shrinks down as density parameters (δ_1 and δ_2) enhance. It is expected because increasing density ratio (δ_1 and δ_2) causes for enhancement in ion density which boosts the soliton to go dipper.

d. It is observed that under certain conditions, the finite amplitude periodic solution may exist in the present plasma system. Actually, the periodicity in the wave profile arises due to the presence of the Jacobi elliptic function in the solution. The amplitude of the periodic significantly depends on the parameters β_1, β_2 and δ_1.

Finally, to the best of our knowledge, this literature expresses some effective new types of analytical solutions (shock, solitary and periodic), especially the finite-amplitude periodic solution incorporating Jacobi elliptic function, for the DAW propagating in plasma circumstance, in the framework of the KP and KPb medium. These solutions could be utilized in other nonlinear mediums which adopt the KP as well as KPb equations. This observation is carried out in parametric space and it is expected that the results observed in the simulation are realistic and effective for studying nonlinear behaviors of DAW in the Astronomical plasma and laboratory plasma. In particular, the dust acoustic solitary structure with two temperatures in a magnetized plasma environment is observed in the rings of Saturn and Jupiter, interstellar molecular clouds. Two temperature ions are also found in earth's magnetotail, earth's polar mesosphere [228, 229, 230].

Chapter 7

Impact of relativistic positron beam on ion-acoustic solitary, periodic and breather waves in Earths' ionospheric region through the framework of KdV and modified KdV equation

[1]

7.1 Introduction

The presence of electron-positron-ion plasmas was confirmed by the Advanced Satellite for Cosmology and Astrophysics (ASCA) in astronomical scenarios under idiosyncratic conditions [231]. Numerous techniques for amassing large amounts of positrons in the lab have been reported in [232, 233, 234, 235]. According to Shan and El-Tantawy [236], the positron beam characteristics and physical factors in a multi-component plasma dramatically alter freak waves. They also highlighted

[1]The research article has been published in the journal of Physica Scripta (IOP)

how the nonlinearity of the plasma environment is significantly affected by the concentration and speed of the positron beam. Using the classical KdV framework, Sarma et al. [129] described many important characteristic of ion-acoustic solitons formed in a particular plasma system with a relativistic positron beam. Shan et al.[126] have shown that the amplitude, and width of solitons propagating in plasma environment, can be altered as a result of the existence of faster positron beam and super-thermal electrons. Once more, Shan & El-Tantawy [236] recently showed that the nonlinearities of the plasma state may be primarily altered by variations in the positron beam speed and positron density. Most studies conducted in the plasma field were of a non-relativistic character [237, 238]. However, when particle speeds are near the speed of light, relativistic effects must be taken into account. Many researchers eventually proved the importance of relativistic interactions in the modulation of plasma wave evolution [239, 240, 241, 242]. In this chapter we study the propagation characteristics of ion-acoustic periodic, soliton, and breather waves in a relativistic EPI plasma with a relativistic positron beam. Applying the conventional reductive perturbation method (RPM) to the fundamental set of fluid equations yields the KdV equation. A mKdV equation is constructed when the KdV model cannot accurately capture the evolution of the nonlinear system. In both models, periodic solutions are derived using Jacobi elliptic functions, and a connection is shown between periodic waves and soliton solutions. Hirota's bilinear approach is used to generate breathers directly from the KdV type framework without utilizing the modified Schrödinger framework inferred from the KdV type framework, a common approach in nonlinear wave studies. Numerical knowledge of numerous physical factors in the ionospheric region is incorporated into the model for describing wave propagation in the Earth's upper layer.

7.2 Governing Equations

In the presence of a relativistic positron beam, we take into account an unmagnetized electron-positron-ion plasma. The charge neutrality criterion is expressed as $n_{i0} + n_{b0} = n_{e0}$ at equilibrium, where n_{j0} stands for the equilibrium concentrations of the jth species ($j = i, e, b$ respectively represent ions, electrons, and positron beams). The basic equations [129] governing the

plasma dynamics can be written as

$$\frac{\partial n_i}{\partial t} + \frac{\partial}{\partial x}(n_i v_i) = 0, \tag{7.1a}$$

$$\frac{\partial v_i}{\partial t} + v_i \frac{\partial v_i}{\partial x} + \frac{\sigma}{n_i}\frac{\partial p_i}{\partial x} = -\frac{\partial \phi}{\partial x}, \tag{7.1b}$$

$$\frac{\partial p_i}{\partial t} + v_i \frac{\partial p_i}{\partial x} + 3p_i \frac{\partial v_i}{\partial x} = 0, \tag{7.1c}$$

$$\frac{\partial n_e}{\partial t} + \frac{\partial}{\partial x}(n_e v_e) = 0, \tag{7.1d}$$

$$\beta_1 n_e \left(\frac{\partial v_e}{\partial t} + v_e \frac{\partial v_e}{\partial x}\right) + \frac{\partial p_e}{\partial x} = n_e \frac{\partial \phi}{\partial x}, \tag{7.1e}$$

$$\frac{\partial p_e}{\partial t} + v_e \frac{\partial p_e}{\partial x} + 3p_e \frac{\partial v_e}{\partial x} = 0 \tag{7.1f}$$

$$\frac{\partial n_b}{\partial t} + \frac{\partial}{\partial x}(n_b v_b) = 0, \tag{7.1g}$$

$$\beta_2 n_b \left(\frac{\partial v_b'}{\partial t} + v_b \frac{\partial v_b'}{\partial x}\right) + \alpha \frac{\partial p_b}{\partial x} = -n_b \frac{\partial \phi}{\partial x}, \tag{7.1h}$$

$$\frac{\partial p_b}{\partial t} + v_b \frac{\partial p_b}{\partial x} + 3p_b \frac{\partial v_b'}{\partial x} = 0, \tag{7.1i}$$

$$\frac{\partial^2 \phi}{\partial x^2} = (1+\delta_b) n_e - \delta_b n_b - n_i, \quad \text{where } \delta_b = \frac{n_{b0}}{n_{i0}}. \tag{7.1j}$$

Here the density and pressure of the jth species are represented by n_j and p_j, respectively. The velocity, charge and mass of the jth species are denoted by v_j, q_j and m_j, respectively. Ions, electrons, and positron beams are denoted by $j = i, e, \text{and } b$, respectively. ϕ is the electrostatic potential, γ is the relativistic factor and k_B is the Boltzmann constant. n_j is normalized by the unperturbed density n_{j0}. Normalizing p_j by $n_{j0} k_B T_j$; v_j by the ion-acoustic speed $c_s = \sqrt{\frac{k_B T_e}{m_i}}$, and the electrostatic potential ϕ by $\frac{k_B T_e}{e}$, we measure the space and time variables by scaling the ion Debye length $\lambda_{di} = \sqrt{\frac{k_B T_e}{4\pi n_{i0} e^2}}$ and the ion plasma period $\omega_{pi}^{-1} = \sqrt{\frac{m_i}{4\pi n_{i0} e^2}}$. Additionally, c is the speed of light in a vacuum, T_j is the temperature of particles of the jth species. The ratio of ion temperature to electron temperature is represented by $\sigma = \frac{T_i}{T_e}$, and the ratio of positron beam temperature to electron temperature is represented by $\alpha = \frac{T_b}{T_e}$. The ratio of electron mass to ion mass is $\beta_1 = \frac{m_e}{m_i}$, and the ratio of positron beam mass to ion mass is $\beta_2 = \frac{m_b}{m_i}$. In addition, $v_b' = v_b\left(1 + \frac{v_b^2}{2c_1^2}\right)$, c_1 is the ratio between c and c_s.

7.3 Nonlinear analysis of KdV equation

To investigate the behavior of wave propagation in electron-positron-ion plasma with relativistic positron beam, we employ RPM to derive the KdV equation, in which the independent variables are stretched as,

$$\xi = \epsilon^{\frac{1}{2}}(x - v_p t), \; \tau = \epsilon^{\frac{3}{2}} t \tag{7.2}$$

where v_p designates the phase velocity of ion-acoustic wave, and ϵ is a small parameter representing the weakness of non-linearity. Expansion of dependent variables are as follows:

$$n_e = 1 + \epsilon n_{e1} + \epsilon^2 n_{e2} + \epsilon^3 n_{e3} + \cdots\cdots, \tag{7.3a}$$

$$n_i = 1 + \epsilon n_{i1} + \epsilon^2 n_{i2} + \epsilon^3 n_{i3} + \cdots\cdots, \tag{7.3b}$$

$$n_b = 1 + \epsilon n_{b1} + \epsilon^2 n_{b2} + \epsilon^3 n_{b3} + \cdots\cdots, \tag{7.3c}$$

$$v_e = \epsilon v_{e1} + \epsilon^2 v_{e2} + \epsilon^3 v_{e3} + \cdots\cdots, \tag{7.3d}$$

$$v_i = \epsilon v_{i1} + \epsilon^2 v_{i2} + \epsilon^3 v_{i3} + \cdots\cdots, \tag{7.3e}$$

$$v_b = v_{b0} + \epsilon v_{b1} + \epsilon^2 v_{b2} + \epsilon^3 v_{b3} + \cdots\cdots, \tag{7.3f}$$

$$p_e = 1 + \epsilon p_{e1} + \epsilon^2 p_{e2} + \epsilon^3 p_{e3} + \cdots\cdots, \tag{7.3g}$$

$$p_i = 1 + \epsilon p_{i1} + \epsilon^2 p_{i2} + \epsilon^3 p_{i3} + \cdots\cdots, \tag{7.3h}$$

$$p_b = 1 + \epsilon p_{b1} + \epsilon^2 p_{b2} + \epsilon^3 p_{b3} + \cdots\cdots, \tag{7.3i}$$

$$\phi = \epsilon\phi_1 + \epsilon^2\phi_2 + \epsilon^3\phi_3 + \cdots\cdots \tag{7.3j}$$

Substituting (7.2) and (7.3) in Eqs.(7.1) and comparing the coefficients of lowest order of ϵ, we obtain the following relations:

$$n_{i1} = \frac{1}{\left(v_p^2 - 3\sigma\right)}\phi_1,\ v_{i1} = \frac{v_p}{\left(v_p^2 - 3\sigma\right)}\phi_1,\ p_{i1} = \frac{3}{\left(v_p^2 - 3\sigma\right)}\phi_1, \tag{7.4}$$

$$n_{e1} = \frac{1}{3 - \beta_1 v_p^2}\phi_1,\ v_{e1} = \frac{v_p}{3 - \beta_1 v_p^2}\phi_1,\ p_{e1} = \frac{3}{3 - \beta_1 v_p^2}\phi_1, \tag{7.5}$$

$$n_{b1} = \frac{1}{\omega\mu}\phi_1,\ v_{b1} = \frac{(v_p - v_{b0})}{\omega\mu}\phi_1,\ p_{b1} = \frac{3}{\mu}\phi_1, \tag{7.6}$$

$$\frac{(1+\delta_b)}{3 - \beta_1 v_p^2} - \frac{1}{v_p^2 - 3\sigma} = \frac{\delta_b}{\omega\mu}, \tag{7.7}$$

where

$$\omega = 1 + \frac{3v_{b0}^2}{2c_1^2},\ \mu = \beta_2 (v_p - v_{b0})^2 - 3\alpha.$$

Then, Eq.(7.7) can be used to compute the phase velocity v_p. Comparing the coefficients of next higher order of ϵ, we find the relationships shown below:

$$\frac{\partial n_{i1}}{\partial\tau} - v_p\frac{\partial n_{i2}}{\partial\xi} + \frac{\partial v_{i2}}{\partial\xi} + \frac{\partial}{\partial\xi}(n_{i1}v_{i1}) = 0, \tag{7.8}$$

$$\frac{\partial v_{i1}}{\partial\tau} - v_p\frac{\partial v_{i2}}{\partial\xi} + v_{i1}\frac{\partial v_{i1}}{\partial\xi} + \sigma\frac{\partial p_{i2}}{\partial\xi} - \sigma n_{i1}\frac{\partial p_{i1}}{\partial\xi} = -\frac{\partial\phi_2}{\partial\xi}, \tag{7.9}$$

$$\frac{\partial p_{i1}}{\partial\tau} - v_p\frac{\partial p_{i2}}{\partial\xi} + v_{i1}\frac{\partial p_{i1}}{\partial\xi} + 3\frac{\partial v_{i2}}{\partial\xi} + 3p_{i1}\frac{\partial v_{i1}}{\partial\xi} = 0, \tag{7.10}$$

$$\frac{\partial n_{e1}}{\partial\tau} - v_p\frac{\partial n_{e2}}{\partial\xi} + \frac{\partial v_{e2}}{\partial\xi} + \frac{\partial}{\partial\xi}(n_{e1}v_{e1}) = 0, \tag{7.11}$$

$$\beta_1\frac{\partial v_{e1}}{\partial\tau}-\beta_1 v_p\frac{\partial v_{e2}}{\partial\xi}-\beta_1 v_p n_{e1}\frac{\partial v_{e1}}{\partial\xi}+\beta_1 v_{e1}\frac{\partial v_{e1}}{\partial\xi}+\frac{\partial p_{e2}}{\partial\xi}=\frac{\partial\phi_2}{\partial\xi}+n_{e1}\frac{\partial\phi_1}{\partial\xi}, \tag{7.12}$$

$$\frac{\partial p_{e1}}{\partial\tau}-v_p\frac{\partial p_{e2}}{\partial\xi}+v_{e1}\frac{\partial p_{e1}}{\partial\xi}+3\frac{\partial v_{e2}}{\partial\xi}+3p_{e1}\frac{\partial v_{e1}}{\partial\xi}=0, \tag{7.13}$$

$$\frac{\partial n_{b1}}{\partial\tau}-(v_p-v_{b0})\frac{\partial n_{b2}}{\partial\xi}+\frac{\partial v_{b2}}{\partial\xi}+\frac{\partial}{\partial\xi}(n_{b1}v_{b1})=0, \tag{7.14}$$

$$\begin{aligned}&\beta_2\left(1+\frac{3}{2c_1^2}v_{b0}^2\right)\frac{\partial v_{b1}}{\partial\tau}+\beta_2\left(1+\frac{3}{2c_1^2}v_{b0}^2\right)(v_{b0}-v_p)\frac{\partial v_{b2}}{\partial\xi}\\&-\beta_2\frac{3}{2c_1^2}v_{b0}(v_p-v_{b0})2v_{b1}\frac{\partial v_{b1}}{\partial\xi}+\beta_2\left(1+\frac{3}{2c_1^2}v_{b0}^2\right)v_{b1}\frac{\partial v_{b1}}{\partial\xi}\\&+\beta_2\left(1+\frac{3}{2c_1^2}v_{b0}^2\right)n_{b1}\frac{\partial v_{b1}}{\partial\xi}(v_{b0}-v_p)+\alpha\frac{\partial p_{b2}}{\partial\xi}=-\frac{\partial\phi_2}{\partial\xi}-n_{b1}\frac{\partial\phi_1}{\partial\xi},\end{aligned} \tag{7.15}$$

$$\begin{aligned}&\frac{\partial p_{b1}}{\partial\tau}+\frac{\partial p_{b2}}{\partial\xi}(v_{b0}-v_p)+v_{b1}\frac{\partial p_{b1}}{\partial\xi}+3\frac{\partial v_{b2}}{\partial\xi}\left(1+\frac{3}{2c_1^2}v_{b0}^2\right)\\&+\frac{9}{2c_1^2}v_{b0}\frac{\partial v_{b1}^2}{\partial\xi}+3p_{b1}\frac{\partial v_{b1}}{\partial\xi}\left(1+\frac{3}{2c_1^2}v_{b0}^2\right)=0,\end{aligned} \tag{7.16}$$

$$\frac{\partial^2\phi_1}{\partial\xi^2}=(1+\delta_b)n_{e2}-\delta_b n_{b2}-n_{i2}. \tag{7.17}$$

From Eqs.(7.8)-(7.17), selecting $\phi_1=\psi$, we finally obtain the following KdV equation:

$$\frac{\partial\psi}{\partial\tau}+A\psi\frac{\partial\psi}{\partial\xi}+B\frac{\partial^3\psi}{\partial\xi^3}=0, \tag{7.18}$$

where

$$A=\frac{R}{P},B=\frac{1}{P},$$

and

$$P=(1+\delta_b)\frac{2\beta_1 v_p}{\left(3-\beta_1 v_p^2\right)^2}+\delta_b\frac{2\beta_2(v_p-v_{b0})}{\omega\mu^2}+\frac{2v_p}{\left(v_p^2-3\sigma\right)^2},$$

$$R=(1+\delta_b)\frac{3\left(1+\beta_1 v_p^2\right)}{\left(3-\beta_1 v_p^2\right)^3}+\delta_b\left(\frac{3}{\omega^2\mu^2}+\frac{3\alpha}{\omega^2\mu^3}+\frac{9\alpha}{\omega\mu^3}-\frac{3v_{b0}(v_p-v_{b0})}{c_1^2\omega^3\mu^2}\right)+\frac{3\left(v_p^2+\sigma\right)}{\left(v_p^2-3\sigma\right)^3}.$$

Nonlinear co-efficient A plays an important role in formation of wave structure. So it is important to study the behaviour of this coefficient with respect to plasma parameters. We have conducted a numerical analysis of the variation of the nonlinear coefficient A with the variation of the parameters α and δ_b in Figure 7.1(a) and Figure 7.1(b), respectively. From Figure 7.1(a), it is clear that (i) A can take on negative, zero, and positive values depending on the value of α; (ii) the value of α at which A equals zero is referred to as the critical value of α, denoted as α_c, and for our current analysis, α_c is approximately 0.207; and (iii) the parameter ranges for the creation of positive (i.e., $\psi>0$) and negative (i.e., $\psi<0$) potential structures can be identified corresponding to $A>0$ and $A<0$. From the observation of Figure 7.1(b), it can be noted that the nonlinear coefficient A exhibits a

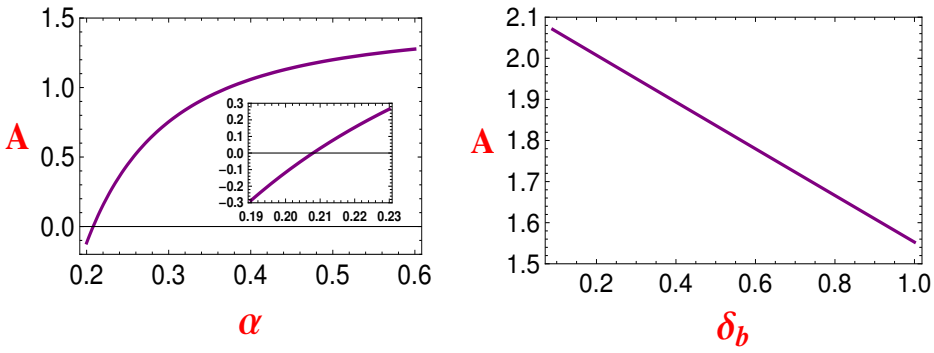

(a) (b)

Figure 7.1: 2D profile of (a) nonlinear coefficient A vs α for $\beta_1 = 0.005$, $\beta_2 = 0.0054$, $\delta_b = 0.5$, $\sigma = 0.1$, $c_1 = 1000$, $\nu_{b0} = 1$, $\nu_p = 1.45$, (b) nonlinear coefficient A vs δ_b for $\beta_1 = 0.005$, $\beta_2 = 0.0054$, $\alpha = 0.3$, $\sigma = 0.1$, $c_1 = 1000$, $\nu_{b0} = 1$, $\nu_p = 1.45$.

strict decrease as δ_b increases. It seems that The sign of A appears to be significantly influenced by the parameters α and δ_b. It is well established that, (i) a negative coefficient for the nonlinear term A results in the formation of rarefactive solitary waves, while (ii) a positive A leads to the existence of compressive solitary waves within this framework. As illustrated in Figure 7.1, both rarefactive and compressive solitary waves are present. Notably, when $A = 0$, the pulse amplitud approaches infinity, indicating that the KdV equation is inadequate for modeling this scenario. Consequently, it is necessary to seek a higher-order nonlinear wave equation to accurately describe the dynamics of nonlinear waves at $A = 0$, as elaborated in section 7.5.

7.4 Soliton, periodic, breather and hybrid solutions of KdV equation

The most prevalent occurrence in all types of nonlinear fields is the soliton, and its modes are typically described as hyperbolic functions. In the past, investigations in plasma physics focused on the nonlinear forms of this wave, such as the soliton and cnoidal waves. Our analysis involves the numerical examination of how the solutions to the KdV equations are affected by changes in the physical parameters consisted with the ionosphere region ([129, 243]), based on the data as, $n_{e0} = 0.11 \times 10^{12} - 0.19 \times 10^{12} m^{-3}$, $n_{i0} = 10^{11} m^{-3}$, $n_{b0} = 10^{10} - 0.9 \times 10^{11} m^{-3}$ with ion and electron temperature as $T_i \approx 0.07$ eV, $T_e \approx 0.2$ eV, $\delta_b = 0.09 - 0.8$, $\sigma = 0.1 - 0.6$, $\alpha = T_b/T_e = 0.2 - 0.6$, $\beta_1 = m_e/m_i = 0.005$ and $\beta_2 = m_b/m_i = 0.0054$.

7.4.1 Periodic solution

In terms of the Jacobian elliptic function, it has recently been discovered that nonlinear periodic waves, such as *sn*, *cn*, and *dn* are formed under specific conditions ([198, 144, 202, 203]). This periodic wave can actively contribute to describe plasma transport processes. We introduce a specific kind of transformation to obtain the periodic wave solution of KdV Eq.(7.18)

$$\psi(\xi,\tau) = \psi(\Theta), \ \textit{where}\ \Theta = k\xi - wt, \tag{7.19}$$

which brings,

$$\frac{1}{2}\left(\frac{d\psi}{d\Theta}\right)^2 + V(\psi) = 0, \tag{7.20}$$

where $V(\psi) = \frac{A}{6Bk^2}\psi^3 - \frac{w}{2Bk^3}\psi^2 + \frac{\Gamma_0}{2Bk^3}$ represents the Sagdeev potential and Γ_0 stands as an integrating constant. Adopting the initial condition $\frac{d\psi(0)}{d\Theta} = 0, \psi(0) = \frac{w}{Ak}$ we have $\Gamma_0 = \frac{2w^3}{3A^2k^2}$, the expression (7.20) is represented below for $\frac{A}{B} > 0$ and $\frac{A}{B} < 0$ respectively as,

$$\left(\frac{d\psi}{d\Theta}\right)^2 = \frac{A}{3Bk^2}[(r_1-\psi)(\psi-r_2)(\psi-r_3)], \tag{7.21}$$

$$\left(\frac{d\psi}{d\Theta}\right)^2 = (-\frac{A}{3Bk^2})[(\psi-r_1)(r_2-\psi)(r_3-\psi)], \tag{7.22}$$

where

$$r_1 = (1+\sqrt{3})\frac{w}{Ak},\ r_2 = \frac{w}{Ak},\ r_3 = (1-\sqrt{3})\frac{w}{Ak}. \tag{7.23}$$

The dispersion co-efficient B is always positive in the current plasma model (7.18) so the term $\frac{A}{3Bk^2}$ changes depending on whether A is positive or negative. For choosing positive values of $\frac{A}{B}$, the real numbers r_1, r_2, r_3 are chosen as $r_1 > r_2 > r_3$ and $r_1 > \psi \geqslant r_2$. On the contrary, the real numbers r_1, r_2, r_3 are ordered as $r_1 < r_2 < r_3$ and $r_1 < \psi \leqslant r_2$ when $\frac{A}{B}$ is negative. As a result, we arrive at the periodic solution as follows:

$$\psi(\xi,\tau) = r_2 + (r_1-r_2)cn^2\left(\frac{\sqrt{\frac{A}{3Bk^2}(r_1-r_3)}}{2}(k\xi - w\tau), \sqrt{\frac{r_1-r_2}{r_1-r_3}}\right), \tag{7.24}$$

where *cn* represents the Jacobi elliptic function, and $\frac{Ak}{3}(r_1+r_2+r_3)$, $r_1 - r_2 = \frac{\sqrt{3}w}{Ak}$, and $4\sqrt{\frac{3Bk^2}{A(r_1-r_3)}}Q(\sqrt{\frac{r_1-r_2}{r_1-r_3}})$ respectively represent velocity, amplitude and wave length of the periodic waves. Here, the complete elliptic integral is denoted by $Q(\sqrt{\frac{r_1-r_2}{r_1-r_3}})$.

7.4.2 Solitary solution

A soliton, commonly known as a solitary wave, is a wave packet that retains its structure while flowing at a constant speed. It is one of their most distinguishing characteristics that the

solitons maintain their shapes as they interact. Now when $\Gamma_0 = 0$, the Eq.(7.20) reduces to

$$\frac{1}{2}\left(\frac{d\psi}{d\Theta}\right)^2 + \frac{A}{6Bk^2}\psi^3 - \frac{w}{2Bk^3}\psi^2 = 0, \tag{7.25}$$

and so solution (7.24) turns to the solitary wave solution as

$$\psi(\xi,\tau) = \frac{3w}{Ak}\ sech^2\left(\sqrt{\frac{w}{4Bk^3}}(k\xi - w\tau)\right), \tag{7.26}$$

Here the terms $\frac{3w}{Ak}$ and $\sqrt{\frac{4Bk^3}{w}}$ represents the peak amplitude and the width of the ion acoustic solitary waves.

7.4.2.1 Discussion on periodic and solitary wave solution for the KdV system

The variation of the plasma parameters δ_b (positron beam to ion density ratio), σ (ion temperature to electron temperature ratio) and α (positron beam temperature to electron temperature ratio) on Sagdeev potential, phase plot, wave structure corresponding to periodic and solitary waves are plotted in Figure 7.2 and Figure 7.3 respectively. Figure 7.2, and Figure 7.3 each contain three rows, where the first position stands for Sagdeev potential, the second position is for phase plane, and 3rd one is for the presentation of the wave structure. By taking into account the identical set of values, the Sagdeev potential, phase plane, and wave structure corresponding to the periodic solution are drawn. We have studied the real zeros of the Sagdeev potential $V(\psi)$ in the forms of ψ_0, ψ_1, and ψ_2 having non-zero finite values of different physical parameters in order to better understand the properties of nonlinear periodic (cnoidal) waves. The Sagdeev potential $V(\psi)$ never vanishes for cnoidal waves at origin (i.e., $V(\psi) \neq 0$ at $\psi = 0$), but it does for solitary waves (i.e., $V(\psi) = 0$ at $\psi = 0$). The potential well particle regularly oscillates between the zeros ψ_0 and ψ_1, according to the Sagdeev potential.

A little potential barrier keeps the oscillating particle from getting to the root value ψ_2. According to the particle's behavior in Figure 7.2(a)-Figure 7.2(c), a nonlinear periodic (cnoidal) wave oscillates between two values of ψ_0 and ψ_1. As a result of the spacing between the repetitions of the wave structures, the nonlinear potential structures of the cnoidal waves are finally repeated, resulting in a wavelength of one unit. When the other parameters are held constant, the Sagdeev potential for various values of the positron beam concentration δ_b is shown in Figure 7.2(a). Figure 7.2(b) and Figure 7.2(c) show the corresponding phase plane and associated periodic structure, respectively. Figure 7.2(c) illustrates the changes in periodic wave patterns as δ_b varies. The graph clearly indicates that as δ_b increases, the amplitude of the periodic wave also increases. This suggests that higher positron beam concentration in plasma leads to ion energization. For this reason, the driving force given by ions thereby actively contributes and plays a crucial role in forming periodic wave greater energetic by enlarging its amplitude. The effect of ion to electron temperature ratio σ on

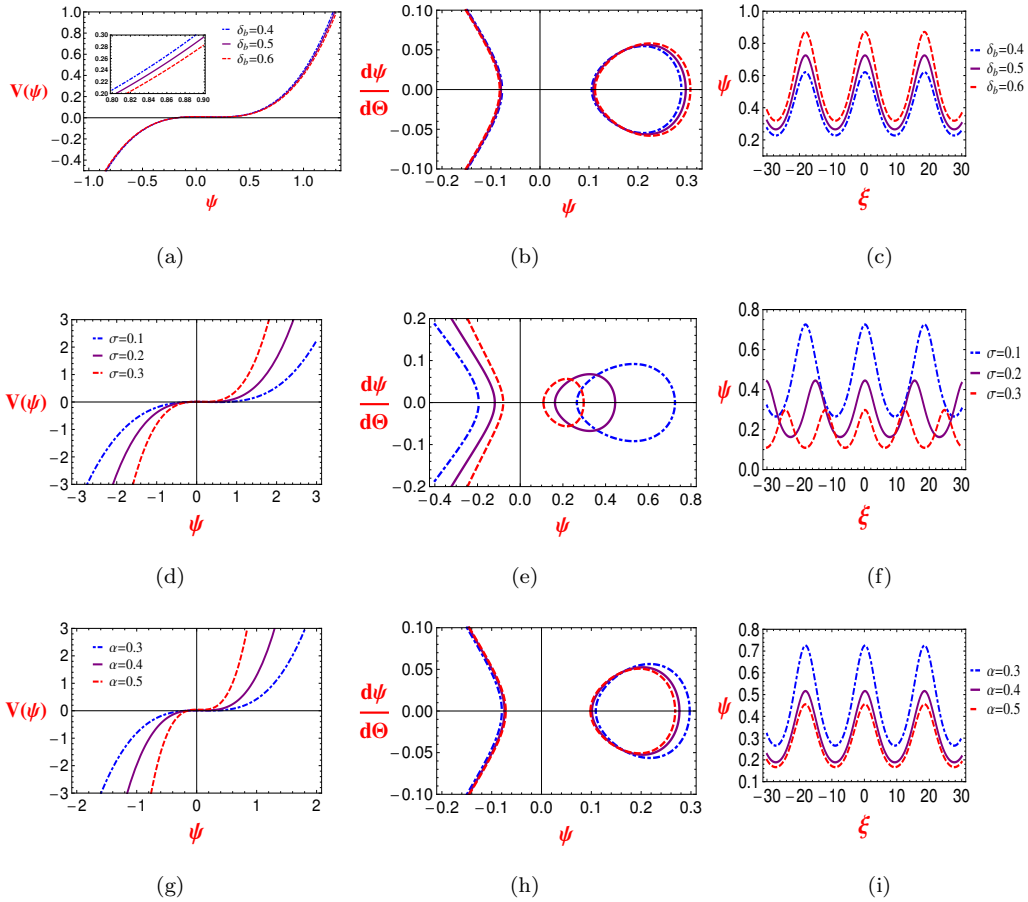

Figure 7.2: (a), (b), and (c) are respectively the variation of δ_b on Sagdeev potential, phase plane, and wave structure corresponding to periodic solution (7.24) for $\beta_1 = 0.005$, $\beta_2 = 0.0054$, $\alpha = 0.3$, $\sigma = 0.1$, $w = 0.2$, $k = 1$, $c_1 = 1000$, $\nu_{b0} = 1$, $\nu_p = 1.45$, $\tau = 1$, $\Gamma_0 = 0.01$. (d), (e), and (f) are respectively the variation of σ on Sagdeev potential, phase plane, and wave structure corresponding to periodic solution (7.24) for $\beta_1 = 0.005$, $\beta_2 = 0.0054$, $\alpha = 0.3$, $\delta_b = 0.5$, $w = 0.2$, $k = 1$, $c_1 = 1000$, $\nu_{b0} = 1$, $\nu_p = 1.45$, $\tau = 1$, $\Gamma_0 = 0.01$. (g), (h), and (i) are respectively the variation of α on Sagdeev potential, phase plane, and wave structure corresponding to periodic solution (7.24) for $\beta_1 = 0.005$, $\beta_2 = 0.0054$, $\sigma = 0.1$, $\delta_b = 0.5$, $w = 0.2$, $k = 1$, $c_1 = 1000$, $\nu_{b0} = 1$, $\nu_p = 1.45$, $\tau = 1$, $\Gamma_0 = 0.01$.

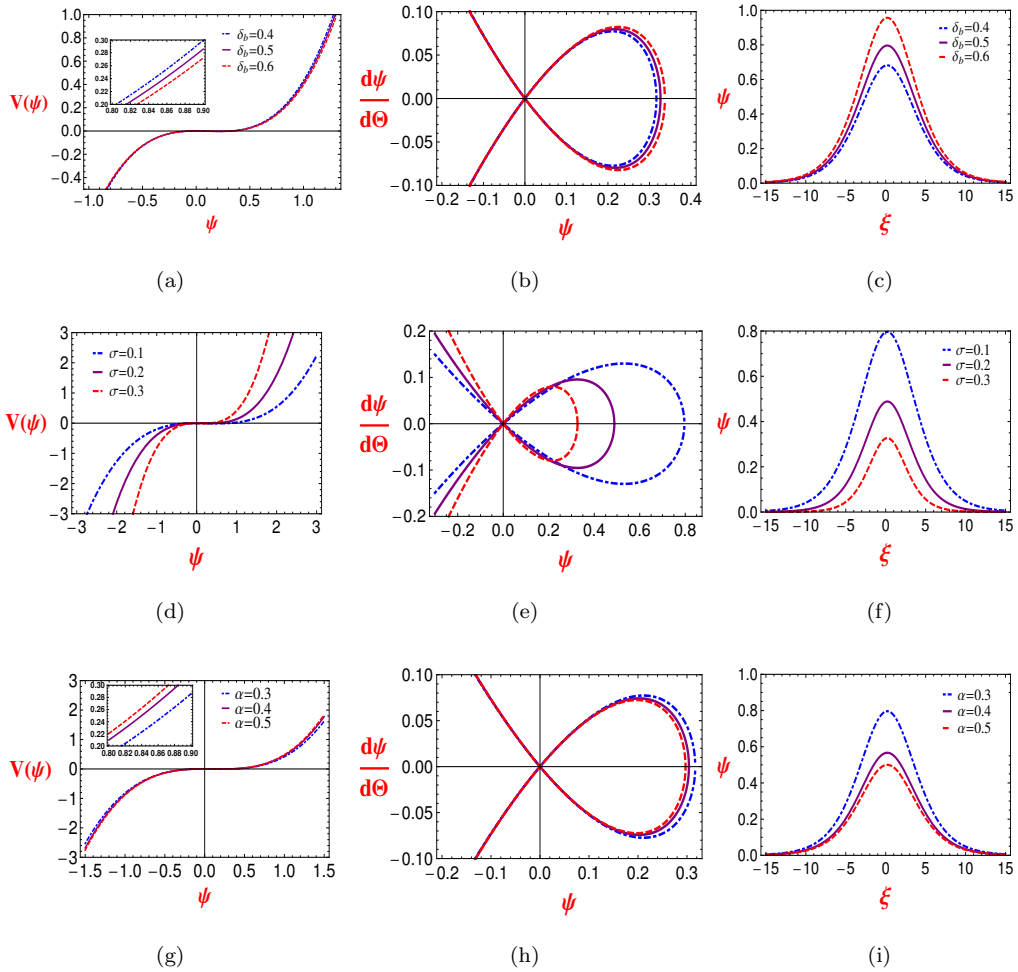

Figure 7.3: (a), (b), and (c) are respectively the variation of δ_b on Sagdeev potential, phase plane, and wave structure corresponding to solitary solution (7.26) for $\beta_1 = 0.005$, $\beta_2 = 0.0054$, $\alpha = 0.3$, $\sigma = 0.1$, $w = 0.2$, $k = 1$, $c_1 = 1000$, $\nu_{b0} = 1$, $\nu_p = 1.45$, $\tau = 1$. (d), (e), and (f) are respectively the variation of σ on Sagdeev potential, phase plane, and wave structure corresponding to solitary solution (7.26) for $\beta_1 = 0.005$, $\beta_2 = 0.0054$, $\alpha = 0.3$, $\delta_b = 0.5$, $w = 0.2$, $k = 1$, $c_1 = 1000$, $\nu_{b0} = 1$, $\nu_p = 1.45$, $\tau = 1$. (g), (h), and (i) are respectively the variation of α on Sagdeev potential, phase plane, and wave structure corresponding to solitary solution (7.26) for $\beta_1 = 0.005$, $\beta_2 = 0.0054$, $\sigma = 0.1$, $\delta_b = 0.5$, $w = 0.2$, $k = 1$, $c_1 = 1000$, $\nu_{b0} = 1$, $\nu_p = 1.45$, $\tau = 1$.

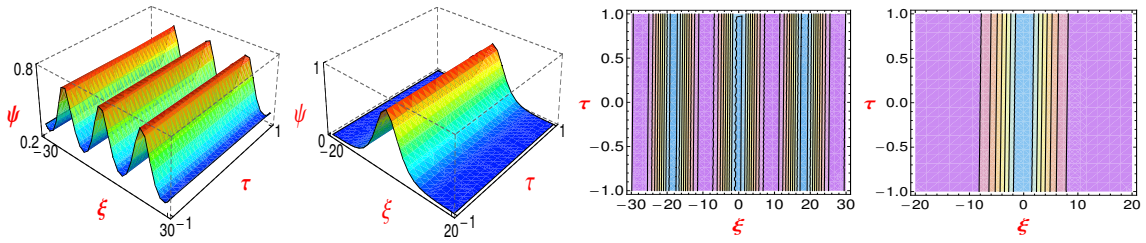

(a) (b) (c) (d)

Figure 7.4: (a) 3D profile of periodic structure (7.24), for $\beta_1 = 0.005$, $\beta_2 = 0.0054$, $\alpha = 0.3$, $\delta_b = 0.5$, $\sigma = 0.1$, $w = 0.2$, $k = 1$, $c_1 = 1000$, $\nu_{b0} = 1$, $\nu_p = 1.45, \Gamma_0 = 0.01$, (b) 3D profile of solitary structure (7.26), for $\beta_1 = 0.005$, $\beta_2 = 0.0054$, $\alpha = 0.3$, $\delta_b = 0.5$, $\sigma = 0.1$, $w = 0.2$, $k = 1$, $c_1 = 1000$, $\nu_{b0} = 1$, $\nu_p = 1.45$, (c) and (d) are Contour plots of the corresponding Figure 7.4(a), and Figure 7.4(b).

Sagdeev potential, phase plot, and wave structure corresponding to periodic wave are presented in Figure 7.2(d), Figure 7.2(e), and Figure 7.2(f) respectively. By observing the distances of the potential curves and the phase plane curves from the vertical axis along parallel to horizontal axis, it is found that the amplitude of periodic wave decreases with enhancing σ as given in Figure 7.2(f). We see negative impact in wave structure due to the increase in ion temperature in comparison to that of the electron. The effect of the parameter α on Sagdeev potential, phase plot, and wave structure corresponding to periodic wave are presented in Figure 7.2(g), Figure 7.2(h), and Figure 7.2(i) respectively. From Figure 7.2(i), it is observed that for enhancing α the amplitude of periodic wave decreases. The structure's characteristics can be described as follows: when the temperature of the positron beam increases in comparison to that of the electron, it has an adverse impact on the system's potential energy. Consequently, the amplitude of the periodic wave exhibits a decreasing pattern.

Figure 7.3(a), Figure 7.3(b), and Figure 7.3(c) respectively, show the Sagdeev potential, phase plot, and wave structure corresponding to a solitary wave for various values of the parameter δ_b while the other parameters are held constant. As before, the characteristics of nonlinear solitary waves are examined using real zeros of $V(\psi)$ in the forms of ψ_0, ψ_1, and ψ_2 with non-zero finite values of various physical parameters. $V(\psi)$ vanishes for solitary waves at origin (i.e., $V(\psi) = 0$ at $\psi = 0$), but it never does for periodic waves. The effect of positron beam concentration on solitary wave structure remains same as we see in periodic wave. Due to the increase in positron beam concentration the amplitude of the solitary wave increases. Figure 7.3(d), Figure 7.3(e), and Figure 7.3(f) respectively, show the effects of the parameter σ on the Sagdeev potential, phase plot, and wave structure corresponding to solitary wave. It can be shown that the amplitude of a single structure strictly reduces with increasing σ as shown in Figure 7.3(f) by looking the distances of the potential curves from the

vertical axis along parallel to horizontal axis and the area covered by the curves of the phase plane. Figure 7.3(g), Figure 7.3(h), and Figure 7.3(i) respectively, exhibit the effects of α on the Sagdeev potential, phase plot, and wave structure corresponding to solitary wave. Figure 7.3(i) shows that with an increase in α, the amplitude of the compressive solitary wave decreases while the width remains relatively constant. This observation leads us to conclude that the nonlinearity of the compressive solitary wave is intensified as α increases. This nonlinear behavior can be attributed to the fact that an increase in the temperature of the positron beam, in comparison to that of the electron, negatively impacts the potential energy of the system. Therefore, as α increases, the amplitude of the compressive solitary wave decreases.

Figure 7.4(a) shows compressive structure of periodic waves whereas, compressive structure of solitary waves are exhibited in Figure 7.4(b). The corresponding contour plots of the above-mentioned figures are plotted in Figure 7.4(c) and Figure 7.4(d). These numerical figures are drawn for a clear presentation of the periodic and solitary structures of the present KdV system.

7.4.3 Bilinear form and K-soliton solution for the KdV equation

A number of studies in nonlinear scientific domains have demonstrated that Hirota's bilinear method [27, 156, 201], is a potential analytical aid for resolving a wider range of nonlinear evolution equations. In the current investigation, we utilize the bilinear form of the KdV model for finding multi-solitons and breathers. Here, we describe the transformation

$$\psi = \frac{12B}{A}\frac{\partial^2}{\partial\xi^2}\ln(\mathcal{H}(\xi,\tau)), \tag{7.27}$$

and utilizing it in the Eq.(7.18), we can acquire the bilinear form of Eq.(7.18) below as,

$$(D_\tau D_\xi + BD_{4\xi})\,\mathcal{H}\cdot\mathcal{H} = 0. \tag{7.28}$$

where $\mathcal{H}$ is a function of ξ, τ, and the Hirota operator is represented by $D_\tau D_\xi$, $D_{4\xi}$ [27, 156, 201]. To find hybrid solutions, the bilinear form of the equation Eq.(7.18) addressed in Eq.(7.28) will be used. The K-soliton solutions of the KdV Eq.(7.18) are obtained by applying Hirota's bilinear approach in the following way,

$$\psi(\xi,\tau) = \psi_\kappa = \frac{12B}{A}\left[\frac{\partial^2}{\partial\xi^2}\ln(\mathcal{H}(\xi,\tau))\right], \tag{7.29}$$

$$\mathcal{H} = 1 + \sum_{j=0}^{K} e^{\kappa_j} + \sum_{j<k} \mathcal{B}_{jk} e^{\kappa_j+\kappa_k} + \sum_{j<k<l} \mathcal{B}_{jk}\mathcal{B}_{jl}\mathcal{B}_{kl} e^{\kappa_j+\kappa_k+\kappa_l} + \cdots + \left(\prod_{j<k}\mathcal{B}_{jk}\right) e^{\sum_{j=1}^{K}\kappa_j}, \tag{7.30}$$

Here

$$\kappa_j = g_j\xi + \Omega_j\tau + \Gamma_j^0,\ \Omega_j = -Bg_j^3,\ j = 1,2,\cdots,K, \tag{7.31}$$

with

$$\mathcal{B}_{jk} = \frac{(g_j - g_k)(B(g_j - g_k)^3 + (\Omega_j - \Omega_k))}{(g_j + g_k)(B(g_j + g_k)^3 + (\Omega_j + \Omega_k))}, \quad 1 \leqslant j < k \leqslant K. \tag{7.32}$$

Here, the values of j, k assume $1, 2, \cdots, K$, where K stands for the soliton numbers and Γ_j^0 for the phase constant. g_j $(j = 1, 2, \cdots, K)$ are real constants chosen at random.

7.4.3.1 2-Soliton solution

When $K = 2$, from Eq.(7.30) we have

$$\mathcal{H} = 1 + e^{\kappa_1} + e^{\kappa_2} + \mathcal{B}_{12} e^{\kappa_1 + \kappa_2}, \tag{7.33}$$

with

$$\kappa_i = g_i \xi - Q g_i^3 \tau + \Gamma_i^0, \; i = 1, 2$$

and

$$\mathcal{B}_{12} = \frac{(g_1 - g_2)(Q(g_1 - g_2)^3 + (\Omega_1 - \Omega_2))}{(g_1 + g_2)(Q(g_1 + g_2)^3 + (\Omega_1 + \Omega_2))}. \tag{7.34}$$

The two-soliton solution for equation Eq.(7.18) can be obtained by replacing Eq.(7.33), into Eq.(7.29).

7.4.3.2 1-Order breather solution

By examining the expression of two-soliton solution and considering complex conjugate conditions, we write the wave vector as,

$$g_1 = p_{R1} + i q_{I1} = g_2^*, \; \Gamma_1^0 = \Gamma_2^0 = 0. \tag{7.35}$$

The declaration $\mathcal{H}$ in Eq.(7.33) is now displayed as

$$\mathcal{H} = 1 + 2e^{m_1} \cos(m_2) + \mathcal{B}_{12} e^{2m_1}, \tag{7.36}$$

and from there, it is learned that the fundamental breather solution is,

$$\begin{aligned} \psi_{br} \quad = \quad & \frac{12B}{A} \frac{(4p^2 \mathcal{B}_{12} e^{2m_1} + 2p^2 e^{m_1} \cos(m_2) - 2e^{m_1} q^2 \cos(m_2) - 4pq e^{m_1} \sin(m_2))}{(1 + \mathcal{B}_{12} e^{2m_1} + 2e^{m_1} \cos(m_2))} - \\ & \frac{12B}{A} \frac{(2\mathcal{B}_{12} p e^{2m_1} + 2p e^{m_1} \cos(m_2) - 2q e^{m_1} \sin(m_2))^2}{(1 + \mathcal{B}_{12} e^{2m_1} + 2e^{m_1} \cos(m_2))^2}, \end{aligned} \tag{7.37}$$

where

$$\begin{aligned} & m_1 = p_{R1} x - (B(p_{R1}^3 - 3p_{R1} q_{I1}^2))\tau, \\ & m_2 = q_{I1} x - (B(3p_{R1}^2 q_{I1} - q_{I1}^3))\tau \quad \text{and} \quad \mathcal{B}_{12} = \frac{q_{I1}^2}{p_{R1}^2}. \end{aligned}$$

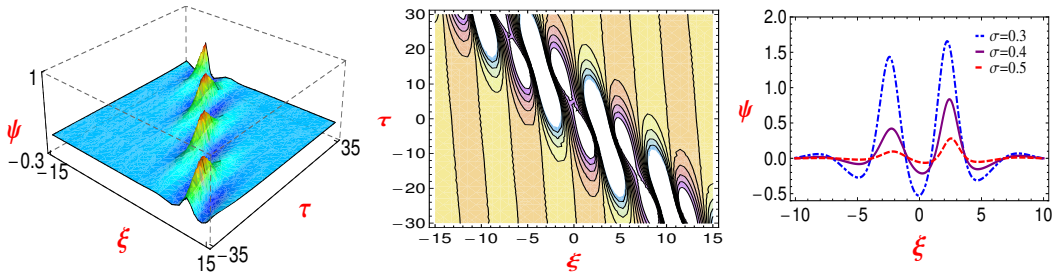

(a) (b) (c)

Figure 7.5: (a) 3D profile of breather structure, for $\beta_1 = 0.005$, $\beta_2 = 0.0054$, $\alpha = 0.4$, $\delta_b = 0.5$, $\sigma = 0.5$, $c_1 = 1000$, $V_{b0} = 1$, $\nu_p = 1.45$, $g_1 = -0.5 - 1.5i = g_2^*$, (b) Contour plot of the corresponding Figure 7.5(a), (c) 2D profile of breather structure, for $\beta_1 = 0.005$, $\beta_2 = 0.0054$, $\alpha = 0.3$, $\delta_b = 0.5$, $c_1 = 1000$, $\nu_{b0} = 1$, $\nu_p = 1.45$, $g_1 = -0.5 - 1.5i = g_2^*$, $\tau = 2$.

7.4.3.3 Three-soliton solution

In this section, we derive some unique patterns of interactions, which are different forms of breather-solitons interacting with solitons from the solution (7.30) with relation (7.32) and when $K = 3$. We investigate the interactions between breather-solitons and other solitons employing the complicated conjugate criteria procedure. Here, $\mathcal{H}$ is selected as an auxiliary function of third order as follows,

$$\mathcal{H} = 1 + e^{\kappa_1} + e^{\kappa_2} + e^{\kappa_3} + \mathcal{B}_{12}e^{\kappa_1+\kappa_2} + \mathcal{B}_{13}e^{\kappa_1+\kappa_3} + \mathcal{B}_{23}e^{\kappa_2+\kappa_3} + \mathcal{B}_{123}e^{\kappa_1+\kappa_2+\kappa_3}, \tag{7.38}$$

where

$$\kappa_i = g_j\xi - Bg_j^3\tau + \Gamma_j^0,\ j = 1,2,3, \quad \& \quad \mathcal{B}_{123} = \mathcal{B}_{12}\mathcal{B}_{13}\mathcal{B}_{23}$$

and $\mathcal{B}_{jk}$, $j,k = 1,2,3$, are provided by (7.32). Because of this, Eq.(7.30) can be used in place of Eq.(7.38) to produce the three-order solution. The three-order solution appears as the three-solitons if all the parameters g_1, g_2 and g_3 are assumed to be real constants.

1-Soliton and 1-order breather solution :

We select a single breather and a single soliton in the following section and merge them to make a hybrid solution to provide more information

$$g_1 = p_{R1} + iq_{I1} = g_2^*,\ g_3 = g_3,\ \Gamma_1^0 = \Gamma_2^0 = 0. \tag{7.39}$$

Then, the $\mathcal{H}$ can be explicitly written as

$$\mathcal{H} = 1 + 2e^{m_1}\cos(m_2) + \mathcal{B}_{12}e^{2m_1} + e^{\kappa_3} + 2\gamma_1 e^{m_1+\kappa_3}\cos(m_2+\sigma_1) + \mathcal{B}_{12}\gamma_1^2 e^{2m_1+\kappa_3} \tag{7.40}$$

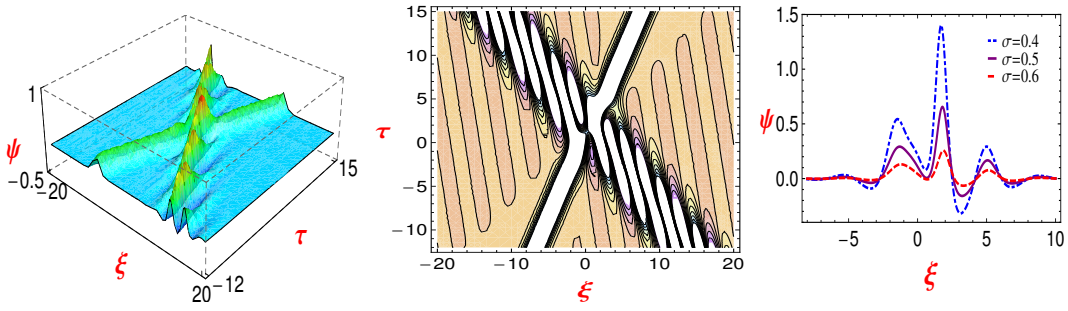

(a) (b) (c)

Figure 7.6: (a) 3D profile for interaction of breather-soliton structure, for $\beta_1 = 0.005$, $\beta_2 = 0.0054$, $\alpha = 0.4$, $\delta_b = 0.5$, $\sigma = 0.5$, $c_1 = 1000$, $\nu_{b0} = 1$, $\nu_p = 1.45$, $g_1 = -0.6 - 1.6i = g_2^*$, $g_3 = 2$; (b) Contour plot of the corresponding Figure 7.6(a), (c) 2D profile of interaction of breather-soliton structure, for $\beta_1 = 0.005$, $\beta_2 = 0.0054$, $\alpha = 0.4$, $\delta_b = 0.5$, $c_1 = 1000$, $\nu_{b0} = 1$, $\nu_p = 1.45$, $g_1 = -0.6 - 1.6i = g_2^*$, $g_3 = 2$, $\tau = 0.5$.

where

$$m_1 = p_{R1}\xi - [B(p_{R1}^3 - 3p_{R1}q_{I1}^2)]\tau,\ m_2 = q_{I1}\xi - [B(3p_{R1}^2 q_{I1} - q_{I1}^3)]\tau,\ \kappa_3 = g_3\xi - Bg_3^3\tau,$$
$$\mathcal{B}_{12} = \frac{q_{I1}^2}{p_{R1}^2},\ \mathcal{B}_{13} = -\frac{(p_{R1} + iq_{I1} - g_3)^2}{(p_{R1} + iq_{I1} + g_3)^2} = \gamma_1 e^{i\sigma_1},\ \mathcal{B}_{13} = \mathcal{B}_{23}^* = \gamma_1 e^{-i\sigma_1}. \tag{7.41}$$

Thus, we obtain a hybrid solution $\psi = \frac{12B}{A}\frac{\partial^2}{\partial\xi^2}\ln(\mathcal{H}(\xi,\tau))$, where $\mathcal{H}$ is determined by Eq.(7.40).

7.4.3.4 Multiple interactive configurations with solitons and breathers

In this part, we describe some innovative interactive topological structures that are composed of breather-solitons as well as solitons collectively and are derived from the solution (7.30) with (7.32) and $K = 4$. By taking into account the complicated conjugate condition technique, we analyse the interacting behaviours between breather-soliton and other types of soltons. We pick $\mathcal{H}$ as the fourth-order auxiliary function

$$\mathcal{H} = 1 + \sum_{i=1}^{4} e^{\kappa_i} + \sum_{1\leqslant i<j\leqslant 4} \mathcal{B}_{ij} e^{\kappa_i+\kappa_j} + \sum_{1\leqslant i<j<k\leqslant 4} \mathcal{B}_{ijk} e^{\kappa_i+\kappa_j+\kappa_k} + \mathcal{B}_{1234} e^{\sum_{i=1}^{4}\kappa_i} \tag{7.42}$$

where $\mathcal{B}_{ij}$, $j = 1, 2, 3$ and $\mathcal{B}_{123} = \mathcal{B}_{12}\mathcal{B}_{13}\mathcal{B}_{23}$ and $\mathcal{B}_{1234} = \mathcal{B}_{12}\mathcal{B}_{13}\mathcal{B}_{14}\mathcal{B}_{23}\mathcal{B}_{24}\mathcal{B}_{34}$ obey the results (7.32), respectively. The fourth-order solution for Eq.(7.18) may be found by putting Eq. (7.42), into Eq.(7.29). There are two different sorts of combinations in the fourth-order situation, and the following are some typical cases:

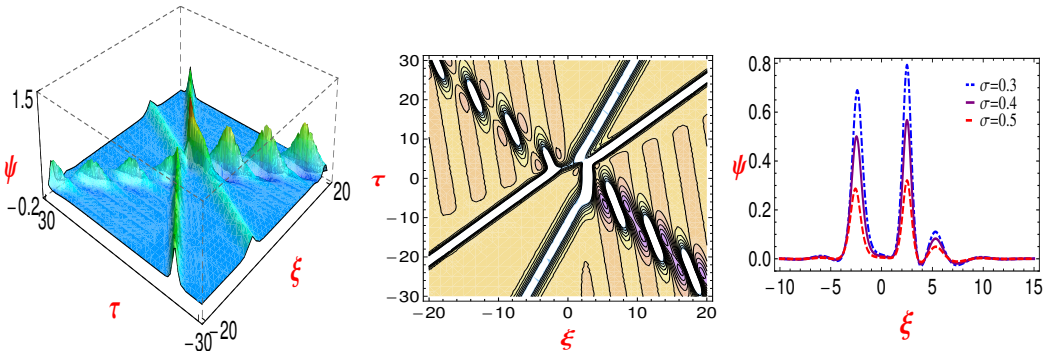

(a) (b) (c)

Figure 7.7: (a) 3D profile for interaction of breather-two-soliton structure, for $\beta_1 = 0.005$, $\beta_2 = 0.0054$, $\alpha = 0.4$, $\delta_b = 0.5$, $\sigma = 0.5$, $c_1 = 1000$, $\nu_{b0} = 1$, $\nu_p = 1.45$, $g_1 = -0.6 - 1.35i = g_2^*$, $g_3 = 2.5$, $g_4 = -1.6$, (b) Contour plot of the corresponding Figure 7.7(a); (c) 2D profile for interaction of breather-soliton structure, for $\beta_1 = 0.005$, $\beta_2 = 0.0054$, $\alpha = 0.4$, $\delta_b = 0.5$, $c_1 = 1000$, $\nu_{b0} = 1$, $\nu_p = 1.45$, $g_1 = -0.6 - 1.35i = g_2^*$, $g_3 = 2.5$, $g_4 = -1.6$, $\tau = 0.5$.

Case I. 1-Order breather and 2-soliton :

We can create a hybrid solution by account of both a 1-order breather and a 2-soliton solution by considering

$$K = 4,\ g_1 = p_{R1} + iq_{I1} = g_2^*,\ g_3 = g_3,\ g_4 = g_4,\ \Gamma_j^0 = 0\,(1 \leqslant j \leqslant 4). \tag{7.43}$$

Therefore, it is possible to express the $\mathcal{H}$ as

$$\begin{aligned}\mathcal{H} \;=\;& 1 + 2e^{m_1}\cos(m_2) + \mathcal{B}_{12}e^{2m_1} + 2\gamma_1 e^{m_1+\kappa_3}\cos(m_2+\sigma_1) + 2\gamma_2 e^{m_1+\kappa_4}\cos(m_2+\sigma_2)\\ &+\mathcal{B}_{12}\gamma_1^2 e^{2m_1+\kappa_3} + 2\mathcal{B}_{12}\gamma_2^2 e^{2m_1+\kappa_4} + \mathcal{B}_{12}\mathcal{B}_{34}\gamma_1^2\gamma_2^2 e^{2m_1+\kappa_3+\kappa_4}\\ &+ 2\mathcal{B}_{34}\gamma_1\gamma_2 e^{m_1+\kappa_3+\kappa_4}\cos(m_2+\sigma_1+\sigma_2),\end{aligned} \tag{7.44}$$

where

$$\begin{aligned}&m_1 = p_{R1}\xi - (Q(p_{R1}^3 - 3p_{R1}q_{I1}^2))\tau,\ m_2 = q_{I1}\xi - (Q(3p_{R1}^2 q_{I1} - q_{I1}^3))\tau, \kappa_3 = g_3\xi - Qg_3^3\tau,\\ &\kappa_4 = g_4\xi - Qg_4^3\tau,\ \mathcal{B}_{12} = \frac{q_{I1}^2}{p_{R1}^2},\ \mathcal{B}_{13} = -\frac{(p_{R1}+iq_{I1}-g_3)^2}{(p_{R1}+iq_{I1}+g_3)^2},\ \mathcal{B}_{13} = \mathcal{B}_{23}^* = \gamma_1 e^{i\sigma_1},\\ &\mathcal{B}_{14} = -\frac{(p_{R1}+iq_{I1}-g_4)^2}{(p_{R1}+iq_{I1}+g_4)^2},\ \mathcal{B}_{14} = \mathcal{B}_{24}^* = \gamma_2 e^{i\sigma_2},\ \mathcal{B}_{34} = -\frac{(g_3-g_4)^2}{(g_3+g_4)^2}.\end{aligned} \tag{7.45}$$

Therefore, we obtain a 1-order breather and 2-soliton solution $\psi = \frac{12B}{A}\left[\frac{\partial^2}{\partial\xi^2}\ln(\mathcal{H}(\xi,\tau))\right]$, where $\mathcal{H}$ is determined by Eq.(7.44).

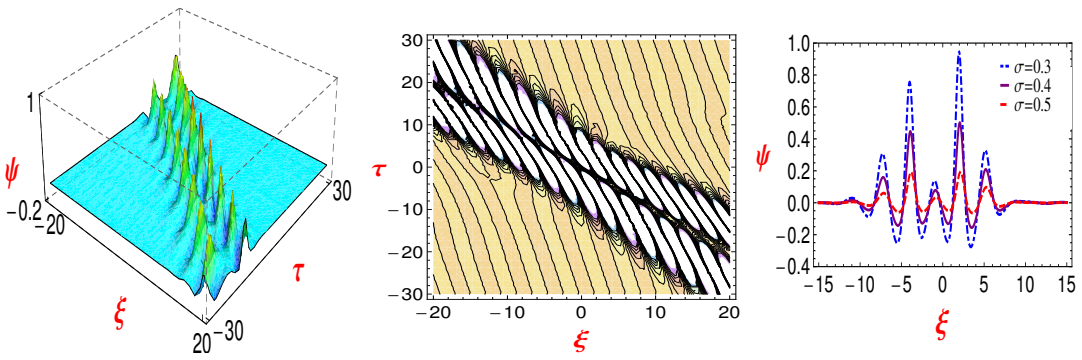

(a) (b) (c)

Figure 7.8: (a) 3D profile of 2-order breather structure, for $\beta_1 = 0.005$, $\beta_2 = 0.0054$, $\alpha = 0.4$, $\sigma = 0.5$, $\delta_b = 0.5$, $c_1 = 1000$, $\nu_{b0} = 1$, $\nu_p = 1.45$, $g_1 = -0.5 - 1.5i = g_2^*$, $g_3 = -0.5 - 1.8i = g_4^*$; (b) Contour plot of the corresponding Figure 7.8(a); (c) 2D profile of two order breather structure, for $\beta_1 = 0.005$, $\beta_2 = 0.0054$, $\alpha = 0.4$, $\delta_b = 0.5$, $c_1 = 1000$, $\nu_{b0} = 1$, $\nu_p = 1.45$, $g_1 = -0.5 - 1.5i = g_2^*$, $g_3 = -0.5 - 1.8i = g_4^*$, $\tau = 0.5$.

Case II. 2-Order breather :

If the established restrictive requirements are satisfied and the solution (7.42) with (7.32) of $K = 4$ is used, it is possible to quickly construct a 2-order breather type wave that is identical to (7.35),

$$g_1 = p_{R1} + iq_{I1} = g_2^*,\ g_3 = g_4^* = r_{R2} + is_{I2},\ \Gamma_1^0 = \Gamma_2^0 = 0. \tag{7.46}$$

Thus, $\mathcal{H}$ can be represented as

$$\begin{aligned}\mathcal{H} \quad = \quad & 1 + 2e^{m_1}\cos(m_2) + \mathcal{B}_{12}e^{2m_1} + 2e^{m_3}{}_{\cos}(m_4) + \mathcal{B}_{34}e^{2m_3} + 2\gamma_3 e^{m_1+m_3}\cos(m_2 + m_4 + \delta_3) + \\ & 2\gamma_4 e^{m_1+m_3}\cos(m_2 - m_4 + \delta_4) + 2\mathcal{B}_{12}\gamma_3\gamma_4 e^{2m_1+m_3}\cos(m_2 + \delta_3 - \delta_4) + \\ & 2\mathcal{B}_{34}\gamma_3\gamma_4 e^{m_1+2m_3}\cos(m_2 + \delta_3 + \delta_4) + \mathcal{B}_{12}\mathcal{B}_{34}\gamma_3^2\gamma_4^2 e^{2(m_1+m_3)},\end{aligned} \tag{7.47}$$

where

$$\begin{aligned}& m_1 = p_{R1}\xi - (Q(p_{R1}^3 - 3p_{R1}q_{I1}^2))\tau,\ m_2 = q_{I1}\xi - (Q(3p_{R1}^2 q_{I1} - q_{I1}^3))\tau, \\ & m_3 = r_{R2}\xi - (Q(r_{R2}^3 - 3r_{R2}s_{I2}^2))\tau,\ m_4 = s_{I2}\xi - (Q(3r_{R2}^2 s_{I2} - s_{I2}^3))\tau, \\ & \mathcal{B}_{12} = \frac{q_{I1}^2}{p_{R1}^2},\ \mathcal{B}_{13} = -\frac{(p_{R1} + i(q_{I1} + ir_{R2} - s_{I2}))^2}{(p_{R1} + iq_{I1} + r_{R2} + is_{I2})^2},\ \mathcal{B}_{13} = \mathcal{B}_{24}^* = \gamma_3 e^{i\delta_3}, \\ & \mathcal{B}_{14} = -\frac{(p_{R1} + i(q_{I1} + ir_{R2} + s_{I2}))^2}{(p_{R1} + iq_{I1} + r_{R2} - is_{I2})^2},\ \mathcal{B}_{14} = \mathcal{B}_{23}^* = \gamma_4 e^{i\delta_4},\ \mathcal{B}_{34} = \frac{s_{I2}^2}{r_{R2}^2}.\end{aligned} \tag{7.48}$$

It is noteworthy that function (7.47) can be substituted into Eq.(7.29) to yield a 2-order breather solution.

7.4.4 Discussion on breather and soliton interaction of the KdV system

In Figure 7.5(a), the breather is represented by the solution (7.37) for the KdV system, taking into account some particular values of the associated parameters and the corresponding contour plot is also presented in Figure 7.5(b). Figure 7.5(c) is drawn for presentation of the impact of σ in breather. It is observed in Figure 7.5(c) that the breather is depressed due to the increase in σ. This characteristic of the structure can be described in the following manner: when the ion's temperature rises in contrast to that of the electron, it negatively affects the potential energy of the system. As a result, the breather demonstrates a declining trend. Figure 7.6(a) is depicted to present the interaction of breather and soliton and the corresponding contour plot is exhibited in Figure 7.6(b). The interactive profile of soliton and breather under the variation of σ is expressed in Figure 7.6(c). The structure of the interaction of bi-soliton and breather is presented in Figure 7.7(a) whose contour plot is given in Figure 7.7(b). The propagation of the interactive wave is briefly described in Figure 7.7(c). The profile of the double breather and the contour plot is presented respectively in Figure 7.8(a) and Figure 7.8(b). As before, in Figure 7.8(c), we find the depressing tendency in breather structure for an enhancement in σ.

7.5 Nonlinear analysis of mKdV equation

The KdV equation is contingent upon A, which is determined by the parameters β_1, β_2, α, δ_b and σ. When specific values are assigned to these parameters (for example $\beta_1 = 0.005$, $\beta_2 = 0.0054$, $\alpha = 0.207$, $\delta_b = 0.5$, $\sigma = 0.1$), a critical point emerges where A equals zero. At this critical point, the nonlinearity disappears, rendering the KdV equation inadequate in describing the nonlinear evolution of perturbation. In such a case, to investigate the wave phenomena in the neighbouring zone of the above mentioned area, higher-order nonlinearity is taken into account to produce a new type of evolution equation, such as the mKdV equation. We introduce the new extended coordinates as follows in order to get the mKdV equation:

$$\xi = \epsilon\left(x - v_p t\right), \tau = \epsilon^3 t. \tag{7.49}$$

Substituting (7.49) and (7.3) in Eqs.(7.1) and comparing the coefficient of lowest order of ϵ, we can obtain the same relations (7.4)-(7.7). Comparing the coefficients of next higher order of ϵ, we get

$$n_{i2} = \frac{3v_p^2 + 3\sigma}{2\left(v_p^2 - 3\sigma\right)^3}\phi_1^2 + \frac{1}{\left(v_p^2 - 3\sigma\right)}\phi_2, \tag{7.50}$$

$$v_{i2} = \frac{v_p^3 + 9\sigma v_p}{2\left(v_p^2 - 3\sigma\right)^3}\phi_1^2 + \frac{v_p}{\left(v_p^2 - 3\sigma\right)}\phi_2, \tag{7.51}$$

$$p_{i2} = \frac{15\nu_p^2 - 9\sigma}{2\left(\nu_p^2 - 3\sigma\right)^3}\phi_1^2 + \frac{3}{\left(\nu_p^2 - 3\sigma\right)}\phi_2, \tag{7.52}$$

$$n_{e2} = \frac{1}{\left(3 - \beta_1\nu_p^2\right)}\phi_2 - \frac{3 + 3\beta_1\nu_p^2}{2\left(3 - \beta_1\nu_p^2\right)^3}\phi_1^2, \tag{7.53}$$

$$\nu_{e2} = \frac{\nu_p}{\left(3 - \beta_1\nu_p^2\right)}\phi_2 - \frac{\nu_p\left(9 + \beta_1\nu_p^2\right)}{2\left(3 - \beta_1\nu_p^2\right)^3}\phi_1^2, \tag{7.54}$$

$$p_{e2} = \frac{3}{\left(3 - \beta_1\nu_p^2\right)}\phi_2 + \frac{9 - 15\beta_1\nu_p^2}{2\left(3 - \beta_1\nu_p^2\right)^3}\phi_1^2, \tag{7.55}$$

$$n_{b2} = -\frac{3}{2c_1^2}\frac{\beta_2\nu_{b0}\left(\nu_p - \nu_{b0}\right)^3}{\omega^3\mu^3}\phi_1^2 + \frac{1}{\omega\mu}\phi_2 + \frac{3}{2\omega^2\mu^2}\phi_1^2$$
$$+\frac{3\alpha}{2\omega^2\mu^3}\phi_1^2 + \frac{9}{2c_1^2}\frac{\alpha\nu_{b0}\left(\nu_p - \nu_{b0}\right)}{\omega^3\mu^3}\phi_1^2 + \frac{9\alpha}{2\omega\mu^3}\phi_1^2, \tag{7.56}$$

,

$$\nu_{b2} = -\frac{3}{2c_1^2}\frac{\beta_2\nu_{b0}\left(\nu_p - \nu_{b0}\right)^4}{\omega^3\mu^3}\phi_1^2 + \frac{\left(\nu_p - \nu_{b0}\right)}{\omega\mu}\phi_2 + \frac{\left(\nu_p - \nu_{b0}\right)}{2\omega^2\mu^2}\phi_1^2$$
$$+\frac{3\alpha\left(\nu_p - \nu_{b0}\right)}{2\omega^2\mu^3}\phi_1^2 + \frac{9}{2c_1^2}\frac{\alpha\nu_{b0}\left(\nu_p - \nu_{b0}\right)^2}{\omega^3\mu^3}\phi_1^2 + \frac{9\alpha\left(\nu_p - \nu_{b0}\right)}{2\omega\mu^3}\phi_1^2, \tag{7.57}$$

$$p_{b2} = -\frac{3}{2c_1^2}\frac{\beta_2^2\nu_{b0}\left(\nu_p - \nu_{b0}\right)^5}{\alpha\omega^2\mu^3}\phi_1^2 + \frac{3}{\mu}\phi_2 + \frac{\beta_2\left(\nu_p - \nu_{b0}\right)^2}{2\alpha\omega\mu^2}\phi_1^2 + \frac{3\beta_2\left(\nu_p - \nu_{b0}\right)^2}{2\omega\mu^3}\phi_1^2$$
$$+\frac{9}{2c_1^2}\frac{\beta_2\nu_{b0}\left(\nu_p - \nu_{b0}\right)^3}{\omega^2\mu^3}\phi_1^2 + \frac{9\beta_2\left(\nu_p - \nu_{b0}\right)^2}{2\mu^3}\phi_1^2 + \frac{3}{2c_1^2}\frac{\beta_2\nu_{b0}\left(\nu_p - \nu_{b0}\right)^3}{\alpha\omega^2\mu^2}\phi_1^2 - \frac{1}{2\alpha\omega\mu}\phi_1^2. \tag{7.58}$$

If we continue to the next order of ϵ, we get

$$\frac{\partial n_{i1}}{\partial\tau} - \nu_p\frac{\partial n_{i3}}{\partial\xi} + \frac{\partial\nu_{i3}}{\partial\xi} + \frac{\partial}{\partial\xi}\left(n_{i1}\nu_{i2}\right) + \frac{\partial}{\partial\xi}\left(n_{i2}\nu_{i1}\right) = 0, \tag{7.59}$$

$$\frac{\partial\nu_{i1}}{\partial\tau} - \nu_p\frac{\partial\nu_{i3}}{\partial\xi} + \nu_{i1}\frac{\partial\nu_{i2}}{\partial\xi} + \nu_{i2}\frac{\partial\nu_{i1}}{\partial\xi} + \sigma\frac{\partial p_{i3}}{\partial\xi} - \sigma n_{i1}\frac{\partial p_{i2}}{\partial\xi} - \sigma n_{i2}\frac{\partial p_{i1}}{\partial\xi} + \sigma n_{i1}^2\frac{\partial p_{i1}}{\partial\xi} = -\frac{\partial\phi_3}{\partial\xi}, \tag{7.60}$$

$$\frac{\partial p_{i1}}{\partial\tau} - \nu_p\frac{\partial p_{i3}}{\partial\xi} + \nu_{i1}\frac{\partial p_{i2}}{\partial\xi} + \nu_{i2}\frac{\partial p_{i1}}{\partial\xi} + 3\frac{\partial\nu_{i3}}{\partial\xi} + 3p_{i1}\frac{\partial\nu_{i2}}{\partial\xi} + 3p_{i2}\frac{\partial\nu_{i1}}{\partial\xi} = 0, \tag{7.61}$$

$$\frac{\partial n_{e1}}{\partial\tau} - \nu_p\frac{\partial n_{e3}}{\partial\xi} + \frac{\partial\nu_{e3}}{\partial\xi} + \frac{\partial}{\partial\xi}\left(n_{e1}\nu_{e2}\right) + \frac{\partial}{\partial\xi}\left(n_{e2}\nu_{e1}\right) = 0, \tag{7.62}$$

$$\beta_1\frac{\partial\nu_{e1}}{\partial\tau} - \beta_1\nu_p\frac{\partial\nu_{e3}}{\partial\xi} - \beta_1\nu_p n_{e1}\frac{\partial\nu_{e2}}{\partial\xi} - \beta_1\nu_p n_{e2}\frac{\partial\nu_{e1}}{\partial\xi} + \beta_1\nu_{e1}\frac{\partial\nu_{e1}}{\partial\xi}$$
$$+\beta_1\nu_{e2}\frac{\partial\nu_{e1}}{\partial\xi} + \beta_1 n_{e1}\nu_{e1}\frac{\partial\nu_{e1}}{\partial\xi} + \frac{\partial p_{e3}}{\partial\xi} = \frac{\partial\phi_3}{\partial\xi} + n_{e1}\frac{\partial\phi_2}{\partial\xi} + n_{e2}\frac{\partial\phi_1}{\partial\xi}, \tag{7.63}$$

$$\frac{\partial p_{e1}}{\partial\tau} - \nu_p\frac{\partial p_{e3}}{\partial\xi} + \nu_{e1}\frac{\partial p_{e2}}{\partial\xi} + \nu_{e2}\frac{\partial p_{e1}}{\partial\xi} + 3\frac{\partial\nu_{e3}}{\partial\xi} + 3p_{e1}\frac{\partial\nu_{e2}}{\partial\xi} + 3p_{e2}\frac{\partial\nu_{e1}}{\partial\xi} = 0, \tag{7.64}$$

$$\frac{\partial n_{b1}}{\partial\tau} - \nu_p\frac{\partial n_{b3}}{\partial\xi} + \frac{\partial\nu_{b3}}{\partial\xi} + \frac{\partial}{\partial\xi}\left(n_{b1}\nu_{b2}\right) + \frac{\partial}{\partial\xi}\left(n_{b2}\nu_{b1}\right) + \nu_{b0}\frac{\partial n_{b3}}{\partial\xi} = 0, \tag{7.65}$$

$$\omega\beta_2\frac{\partial \nu_{b1}}{\partial \tau}-\omega\beta_2\left(\nu_p-\nu_{b0}\right)\frac{\partial \nu_{b3}}{\partial \xi}-\frac{1}{2c_1^2}\beta_2\left(\nu_p-\nu_{b0}\right)\frac{\partial \nu_{b1}^3}{\partial \xi}-\frac{3}{c_1^2}\beta_2\nu_{b0}\left(\nu_p-\nu_{b0}\right)\frac{\partial}{\partial \xi}\left(\nu_{b1}\nu_{b2}\right)$$
$$+\omega\beta_2\nu_{b1}\frac{\partial \nu_{b2}}{\partial \xi}+\omega\beta_2\nu_{b2}\frac{\partial \nu_{b1}}{\partial \xi}+\frac{3}{2c_1^2}\beta_2\nu_{b0}\nu_{b1}\frac{\partial \nu_{b1}^2}{\partial \xi}-\omega\beta_2\left(\nu_p-\nu_{b0}\right)n_{b1}\frac{\partial \nu_{b2}}{\partial \xi}$$
$$-\frac{3}{2c_1^2}\beta_2\nu_{b0}\left(\nu_p-\nu_{b0}\right)n_{b1}\frac{\partial \nu_{b1}^2}{\partial \xi}+\omega\beta_2 n_{b1}\nu_{b1}\frac{\partial \nu_{b1}}{\partial \xi}-\omega\beta_2\left(\nu_p-\nu_{b0}\right)n_{b2}\frac{\partial \nu_{b1}}{\partial \xi}$$
$$+\alpha\frac{\partial p_{b3}}{\partial \xi}=-\frac{\partial \phi_3}{\partial \xi}-n_{b1}\frac{\partial \phi_2}{\partial \xi}-n_{b2}\frac{\partial \phi_1}{\partial \xi}, \tag{7.66}$$
$$\frac{\partial p_{b1}}{\partial \tau}-\left(\nu_p-\nu_{b0}\right)\frac{\partial p_{b3}}{\partial \xi}+\nu_{b1}\frac{\partial p_{b2}}{\partial \xi}+\nu_{b2}\frac{\partial p_{b1}}{\partial \xi}+3\omega\frac{\partial \nu_{b3}}{\partial \xi}+3\omega p_{b1}\frac{\partial \nu_{b2}}{\partial \xi}$$
$$+\frac{9}{2c_1^2}\nu_{b0}p_{b1}\frac{\partial \nu_{b1}^2}{\partial \xi}+\frac{3}{2c_1^2}\frac{\partial \nu_{b1}^3}{\partial \xi}+\frac{9}{c_1^2}\nu_{b0}\frac{\partial}{\partial \xi}\left(\nu_{b1}\nu_{b2}\right)+3\omega p_{b2}\frac{\partial \nu_{b1}}{\partial \xi}=0, \tag{7.67}$$
$$\frac{\partial^2\phi_1}{\partial \xi^2}=\left(1+\delta_b\right)n_{e3}-\delta_b n_{b3}-n_{i3}. \tag{7.68}$$

From Eqs.(7.59)-(7.68), selecting $\phi_1=\psi$, we finally obtain the following mKdV equation

$$\frac{\partial \psi}{\partial \tau}+A_1\psi^2\frac{\partial \psi}{\partial \xi}+B\frac{\partial^3\psi}{\partial \xi^3}=0, \tag{7.69}$$

where

$$A_1=\frac{R_1}{P}, B=\frac{1}{P},$$

and

$$\begin{aligned}
P &= \left(1+\delta_b\right)\frac{2\beta_1\nu_p}{\left(3-\beta_1\nu_p^2\right)^2}+\delta_b\frac{2\beta_2\left(\nu_p-\nu_{b0}\right)}{\omega\mu^2}+\frac{2\nu_p}{\left(\nu_p^2-3\sigma\right)^2},\\
R_1 &= -\left(1+\delta_b\right)\frac{3(5\beta_1^2\nu_p^4+30\beta_1\nu_p^2+9)}{2\left(3-\beta_1\nu_p^2\right)^5}+\delta_b(-\frac{30}{2c_1^2}\frac{\nu_{b0}\left(\nu_p-\nu_{b0}\right)}{\omega^4\mu^3}-\frac{3}{2c_1^2}\frac{\left(\nu_p-\nu_{b0}\right)^2}{\omega^4\mu^3}+\frac{13}{2\omega^3\mu^3}+\\
&\frac{12\alpha}{\omega^3\mu^4}+\frac{\beta_2\left(\nu_p-\nu_{b0}\right)^2}{\omega^3\mu^4}-\frac{81}{2c_1^2}\frac{\alpha\nu_{b0}\left(\nu_p-\nu_{b0}\right)}{\omega^3\mu^4}+\frac{81\alpha}{2\omega^2\mu^4}+\frac{3\beta_2\left(\nu_p-\nu_{b0}\right)^2}{2\omega^2\mu^4}\\
&+\frac{27}{2c_1^4}\frac{\nu_{b0}^2\left(\nu_p-\nu_{b0}\right)^2}{\omega^5\mu^3}+\frac{3\alpha\beta_2\left(\nu_p-\nu_{b0}\right)^2}{\omega^3\mu^5}+\frac{9\alpha^2}{2\omega^3\mu^5}+\frac{27\alpha\beta_2\left(\nu_p-\nu_{b0}\right)^2}{2\omega^2\mu^5}+\frac{81\alpha^2}{2\omega^2\mu^5}+\frac{81\alpha^2}{\omega\mu^5}\\
&+\frac{27\alpha\beta_2\left(\nu_p-\nu_{b0}\right)^2}{2\omega\mu^5}-\frac{3}{2\omega^2\mu^3})+\frac{3\left(9\sigma^2+30\sigma\nu_p^2+5\nu_p^4\right)}{2\left(\nu_p^2-3\sigma\right)^5}-\frac{36}{2c_1^2}\frac{\alpha\nu_{b0}\left(\nu_p-\nu_{b0}\right)}{\omega^4\mu^4}.
\end{aligned} \tag{7.70}$$

7.6 Solutions of mKdV equation

7.6.1 Periodic wave structure of the mKdV equation

To observe nonlinear periodic waves in plasma environment, we now consider the mKdV framework. Utilizing the transformation (7.19), we derive a connection from Eq.(7.69) in below as,

$$\frac{1}{2}\left(\psi'\right)^2+V(\psi)=0. \tag{7.71}$$

The Sagdeev potential $V(\psi)$ reads

$$V(\psi) = \frac{A_1}{12Bk^2}\psi^4 - \frac{w}{2Bk^3}\psi^2 - \frac{\Gamma_1}{Bk^3}, \tag{7.72}$$

and Γ_1 is an integrating constant. A different approach to construct the equation is as follows:

$$(\psi')^2 = \frac{A_1}{6Bk^2}(r_1 - \psi^2)(\psi^2 - r_2), \tag{7.73}$$

where $r_1 = \frac{3w}{A_1 k} + \sqrt{\frac{9w^2}{A_1^2 k^2} + \frac{12\Gamma_1}{A_1 k}}$, $r_2 = \frac{3w}{A_1 k} - \sqrt{\frac{9w^2}{A_1^2 k^2} + \frac{12\Gamma_1}{A_1 k}}$ also $r_1 > 0$ and $r_2 < 0$.

$$\sqrt{\frac{A_1}{6Bk^2}}\,\Theta = \int \frac{dr}{\sqrt{(r_1 - \psi^2)(\psi^2 - r_2)}}. \tag{7.74}$$

Using the following transformation

$$\psi = \sqrt{r_1}\,\cos\theta, \tag{7.75}$$

we get

$$\begin{aligned}\sqrt{\frac{A_1}{6Bk^2}}\,\Theta &= \int \frac{d\psi}{\sqrt{(r_1 - \psi^2)(\psi^2 - r_2)}} \\ &= \frac{1}{\sqrt{r_1 - r_2}} \int \frac{d\theta}{\sqrt{1 - \kappa_1^2 {}^2\theta}},\end{aligned} \tag{7.76}$$

where $\kappa_1^2 = \frac{r_1}{r_1 - r_2}$. Jacobi's elliptic sine function [198, 144, 202, 203], which gives us the following results in this instance, is:

$$\sin\theta = sn\left(\sqrt{\frac{A_1}{6Bk^2}(r_1 - r_2)}\;\Theta, \kappa_1\right). \tag{7.77}$$

As a result, the answer to Eq. (7.73) is

$$\psi(\Theta) = \sqrt{r_1}\;cn\left(\sqrt{\frac{A_1}{6Bk^2}(r_1 - r_2)}\;\Theta, \kappa_1\right). \tag{7.78}$$

Hence, the periodic wave solution of mKdV Eq.(7.69) has the following formula:

$$\psi(\xi, \tau) = \sqrt{r_1}\;cn\left[\sqrt{\frac{A_1}{6Bk^2}(r_1 - r_2)}\;(k\xi - w\tau), \sqrt{\frac{r_1}{r_1 - r_2}}\right]. \tag{7.79}$$

It is evident that the periodic wave's amplitude is $\sqrt{r_1}$.

7.6.2 Solitary wave structure of mKdV equation

Now if $\Gamma_1 = 0$, then $r_1 = \frac{6w}{A_1 k}$, $r_2 = 0$ and then $\kappa_1 = 1$ and so the periodic solution (7.79) becomes a single solution as

$$\psi(\xi, \tau) = \psi_0\;sech\left(\frac{k\xi - w\tau}{w_d}\right). \tag{7.80}$$

where the amplitude reads $\psi_0 = \pm\sqrt{\frac{6w}{A_1 k}}$ and width reads $w_d = \sqrt{\frac{Bk^3}{w}}$.

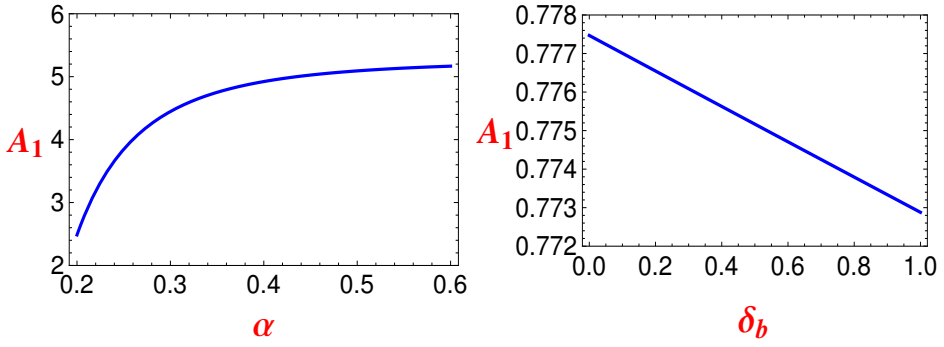

(a) (b)

Figure 7.9: 2D profile of (a) nonlinear coefficient A_1 vs α for $\beta_1 = 0.005$, $\beta_2 = 0.0054$, $\delta_b = 0.5$, $\sigma = 0.2$, $c_1 = 1000$, $\nu_{b0} = 1$, $\nu_p = 1.45$, (b) nonlinear coefficient A_1 vs δ_b for $\beta_1 = 0.005$, $\beta_2 = 0.0054$, $\alpha = 0.3$, $\sigma = 0.2$, $c_1 = 1000$, $\nu_{b0} = 1$, $\nu_p = 1.45$.

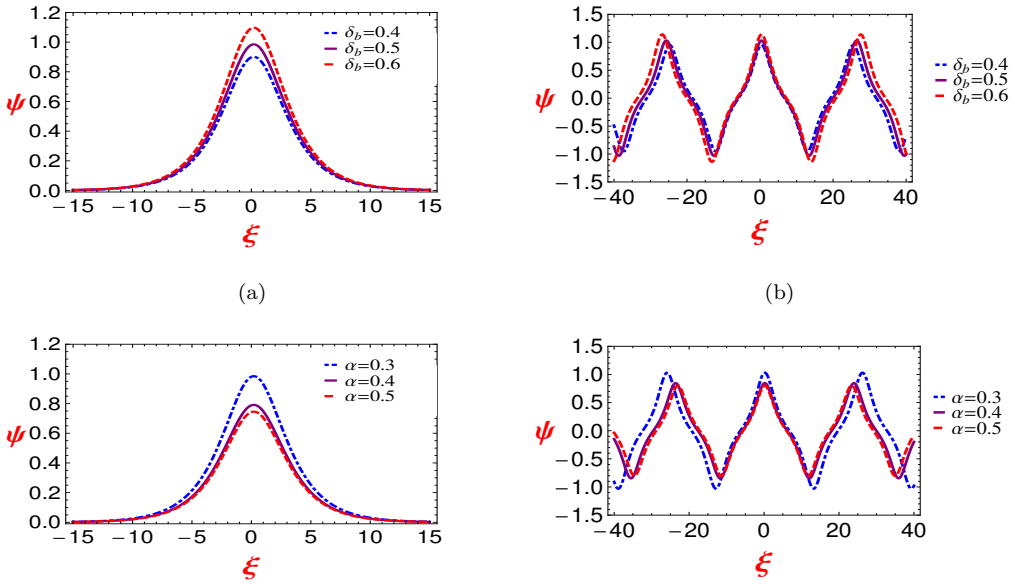

(a) (b)

(c) (d)

Figure 7.10: (a) The wave structure corresponding to solitary solution (7.80) for $\beta_1 = 0.005$, $\beta_2 = 0.0054$, $w = 0.2$, $k = 1$, $c_1 = 1000$, $\nu_{b0} = 1$, $\nu_p = 1.45$, $\tau = 1$, $\Gamma_1 = 0$, $\sigma = 0.1$, and $\alpha = 0.3$, (b) is the wave structure corresponding to periodic solution (7.79) for $\beta_1 = 0.005$, $\beta_2 = 0.0054$, $w = 0.2$, $k = 1$, $c_1 = 1000$, $\nu_{b0} = 1$, $\nu_p = 1.45$, $\tau = 1$, $\Gamma_1 = 0.01$, $\sigma = 0.1$, and $\alpha = 0.3$, (c) is the wave structure corresponding to solitary solution (7.80) for $\beta_1 = 0.005$, $\beta_2 = 0.0054$, $w = 0.2$, $k = 1$, $c_1 = 1000$, $\nu_{b0} = 1$, $\nu_p = 1.45$, $\tau = 1$, $\Gamma_1 = 0$, $\sigma = 0.1$, $\delta_b = 0.5$, (d) is the wave structure corresponding to periodic solution (7.79) for $\beta_1 = 0.005$, $\beta_2 = 0.0054$, $w = 0.2$, $k = 1$, $c_1 = 1000$, $\nu_{b0} = 1$, $\nu_p = 1.45$, $\tau = 1$, $\Gamma_1 = 0.01$, $\sigma = 0.1$, $\delta_b = 0.5$.

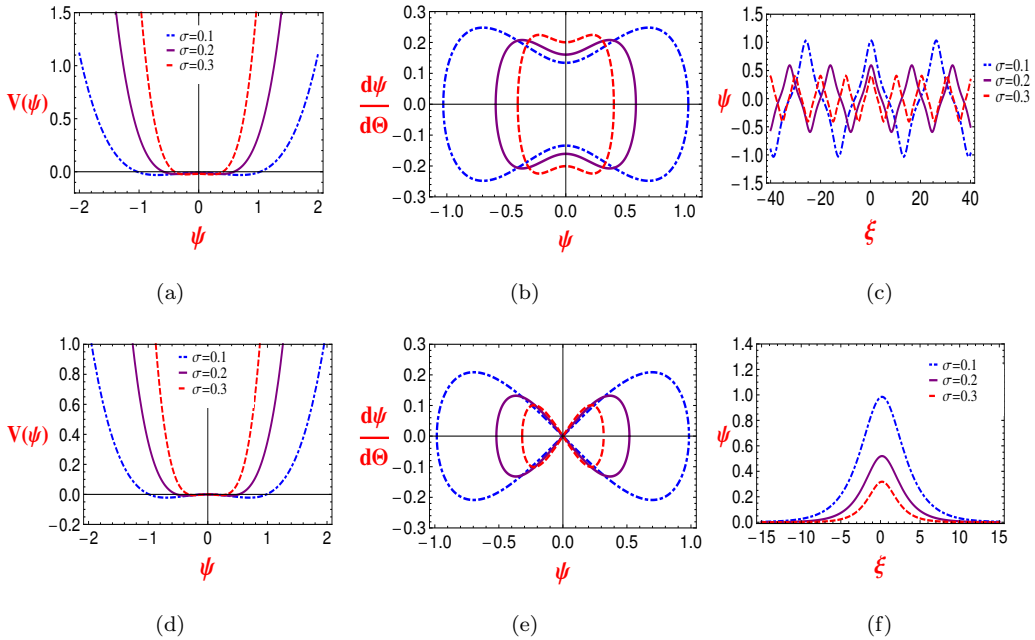

Figure 7.11: (a), (b), and (c) are the variation of σ on Sagdeev potential, phase plane, and wave structure corresponding to periodic solution (7.79) respectively for $\beta_1 = 0.005$, $\beta_2 = 0.0054$, $\alpha = 0.3$, $\delta_b = 0.5$, $w = 0.2$, $k = 1$, $c_1 = 1000$, $\nu_{b0} = 1$, $\nu_p = 1.45$, $\tau = 1$, $\Gamma_1 = 0.01$. (d), (e), and (f) are the variation of σ on Sagdeev potential, phase plane, and wave structure corresponding to solitary solution (7.80) respectively for $\beta_1 = 0.005$, $\beta_2 = 0.0054$, $\alpha = 0.3$, $\delta_b = 0.5$, $w = 0.2$, $k = 1$, $c_1 = 1000$, $\nu_{b0} = 1$, $\nu_p = 1.45$, $\Gamma_1 = 0$, $\tau = 1$.

7.6.3 Breather wave solution for the mKdV equation

We first replace ξ by $YB^{1/3}$, ψ by $\sqrt{24}VA_1^{-1/2}B^{1/6}$ and τ by T, Eq.(7.69) is then simplified into the standard mKdV equation as,

$$\frac{\partial V}{\partial T} + 24V^2\frac{\partial V}{\partial Y} + \frac{\partial^3 V}{\partial Y^3} = 0. \tag{7.81}$$

Utilizing the transformation

$$V = \arctan\left(\frac{\mathcal{F}(Y,T)}{\mathcal{G}(Y,T)}\right)_Y = \frac{\mathcal{F}_Y\mathcal{G} - \mathcal{F}\mathcal{G}_Y}{\mathcal{F}^2 + \mathcal{G}^2}, \tag{7.82}$$

in Eq.(7.81), we get the bilinear form of Eq.(7.81) as

$$D_T(\mathcal{F}.\mathcal{G}) + D_Y^3(\mathcal{F}.\mathcal{G}) = 0, \tag{7.83a}$$

$$D_Y^2(\mathcal{F}.\mathcal{F} + \mathcal{G}.\mathcal{G}) = 0, \tag{7.83b}$$

where the real variables Y and T are represented by the functions $\mathcal{F}$ and $\mathcal{G}$, and the Hirota operator is represented by D_T, D_Y^2, D_Y^3 [27, 156, 201]. The soliton and periodic solutions of the KdV and mKdV equations have been already studied. Specifically, now we focus on a unique form of breather solution within the mKdV equation [244]. These breathers represent special instances of two-soliton solutions, which manifest as spatially localized and time-periodic solutions. The breather solution is characterized by a bound two-soliton solution with complex conjugated wave vectors. By analyzing the expression of the two-soliton solution [245, 246] within the framework of Eqs.(7.83), we can gain further insights. Assuming,

$$\mathcal{F} = 1 + e^{\kappa_1} + e^{\kappa_2} + \mathcal{A}_{12}e^{\kappa_1+\kappa_2}, \tag{7.84a}$$

$$\mathcal{G} = 1 - e^{\kappa_1} - e^{\kappa_2} + \mathcal{A}_{12}e^{\kappa_1+\kappa_2} \tag{7.84b}$$

with

$$\kappa_j = g_j(Y + w_jT) + \Gamma_j^0,\ j = 1, 2$$

and under certain complex conjugate conditions, we find the wave vectors as,

$$g_1 = p_1 + iq_1 = g_2^*,\ \Gamma_1^0 = \Gamma_2^0 = 0. \tag{7.85}$$

Separating real and imaginary parts of κ_j as, $\kappa_1 = \theta_1 + i\theta_2$, $\kappa_2 = \theta_1 - i\theta_2$, the solutions $\mathcal{F}$ and $\mathcal{G}$ of Eqs.(7.83) in Eq.(7.84) can be written as

$$\mathcal{F} = 1 + 2e^{\theta_1}\cos(\theta_2) + \mathcal{A}_{12}e^{2\theta_1}, \tag{7.86a}$$

$$\mathcal{G} = 1 - 2e^{\theta_1}\cos(\theta_2) + \mathcal{A}_{12}e^{2\theta_1}. \tag{7.86b}$$

As a consequence of the gauge property [27, 247], $\mathcal{F}$ and $\mathcal{G}$ refer to the following

$$\mathcal{F} = e^{-\theta_1} + 2\cos(\theta_2) + \mathcal{A}_{12}e^{\theta_1}, \tag{7.87a}$$

$$\mathcal{G} = e^{-\theta_1} - 2\cos(\theta_2) + \mathcal{A}_{12}e^{\theta_1}. \tag{7.87b}$$

Now, we aim to find the breather-wave solutions of Eq.(7.69) using an extended version of test functions known as the extended homoclinic test approach [248, 249, 250]. We consider the following functions as,

$$\mathcal{F} = r_2 e^{\theta_1} + r_1\cos(\theta_2) + e^{-\theta_1}, \tag{7.88a}$$

$$\mathcal{G} = r_4 e^{\theta_1} + r_3\cos(\theta_2) + e^{-\theta_1}, \tag{7.88b}$$

$$\theta_1 = g_1(Y + c_1\tau),\ \theta_2 = g_2(Y + c_2\tau).$$

We shall eventually compute the constants used in the equation below. Replacing Eq.(7.88) into Eqs.(7.83) and bring altogether the coefficients of $e^{j\theta_1}$, $\cos(\theta_2)e^{j\theta_1}$ and $\sin(\theta_2)e^{j\theta_1}$, for $(j = -1, 0, 1)$ disappear, we obtained the following algebraic equations:

$$\text{coeff.of } e^{\theta_1}\cos(\theta_2) : (-g_1^3 r_1 r_4 + g_1^3 r_2 r_3 + 3g_1 g_2^2 r_1 r_4 - 3g_1 g_2^2 r_2 r_3 - c_1 g_1 r_1 r_4 + c_1 g_1 r_2 r_3) = 0, \tag{7.89a}$$

$$\text{coeff. of } \ e^{-\theta_1}\cos(\theta_2) : (g_1^3 r_1 - g_1^3 r_3 - 3g_1 g_2^2 r_1 + 3g_1 g_2^2 r_3 + c_1 g_1 r_1 - c_1 g_1 r_3) = 0, \tag{7.89b}$$

$$\text{coeff. of } e^{\theta_1}\sin(\theta_2) : (-3g_1^2 g_2 r_1 r_4 + 3g_1^2 g_2 r_2 r_3 + g_2^3 r_1 r_4 - g_2^3 r_2 r_3 - c_2 g_2 r_1 r_4 + c_2 g_2 r_2 r_3) = 0, \tag{7.89c}$$

$$\text{coeff. of } e^{-\theta_1}\sin(\theta_2) : (-3g_1^2 g_2 r_1 + 3g_1^2 g_2 r_3 + g_2^3 r_1 - g_2^3 r_3 - c_2 g_2 r_1 + c_2 g_2 r_3) = 0, \tag{7.89d}$$

$$\text{coefficient of} \quad e^{0.\theta_1}e^{0.\theta_2} : 8g_1^3 r_2 - 8g_1^3 r_4 + 2c_1 g_1 r_2 - 2c_1 g_1 r_4 = 0, \tag{7.89e}$$

and

$$\text{coefficient of} \quad e^{\theta_1}\cos(\theta_2) : (2g_1^2 r_1 r_2 + 2g_1^2 r_3 r_4 - 2g_2^2 r_1 r_2 - 2g_2^2 r_3 r_4) = 0, \tag{7.90a}$$

$$\text{coefficient of} \quad e^{-\theta_1}\cos(\theta_2) : (2g_1^2 r_1 + 2g_1^2 r_3 - 2g_2^2 r_1 - 2g_2^2 r_3) = 0, \tag{7.90b}$$

$$\text{coefficient of} \quad e^{\theta_1}\sin(\theta_2) : (4g_1 g_2 r_1 r_2 + 4g_1 g_2 r_3 r_4) = 0, \tag{7.90c}$$

$$\text{coefficient of} \quad e^{-\theta_1}\sin(\theta_2) : (-4g_1 g_2 r_1 - 4g_1 g_2 r_3) = 0, \tag{7.90d}$$

$$\text{coefficient of} \quad e^{0.\theta_1}e^{0.\theta_2} : -2g_2^2 r_1^2 - 2g_2^2 r_3^2 + 8g_1^2 r_2 + 8g_1^2 r_4 = 0. \tag{7.90e}$$

By solving the above algebraic equations, we obtain

$$r_2 = \frac{g_2^2}{4g_1^2},\ r_4 = \frac{g_2^2}{4g_1^2},\ r_3 = -r_1,\ c_1 = -g_1^2 + 3g_2^2,\ c_2 = g_2^2 - 3g_1^2, \tag{7.91}$$

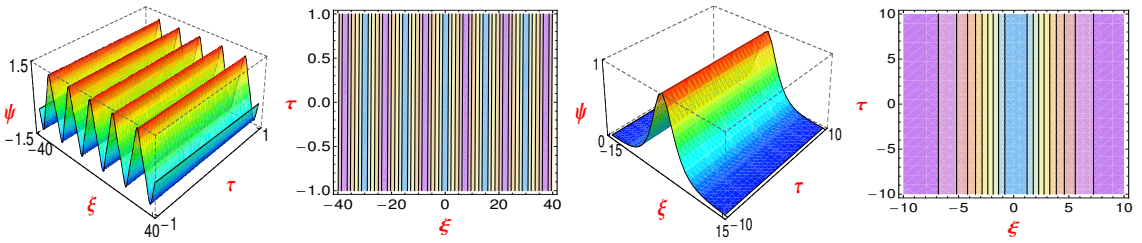

(a) (b) (c) (d)

Figure 7.12: (a) 3D profile of periodic structure (7.79) for $\beta_1 = 0.005$, $\beta_2 = 0.0054$, $\alpha = 0.3$, $\sigma = 0.1$, $\delta_b = 0.5$, $w = 0.2$, $k = 1$, $c_1 = 1000$, $\nu_{b0} = 1$, $\nu_p = 1.45$, $\Gamma_1 = 0.01$, (b) Contour plot of the corresponding Figure 7.12(a);(c) 3D profile of solitary structure (7.80) for $\beta_1 = 0.005$, $\beta_2 = 0.0054$, $\alpha = 0.3$, $\sigma = 0.1$, $\delta_b = 0.5$, $w = 0.2$, $k = 1$, $c_1 = 1000$, $\nu_{b0} = 1$, $\nu_p = 1.45$, (d) Contour plot of the corresponding Figure 7.12(c).

Following some calculations using Eq.(7.88), we arrive at

$$\mathcal{F} = 2\sqrt{r_2}\cosh(\theta_1) + r_1\cos(\theta_2),\ \mathcal{G} = 2\sqrt{r_4}\cosh(\theta_1) - r_{1\cos}(\theta_2). \tag{7.92}$$

Substituting Eq.(7.92) into Eq.(7.82), Eq.(7.69) has the following breather solutions in addition to the relations (7.91),

$$\psi_{br} = -\sqrt{\frac{24}{A_1}}B^{1/6}\,\frac{r_1(\sqrt{r_2}+\sqrt{r_4})(\sinh\eta_1\cos\eta_2 g_1 + \sin\eta_2\cosh\eta_1 g_2)}{(2\sqrt{r_2}\cosh(\eta_1) + r_{1\cos}(\eta_2))^2 + (2\sqrt{r_4}\cosh(\eta_1) - r_{1\cos}(\eta_2))^2}, \tag{7.93}$$

where

$$\eta_1 = g_1\left(\frac{\xi}{B^{1/3}} + (-g_1^2 + 3g_2^2)\tau\right),\ \eta_2 = g_2\left(\frac{\xi}{B^{1/3}} + (g_2^2 - 3g_1^2)\tau\right). \tag{7.94}$$

A homoclinic breather wave results from the interaction of the breather and homoclinic waves. A homoclinic breather wave form results from the interaction of two homoclinic waves. The hyperbolic functions $\sinh(\eta_1)$ and $\cosh(\eta_1)$, as well as the trigonometric functions $\sin(\eta_2)$ and $\cos(\eta_2)$, can be obtained to make up the answer (7.93). The breather wave propagates through periodic oscillation at a velocity

$$\nu_\xi = (3g_1^2 - g_2^2)B^{1/3}. \tag{7.95}$$

7.6.4 Discussion of the periodic, solitary and breather structures of the mKdV equation

It can be seen from solution (7.93) that solitons only occur in the case where $A_1 > 0$. Figure 7.9 illustrates how the coefficient A_1 varies in relation to the parameters α, δ_b. Based on varying values of α, δ_b, Figure 7.9 shows that all of the coefficient care values are positive. Thus,

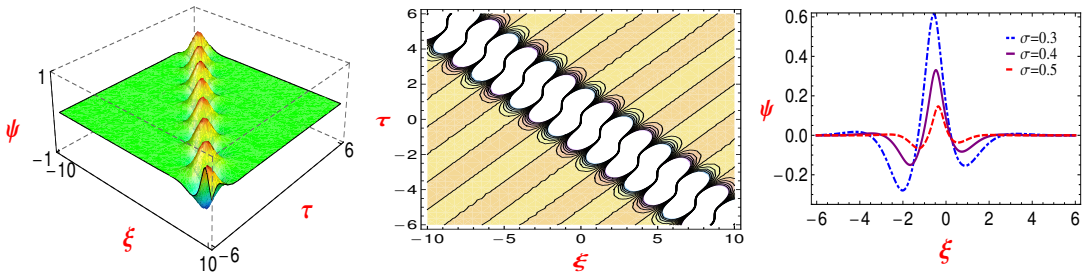

(a) (b) (c)

Figure 7.13: (a) 3D profile of breather structure (7.93) for $\beta_1 = 0.005$, $\beta_2 = 0.0054$, $\alpha = 0.3$, $\delta_b = 0.5$, $\sigma = 0.3$, $c_1 = 1000$, $\nu_{b0} = 1$, $\nu_p = 1.45, r_1 = 1$, $r_2 = -1, r_3 = 1$, $g_1 = 1$, $g_2 = 1$, (b) Contour plot of the corresponding Figure 7.13(a); (c) 2D profile of breather structure for $\beta_1 = 0.005$, $\beta_2 = 0.0054$, $\alpha = 0.3$, $\delta_b = 0.5$, $c_1 = 1000$, $\nu_{b0} = 1$, $\nu_p = 1.45, r_1 = 1$, $r_2 = -1, r_3 = 1$, $g_1 = 1$, $g_2 = 1$, $\tau = 0.5$.

for $\beta_1 = 0.005$, $\beta_2 = 0.0054$, $\delta_b = 0.5$, $\sigma = 0.2$, $c_1 = 1000$, $\nu_{b0} = 1$, $\nu_p = 1.45$, we see that the single waves are only compressive ones. In the mKdV framework, Figure 7.10(a) and Figure 7.10(b) illustrate the impact of δ_b on the solitary and periodic waves. Figure 7.10(a) shows that raising δ_b results in a boost in the amplitude of the solitary wave. Specifically, for $\delta_b \in (0.4, 0.6)$, the amplitude of the solitary wave in Figure 7.10(a) increases within the range of $(0.89, 1.09)$. This is observed while keeping the other parameters constant at $\sigma = 0.1$, and $\alpha = 0.3$. Similarly, in Figure 7.3(c), the KdV model demonstrates a similar pattern where the amplitude of the solitary wave lies within the range of $(0.69, 0.97)$ for the same values of δ_b. Other plasma parameters are the same as mentioned above. This study reveals that a rise in positron beam concentration results in a greater increase in amplitude in the mKdV model compared to the KdV model. Similar observations can be made in Figure 7.2(c) and Figure 7.10(b) for the periodic wave in both models.

Figure 7.10(c) and Figure 7.10(d) illustrate the influence of α on both solitary and periodic wave profiles in the mKdV framework. From Figure 7.10(c), it is clear that as α increases, the amplitude of the solitary wave decreases. The amplitude of the solitary wave range from 0.76 to 0.98 when $\alpha \in (0.3, 0.5)$, keeping other plasma parameters constant at $\sigma = 0.1$, and $\delta_b = 0.5$. On the other hand, in the KdV model (Figure 7.3(i)), the amplitude of the solitary wave range from 0.5 to 0.8 for the same values of α. Other plasma parameters are the same as mentioned above. However, it is evident that increasing the temperature of positron beam, compared to that of the electron, results in a more increase in the amplitude of the solitary wave within the mKdV framework compared to the KdV model. A similar observation can be made in Figure 7.2(i) and Figure 7.10(d) for enhancing α in both models.

Now, we talk about how the plasma parameter σ, which is the ratio of the temperature of an ion

to that of an electron, affects the wave propagation in the current plasma system. The fluctuation of the Sagdeev potential, the phase plot, and the related periodic solutions are each depicted in Figure 7.11(a), Figure 7.11(b), and Figure 7.11(c) respectively. It is evident from the distances of the Sagdeev potential curves and the phase plane curves from the vertical axis along parallel to horizontal axis that the periodic waves' amplitude shrinks to enhance the ion to electron temperature ratio parameter σ, as seen in Figure 7.11(c). Figure 7.11(d), Figure 7.11(e), and Figure 7.11(f), respectively, show the fluctuation of the Sagdeev potential, the phase plot, and the associated single solutions. By examining the distances of the Sagdeev potential curves and the phase plane curves from the vertical axis along parallel to horizontal axis (see. Figure 7.11(f)), it is clear that the amplitude of the solitary wave shrinks for enhancing the ion to electron temperature ratio parameter σ. The solitary wave's amplitude varies between 0.33 and 0.99 for $\sigma \in (0.1, 0.3)$, with $\alpha = 0.3$, and $\delta_b = 0.5$ remaining the same. Figure 7.3(f) illustrates a similar trend in the KdV model, with the amplitude ranging from 0.33 to 0.8 for same values of σ. The other plasma parameters remain unchanged. The Figure 7.12(a) and Figure 7.12(c) also depict the three-dimensional figure of a periodic and solitary wave of the mKdV model respectively, and their related contour mapping are shown respectively in Figure 7.12(b) and Figure 7.12(d). The periodic breather for the system under consideration is shown in Figure 7.13(a) through the solution (7.93), taking into account the specific values of the relevant parameters. The contour plot Figure 7.13(b) beautifully depict the top and bottom panels of the breather presented in Figure 7.13(a). Figure 7.13(c) illustrates the fluctuation of the parameter σ on the breather wave. It can be seen from the preceding image that increasing σ causes the breather's amplitude to shrink. The rise in ion temperature has caused a negative effect on the wave structure when compared to the electron's temperature. Furthermore, as σ increases, the wave velocity also significantly increases, consequently causing the wave to move forward.

7.7 Conclusion

Previously, inhomogeneous Burgers type models were used to investigate the motion of ion-acoustic wave in EPI plasma medium containing a relativistic positron beam [251]. For the first time, utilizing the KdV and mKdV models derived from the fundamental equation of plasma dynamics in a parametric setting, this article investigates the propagating characteristic of ion-acoustic periodic, solitary, and breather waves propagate in electron-ion plasmas with relativistic positron beams. *Numerical research reveals that* δ_b *(ratio of positron beam density to ion density),* α *(ratio of positron beam temperature to electron temperature) and* σ *(ratio of ion temperature to electron temperature) affect the wave dynamics in current plasma environment.* The presence of relativistic positron beams has a significant impact on the behavior of nonlinear waves, causing changes in the amplitude and width of wave structures. The analytical solutions of KdV and mKdV equations are numerically

analyzed and physical significance can be attributed to the fact that positron beams which are energy ingredient to the plasma system play a key role in destructing nonlinearity of the system as the beam concentration increases. In both periodic and solitary waves, the same type of propagating behavior is observable for variations in the parameters σ and α for KdV and mKdV models. An increase in the values of σ and α result in increased nonlinearity within the system, leading to a decrease in the amplitude of wave potentials. A negative impact follows on wave structures for enhancement in both parameters.

Breathers are typically contracted from KdV-type models using Schördinger-type models, which are produced from the aforementioned models via appropriate transformations. It needs to be noted that this study directly investigates numerous breather solutions from the KdV and mKdV models by assuming conjugates on the wave vectors. This article also emphasizes how different parameters affect the motion of breathers and its interactions. Under the same variations of parameters, the same type of behavior is observed in breather and solitary encounters. Our research may shed light on the dynamic behavior of solitons, periodic waves, breathers, and many other hybrid solitons propagation in the ionospheric region of the Earth's upper layer.

Chapter 8

Conclusions and future works

8.1 Conclusions

Different analytic techniques are introduced derive the solutions of different nonlinear models. On the other hand integrability of the aforementioned models is checked using painlevé property and Lax pair. Especially, the Hirota bilinear approach is employed to find soliton, shock, breather and various types' hybrid solutions for the autonomous as well as non-autonomous nonlinear evaluation equations. The incorporation of non-homogeneous forced terms offers a broader perspective in the examination of nonlinear wave propagation within disperse media. In the early chapters, we explore the behavior of this nonlinear wave as it evolves with changes in the order of the fractional time derivative. Additionally, we analyze the interplay between parameters such as the external periodic force coefficient and the frequency of the periodic force, illustrating these interactions through simulations. In the second phase, two nonlinear models namely KP and KPb are utilized to analyze the dynamical characteristic of IAW in dusty plasma. Finally, the impact of positron beam in the dynamics of IAW is studied in the previous chapter. The key finding of our investigation is addressed below in brief.

We study the integrability, exact solutions, and qualitative aspects of the non-autonomous Kadomtsev-Petviashvili (NKP) problem in chapter (2). Lax pairings, infinite conservation laws, and bilinear Bäcklund are used to study the features of integrability. For the aforementioned equation to be integrable, there are a few compatibility requirements.Using a binary Bell-polynomial obtained from the bilinear Bäcklund transformation, the infinite conservation rules of the NKP equation are shown directly. Using the Riemann theta function, the quasi-periodic solutions are obtained from the Bell-polynomial of the NKP equation. Numerical graphs and figures illustrate the important

roles played by the forcing and damping terms in the quasi-periodic waves. In the asymptotic analysis of the quasi-periodic solution, we investigate single soliton and bi-soliton solutions derived from the one and two periodic solutions of the NKP equation. It is therefore expected that periodic solutions may evolve into soliton or multi-soliton forms, contingent upon the periodicity of the quasi-periodic solution. Comprehensive studies have been conducted on the lump and breather waves of the NKP equation, taking into account variations in the forcing components. The findings indicate that various backgrounds of these wave quantities emerge as a result of different types of forcing components, alongside a notable diminishing effect in the breather wave attributed to the damping term. An analytical assessment has been performed to determine the maximum possible altitude of a lump. Additionally, a significant observation from the current studies is that both horseshoe-type lumps and breathers may arise due to the influence of externally applied forces on the NKP system.

In chapter (3), the integrability of the non-autonomous KP-mKP equation is analyzed through the lens of Painlevé integrability. A novel criterion for Painlevé integrability is introduced, which aligns precisely with the conditions necessary for the formulation of the Bilinear equation. Additionally, the chapter presents the development of two-component Lax systems and a four-field bilinear Bäcklund transformation, utilizing these mixed variables for the non-autonomous KP-mKP equation. By implementing appropriate parameter constraints and employing the long wave limiting process, various solutions are derived, including K-soliton solutions, $\mathfrak{m}$-breather solutions (for $\mathsf{K} = 2\mathfrak{m}$), hybrid solutions composed of both breathers and solitons (for $\mathsf{K} = 2\mathfrak{m} + \mathsf{k}$), as well as K-order smooth positons and $\mathfrak{m}$th-order breather positons for the non-autonomous KP-mKP equation. In the context of the non-autonomous KP-mKP system, a variety of intricate solution structures have been developed within the relevant parametric regions. These include configurations such as the kinky-breather, double kinky-breather, horseshoe-shaped breather, periodic position, kinky-breather-position, horseshoe-shaped breather-position, parabolic horseshoe-type breather, and double horseshoe-type breather, among others. The concept of modulation instability is employed to assess the stability of the derived solutions. Additionally, wave dispersion phenomena are utilized to elucidate the relationship between the phase velocity of the wave and its wave number. A qualitative analysis of the non-autonomous KP-mKP system reveals the presence of multistability, highlighting the solution's dependence on various parameters. This multistability signifies the coexistence of different types of solutions, including periodic, soliton, and shock solutions, corresponding to distinct sets of initial conditions. Typically, the behavior of nonhomogeneous evolution equations is examined primarily in two dimensions. However, adopting a three-dimensional perspective enables the damping coefficient to exert a considerable influence on dynamic behavior. Additionally, an analysis of the phase space concerning the non-autonomous KP-mKP system reveals numerous intriguing dynamic characteristics. The presence of various unstable spirals within the phase space suggests a rise in internal energy, which reflects the instability of the solutions. Moreover, an increase in

the intensity of the external periodic force contributes to the emergence of chaotic solutions. The emergence of chaos via intermittency indicates the presence of turbulence. Our analysis reveals that a significant amplitude of external force is necessary to induce instability and chaos through the distortion of low-energy orbits. Conversely, a comparatively minor amplitude of external force can produce intermittency and chaos by altering high-energy orbits. Therefore, systems characterized by low total energy exhibit greater stability against external disturbances than those in a high-energy state.

The exact solutions of the KP-mKP equation is also studied by employing complete discrimination system for polynomial method (CDSPM) in chapter (4). A spectrum of wave features including solitary waves, kink waves, shock waves, rational functions, exponential, singular waves, hyperbolic waves, and periodic waves derived from the KP-mKP equation. These solutions are qualitatively analyzed through numerical graphs, offering fresh insights into the properties of Jacobian elliptic functions. the existence and validity of the various topological structures of the solutions are confirmed from the phase portrait of the dynamical system.

In chapter (5), exact solutions of damped Gardner-Burger (dGB) equation is investigated using G'/G method and the method of undetermined coefficients. Different types of solutions such as kink soliton solution, singular periodic solution, rational solution, rarefactive soliton solution are obtained and with that effects of the coefficients of Burgers term and damping on solution structure also investigated for the dGB equation. In our observation we see rarefactive soliton for the damped Gardner-Burgers system, which gets deeper for higher values of damping and burgers coefficients. The amplitude of the damped Gardner-Burger's kink soliton increases with an increase in the dampness, On the other hand, higher values of burgers coefficient can reduce the height of the kink soliton of the damped Gardner-Burgers equation.

We conduct a further examination of the propagating characteristics of dust acoustic shocks, solitary waves, and periodic waves within a dusty plasma environment by introducing the KPb model (chapter (6)). The KPb system encompasses kink (or anti-kink) shaped shocks and solitary-type solitons. The presence of viscosity and the inter-collision of plasma particles contribute to the emergence of the Burgers effect within the KPb framework. Our findings indicate that an increase in the Burgers coefficient or viscosity coefficient (ζ_0) results in a downward movement of the solitary wave soliton. This outcome is anticipated, as an increase in ζ_0 leads to a reduction in the system's energy. Additionally, the amplitude of the kink is observed to rise with the increase in dissipation associated with the enhancement of ζ_0. The emergence of the wave structure in the current system is also significantly influenced by the ion temperature ratio β_1. It is observed that the dust acoustic shock increases (decreases) as β_1 increases, whereas increasing β_1 results in a reduction of the solitary type wave solution's depth. A similar conclusion can be drawn regarding parameter β_2. The soliton decreases both alone and in conjunction with the enhancement of density parameters (δ_1 and δ_2).

This is predicted since a higher density ratio (δ_1 and δ_2) leads to an increase in ion density, which in turn causes the dust acoustic soliton to become more intense. The KPb system has a limited amplitude periodic solution under specific circumstances. There is a considerable dependence of the periodic amplitude on the parameters β_1, β_2, and δ_1.

In chapter (7), we investigates the propagating characteristic of ion-acoustic periodic, solitary, and breather waves propagate in electron-ion plasmas with relativistic positron beams. Numerical research reveals that δ_b (ratio of positron beam density to ion density) has a significant impact in determining the amplitude and width of wave structures. Positron beams which are energy ingredient to the plasma system play a key role in destructing nonlinearity of the system as the beam concentration increases. On the other hand an increase in the values of σ (ratio of ion temperature to electron temperature) and α (ratio of positron beam temperature to electron temperature) result in increased nonlinearity within the system, leading to a decrease in the amplitude of ion acoustic wave potentials.

8.2 Future work

In the near future, we intend to investigate the integrability of certain variable coefficient nonlinear evolution equations, employing a methodology akin to that of our current research. Additionally, we aim to derive exact or hybrid solutions utilizing more robust techniques, such as the Darboux transformation. In this context, the inverse scattering method will also be relevant for obtaining analytical solutions of NLEEs with an initial seed solution. Furthermore, plasma fluid models present a rich domain of strongly nonlinear dynamic and evolutionary systems, characterized by various geometric and topological structures, including solitons, kinks, vortices, rogue waves, and others. The future study could be expanded in either of these directions, incorporating weak or strong perturbations from external source terms, as well as factors such as damping and viscosity. This report additionally examines the effects of periodic forcing and damping. In practical scenarios, it is probable that various forms of external perturbations, such as Exponential and Gaussian forcing, as well as Sech-hyperbolic forcing, may occur, often in combination with other force terms. A thorough exploration of these source terms would undoubtedly yield significant insights. For example, the Sec-hyperbolic soliton surface geometry is characterized by its smoothness, at least under the assumed conditions, and is anticipated to maintain this smoothness for a sufficiently extended time period before dissipating. In cases of strong perturbation, the initially smooth solitonic structure is expected to evolve into intricate fractal-like geometries over time, even in the absence of external disturbances. Furthermore, it would be beneficial to expand upon the current research by employing the innovative asymptotic method [252, 253, 254, 255, 256] recently developed to achieve the aforementioned objectives.

Publications from the content of the Thesis

1. **Tanay Sarkar**, Santanu Raut, and Prakash Chandra Mali (2022): **The classification of the exact single travelling wave solutions to the constant coefficient KP-mKP equation employing complete discrimination system for polynomial method**, Computational and Mathematical Methods, 2022.

2. **Tanay Sarkar**, Santanu Raut, and Prakash Chandra Mali (2023): **Studies on the dust acoustic shock, solitary, and periodic waves in an unmagnetized viscous dusty plasma with two-temperature ions**, Brazilian Journal of Physics, 53(1), 12.

3. Santanu Raut, Ranjan Barman, and **Tanay Sarkar** (2023): **Integrability, breather, lump and quasi-periodic waves of non-autonomous Kadomtsev–Petviashvili equation based on Bell-polynomial approach**, Wave Motion, 119, 103125.

4. **Tanay Sarkar**, Raut, S., and N. M. Chadha (2023, August): **Analytical solutions of damped gardner-burgers equation using two expansion methods**, In AIP Conference Proceedings (Vol. 2852, No. 1). AIP Publishing.

5. Santanu Raut, **Tanay Sarkar**, Subrata Roy, and Aniriddha Palit (2024): **Characteristic of integrability of nonautonomous KP-modified KP equation and its qualitative studies: soliton, shock, periodic waves, breather, positons and soliton interactions**, Nonlinear Dynamics, 112, 9323–9354.

6. Ashim Roy, **Tanay Sarkar**, Subrata Roy, Santanu Raut (2024): **Impact of relativistic positron beam on ion-acoustic solitary, periodic and breather waves in Earths' ionospheric region through the framework of KdV and modified KdV equation**, Physica Scripta, 99(12), 125603.

Bibliography

[1] Rogers, C., and Shadwick, W.R. (1982) Bäcklund transformations and their application (Mathematics in Science and Engineering), Academic Press, New York, vol. 161.

[2] Ablowitz, M. J., & Clarkson, P. A. (1991) Solitons, nonlinear evolution equations and inverse scattering (Vol. 149), Cambridge university press.

[3] Kudryashov, N. A. (1990) Exact solutions of the generalized Kuramoto-Sivashinsky equation, Physics Letters A, 147(5-6), 287-291.

[4] Hirota, R. (1971) Exact solution of the Korteweg—de Vries equation for multiple collisions of solitons, Physical Review Letters, 27(18), 1192.

[5] Wazwaz, A. M. (2007) The tanh–coth method for solitons and kink solutions for nonlinear parabolic equations, Applied Mathematics and Computation, 188(2), 1467-1475.

[6] Grimshaw, R. (1981) Evolution equations for long, nonlinear internal waves in stratified shear flows, Studies in Applied Mathematics, 65(2), 159-188.

[7] Helal, M. A., & El-Eissa, H. N. (1996) Shallow water waves and Korteweg-de Vries equation (oceanographical application), Pure Mathematics and Applications, 7(3-4), 263-282.

[8] Alhejaili, W., Roy, S., Raut, S., Roy, A., Salas, A. H., Aboelenen, T., & El-Tantawy, S. A. (2024) Analytical solutions to (modified) Korteweg–de Vries–Zakharov–Kuznetsov equation and modeling ion-acoustic solitary, periodic, and breather waves in auroral magnetoplasmas, Physics of Plasmas, 31(8).

[9] Fuchssteiner, B. (1993) Integrable nonlinear evolution equations with time-dependent coefficients, Journal of mathematical physics, 34(11), 5140-5158.

[10] Johnpillai, A. G., & Khalique, C. M. (2011) Variational approaches to conservation laws for a nonlinear evolution equation with time dependent coefficients, Quaestiones Mathematicae, 34(2), 235-245.

[11] Liu, H., Li, J., & Liu, L. (2010) Painlevé analysis, Lie symmetries, and exact solutions for the time-dependent coefficients Gardner equations, Nonlinear Dynamics, 59(3), 497-502.

[12] Xiao-Yan, T., Yuan, G., Fei, H., & Sen-Yue, L. (2009) Variable coefficient nonlinear systems derived from an atmospheric dynamical system, Chinese Physics B, 18(11), 4622.

[13] Liu, J. G., & Osman, M. S. (2022) Nonlinear dynamics for different nonautonomous wave structures solutions of a 3D variable-coefficient generalized shallow water wave equation, Chinese Journal of Physics, 77, 1618-1624.

[14] Wang, Y. F., Tian, B., Li, M., Wang, P., & Wang, M. (2014) Integrability and soliton-like solutions for the coupled higher-order nonlinear Schrödinger equations with variable coefficients in inhomogeneous optical fibers, Communications in Nonlinear Science and Numerical Simulation, 19(6), 1783-1791.

[15] Tian, S. F., & Zhang, H. Q. (2014) On the integrability of a generalized variable-coefficient forced Korteweg-de Vries equation in fluids, Studies in Applied Mathematics, 132(3), 212-246.

[16] Ghosh, U., Roy, S., Biswas, S., & Raut, S. (2024) A non-autonomous fractional granular model: Multi-shock, Breather, Periodic, Hybrid solutions and Soliton interactions, Chaos, Solitons & Fractals, 187, 115393.

[17] Raut, S., Mondal, K. K., Chatterjee, P., & Roy, A. (2021) Two-dimensional ion-acoustic solitary waves obliquely propagating in a relativistic rotating magnetised electron–positron–ion plasma in the presence of external periodic force, Pramana, 95(2), 73.

[18] Roy, A., Mondal, K. K., Chatterjee, P., & Raut, S. (2022) Influence of external periodic force on ion acoustic waves in a magnetized dusty plasma through forced KP equation and modified forced KP equation, Brazilian Journal of Physics, 52(3), 65.

[19] Moser, J. (1980) Various aspects of integrable Hamiltonian systems, Dynamical Systems: Lectures given at a Summer School of the Centro Internazionale Matematico Estivo (CIME), held in Bressanone (Bolzano), Italy, June 19–27, 1978, 137-195.

[20] Ablowitz, M. J., & Segur, H. (1981) Solitons and the inverse scattering transform, Society for Industrial and Applied Mathematics, Philadelphia.

[21] Ablowitz, M. J., Kaup, D. J., Newell, A. C., & Segur, H. (1974) The inverse scattering transform-Fourier analysis for nonlinear problems, Studies in applied mathematics, 53(4), 249-315.

[22] Novikov, S., Manakov, S. V., Pitaevskii, L. P., & Zakharov, V. E. (1984) Theory of solitons: the inverse scattering method, Springer Science & Business Media.

[23] Ponce, G. (1993) Lax pairs and higher order models for water waves, Journal of differential equations, 102(2), 360-381.

[24] Lou, S. Y., & Hu, X. B. (1997) Infinitely many Lax pairs and symmetry constraints of the KP equation, Journal of Mathematical Physics, 38(12), 6401-6427.

[25] Al Khawaja, U. (2010) A comparative analysis of Painlevé, Lax pair, and similarity transformation methods in obtaining the integrability conditions of nonlinear Schrödinger equations, Journal of Mathematical Physics, 51(5).

[26] Gardner, C.S., Greene, J.M., Kruskal, M.D., and Miura, R.M. (1967) Method for Solving the Korteweg-de Vries Equation, Phys. Rev. Lett. 19, 1095–1097.

[27] Hirota, R. (2004) The direct method in soliton theory (No. 155), Cambridge University Press, Cambridge.

[28] Conte, R. M., & Musette, M. (2008) The Painlevé Handbook, Dordrecht: Springer Science+ Business Media B.V.

[29] Conte, R. (Ed.). (2012) The Painlevé property: one century later, Springer Science & Business Media.

[30] Lamb Jr, G. L. (1974) Bäcklund transformations for certain nonlinear evolution equations, Journal of Mathematical Physics, 15(12), 2157-2165.

[31] Wadati, M., Sanuki, H., & Konno, K. (1975) Relationships among inverse method, Bäcklund transformation and an infinite number of conservation laws, Progress of theoretical physics, 53(2), 419-436.

[32] Konno, K., Sanuki, H., & Ichikawa, Y. H. (1974) Conservation laws of nonlinear-evolution equations, Progress of Theoretical Physics, 52(3), 886-889.

[33] Hereman, W. (2006) Symbolic computation of conservation laws of nonlinear partial differential equations in multi-dimensions, International journal of quantum chemistry, 106(1), 278-299.

[34] Fokas, A. S. (1987) Symmetries and integrability, Studies in Applied Mathematics, 77(3), 253-299.

[35] Biswas, S., Ghosh, U., & Raut, S. (2023) Construction of fractional granular model and bright, dark, lump, breather types soliton solutions using Hirota bilinear method, Chaos, Solitons & Fractals, 172, 113520.

[36] Chen, H. H. (1975) A Bäcklund transformation in two dimensions, Journal of Mathematical Physics, 16(12), 2382-2384.

[37] Wazwaz, A. M. (2004) The tanh method for traveling wave solutions of nonlinear equations, Applied Mathematics and Computation, 154(3), 713-723.

[38] Wang, M., Li, X., & Zhang, J. (2008) The (G'/G)-expansion method and travelling wave solutions of nonlinear evolution equations in mathematical physics, Physics Letters A, 372(4), 417-423.

[39] Matveev, V. B. (1992) Positon-positon and soliton-positon collisions: KdV case, Physics Letters A, 166(3-4), 209-212.

[40] Dubard, P., Gaillard, P., Klein, C., & Matveev, V. B. (2010) On multi-rogue wave solutions of the NLS equation and positon solutions of the KdV equation, The European Physical Journal Special Topics, 185(1), 247-258.

[41] Vishnu Priya, N., Senthilvelan, M., & Lakshmanan, M. (2013) Akhmediev breathers, Ma solitons, and general breathers from rogue waves: A case study in the Manakov system, Physical Review E—Statistical, Nonlinear, and Soft Matter Physics, 88(2), 022918.

[42] Dudley, J. M., Dias, F., Erkintalo, M., & Genty, G. (2014) Instabilities, breathers and rogue waves in optics, Nature Photonics, 8(10), 755-764.

[43] Raut, S. (2024) Integrability, and stability aspects for the non-autonomous perturbed Gardner KP equation: Solitons, breathers, Y-type resonance and soliton interactions, Wave Motion, 130, 103373.

[44] Satsuma, J., & Ablowitz, M. J. (1979) Two-dimensional lumps in nonlinear dispersive systems, Journal of Mathematical Physics, 20(7), 1496-1503.

[45] Ma, W. X., & Zhang, L. (2020) Lump solutions with higher-order rational dispersion relations, Pramana, 94, 1-7.

[46] Ma, W. X., Zhou, R., & Gao, L. (2009) Exact one-periodic and two-periodic wave solutions to Hirota bilinear equations in (2+ 1) dimensions, Modern Physics Letters A, 24(21), 1677-1688.

[47] Qin, C. Y., Tian, S. F., Zou, L., & Ma, W. X. (2018) Solitary wave and quasi-periodic wave solutions to a (3+ 1)-dimensional generalized Calogero-Bogoyavlenskii-Schiff equation, Adv. Appl. Math. Mech, 10(4), 948-977.

[48] Michel, A., Wang, A., Hu, B., Nashed, Z., & Taft, E. (2001) Qualitative theory of dynamical systems, CRC Press.

[49] Bhatia, N. P., & Szegö, G. P. (2002) Stability theory of dynamical systems, Springer Science & Business Media.

[50] Shil'nikov, L. P. (2001) Methods of qualitative theory in nonlinear dynamics (Vol. 5), World Scientific.

[51] Palit, A., Roy, A., & Raut, S. (2022) Qualitative studies of the influence of damping and external periodic force on ion-acoustic waves in a magnetized dusty plasma through modified ZK equation, Brazilian Journal of Physics, 52(4), 110.

[52] Strogatz, S. H. (2018) Nonlinear dynamics and chaos: with applications to physics, biology, chemistry, and engineering, CRC press.

[53] Raut, S., Sarkar, T., Roy, S., & Palit, A. (2024) Characteristic of integrability of nonautonomous KP-modified KP equation and its qualitative studies: soliton, shock, periodic waves, breather, positons and soliton interactions, Nonlinear Dynamics, 112, 9323-9354.

[54] Chadha, N. M., Tomar, S., & Raut, S. (2023) Parametric analysis of dust ion acoustic waves in superthermal plasmas through non-autonomous KdV framework, Communications in Nonlinear Science and Numerical Simulation, 123, 107269.

[55] Ichimaru, S. (1993) Nuclear fusion in dense plasmas, reviews of modern physics, 65(2), 255.

[56] Lakhina, G. S., Singh, S. V., Kakad, A. P., Verheest, F., & Bharuthram, R. (2008) Study of nonlinear ion-and electron-acoustic waves in multi-component space plasmas, Nonlinear Processes in Geophysics, 15(6), 903-913.

[57] Sreeraj, T., Singh, S. V., & Lakhina, G. S. (2016) Coupling of electrostatic ion cyclotron and ion acoustic waves in the solar wind, Physics of Plasmas, 23(8).

[58] Chen, F. F. (1995) Industrial applications of low-temperature plasma physics, Physics of Plasmas, 2(6), 2164-2175.

[59] Ito, T., Izaki, T., & Terashima, K. (2001) Application of microscale plasma to material processing, Thin solid films, 386(2), 300-304.

[60] Levchenko, I., Xu, S., Mazouffre, S., Lev, D., Pedrini, D., Goebel, D., ... & Bazaka, K. (2020) Perspectives, frontiers, and new horizons for plasma-based space electric propulsion, Physics of Plasmas, 27(2).

[61] Rezaei, F., Vanraes, P., Nikiforov, A., Morent, R., & De Geyter, N. (2019) Applications of plasma-liquid systems: A review, Materials, 12(17), 2751.

[62] Merlino, R. L. (2014) 25 years of dust acoustic waves, Journal of Plasma Physics, 80(6), 773-786.

[63] Shukla, P. K., & Ali, S. (2005) Dust acoustic waves in quantum plasmas, Physics of plasmas, 12(11), 114502.

[64] Shukla, P. K., & Mamun, A. A. (2015) Introduction to dusty plasma physics, CRC press.

[65] Zabusky, N. J., & Kruskal, M. D. (1965) Interaction of" solitons" in a collisionless plasma and the recurrence of initial states, Physical review letters, 15(6), 240.

[66] Lax, P. D. (1968) Integrals of nonlinear equations of evolution and solitary waves, Communications on Pure and Applied Mathematics, 21(5), 467–490.

[67] Fokas, A. S. (2022) Integrable nonlinear evolution equations in three spatial dimensions, Proceedings of the Royal Society A: Mathematical, Physical and Engineering Sciences, 478(2263), 20220074.

[68] Weiss, J., Tabor, M., & Carnevale, G. (1983) The Painlevé property for partial differential equations, Journal of Mathematical Physics, 24(3), 522-526.

[69] Korteweg, D. J., & De Vries, G. (1895) XLI. On the change of form of long waves advancing in a rectangular canal, and on a new type of long stationary waves, The London, Edinburgh, and Dublin Philosophical Magazine and Journal of Science, 39(240), 422-443.

[70] Saha, D., Chatterjee, P., & Raut, S. (2023) Multi-shock and soliton solutions of the Burgers equation employing Darboux transformation with the help of the Lax pair, Pramana, 97(2), 54.

[71] Chatterjee, P., Saha, D., Wazwaz, A. M., & Raut, S. (2023) Explicit solutions of the Schamel–KdV equation employing Darboux transformation, Pramana, 97(4), 172.

[72] Pal, N. K., Nasipuri, S., Chatterjee, P., & Raut, S. (2024) Bilinear Bäcklund transformation, Lax pair, Darboux transformation, multi-soliton, periodic wave, complexiton, higher-order breather and rogue wave for geophysical Boussinesq equation, Pramana, 98(3), 110.

[73] Holmes, P. (1990) Poincaré, celestial mechanics, dynamical-systems theory and "chaos", Physics Reports, 193(3), 137-163.

[74] Verhulst, F. (2016) Henri Poincaré's inventions in dynamical systems and topology, The foundations of chaos revisited: from Poincaré to recent advancements, 1-25.

[75] Birkhoff, G. D. (1927) Dynamical systems, American Mathematical Society (Vol. 9).

[76] Lorenz, E. N. (1963) Deterministic nonperiodic flow, Journal of atmospheric sciences, 20(2), 130-141.

[77] Revans, D. (1933) Low-frequency oscillations in ionized gases, Proceedings of the Physical Society, 45(2), 139-148

[78] Ikezi, H., Taylor, R. J., & Baker, D. R. (1970) Formation and interaction of ion-acoustic solitions, Physical Review Letters, 25(1), 11.

[79] Ikezi, H. (1973) Experiments on ion-acoustic solitary waves, Research Report: IPPJ.

[80] Thompson, C., Barkan, A., D'angelo, N., & Merlino, R. L. (1997) Dust acoustic waves in a direct current glow discharge, Physics of Plasmas, 4(7), 2331-2335.

[81] Tonks, L., and Langmuir, I. (1929) Oscillations in Ionized Gases, Phys. Rev. 33(2), 195.

[82] Post, R. F. (1956) Controlled fusion research—an application of the physics of high temperature plasmas, Reviews of Modern Physics, 28(3), 338.

[83] Gill, R. D. (Ed.). (2013) Plasma physics and nuclear fusion research, Academic Press.

[84] Rao, N. N., Shukla, P. K., & Yu, M. Y. (1990) Dust-acoustic waves in dusty plasmas, Planetary and space science, 38(4), 543-546.

[85] Barkan, A., Merlino, R. L., D'Angelo, N. (1995) Laboratory observation of the dust-acoustic wave mode, Physics of Plasmas, 2(10), 3563–3565.

[86] Kadomtsev, B. B., & Petviashvili, V. I. (1970) On the stability of solitary waves in weakly dispersing media, In Doklady Akademii Nauk (Vol. 192, No. 4, pp. 753-756), Russian Academy of Sciences.

[87] Ablowitz, M. J., & Segur, H. (1979) On the evolution of packets of water waves, Journal of Fluid Mechanics, 92(4), 691-715.

[88] Pelinovsky, D. E., Stepanyants, Y. A., & Kivshar, Y. S. (1995) Self-focusing of plane dark solitons in nonlinear defocusing media, Physical Review E, 51(5), 5016.

[89] Chen, H. H. (1975) A Bäcklund transformation in two dimensions, Journal of Mathematical Physics, 16(12), 2382-2384.

[90] Satsuma, J. (1976) N-soliton solution of the two-dimensional Korteweg-de Vries equation, J. Phys. Soc. Japan 40, 286-90.

[91] Manakov, S. V. (1981) Inverse scattering transform for the time-dependent Schrödinger equation and Kadomtsev-Petviashvili equation, Physica D (Amsterdam);(Netherlands), 3(1/2).

[92] Fokas, A. S., & Ablowitz, M. J. (1983) On the Inverse Scattering of the Time-Dependent Schrödinger Equation and the Associated Kadomtsev-Petviashvili (I) Equation, Studies in Applied Mathematics, 69(3), 211-228.

[93] Ablowitz, M. J., Yaacov, D. B., & Fokas, A. S. (1983) On the inverse scattering transform for the Kadomtsev-Petviashvili equation, Studies in Applied Mathematics, 69(2), 135-143.

[94] Li, L., Xie, Y., Yan, Y., Wang, M. (2022) A new extended (2+1)-dimensional Kadomtsev-Petviashvili equation with N-solitons, periodic solutions, rogue waves, breathers and lump waves, Results Phys. 39, 105678.

[95] Wazwaz, A. M. (2023) Painlevé integrability and lump solutions for two extended (3 + 1)- and (2 + 1)-dimensional Kadomtsev–Petviashvili equations, Nonlinear Dyn 111, 3623–3632.

[96] Konopelchenko, B. G., & Dubrovsky, V. G. (1984) Some new integrable nonlinear evolution equations in 2+ 1 dimensions, Physics Letters A, 102(1-2), 15-17.

[97] Naz, R., Ali, Z., & Naeem, I. (2013) Reductions and new exact solutions of ZK, Gardner KP, and modified KP equations via generalized double reduction theorem, Abstract and Applied Analysis (Vol. 2013, No. 1, p. 340564), Hindawi Publishing Corporation.

[98] Wazwaz, A. M. (2014) Multiple kink solutions for the (2+ 1)-dimensional integrable Gardner equation, Proc. Romanian Acad. A, 15(3), 241-246.

[99] Clarkson, P. A. (1990) Painlevé analysis and the complete integrability of a generalized variable-coefficient Kadomtsev-Petviashvili equation, IMA journal of applied mathematics, 44(1), 27-53.

[100] Tian, S. F., & Zhang, H. Q. (2012) On the integrability of a generalized variable-coefficient Kadomtsev–Petviashvili equation, Journal of Physics A: Mathematical and Theoretical, 45(5), 055203.

[101] Yan, X., Liu, J., & Xin, X. (2023) Soliton solutions and lump-type solutions to the (2+ 1)-dimensional Kadomtsev-Petviashvili equation with variable coefficient, Physics Letters A, 457, 128574.

[102] Ma, W. X. (2015) Lump solutions to the Kadomtsev–Petviashvili equation, Physics Letters A, 379(36), 1975-1978.

[103] Chow, K. W., Lai, W. C., Shek, C. K., & Tso, K. (1998) Positon-like solutions of nonlinear evolution equations in (2+ 1) dimensions, Chaos, Solitons & Fractals, 9(11), 1901-1912.

[104] Borhanifar, A., Jafari, H., & Karim, S. A. (2008) New solitons and periodic solutions for The kadomtsev-Petviashvili equation, The Journal of Nonlinear Sciences and its Applications, 1(4), 224-229.

[105] Aslan, I. (2012) On the application of the Exp-function method to the KP equation for N-soliton solutions, Applied Mathematics and Computation, 219(6), 2825-2828.

[106] Khan, K., & Akbar, M. A. (2015) Exact traveling wave solutions of Kadomtsev–Petviashvili equation, Journal of the Egyptian Mathematical Society, 23(2), 278-281.

[107] Gu, Y., & Meng, F. (2019) Searching for Analytical Solutions of the (2+ 1)-Dimensional KP Equation by Two Different Systematic Methods, Complexity, 2019(1), 9314693.

[108] Konopelchenko, B. G. (1991) Inverse spectral transform for the (2+ 1)-dimensional Gardner equation, Inverse Problems, 7(5), 739.

[109] Wazwaz, A. M. (2008) Solitons and singular solitons for the Gardner-KP equation, Applied Mathematics and Computation, 204(1), 162–169.

[110] Liu, H.,and Yan, F. (2014) Bifurcation and exact travelling wave solutions for Gardner–KP equation, Applied Mathematics and Computation, vol. 228, pp. 384–394.

[111] Jawad, A.J.A.M., Mirzazadeh, M., and Biswas, A. (2015) Dynamics of shallow water waves with Gardner-Kadomtsev-Petviashvili equation, Discrete & Continuous Dynamical Systems-S, vol. 8, no. 6, pp. 1155, 2015.

[112] Boateng, K., Yang, W., Yaro, D., and Otoo,M. E. (2020) Jacobi Elliptic Function Solutions and Traveling Wave Solutions of the (2 + 1)-Dimensional Gardner-KP Equation, Mathematical Methods in the Applied Sciences, vol. 43, no. 21, 6131–10.

[113] Wang, M. (1996) Exact solutions for a compound KdV-Burgers equation, Physics Letters A, 213(5-6), 279-287.

[114] Zhang, W., Chang, Q., & Jiang, B. (2002) Explicit exact solitary-wave solutions for compound KdV-type and compound KdV–Burgers-type equations with nonlinear terms of any order, Chaos, Solitons & Fractals, 13(2), 311-319.

[115] Li, B., Chen, Y., & Zhang, H. (2003) Explicit exact solutions for compound KdV-type and compound KdV–Burgers-type equations with nonlinear terms of any order, Chaos, Solitons & Fractals, 15(4), 647-654.

[116] Kaya, D. (2004) Solitary-wave solutions for compound KdV-type and compound KdV–Burgers-type equations with nonlinear terms of any order, Applied mathematics and computation, 152(3), 709-720.

[117] Duan, W. S. (2001) Weakly two-dimensional dust acoustic waves, Physics of Plasmas, 8(8), 3583-3586.

[118] Lin, M. M., & Duan, W. S. (2005) The Kadomtsev–Petviashvili (KP), MKP, and coupled KP equations for two-ion-temperature dusty plasmas, Chaos, Solitons & Fractals, 23(3), 929-937.

[119] Dorranian, D., & Sabetkar, A. (2012) Dust acoustic solitary waves in a dusty plasma with two kinds of nonthermal ions at different temperatures, Physics of plasmas, 19(1).

[120] Saini, N. S., Kaur, N., & Gill, T. S. (2015) Dust acoustic solitary waves of Kadomstev–Petviashvili (KP) equation in superthermal dusty plasma, Advances in Space Research, 55(12), 2873-2882.

[121] Gill, T. S., Saini, N. S., & Kaur, H. (2006) The Kadomstev–Petviashvili equation in dusty plasma with variable dust charge and two temperature ions, Chaos, Solitons & Fractals, 28(4), 1106-1111.

[122] Pakzad, H. R., & Javidan, K. (2009) Solitary waves in dusty plasmas with variable dust charge and two temperature ions, Chaos, Solitons & Fractals, 42(5), 2904-2913.

[123] Seadawy, A. R. (2017) Solitary wave solutions of two-dimensional nonlinear Kadomtsev–Petviashvili dynamic equation in dust-acoustic plasmas, Pramana, 89, 1-11.

[124] Xue, J. K. (2003) Kadomtsev-Petviashvili (KP) Burgers equation in a dusty plasmas with non-adiabatic dust charge fluctuation, The European Physical Journal D-Atomic, Molecular, Optical and Plasma Physics, 26, 211-214.

[125] Shah, A., & Mahmood, S. (2012) Impact of Positron Beam on Nonlinear Energy Transport in Electron–Ion Plasma, Journal of the Physical Society of Japan, 81(8), 084501.

[126] Ali Shan, S., El-Tantawy, S. A., & Moslem, W. M. (2013) On the fully nonlinear acoustic waves in a plasma with positrons beam impact and superthermal electrons, Physics of Plasmas, 20(8).

[127] Shah, A., Mahmood, S., & Haque, Q. (2012) Ion acoustic shock waves in presence of superthermal electrons and interaction of classical positron beam, Physics of Plasmas, 19(3).

[128] Ali Shan, S., Ur-Rehman, A., & Mushtaq, A. (2017) Ion-acoustic solitary waves in a positron beam plasma with electron trapping and nonextensivity effects, Physics of Plasmas, 24(3).

[129] Sarma, R., Misra, A. P., & Adhikary, N. C. (2018) Nonlinear ion-acoustic solitary waves in an electron-positron-ion plasma with relativistic positron beam, Chinese Physics B, 27(10), 105207.

[130] Gaillard, P. (2021) The mKdV equation and multi-parameters rational solutions, Wave Motion, 100, 102667.

[131] Wadati, M. (1973) The modified Korteweg-de Vries equation, Journal of the Physical Society of Japan, 34(5), 1289-1296.

[132] Miura, R. M., Gardner, C. S., & Kruskal, M. D. (1968) Korteweg-de vries equation and generalizations. II. Existence of conservation laws and constants of motion, Journal of Mathematical physics, 9(8), 1204-1209.

[133] Jimbo, M., Kruskal, M. D. and Miwa, T. (1982) The Painlevé Test for the Self-dual Yang-Mills Equations, Physics Letters A, 92(2), 59-60.

[134] Bell, E. T. (1934) Exponential polynomials, Annals of Mathematics, 258-277.

[135] Gilson, C., Lambert, F., Nimmo, J., & Willox, R. (1996) On the combinatorics of the Hirota D-operators, Proceedings of the Royal Society of London. Series A: Mathematical, Physical and Engineering Sciences, 452(1945), 223-234.

[136] Lambert, F., Loris, I., & Springael, J. (2001) Classical Darboux transformations and the KP hierarchy, Inverse Problems, 17(4), 1067.

[137] Hon, Y. C., & Fan, E. (2012) Binary Bell polynomial approach to the non-isospectral and variable-coefficient KP equations, IMA Journal of Applied Mathematics, 77(2), 236-251.

[138] Lambert, F., & Springael, J. (1997) Construction of Bäcklund transformations with binary Bell polynomials, Journal of the Physical Society of Japan, 66(8), 2211-2213.

[139] Lambert, F., & Springael, J. (2008) Soliton equations and simple combinatorics, Acta Applicandae Mathematicae, 102, 147-178.

[140] Lü, X., Lin, F., & Qi, F. (2015) Analytical study on a two-dimensional Korteweg–de Vries model with bilinear representation, Bäcklund transformation and soliton solutions, Applied Mathematical Modelling, 39(12), 3221-3226.

[141] Lax, P. D. (1969) Integrals of nonlinear equations of evolution and solitary waves, Matematika, 13(5), 128-150.

[142] Yomba, E. (2010) Jacobi elliptic function solutions of the generalized Zakharov–Kuznetsov equation with nonlinear dispersion and t-dependent coefficients, Physics Letters A, 374(15-16), 1611–1615.

[143] Liu, C. S. (2005) New exact envelope traveling wave solutions of high-order dispersive cubic-quintic nonlinear Schrödinger equation, Communications in theoretical physics, 44(5), 799.

[144] Sarkar, T., Raut, S., Mali, P. C. (2022) The Classification of the Exact Single Travelling Wave Solutions to the Constant Coefficient KP-mKP Equation Employing Complete Discrimination System for Polynomial Method, Computational and Mathematical Methods, vol. 2022: Article ID 3844031, 14 pages.

[145] Raut, S., Saha, S., Das, A. N., & Talukder, P. (2023) Complete discrimination system method for finding exact solutions, dynamical properties of combined Zakharsov-Kuznetsov-modified Zakarsov-Kuznetsov equation, Alexandria Engineering Journal, 76, 247-257.

[146] Awawdeh, F., jaradat, H. M., Al-Shara, S. (2012) Applications of a simplified bilinear method to ion-acoustic solitary waves in plasma, Eur. Phys. J. D, 66(2), 40.

[147] Hereman, W., and Nuseir, A. (1997) Symbolic methods to construct exact solutions of non-linear partial differential equations, Math. Comput. Simul. 43, 13–27.

[148] Ma, W. X. (2020) N-soliton solutions and the Hirota conditions in (2+ 1)-dimensions, Optical and Quantum Electronics, 52(12), 511.

[149] Alhejaili, W., Roy, S., Raut, S., Roy, A., Salas, A. H., Aboelenen, T., & El-Tantawy, S. A. (2024) On the integrability, multi-shocks, high-order kinky-breathers, L-lump–kink solutions for the non-autonomous perturbed potential Kadomtsev–Petviashvili equation, Nonlinear Dynamics, 1-25.

[150] Layek, G. C. (2015) An introduction to dynamical systems and chaos (Vol. 449), Springer: New Delhi, India.

[151] Lakshmanan, M., & Rajaseekar, S. (2012) Nonlinear dynamics: integrability, chaos and patterns, Springer Science & Business Media.

[152] Wei, G.M., Gao, Y.T., Hu, W. and Zhang, C.Y. (2006) Painlevé analysis, auto-Bäcklund transformation and new analytic solutions for a generalized variable-coefficient Korteweg-de Vries (KdV) equation, The European Physical Journal B-Condensed Matter and Complex Systems, 53(3), pp.343-350 .

[153] Liu, Y., Gao, Y. T., Sun, Z. Y., & Yu, X. (2011) Multi-soliton solutions of the forced variable-coefficient extended Korteweg–de Vries equation arisen in fluid dynamics of internal solitary waves, Nonlinear Dynamics, 66(4), 575-587.

[154] Yu, X., Gao, Y. T., Sun, Z. Y., & Liu, Y. (2012) Wronskian solutions and integrability for a generalized variable-coefficient forced Korteweg–de Vries equation in fluids, Nonlinear Dynamics, 67(2), 1023-1030.

[155] Li, M., Xiao, J. H., Wang, M., Wang, Y. F., & Tian, B. (2013) Solitons for a forced extended Korteweg-de Vries equation with variable coefficients in atmospheric dynamics, Zeitschrift fuer Naturforschung. A: Physical Sciences, 68(3-4), 235-244.

[156] Roy, S., Raut, S., Kairi, R. R., & Chatterjee, P. (2022) Integrability and the multi-soliton interactions of non-autonomous Zakharov–Kuznetsov equation, The European Physical Journal Plus, 137(5), 1-14.

[157] Sen A., Tiwari S., Mishra S., Kaw P. (2015) Nonlinear wave excitations by orbiting charged space debris objects, Advances in Space Research, 56(3), 429.

[158] Aslanov V. S., Yudintsev V. V. (2015) Dynamics, analytical solutions and choice of parameters for towed space debris with flexible appendages, Advances in Space Research, 55, 660–667.

[159] Raut, S., Roy, A., Mondal, K. K., Chatterjee, P. and Chadha, N. M. (2021) Non-stationary Solitary Wave Solution for Damped Forced Kadomtsev-Petviashvili Equation in a Magnetized Dusty Plasma with q-Nonextensive Velocity Distributed Electron, International Journal of Applied and Computational Mathematics, 7(6), pp.1-20.

[160] Shen, Y. J., Gao, Y. T., Yu, X., Meng, G. Q., & Qin, Y. (2014) Bell-polynomial approach applied to the seventh-order Sawada–Kotera–Ito equation, Applied Mathematics and Computation, 227, 502-508.

[161] Wang, C., (2016) Spatiotemporal deformation of lump solution to (2+ 1)-dimensional KdV equation, Nonlinear Dynamics, 84(2), pp.697-702.

[162] Jordan, P. M., & Puri, A. (2005) A note on traveling wave solutions for a class of nonlinear viscoelastic media, Physics Letters A, 335(2-3), 150-156.

[163] Zhou, J. K. (1986) Differential transformation and its applications for electrical circuits, Huazhong University Press.

[164] Raut, S., Roy, S., Saha, S., & Das, A. N. (2022) Studies on the Dust–Ion–Acoustic Solitary Wave in Planar and Non-Planar Super-Thermal Plasmas with Trapped Electrons, Plasma Physics Reports, 48(6), 627-637.

[165] Ray, A. K., & Bhattacharjee, J. K. (2007) Standing and travelling waves in the shallow-water circular hydraulic jump, Physics Letters A, 371(3), 241-248.

[166] Wang, R. R., Wang, Y. Y. and Dai, C. Q. (2022) Influence of higher-order nonlinear effects on optical solitons of the complex Swift-Hohenberg model in the mode-locked fiber laser, Optics & Laser Technology, 152, p.108103.

[167] Yan, Z. (2003) Generalized method and its application in the higher-order nonlinear Schrödinger equation in nonlinear optical fibres, Chaos, Solitons & Fractals, 16(5), 759-766.

[168] Whitham, G.B. (1974) Linear and nonlinear waves, Wiley-Interscience, 1974, 651.

[169] Roy, A., Raut, S., & Barman, R. (2022) Studies on the Effect of Dust–Ion Collision on Dust–Ion Acoustic Solitary Waves in a Magnetized Dusty Plasma in the Framework of Damped KP Equation and Modified Damped KP Equation, Plasma Physics Reports, 48(4), 367-383.

[170] Dorranian, D. and Sabetkar, A. (2012) Dust acoustic solitary waves in a dusty plasma with two kinds of nonthermal ions at different temperatures, Physics of plasmas, 19(1).

[171] Ablowitz, M. J., Ramani, A., & Segur, H. (1980) A connection between nonlinear evolution equations and ordinary differential equations of P-type. II, Journal of Mathematical Physics, 21(5), 1006-1015.

[172] Hu, X. and Chen, Y. (2012) A direct procedure on the integrability of nonisospectral and variable-coefficient MKdV equation, Journal of Nonlinear Mathematical Physics, 19(01), 1250002.

[173] Ma, W. X. (2013) Bilinear equations and resonant solutions characterized by Bell polynomials, Reports on Mathematical Physics, 72(1), 41-56.

[174] Wang, Y. Y., Su C. Q., Liu X. Q., Li J. G. (2018) Nonautonomous solitons for an extended forced Korteweg–de Vries equation with variable coefficients in the fluid or plasma, Waves Random Complex Media, 28(3), 411–25.

[175] Raut, S., Ma, W. X., Barman, R. and Roy, S. (2023) A non-autonomous Gardner equation and its integrability: Solitons, positons and breathers, Chaos, Solitons & Fractals, 176, 114089.

[176] Xing, Q., Wu, Z., Mihalache, D., & He, J. (2017) Smooth positon solutions of the focusing modified Korteweg–de Vries equation, Nonlinear Dynamics, 89, 2299-2310.

[177] Xing, Q., Wang, L., Mihalache, D., Porsezian, K., & He, J. (2017) Construction of rational solutions of the real modified Korteweg-de Vries equation from its periodic solutions, Chaos: An Interdisciplinary Journal of Nonlinear Science, 27(5), 053102.

[178] Schiebold, C. (2017) Asymptotics for the multiple pole solutions of the nonlinear Schrödinger equation, Nonlinearity, 30, 2930–2981.

[179] Zhang, Y., Tao, X., Yao, T., & He, J. (2020) The regularity of the multiple higher-order poles solitons of the NLS equation, Studies in Applied Mathematics, 145(4), 812-827.

[180] Bilman, D., Buckingham, R. (2019) Large-order asymptotics for multiple-pole solitons of the focusing nonlinear schrödinger equation. Journal of Nonlinear Science, 29, 2185–2229.

[181] Wang, L., He, J., Xu, H., Wang, J., & Porsezian, K. (2017) Generation of higher-order rogue waves from multibreathers by double degeneracy in an optical fiber, Physical Review E, 95(4), 042217.

[182] Zhang, Z., Yang, X. Y., Li, B. (2020) Novel soliton molecules and breather-positon on zero background for the complex modified KdV equation, Nonlinear Dynamics, 100, 1551.

[183] Manafian, J., Ilhan, O. A., & Alizadeh, A. A. (2020) Periodic wave solutions and stability analysis for the KP-BBM equation with abundant novel interaction solutions, Physica Scripta, 95(6), 065203.

[184] Ahmed, S., Ashraf, R., Seadawy, A. R., Rizvi, S.T. R., Younis, M., Althobaiti, A., El-Shehawi, A. M. (2021) Lump, multi-wave, kinky breathers, interactional solutions and stability analysis for general (2+1)-rth dispersionless Dym equation, Results in Physics, 25, 104160.

[185] Yokus, A., Isah, M. A. (2022) Stability analysis and solutions of (2+1)-Kadomtsev–Petviashvili equation by homoclinic technique based on Hirota bilinear form, Nonlinear Dynamics, 109, 3029–3040.

[186] Schneider, T.M., Eckhardt, B. and Yorke, J.A. (2007) Turbulence transition and the edge of chaos in pipe flow, Physical review letters, 99(3), 034502.

[187] Chen, M., Sun, M., Bao, H., Hu, Y. and Bao, B. (2019) Flux–charge analysis of two-memristor-based Chua's circuit: dimensionality decreasing model for detecting extreme multistability, IEEE Transactions on Industrial Electronics, 67(3), 2197-2206.

[188] Li, H., Li, K., Chen, M. and Bao, B. (2020) Coexisting infinite orbits in an area-preserving Lozi map, Entropy, 22(10), 1119.

[189] Abdul Rahim, M. F., Natiq, H., Fataf, N.A.A. and Banerjee, S. (2019) Dynamics of a new hyperchaotic system and multistability, The European Physical Journal Plus, 134, 1-9.

[190] Kodama, Y. (2018) Solitons in two-dimensional shallow water, Society for Industrial and Applied Mathematics.

[191] Seadawy, A. R. (2017) Solitary wave solutions of two-dimensional nonlinear Kadomtsev–Petviashvili dynamic equation in dust-acoustic plasmas, Pramana, 89(3), 1-11.

[192] Raut, S., Mondal, K. K., Chatterjee, P., and Roy, A. (2021) Propagation of dust-ion-acoustic solitary waves for damped modified Kadomtsev–Petviashvili–Burgers equation in dusty plasma with a q-nonextensive nonthermal electron velocity distribution, SeMA Journal, 78(4), 571-593.

[193] Liu, C. S. (2006) All Single Traveling Wave Solutions to (3+1)-Dimensional Nizhnok Novikov Veselov Equation, Commun. Theor. Phys. (Beijing, China), 45, 991–992.

[194] Liu, C. S. (2007) The classification of travelling wave solutions and superposition of multi-solutions to Camassa–Holm equation with dispersion, Chinese Phys, 16(7), 1832.

[195] Liu, C. S. (2005) Exact travelling wave solutions for (1+1)-dimensional dispersive long wave equation, Chinese Physics, 14(9), 1710–1715.

[196] Yang, L., Hou, X. R., and Zeng, Z. B. (1996) A complete discrimination system for polynomials, Science in China, Series E, 39(6), 628-646.

[197] Kai, Y., Chen, S., Zheng, B., Zhang, K., Yang, N., and Xu, W. (2020) Qualitative and quantitative analysis of nonlinear dynamics by the complete discrimination system for polynomial method, Chaos, Solitons & Fractals, 141, 110314, 2020.

[198] Byrd, P. F., and Friedman, M. D. (1971) Handbook of Elliptic Integrals for Engineers and Scientists, Springer-Verlag Berlin Heidelberg New York.

[199] Guckenheimer, J., and Holmes, P. (2013) Nonlinear oscillations, dynamical systems, and bifurcations of vector fields, Springer Science Business Media, 42.

[200] Jhangeer, A., Hussain, A., Junaid-U-Rehman, M., Baleanu, D., and Riaz., M. B. (2021) Quasi-periodic, chaotic and travelling wave structures of modified Gardner equation, Chaos, Solitons & Fractals, 143, 110578.

[201] Raut, S., Barman, R., and Sarkar, T. (2023) Integrability, breather, lump and quasi-periodic waves of non-autonomous Kadomtsev–Petviashvili equation based on Bell-polynomial approach, Wave Motion, 119, 103125.

[202] Raut, S., Sarkar, T., Mali, P. C., Alotaibi, B. M., Ismaeel, S., and El-Tantawy, S. A. (2023) On the propagation and interaction of ion-acoustic solitary, periodic, shock, and breather waves in a non-Maxwellian electron–positron–ion magnetoplasma, Physics of Fluids, 35(5), 053111.

[203] Sarkar, T., Roy, S., Raut, S., and Mali, P. C. (2023) Studies on the Dust Acoustic Shock, Solitary, and Periodic Waves in an Unmagnetized Viscous Dusty Plasma with Two-Temperature Ions, Brazilian Journal of Physics, 53(1), 12.

[204] Miller, H. R., Wiita, P. J. (1987) Active Galactic Nuclei, (Berlin: Springer) 202.

[205] Gurevich, A. V., Istomin, Y. (1993) Physics of the Pulsar Magnetosphere, (Cambridge: Cambridge University Press).

[206] Goldreich, P., Julian, W. H. (1969) Pulsar Electrodynamics, Astrophys. J., 157.

[207] Michel, F. C. (1982) Theory of pulsar magnetospheres, Rev. Mod. Phys., 54, 1.

[208] Tandberg-Hansen, E., Emslie, A. G. (1988) The Physics of Solar Flares, Cambridge University Press, Cambridge, 14.

[209] Goertz, C. K. (1989) Dusty plasmas in the solar system, Rev. Geophys., 27(2), 271-292.

[210] Havens, O., Melandso, F., Aslaksen, T. K., Nitter, T. (1992) Collisionless Braking of Dust Particles in the Electrostatic Field of Planetary Dust Rings, Physica Scripta, 45(5), 491-496.

[211] Whipple, E. C., Northrop, T. G., Mendis, D. A. (1985) The electrostatics of a dusty plasma, J. Geophys. Res., 90(A8), 7405-7413.

[212] Chu, J. H., Du, J. B, Lin, I. (1994) Coulomb solids and low-frequency fluctuations in RF dusty plasmas, Phys. D: Appl. Phys, 27(2), 296.

[213] Pieper, J. B., Goree, J. (1996) Dispersion of Plasma Dust Acoustic Waves in the Strong-Coupling Regime. Physical Review Letters, 77(15), 3137–3140.

[214] Prabhakara, H. R., Tanna, V. L. (1996) Trapping of dust and dust acoustic waves in laboratory plasmas. Physics of Plasmas, 3(8), 3176–3181.

[215] Verheest, F. (1992) Nonlinear dust-acoustic waves in multispecies dusty plasmas, Planetary and Space Science, 40(1), 1–6.

[216] Shukla, P. K., Silin, V. P. (1992) Dust ion-acoustic wave, Physica Scripta, 45(5), 508–508.

[217] Melandso/, F. (1996) Lattice waves in dust plasma crystals, Physics of Plasmas, 3(11), 3890–3901.

[218] Verheest, F. (1996) Waves and instabilities in dusty space plasmas, Space Sci. Rev., 77(3-4), 267-302.

[219] Shukla, P. K., Mamun, A. A. (2002) Introduction to Dusty Plasma Physics, 1st ed. (IOP, London, 2002)

[220] Rahman, A. U., Khalid, M., Zeb, A. (2019) Compressive and rarefactive ion acoustic nonlinear periodic waves in nonthermal plasmas, Brazilian Journal of Physics, 49(5), 726-733.

[221] Melands, F., Aslaksen, T.,and Havnes, O. (1993) A new damping effect for the dust-acoustic wave, Planetary and Space Science, 41(4), 321–325.

[222] Melandso, F. (1996) Lattice waves in dust plasma crystals, Physics of Plasmas, **3**(11), 3890–3901.

[223] Nejoh, Y. N. (1997) The dust charging effect on electrostatic ion waves in a dusty plasma with trapped electrons, Physics of Plasmas, 4(8), 2813–2819.

[224] Xie, B., He, K., Huang, Z. (1999) Dust-acoustic solitary waves and double layers in dusty plasma with variable dust charge and two-temperature ions, Physics of Plasmas, 6(10), 3808–3816.

[225] Washimi, H., Taniuti, T. (1966) Propagation of Ion-Acoustic Solitary Waves of Small Amplitude, Physical Review Letters, 17(19), 996–998.

[226] Khalid, M., Khan, M., Rahman, A. U., and Hadi, F. (2022) Nonlinear periodic structures in a magnetized plasma with Cairns distributed electrons, Indian journal of Physics, **96**(6), 1783-1790.

[227] Khalid, M., Khan, M., Muddasir., Rahman, A. U., and Irshad, M. (2021) Periodic and localized structures in dusty plasma with Kaniadakis distribution, Zeitschrift für Naturforschung A, 76(10), 891-897.

[228] Maier, E. J., and Hoffman, J. H. (1974) Observation of a two-temperature ion energy distribution in regions of polar wind flow. Journal of Geophysical Research, 79(16), 2444-2447.

[229] Moslem, W. M. (2005) Obliquely propagating dust-acoustic solitary waves in cosmic dust-laden plasmas. Chaos, Solitons & Fractals, 23(3), 939-947.

[230] Tagare, S. G., Singh, S. V., Reddy, R. V., and Lakhina, G. S. (2004) Electron acoustic solitons in the Earth's magnetotail. Nonlinear Processes in Geophysics, 11(2), 215-218.

[231] Kotani, T., Kawai, N., Matsuoka, M., & Brinkmann, W. (1996) Iron-line diagnostics of the jets of SS 433, Publications of the Astronomical Society of Japan, 48(4), 619-629.

[232] Cowan, T. E., Perry, M. D., Key, M. H., Ditmire, T. R., Hatchett, S. P., Henry, E. A., ... & Kühl, T. (1999) High energy electrons, nuclear phenomena and heating in petawatt laser-solid experiments, Laser and Particle Beams, 17(4), 773-783.

[233] Greaves, R. G., & Surko, C. M. (1995) An electron-positron beam-plasma experiment, Physical review letters, 75(21), 3846.

[234] Surko, C. M., Leventhal, M., & Passner, A. J. P. R. L. (1989) Positron plasma in the laboratory, Physical Review Letters, 62(8), 901.

[235] Weber, M. H., Pilant, L., & Lynn, K. G. (2007) Small accelerator based intense positron beam sources, physica status solidi c, 4(10), 3953-3956.

[236] Ali Shan, S., & El-Tantawy, S. A. (2016) The impact of positrons beam on the propagation of super freak waves in electron-positron-ion plasmas, Physics of Plasmas, 23(7).

[237] Adhikary, N. C., Deka, M. K., Dev, A. N., & Sarmah, J. (2014) Modified Korteweg–de Vries equation in a negative ion rich hot adiabatic dusty plasma with non-thermal ion and trapped electron, Physics of Plasmas, 21(8).

[238] Adhikary, N. C., Misra, A. P., Deka, M. K., & Dev, A. N. (2017) Nonlinear dust-acoustic solitary waves and shocks in dusty plasmas with a pair of trapped ions, Physics of Plasmas, 24(7).

[239] Gill, T. S., Singh, A., Kaur, H., Saini, N. S., & Bala, P. (2007) Ion-acoustic solitons in weakly relativistic plasma containing electron–positron and ion, Physics Letters A, 361(4-5), 364-367.

[240] Gill, T. S., Bains, A. S., & Saini, N. S. (2009) Ion acoustic soliton in weakly relativistic magnetized electron–positron–ion plasma, Canadian Journal of Physics, 87(8), 861-866.

[241] Shah, A., Haque, Q., & Mahmood, S. (2011) Electrostatic compressive and rarefactive shocks and solitons in relativistic plasmas occurring in polar regions of pulsar, Astrophysics and Space Science, 335, 529-537.

[242] Dev, A. N., Deka, M. K., Sarma, J., Saikia, D., & Adhikary, N. C. (2016) K–P–Burgers equation in negative ion-rich relativistic dusty plasma including the effect of kinematic viscosity, Chinese Physics B, 25(10), 105202.

[243] Abdikian, A., and Ghanbari, B. (2023) On a modified Korteweg–de Vries equation for electrostatic structures in relativistic degenerate electron-positron plasma, Results in Physics, 48, 106399.

[244] Xing, Q., Wang, L., Mihalache, D., Porsezian, K., & He, J. (2017) Construction of rational solutions of the real modified Korteweg-de Vries equation from its periodic solutions, Chaos: An Interdisciplinary Journal of Nonlinear Science, 27(5).

[245] Hirota, R. (1972) Exact solution of the modified Korteweg-de Vries equation for multiple collisions of solitons, Journal of the Physical Society of Japan, 33(5), 1456-1458.

[246] Zhang, Z., Li, B., Chen, J., & Guo, Q. (2021) Construction of higher-order smooth positons and breather positons via Hirota's bilinear method, Nonlinear Dynamics, 105(3), 2611-2618.

[247] Liu, S. Z., & Zhang, D. J. (2021) General description on extended homoclinic orbit solutions of the KdV-type bilinear equations, Modern Physics Letters B, 35(05), 2150092.

[248] Najafi, M., Najafi, M., & Darvishi, M. T. (2012) New exact solutions to the (2+ 1)-dimensional Ablowitz—Kaup—Newell—Segur equation: modification of the extended homoclinic test approach, Chinese Physics Letters, 29(4), 040202.

[249] Wang, X. B., Tian, S. F., Qin, C. Y., & Zhang, T. T. (2017) Dynamics of the breathers, rogue waves and solitary waves in the (2+ 1)-dimensional Ito equation, Applied Mathematics Letters, 68, 40-47.

[250] Wang, X. B., Tian, S. F., Yan, H., & Zhang, T. T. (2017) On the solitary waves, breather waves and rogue waves to a generalized (3+ 1)-dimensional Kadomtsev–Petviashvili equation, Computers & Mathematics with Applications, 74(3), 556-563.

[251] Singla, S., Kaur, M., & Saini, N. S. (2022) Ion-acoustic shocks in multicomponent plasma with relativistic positron beam, Journal of Astrophysics and Astronomy, 43(2), 70.

[252] Raut, S., & Datta, D. P. (2009) Analysis on a fractal set, Fractals, 17(01), 45-52.

[253] Raut, S., & Datta, D. P. (2010) Non-archimedean scale invariance and cantor sets, Fractals, 18(01), 111-118.

[254] Datta, D. P., & Raut, S. (2006) The arrow of time, complexity and the scale free analysis. Chaos, Solitons & Fractals, 28(3), 581-589.

[255] Raut, S., & Datta, D. P. (2009) ERRATUM:" Analysis on a Fractal Set," Raut and Datta, Fractals, 17(04), 547-547.

[256] Datta, D. P., Raut, S., & Raychoudhuri, A. (2011) Ultrametric Cantor sets and growth of measure, P-Adic Numbers, Ultrametric Analysis, and Applications, 3(1), 7-22.